INFLUENCE OF WELD PROFILE ON FATIGUE CRACK GROWTH IN TUBULAR WELDED JOINTS

RIMON F. KARE

Submitted for the Degree of
Doctor of Philosophy

Department of Mechanical Engineering and Aeronautics

CITY UNIVERSITY

JUNE 1989

TABLE OF CONTENTS

LIST OF FIGURES

LIST OF TABLES

ACKNOWLEDGEMENTS

I would like to thank my supervisor Dr. D.L. McDiarmid for his help and constant encouragement. I would also like to thank Professor W.D. Dover for the opportunity to undertake the study required to produce this Thesis, the helpful discussions and for making the facilities at University College London available to me.

Thanks are due to the technical staff in the Mechanical Engineering Department particularly at University College London.

I am grateful to my parents for their understanding throughout my years of study.

My thanks to Celia for her invaluable support and encouragement.

TO HANI MY YOUNGER BROTHER R.I.P.

ABSTRACT

This thesis investigates the influence of weld profile on fatigue crack growth in tubular welded joints used in the construction of offshore platforms.

An experimental strain analysis has been conducted on three multiplanar steel joints having the same overall geometry but different weld profiles and loaded in out-of-plane bending. This was used to study the effect that controlling the weld profile has upon the stresses in the vicinity of the brace/chord intersection. The same joint configuration, for which the applied loads are reacted by a second brace, was also analysed using a thick shell finite element model and the results compared.

The weld angle α and weld toe radius ρ of the steel models were measured. These values and coordinates of a saddle position from the finite element model were used to generate a number of two-dimensional models of a saddle position. The 2-D models were analysed under plane strain conditions with the boundary conditions calculated from the global finite element analysis using a substructuring technique in order to calculate through thickness stress distributions. The results from this analysis are compared with T-butt joint results.

A series of fatigue tests were conducted on the multibrace nodes in out-of-plane bending under fully reversed constant amplitude loading. The data on crack length and crack depth was collected for relatively small fatigue cracks in the early stages of fatigue damage. Thirteen chord cracks are reported (5 for AWS profile, 6 for C1 profile and 2 for C2 profile).

Experimental stress intensity calibration factors were produced for the deepest point of the crack. The Niu-Glinka weight function was used to predict the distribution of the stress intensity calibration factor Y for the deepest point of the crack. The results indicate that the Niu-Glinka weight function method combined with either linear moment release or quadratic moment release model provides a satisfactory method for calculating the stress intensity factors for fatigue cracks in tubular welded joints.

Crack initiation life in the tubular joints was predicted using the local strain approach. A fatigue fracture mechanics model is proposed to predict the crack propagation life of a tubular joint. The results are compared on the basis of different weld profiles and with the experimental fatigue data.

NOMENCLATURE

A B C D	four saddle positions
E F G H	four crown positions
E	modulus of elasticity
F_r	geometric stress intensity correction factor for a semi-elliptical surface crack emanating from an angular corner α in a plate of finite thickness and finite width under uniform tension
H	generalised modulus of elasticity
K	local stress concentration factor
K_G	geometric stress concentration factor
K_W	component of SCF due to weld notch effect
K'	material constant
K_t	theoretical stress concentration factor
K_σ	stress concentration factor, σ divided by S
K_ε	strain concentration factor
K_r	reference stress intensity factor
L	weld leg length
R	chord radius
SCF	stress concentration factor (tubular joints)
SCNF	strain concentration factor (tubular joints)
T	chord thickness
Y	geometric stress intensity calibration factor
X Y Z	tubular joints 1, 2, 3 respectively
b	fatigue strength exponent
c	fatigue ductility exponent
e	nominal strain
m(x,a)	weight function
n'	material constant
r	brace radius
t	brace thickness
α	weld angle
ρ	weld toe radius
ε	maximum strain

σ	elastic-plastic stress
$\Delta\varepsilon$	total strain range
ε'_f	fatigue ductility coefficient
$\Delta\sigma$	total stress range
σ'_f	fatigue strength coefficient
$u_r(x,a)$	crack opening displacement corresponding to the reference stress intensity factor

1 CHAPTER ONE

REVIEW OF THE LITERATURE

1.1 Scope of chapter

A number of research programmes have reported on the problems of fatigue and fracture behaviour of complex steel welded structures. Consequently a large data and research base exists on the various aspects that influence the behaviour of tubular welded joints. This chapter presents a review of the literature. The main areas of the review are:

(i) The stress fields that exist at the intersections of these tubes and the methods of stress analysis used to determine the magnitude of these stresses.

(ii) The different methodologies available for designing against fatigue fracture of welded structures.

(ii)The geometry of the weld profile and the codes that govern the welding procedures of steel structures.

1.2 Introduction

The rapid development of the offshore oil and gas industry and its continuing expansion into ever more hostile environments such as the northern North Sea has led to increasing demands being made upon the technology used. In response to initial development in the North Sea the 1970's saw the start of a number of research programmes concerned with the fatigue behaviour of offshore structures. A significant outcome of these programmes was the publication of the Department of Energy Guidance Notes for Offshore Industry [1.1] and the SERC Cohesive Fatigue Programme 1983-85 [1.2]. The primary aim of these programmes was to produce a broad fatigue database and reliable methods of using data for design and certification of tubular welded connections. A further aim was to investigate the various stress analysis techniques and to determine procedures for the measurement of the 'hot spot' stress concentration factors.

Steel jacket offshore structures consist primarily of tubular joints which are formed by the intersection of brace and chord members, with the ouside diameter of the brace less than or equal to the outside diameter of the chord. A schematic diagram showing wellhead and productions constructed using welded steel tubular connections is shown in Figure 1.1. The complex intersection induces large distortions of the nominal stress fields in each of the tubular members giving rise to severe stress concentrations. The joint deformation and distribution of stresses and in particular peak stresses play a major part in the design of offshore structures. Detailed analysis is therefore required to determine the magnitude of the peak stresses and the deformations caused. The different methods available to conduct a stress analysis study are experimental techniques which include acrylic models, steel models and photoelasticity, and numerical methods which are primarily the finite element technique. These are discussed in the light of the existing design codes and relevant published work.

In terms of the design and fatigue life assessment of a structural component, two basic approaches are available. The first and more generally used method is the empirically derived relationship between applied stress range and fatigue life (S-N approach). For tubular joints this approach requires that the number of cycles to failure can be related to the 'hot spot stress'. This provides a stress-life curve which could be used to predict the total fatigue life of a structure. However, for crack growth or remaining life prediction the second method which is based on linear elastic fracture mechanics is used. This method considers the growth rate of an existing defect at each stage in its propagation and since for welded structures initiation is a very small part of the total fatigue life, fracture mechanics would seem to be an appropriate technique for assessing the life of a structure. However, the method is complex and a number of parameters need to be considered. One principle parameter is the stress intensity factor.

For engineering components and particularly welded structures the cracks developed are normally semi-elliptical in nature and if fracture mechanics models are to be used in order to predict the remaining life of a structure containing this type of crack then calculation of stress intensity factors for relevant crack-load configurations will have to be undertaken. The stress intensity factor for a crack in a welded joint depends on the global geometry of the joint as well as the local geometry of the weld profile and the type of loading. Therefore, the evaluation of stress intensity

factors for any type of structure, requires analysis of all these parameters. The derivation of formulae for this analysis can be approached using classical solutions or numerical methods, and these techniques are reviewed in section 1.6.

A third but less widely used method for tubular joints needs to be mentioned in this context, which is the local stress-strain approach to crack initiation. The aim of this approach is to predict the number of loading cycles necessary to initiate a crack in a component. This predictive technique is based on the assumption that the fatigue behaviour of a notch can be approximated by a small plain specimen subjected to the same stress-strain history as the notch tip. This technique in conjunction with fracture mechanics analysis will provide the basis for a fatigue life model.

The final section of this chapter will consider the different aspects that govern the weld profile of a tubular connection. The effect of the weld profile on the stress distribution at the toe of the weld and subsequent fatigue test results are also reviewed.

1.3 Stress distributions at tubular joints

Stresses in tubular joints arise from three main causes:

1. The basic structural response of the joint to the applied load. This is termed the nominal stress

2. Further, to maintain continuity at the intersection, the tubular walls deform, giving rise to deformation stresses.

3. Finally, the weld introduces a geometrical discontinuity, giving rise to notch stresses.

Nominal stresses arise due to the tubes behaving as beam-columns, and may be calculated by frame analysis of the structure.

Geometric stresses result from the differences in deformation between the brace and the chord under load. Consider a T joint under axial tensile brace load, the brace extends only very slightly, whereas the circular cross section of the chord becomes significantly elongated to a pear-shaped section. The differences in deformation require the tube walls to bend so that the brace and chord remain in contact at the weld.

Local stresses arise because of the geometric discontinuity of the tube walls at the weld toes, where an abrupt change of the section occurs, which in turn increases until the weld root is reached. The local stresses do not propagate far through the wall thickness, and therefore a local region with stresses varying rapidly in three dimensions is present. The weld also stiffens the walls of the tubular joint locally, and thus affects the local stresses up to and beyond the position of the weld toe. However, in this small region the effect of this stress decays very sharply.

1.3.1 Stress concentration factor - review of codes

The welding process and the geometry of a tubular give rise to stress raisers which cause the stress at the intersection to greatly exceed the nominal brace stress. The maximum stress is termed the hot spot stress. The stress concentration factor is a non-dimensional parameter defined as the ratio of the stress measured at the intersection to the nominal brace stress. The different design codes refer to this stress and a short review is presented on the interpretations of the different design codes with refernce to the SCF and the hot spot stress.

1.3.2 American Petroleum Institute - API RP2A

This design code [1.3] defines the 'hot spot' strain as that which would be measured by a strain gauge element adjacent to and perpendicular to the toe of the weld, after stable strain cycles have been achieved. This implies that no extrapolation to the weld toe is required, and would therefore consider local stresses at tubular connections in terms of the geometric SCF. This is because the API code makes provisions for the severity of the notch at the weld toe by assigning different S-N curves X and X′ for the different weld profile qualities. The code allows for the use of empirical equations, derived from finite element analysis, to predict the SCF. However, in using these equations differences between mid-plane intersections and actual hot spot locations must be taken into account as well as the stiffening effect of the weld geometry.

1.3.3 American Welding Society Structural Code AWS D1.1-84

The AWS [1.4] states that this is the stress or strain on the outside surface of intersecting members at the toe of the weld joining them, measured after shakedown in model or prototype connection, or calculated with best available

theory. AWS states that the 'hot spot' stress or strain can be determined by testing an accurately scaled model, or by theoretical analysis, and gives the finite element method as an example.

1.3.4 BS 6235: 1982

This code [1.5] defines the 'hot spot' stress as that stress which is as near as possible to the intersection, without being influenced by the weld profile. It also states that the SCF should be determined by methods such as parametric equations, finite element analyses, or experimental methods. This is significantly different from other codes as it implies that the 'hot spot' refers to the 'local' deformation stress.

1.3.5 UK Department of Energy Guidance Notes

This document [1.1] defines the 'hot spot' stress as the greatest value of stress around the brace/chord intersection of the extrapolation to the weld toe of the geometric stress distribution near the weld toe. This stress incorporates the effects of overall joint geometry, but omits the stress concentrating influence of the weld itself. Figure 1.2. shows an example of the stress distribution in the chord.

The extrapolation to the weld toe hot spot stress concept, was therefore developed to provide a consistent definition of fatigue stress for use in a conventional S-N approach to fatigue performance. This extrapolation technique overcomes the difficulties associated with the measurement of weld toe stresses and the extent their influence has on the maximum surface stress. It relies on the linear extrapolation to the weld toe of stresses measured at prescribed distances from it. These distances are given by Irvine [1.6] and shown in Figure 1.3. for T and X tubular joints.

Irvine reports that wall bending stresses decay away fairly linearly in the axial direction of the brace for a distance of $0.8(rt)^{0.5}$, and they become negligible at about $5(rt)^{0.5}$ from the weld toe. For the chord the linear region for stress decay is more difficult to define, but over about 5° of arc, the stress is fairly linear. It is further noted that in certain locations of certain tubular joints, the stress

obtained perpendicular to the weld toe may not be the maximum principle stress. The value of stress quoted as the hot spot stress is taken as the (conservative) value of extrapolated maximum principle stress.

1.3.6 Estimation of stress concentration factors

1.3.6.1 Parametric equations

The parametric equations are basically design formulae used by the design engineer to assess the magnitude of the stress concentration factor at the pertinent positions along the brace/chord intersection. These equations were developed by fitting analytical or model SCF data to equations which are functions of non-dimensional tubular joint geometric parameters. A number of equations exist for different joint geometry and loading conditions. The most widely used are the Kuang [1.7], Gibstein [1.8] and Wordsworth/Smedley [1.9] equations which deal exclusively with co-planar tubular connections.

Kuang used the FE method to develop a comprehensive set of semi-empirical formulae for T, Y, K and KT joints. The SCF values presented are those obtained at the intersection line of the mid-surface between the brace and chord, and must therefore be accounted for when comparing SCF values from model analysis. The chord end conditions for axial and in-plane bending IPB analyses were taken as simply supported. For out-of-plane OPB moment loaded cases, the chord ends were fixed to provide the necessary torsional restraint.

Gibstein carried out FE study on T joints, the chord length and end conditions were also investigated. The analyses were for axial, IPB and OPB. Gibstein found that the difference in chord boundary conditions produced a 5% difference in the case of axial loading and no difference in the case of IPB between the SCF values. It must be noted that the influence of α (ratio of chord lenght to chord radius) was not investigated, even though it appears in the SCF formulation of axial loading.

The correction factor for the influence of α was taken from Kuang's analysis. The formulae for SCFs in the brace have been modified by a factor of 0.8 to allow for the differences between predicted and experimental SCFs.

Wordsworth *et al* derived empirical formulae for SCF in T, Y, KT and X joints. The data for the parametric study were obtained from acrylic model testing. No attempt was made to model the fillet welds. The formulae are intended to yield the gross deformation stress concentration factors.

A major disadvantage in the use of parametric equations to assess the peak stresses at intersections, is the implication that for complex joints the stress distributions around individual braces do not interact. However this is not the case when bracing members are nearer to each other than two or three diameter distances. Depending on the load and direction of load, the presence of such braces can cause either over prediction or under prediction of the SCF. Also none of the equations in question, cover joints with overlapped braces or internal or external stiffeners. All three sets of equations impose limits upon the range of validity for values of α, β, γ and τ. Each set of equations assumes freely supported chord end conditions with a minimum chord length to radius ratio (α) so as to avoid interaction of chord loading stress concentration and tubular connection stress concentration, and incorporate chord beam bending stresses.

1.4 Methods of stress analysis

The complexity of the stress distribution at the welded intersection of a tubular joint has proved to be a difficult problem. Both experimental and analytical solutions continue to be used. A summary of the different techniques is presented. The main techniques used are:

1. Strain gauged steel models (full/small scale)
2. Finite element method
3. Strain gauged acrylic models
4. Photoelastic method

1.4.1 Strain gauged steel models

Steel models are usually scaled down versions of the real joint and are often fatigue tested after the stress analysis. The welds are present and therefore a more realistic situation is tested. As strain gauging is a costly and time consuming process they are used at a limited number of points. Therefore the risk exists of not having a strain gauge at the peak stress location. It is not possible to accurately

measure the strain values at the hot spot region due to the physical size of the weld. The presence of notch stresses very close to the weld toe also causes large errors in the measured strain for very small errors in the positioning of the strain gauge. Consequently the 'hot spot' strain approach is used as described in section 1.3.1.4. A detailed discussion of experimental procedures and techniques was presented by Irvine. The results obtained from steel models are considered the most realistic and thus form the basis for comparison with data from other methods.

1.4.2 Finite element analysis

The FE method is a numerical analysis tool which may be used to obtain approximate solutions to problems in linear elasticity with the aid of a digital computer. The first step in the FE analysis is the discretisation of a continuum with infinite degrees of freedom into a mesh, yielding an equivalent system with a finite number of degrees of freedom. This mesh is composed of elements of simple geometric shape, with freedoms defined at a number of nodes. The elements have an assumed displacement field, enabling relationships between nodal forces and nodal displacements to be obtained for each element. The stiffness matrix which defines these relationships may be derived directly using an energy theorem such as the principle of minimum total potential energy. These equations are then assembled into a global system which describes the force/displacement relationships for the overall structure. When the boundary conditions are introduced, this set of simultaneous equations may be solved for the unknown displacements, from which the stresses acting in each element may then be extracted. The solution so obtained satisfies all the equations of linear elasticity except those for equilibrium. Although this is violated between elements it is still satisfied in an overall sense. The accuracy of the results increases with the fineness of the mesh in those regions where the stresses vary rapidly and for tubular joints these regions are the brace/chord intersections.

A mesh generator for tubular joints should therefore be capable of producing relatively fine elements in the vicinity of any brace/chord intersections. Conversely, near the ends of the chord and braces where the stresses vary very slowly, the program should generate coarse elements in order to avoid unnecessary computational effort.

A number of different element formulations are available for the analysis of tubular joints. These may be categorised as follows

1. Facet shell/plate elements
2. Thin-shell elements
3. Thin/thick shell elements
4. Three dimensional elements

The choice of an element for a tubular joint analysis, depends on the geometry of the joint and the purpose for which the results of the joint analysis are to be used. Early FE work utilised the Facet shell/plate elements because of their simplicity. However, these type of elements introduce geometrical errors, and in addition the coupling which exists in shells between membrane forces and bending moments is not reproduced in these formulations at the element level. For these reasons the more advanced curved elements are preferred in shell analysis.

The curved shell elements may be thin-shells or thick-shells, the distinction being that for thin-shells it is assumed that the through thickness normals in the undeformed shell remain straight and normal to top and bottom surfaces in the deformed shell. However, in thick-shells, the through-thickness normals may take an angular deflection with respect to the top and bottom surfaces, thus permitting shear deformations. Elements based on this formulation include the Ahmad element [1.10] and the Complex semi loof elements [1.11]. One significant disadvantage in the use of shell elements for the analysis of tubular intersections is that the weld is not modelled and thus the three-dimensional stresses in the joint are lost. This could lead to spurious local bending of the member walls to be induced, particularly in the brace.

The three-dimensional elements give improved modelling in the intersection region and could also be used to model the whole tubular joint. However, the use of three-dimensional elements at a tubular intersection will introduce a sharp notch in the model which in theory could give rise to infinite stresses at the notch tip. The use of a very fine mesh in this region will merely predict unrealistically high SCFs, and to avoid this the stresses should be calculated at some characteristic distance from the intersection which has the additional advantage that this may be chosen to coincide with typical strain gauge positions used in

laboratory tests. The three-dimensional elements are normally used for specific applications such as fracture mechanics studies of small defects at tubular joints. An efficient use of these elements is to combine them in a conforming manner with shell elements which may be used to model the position of tubular section remote from the intersection.

1.4.3 Acrylic models

Acrylic models are made from commercially available cast acrylic tubes. The procedures for obtaining the stress distributions are similar to those for the steel models. As the weld is not modelled, the stresses are extrapolated to the tube intersection line on the external surface. The main advantage of this technique is that as the material is readily available, easy to machine, and has a low Young's modulus it is extremely rapid and cheap to use. This method provides an alternative to the finite element method in the case of complex joints, as the models can be fabricated relatively quickly. The disadvantage of acrylic models, in addition to those noted for steel models are:

1. Acrylic suffers from visco-elastic effects thus readings have to be timed.
2. Strain gauges can be damaged, due to poor heat dissipation of acrylic.

In the review conducted by Irvine [1.12] of the stress analysis methods used in the UKOSRP 1, a steel T joint subjected to axial brace load was used to study the differences between the techniques described above. Figure 1.4. shows the outside surface stress distributions obtained for a saddle position compared with other data. The results show that the closest agreement was achieved between the steel model results (considered the most realistic), and the photoelastic results. This is due to the fact that both techniques model the weldments. The absence of weld in the acrylic model, and the lack of physical thickness in the thin shell finite element analysis, contributed to the differences in stress distributions and SCF values at the critical positions.

1.4.4 Photoelastic method

Three dimensional photoelasticity is an experimental technique for stress and strain analysis. It is particularly useful for joints with complicated geometry and or loading conditions. The technique provides quantitative evidence of highly

stressed areas, and peak stresses at the exterior and interior of the joints. This allows for a complete three-dimensional stress pattern to be determined in the region of the intersection.

The method employs the 'frozen-stress' technique. This is conducted by simply heating the model to its stress annealing temperature, applying a load and then allowing it to cool slowly under load. Once cooled under room temperature the load is removed but the strain pattern is locked in the model. Slices are then dissected from the regions of interest for optical examination.

The most important advantage of photoelasticity is the ability to study the overall stress field. The technique of manufacture allows for the weldment to be modelled. However, this method should be regarded as a complete experimental method in its own right as it involves destruction of test pieces thus making it expensive and only one test can be performed per model. Great care is required during manufacture of the model as well as in the experimental stages.

1.5 Stress distributions at weld toes

It is well known that the fatigue strength of welded joints is significantly affected by the stress concentration at the weld toes. Research is continuing in this area in order to characterise the state of stress that exists in this region. If this stress field could be characterised then fatigue fracture mechanics models could be developed for early crack growth.

Koibuchi *et al* [1.13] studied the effect of weld toe radius on the fatigue life of plate structural steel. The radii were measured and the most frequent values ranged between 0.5-0.7 mm. Much smaller radii however, were also found. The brittle lacquer method was then used to search for the highly stressed parts along the welded line. These parts were then strain gauged. Measurement from the welded toe showed significantly different values compared with those of the plate specimens with side notches. The authors also noted that it is the toe radius ρ and not α the weld angle that governs the stress concentration factor at the weld toe.

Itoh [1.14] showed the effect that weld toe configuration has on the propagation behaviour of cracks greater than 1 mm in depth for welded butt joints in C-Mn-Si steel. The stress concentration factor and its scatter for the as welded bead (mean value = 2.17, standard deviation = 0.40) was decreased to (mean value = 1.61,

standard deviation = 0.24) by toe grinding. The weld toe grinding has clearly achieved a reduction in the SCF and in the scatter of these values. Initial crack growth was found to be rapid and was governed by the influence of the weld toe stresses but the propagation behaviour was unaffected.

Gibstein [1.15] reported the results of a number of tests which were carried out at DnV on tubular welded joints of T, X, Y and K configurations, in an attempt to provide information on the stress conditions near the weld toe and the influence of the weld and its geometry on the distribution of the stress. Gibstein distinguishes the joints by their particular strain distributions. The 'ordinary' weld joints exhibited a notch effect, and therefore a varying strain distribution giving rise to sharp increases in the stress at the locality of the weld toes. This variation in strain is evident between different joints as well as between closely spaced locations along the same weld toe. With the sections designated 'notch free' the stress distribution was linear and extended into the toe region, indicating the absence of discontinuities at the weld toe. These conditions were found to be common at the weld toes on the brace sides of the welds. This possibly explains why fatigue failures do not frequently occur on the brace side of tubular joints. The effect of the notch on the strain distribution at the weld toe for tubular joints was presented as the ratio of stress at the weld toe, divided by stress at the same position which corresponds to a notch free condition. For chord weld toes this ratio was found to range between 1.24 and 1.36.

Dover and Connolly [1.16] adopted a similar approach in assessing the notch effect at the weld toes. Strain gauges were placed in the weld toe regions and linear region of the chord side of the steel models. The weld toe SCF K_W was found to be greater than the extrapolated geometric SCF K_G. K_W values were calculated by subtracting K_G from K (value measured at weld toe). However, if we use the definition of K_W as that given by Gibstein then K_W values fall in a range of 1.33 - 1.59, slightly higher than those reported in Ref. [1.15]. The absence of large variations in both sets of results suggests that the strain gauges were placed too far from the weld toe and would therefore not include the full effect of the notch. It was concluded by the authors that if K_W could be accurately determined then it may be possible to develop models for early fatigue crack growth prediction.

Pappalettere *et al*, [1.17 & 1.18] used cruciform specimens with different weld toe radii and various weld penetration defined as percentage lack of penetration (% LOP). This was complemented with work carried out using finite element models with identical geometries to those of the cruciform specimens. The range of weld toe radii were $0.8 \leq r/t \leq 0.316$ and an LOP 0%, 50% and 100%. Concentration gauges with 0.51 mm grids and 0.79 mm grids were used to measure the strains. An empirical expression was derived showing the variation of the maximum stress indices, $K = \sigma_{local}/\sigma_{nominal}$ as a function of (r/T)

$$K = A(r/T)^b \qquad 1.1$$

A & b are constants.

For the second part of the analysis the finite element method was used to determine the magnitude and positions of SCF and surface stress distribution in fillet welded T plate joints. All the models were generated with constant: r = 1 mm, weld angle 45° and weld leg length 1.5t. The range of wall thicknesses was t = 2 mm to t = 100 mm. Typical surface stress distribution are shown in Figure 1.5.

Lawrence *et al* [1.19] conducted a similar analysis using the FEM. Surface and through thickness stresses were obtained. The position of maximum stress was found to lie in a very small region approximately 0.16 r (r = weld toe = 0.76 mm). The variation in K as a function of t/r is presented

$$K = 1 + \alpha(t/r)^{0.5} \qquad 1.2$$

the constant α represents the macrogeometry and loading condition of the weldment.

1.6 Fatigue design methods

The life of a structure which fails by fatigue, may be divided broadly into three stages, namely (a) crack initiation, (b) crack growth (c) final failure. In traditional design methods no distinction is made between the three stages; crack initiation and subsequent growth are treated as a single process, and member failure has an arbitrary definition such as the appearance of a through-thickness crack. However, a number of different approaches have evolved for design against fatigue failure.

These methods fall within three categories namely the classical S-N approach, the local stress-strain method and the fracture mechanics approach to crack initiation and crack growth. The first two approaches are primarily associated with initiation studies, although neither method obtains explicit information on initiation of a specific crack size, rather data is obtained on cycles to specimen failure. The fracture mechanics approach seeks to address both initiation and crack propagation in a specimen. Information on initiation is obtained in terms of number of cycles to initiate a crack of a given size. Crack propagation studies deals exclusively with propagation of pre-existing cracks.

A large data base exists for welded structures but it can only be used for traditional S-N curve fatigue design methods. These methods are likely to continue to be used as primary design tools. However, a number of research programmes are now actively seeking fracture mechanics modelling of early as well as established crack growth. This could provide a tool for evaluating non-destructive test results assessing structural reliability once cracks are detected in service and determining the feasibility of extending the lives of existing structures beyond their original design lives. A short summary of the different fatigue methodoligies is presented below.

1.6.1 Classical S-N approach

The philosophy of this approach is relatively simple and has changed little since it was first used by Wohler [1.20] in his pioneering studies of metal fatigue in 1860. The material's fatigue properties are characterised in terms of the applied nominal stress, S, and the resulting cycles to failure, N. Testing is often conducted under completely reversed bending or tension thus, S, corresponds to the nominal stress amplitude at zero mean stress. However, the S-N curve is influenced by a number of variables e.g. the effect of loading in terms of bending versus tension loading, specimen size and geometry, environment and localised residual stresses. All of these variables are incorporated in the fatigue analysis using empirically based correction factors.

The principal characteristics of the S-N curve, are that a decrease in the applied stress amplitude results in an increase in the number of cycles to failure, and a gradual reduction in the applied stress amplitude can establish the existance or otherwise of a fatigue limit.

The main advantages in using this method is that the data is relatively easy to obtain, a large amount of data already exists and the method is simple to apply. However, the S-N method is based on specimen failure and not crack initiation. It does not consider the cyclic hardening/softening of the material, nor does it address the local plasticity effects. It considers the local stress in the region of stress concentration in the component to be $K_t S$, where K_t is the elatic stress concentration factor. Thus, design against fatigue merely involves manipulating K_t and S so that their product is less than either the fatigue limit or the desired fatigue life. Therefore, for complex geometries the local stress and strain conditions are unknown at positions of stress concentrations where fatigue crack initiation will inevitably occur, such as the toe of a welded structure.

A typical S-N curve is drawn on a coordinate system where the ordinate describes the stress range and the abscissa describes the number of cycles to failure. Logarithmic scales are conventionally used for both axes. For welded tubular joints it is necessary to define the two parameters that describe the S-N curve, stress range and failure criterion, prior to analysis of data.

The stress range is referred to as the 'hot spot stress' range and is defined as the maximum stress obtained by a linear extrapolation to the weld toe of the maximum stress distribution near the weld toe but far enough away from it not to be influenced by the 'notch' stress. For design purposes regarding as yet unbuilt joints, the empirical parametric equations could be used to determine the hot spot stress for simple types of joints. The failure criterion however, is divided in three stages:

i) N_1 : First discernable surface crack, usually detected from visual inspection or strain gauge monitoring adjacent to the weld toe where the hot spot stress is measured.

ii) N_2 : First through thickness cracking detected by a) visual means b) internally applied air pressure c) strain gauging.

iii) N_3 : End of test defined as a) extensive cracking b) member pull out.

N_1 is liable to considerable error and in service N_1 cracks and laboratory N_1 cracks are considerably different in sizes. N_3 does not normally occur in service. Therefore the relevant life of a joint is defined as N_2 which can be more accurately

measured than either of the two other values and as is shown from existing data the degree of scatter is considerably lower than for N_1 or N_3 values. Also these cracks could be detected and repaired.

1.6.2 Local strain approach

The second of the fatigue methodologies reviewed here is the local strain approach. This is not a technique that has enjoyed widespread use in the fatigue assessment of offshore welded structures. It is primarily concerned with the initiation part of the fatigue life and thus seeks to predict the number of cycles to crack initiation. However, it does not quantify the size of a crack to the end of initiation and the begining of the propagation period, and consequently initiation as a fraction of total life cannot be accurately defined.

The first step in the calculation process is to identify the likely crack initiation locations. For welds typically found in offshore structures, cracks usually initiate at the weld toe. This technique is based on the hypothesis that the fatigue behaviour of a notch e.g. at the weld toe can be approximated by the behaviour of a small plain specimen subjected to the same stress strain history as the notch at the weld toe. Assuming that crack initiation is defined on the same basis for both situations, then the number of cycles to crack initiation in the plain specimen should be equal to the number of cycles to initiate a crack at the weld toe. During these early stages of initiation the notch zone is under high concentration of stress which leads to plastic deformation of the region. The local strain approach accounts for such behaviour and plasticity effects are explicitly treated in this method.

The input data required for this approach are the load and environment histories of the structural component as well as the material fatigue properties. Mechanics analysis is used to relate nominal loadings to stress and strain amplitudes, and mean stresses in the critical region of stress concentration. This information is then used to assess fatigue damage by using the rules for cycle counting and damage accumulation. The material fatigue properties relate to the cycle stress strain as well as the strain life relationships.

1.6.2.1 Sress-strain material behaviour under cyclic loading

Most engineering materials harden or soften [1.21,1.22] to a stable condition under cyclic loading resulting in the need for a stress strain curve that is specific to cyclic loading. These material properties are usually obtained in the uniaxial state of stress by testing unnotched specimens. The test is conducted under constant amplitude controlled strain test, initially rapid softening or hardening occurs and after that an approximately stable stress strain hysteresis loop is formed as shown in Figure 1.6. If loops taken from the tests at several different strain levels are plotted in the same σ - ε coordinates a cyclic stress strain curve is defined by the locus of the loop tips OABC. Figure 1.7 shows cyclic stress strain curves for tension and compression, OABC and OADEF seldom differ significantly.

In many cases it is assumed that all stable hysteresis loop traces follow a unique curve which may be mathematically described by the Ramborg-Osgood equation.

$$\frac{\Delta\varepsilon}{2}=\frac{\Delta\sigma}{2E}+\left(\frac{\Delta\sigma}{2K'}\right)^{1/n'} \qquad 1.3$$

$\Delta\varepsilon$ is the total strain range in plane strain

$\Delta\sigma$ is the total stress range

K' is a material constant

n' is a material constant

For complex load histories, procedures are already established for counting fatigue cycles. Dowling [1.23] has shown that the "rain-flow" method, which counts cycles as closed stress strain hysteresis loops, is most effective for a wide range of variable amplitude histories. The other aspect of damage assessment, namely damage accumulation, is adequately treated using linear damage laws such as the Palmgren-Miner rule [1.24,1.25].

$$D=\Sigma\frac{n_i}{N_i} \qquad 1.4$$

n_i is the number of cycles of a given strain range, and N_i is the number of cycles to failure for the same strain range.

Although such linear damage laws cannot account for load interactions, these effects can be accounted for when generating the cyclic strain life information.

A mechanics analysis is used to establish a relationship between the nominal stress, nominal strain, and the notch stress and notch strain fields. These relationships can either be determined from elastic plastic finite element analysis or from simple engineering approximations such as Neuber's rule [1.26,1.27]. Neuber postulated that for a material which deforms nonlinearly, the theoretical stress concentration factor, K_t is equal to the geometric mean of the actual stress K_σ , and strain concentration, K_ε\ factors. That is,

$$K_t = \sqrt{(K_\sigma K_\varepsilon)} \qquad 1.5$$

K_t is the theoretical stress concentration factor, a constant for a given geometry and loading

K_σ is the stress concentration factor, σ divided by S, not a constant when yielding occurs

$K\varepsilon$ is the strain concentration factor, ε divided by e, not a constant when yielding occurs

An alternative to Neuber's rule is the equivalent strain energy density concept which is based on the assumption that the total strain energy density in the plastic zone ahead of the notch tip is equal to the strain energy density calculated on the basis of the hypothetical elastic stress field which would exist in the absence of plastic yielding. This approach has been shown to provide more accurate estimation of the local strain.

1.6.2.2 Fatigue properties

The fatigue properties are characterised by the ε - N relation obtained from smooth simple laboratory specimens. The most popular is the Manson-Coffin relation [1.28] determined under tension-compression strain control loading. For most engineering metallic materials the ε - N relation can be satisfactorily approximated by the following equation;

$$\frac{\Delta\varepsilon}{2} = \frac{\sigma'_f}{E}(2N_f)^b + \varepsilon'_f(2N_f)^c \qquad 1.6$$

$\Delta\varepsilon$ total strain range

σ'_f	fatigue strength coefficient
ε'_f	fatigue ductility coefficient
E	modulus of elasticity
b	fatigue strength exponent
c	fatigue ductility exponent.

To calculate damage under variable amplitude loading Miner's rule is used, as in the S/N approach.

The major disadvantage of the local strain approach is that it only deals with the crack initiation phase of fatigue life, not total life. A further disadvantage is the complexity of the method as compared with the S-N approach. However, the fact that plasticity effects are dealt with realistically, provides a significant advantage over for example the S-N approach. The disadvantages associated with the complex nature of the method may be overcome by developing the appropriate computer algorithms to perform the analysis. One further advantage is that it does not rquire any testing of large scale components

1.6.3 Fracture mechanics

The design of a structure using the fracture mechanics approach, involves the selection of portions of the structure requiring closer examination, and then the quantification of the behaviour of defects at these locations. For tubular welded joints it is assumed *a Priori* that defects exist. The size of the defect is determined mainly by the inspection method used. Once initial crack size has been assumed, the analysis is concerned with calculating the growth of the crack until failure occurs. The main parameters that determine the onset of fracture are the crack size, the stresses surrounding the crack location, and material toughness.

The fracture mechanics approach, seeks to relate conditions of stress and strain fields in the vicinity of a crack tip to the stress acting on the crack face and the crack depth. Various fracture mechanics parameters have been introduced in this subject, but the one parameter that characterises the stress field at the crack tip is the stress intensity factor K. This parameter can correlate the crack growth and fracture behaviour of materials provided that the crack tip stress field remains predominantly elastic.

All stress systems in the vicinity of a crack tip may be derived from three modes of loading as shown in Figure 1.8. The opening mode (mode I) is considered as the most important, particularly in fatigue. For a crack subjected to loading which causes mode I deformation, the stress components in the vicinity of the crack tip are of the form

$$f = \frac{K_I}{(2\pi r)^{1/2}} g(\theta) \qquad 1.7$$

r and θ (Figure 1.9) are the polar coordinates of the point under consideration, and g is a function of the angular position. From the above equation, for the condition of r = 0 at the crack tip, the stresses in theory become infinite, that is the stress fields become infinite. The strength of the singularity is given by K_I, the stress intensity. Under the assumptions of linear elasticity, valid for fatigue crack growth problems, the stress intensity factor characterises the stress-strain field at the crack tip. In view of this fact Paris *et al* (1.29) proposed a power law relating crack growth rate to the stress intensity factor range, K, caused by a stress cycle:

$$\frac{da}{dN} = c(\Delta K)^m \qquad 1.8$$

where da/dN is the crack extension per load cycle, c and m are material parameters and

$$K = (K_I)_{max} - (K_I)_{min} \qquad 1.9$$

where $(K_I)_{max}$ and $(K_I)_{min}$ are the maximum and minimum stress intensity factors respectively in each load cycle. By integrating equation 1.8 with respect to the variable a, the fatigue propagation life can be determined

$$N_p = \frac{1}{c} \int_{a_i}^{a_f} \frac{da}{c(\Delta K)^m} \qquad 1.10$$

where a_i and a_f are initial and final crack sizes.

In the case of tubular joints, this calculation of N_p depends on developing a stress intensity factor specific for tubular joints, and so far this has not proved to be an easy exercise. This is mainly due to the complex stress distribution produced by

the variation in restraint between brace and chord under applied loading. Thus there is a varying stress distribution through the region where the crack will grow.

In general most of the stresses are due to secondary bending between chord and brace, and therefore one would expect that as the crack grows through the neutral axis, the crack growth rate would decrease in the depth direction. In fact the situation at the welded intersection is very complex and a solution to this problem is not available. However, there is a need for simplified expressions for stress intensity factors for cracks in tubular joints, in order to enable fracture mechanics to be used for the purpose of fatigue design.

The methods which are generally used to calculate stress intensity factors are:

(a) Classical solutions for idealised geometries corrected to represent tubular joints

(b) Numerical methods

(c) Semi-empirical solutions based on experimental data.

1.6.3.1 Classical solutions

A number of solutions exist for cracks in bodies with simple configurations under various loading conditions. These provide the basis from which approximations for stress intensity factor solutions are derived for a crack in a more complex geometric configuration. As an example, for a surface crack in a welded cruciform, the correction factor Y may be expressed as:

$$Y = Y_E Y_S Y_W Y_G Y_K \qquad 1.11$$

where Y_E accounts for the crack shape, for part-through cracks, Y_S is the front free surface correction, Y_W is the finite width correction, Y_G corrects for non-uniform applied stress, and Y_K is the correction factor for the geometrical discontinuity caused by the presence of the adjacent weld.

Using existing published solutions, it is often possible to evaluate the correction factors individually. A number of references e.g.[1.30] are available which show examples of derivations of stress intensity factors for particular cases.

1.6.3.2 Numerical methods

One of the most powerful methods of computing the stress intensity factors for general stress fields, is the weight function method. This method was first proposed by Bueckner [1.31] and Rice [1.32] and the basis of this technique is that it separates the effect of component geometry from that of the imposed loading, since once a weight function has been derived for a particular geometry and loading, the same weight function can be used for other loadings applied to the same geometry.

First a reference stress intensity factor and a crack face opening displacement function for the geometry of interest and any mode of loading, is developed. Using these solutions the weight function can then be derived, and the stress intensity factor K_I calculated for other stress states. One such weight function method, was proposed by Oore-Burns [1.33] for calculation of stress intensity factors SIF for an embedded irregular shaped crack in an infinite body.

Niu-Glinka [1.34] have also derived a weight function for semi-elliptical cracks emanating from the weld toe of T-butt welded joints. Once the weight function has been calculated it is then used to calculate the stress intensity factor using the following equation:

$$K = \int_0^a m(x,a)\sigma(x)dx \qquad 1.12$$

$m(x,a)$ is the weight function, $\sigma(x)$ is the stress distribution in the potential of the crack plane.

Experimental crack growth results can be used to calculate stress intensity factor range from the relationship:

$$K = Y\,\sigma\sqrt{\pi a} \qquad 1.13$$

Y is the stress intensity factor calibration and is dependent on the applied stress. Combining the Paris crack growth law with the above variation in Y can be represented for experimental results as:

$$Y_{exp} = \frac{1}{\Delta\sigma\sqrt{\pi a}}\left(\frac{1}{c}\frac{da}{dn}\right)^{1/m} \qquad 1.14$$

c and m are material constants and ΔK is the range of the stress intensity factor. In this case Y corresponds to an experimental calibration and is termed Y_{exp}.

One advantage in using the fracture mechanics approach, is that it analyses crack growth, and with the improvements in NDT techniques, a better assessment of remaining life of a cracked structure can therefore be made.

Another advantage is the effect of the parameters, which influence the fatigue life, such as environment conditions and plate thickness, which may be assessed individually.

A major disadvantage is the complexity of the method. Detailed information is required e.g. initial flaw size, and material crack growth properties for the analysis. Also this technique requires further development in terms of variable amplitude loading and elasto-plastic analysis.

1.7 Weld profile

1.7.1 Introduction

The weld profile of a tubular connection is recognised as being a significant parameter in the assessment of the fatigue life of a tubular joint. The geometric parameters of the weld i.e. weld angle α and weld toe radius ρ have been shown to influence the through thickness stress distributions for T-butt joints [1.35] and the local stress at the toe of the weld for tubular welded joints[1.36]. Also the research programmes (UKOSRP 1) and the Cohesive Programmes commented on the observation that the fatigue strength gradually decreased as the connection size increased. However, it was argued that the decrease in fatigue strength was related to both the increase in chord wall thickness and to the weld profile, the two factors being interdependent. These initial studies provided the basis for investigating the fatigue behaviour of tubular welded structures where the weld profile is controlled during the fabrication stages. The fatigue testing of these joints would then complement the design S-N curves which already exist. For convenience the size of the node was referenced to the chord wall thickness.

At that time it was appreciated that the scaling up of joint size had implications for the relative sizes of chord wall thickness and weld reinforcement, and there was a possibility that the thickness effect could perhaps be mitigated by modifying the weld profile. This would imply that modifying the weld profile for a single size of joint could produce a different fatigue life. These modifications to the weld procedure in order to enhance the fatigue life are termed Controlled Weld Profile (CWP).

The CWP approach is based on the premise that increasing the weld leg length would cause the stress field near the weld toe (which controls early crack growth) to be effectively moved further away from the brace/chord intersection, and into a region of lower stress which would therefore result in a longer time to crack initiation. Clearly a comprehensive stress analysis study would have to be undertaken to assess the strength of the stress field in the region close to the intersection of the brace and chord, for both standard, and modified weld profiles. In order that this value of stress can be used in assessing fatigue properties of a tubular joint, it must be measured in accordance with United Kingdom Offshore Steels Research Project (UKOSRP I) [1.36] recommendations.

However, the modifications of the weld geometric parameters could influence the local elastic stresses at the toe of the weld as well as the global stresses which arise due to the joint requiring to maintain geometric compatibility between brace and chord under applied loading. These local stresses at weld toes are discussed and will form the basis for comparison with the results of the strain measurements conducted on the steel joints and FE analysis work from this project.

The procedure for fabrication and inspection of welded structures is governed by engineering codes of which the most widely used is the AWS D1.1 [1.4]. For this project two types of weld profile were investigated;

1. The profile manufactured to AWS D1.1-1984 code
2. A modified version of the welding procedure used for AWS D1.1 profile was developed and designated Controlled Weld Profile CWP.

Therefore, this review of the section weld profile is conducted with particular reference to the AWS D1.1 code.

1.7.2 Profile controlled welds

Welded joints that conform to the requirements of the AWS D1.1 are referred to as 'profile controlled' welds. The code specifies a series of idealised sections of full penetration welds for connecting tubular members. The elements of such sections include the profiling stage of the members to be welded, specification of weld leg length, the maximum allowable weld toe undercutting, and the profiling of the weld outer surface. The code also defines methods of reducing or eliminating local stress concentrations where crack-like defects occur at the toe of the weld. This definition specifies that in order for the local stress concentration effect to be reduced then the profile of the weld should in general be concave, and at the weld toes be radiused so that it merges smoothly into the base metal.

Further conditions are stipulated and these are; where the weld is enclosed in an angle of less than 90°, the profile should be shown as entirely concave and where the angle is greater than 90°, a straight profile may connect the concave weld toe. The radiusing of the weld toe is generally taken as half the brace thickness with a minimum value of 10 mm.

The API [1.3] code however, defines specific guidance on weld profile acceptability. A finished weld is now designated as profiled or non-profiled, and these two classes of weld are assigned to considerably different S-N fatigue design curves, designated X and X′ respectively for API code and X_1 and X_2 for the AWS code. It also states that the capping layer should be applied in order that the as welded surface merges smoothly with the adjoining base metal and approximates a concave profile. The clear difference between the S-N fatigue life curves shown in Figure 1.10 appropriate to each type of weld obviously places significant importance on the definition of profile control. Therefore, both API and AWS D1.1 specify tests or treatments to help establish what a 'profile controlled' weld is. These tests are summarised below:

i) Passing the dime test in the as welded condition.

ii) Weld toe grinding - API specifies that the grinding marks should be transverse to the weld axis.

iii) Weld toe hammer peening followed by Magnetic Particle Inspection (MPI). MPI is to be applied to all weldments at connections of non-redundant structures.

However, these elements are currently the subject of a review and possible amendments by both API and AWS. Fracture mechanics solutions are being sought for a number of tubular joint geometries containing various profiles of different standard weld quality. It is hoped that these solutions will provide the basis for these amendments.

In practical terms the achievement or otherwise of profiled welds was demonstrated in the tubular joints manufactured for the UKOSRP I [1.36] and the ECSC [1.37] programmes. These have been manufactured to AWS D1.1 specification.

The tubular joints used in the UKOSRP I programme were manufactured with single-sided full penetration welds. The dime standard was applied in the region of the anticipated hot spot. Deficient profiles were repaired by cutting out and re-welding. Weld toe grinding was not used. Figure 1.11 shows illustrations of idealised boundaries between weld metal and parent plate material as taken from weld penetration drawings. The smaller connections, using fewer weld runs across the weld face, show relatively poor profiling and are seen to be dominated by the geometry of individual weld runs as shown in Figure 1.12. The larger connections require a greater number of weld face runs and this allows the welder to build up better profiles as demonstrated in the profile shown in Figure 1.13.

In practice weld profile is easier to control with an increase in the weld size and number of the weld runs. Weld toe detail, however, still depends on the geometry of the weld toe run, which is often laid down very early in the welding process to establish a base for building up the weld. This feature of weld toe condition is clearly demonstrated in the case of the French tubular joints. Figure 1.14. shows weld profiles with weld toe/base metal intersection exhibiting generally sharp corners with little evidence of weld toe radiusing having been attempted. On the whole the Dutch programme shows more varied standard of toe profiling. Both well radiused, Figure 1.15., and completely sharp cornered profiles, Figure 1.16., are evidence of the varied standard achieved.

1.7.3 Effect of weld profile on fatigue test results

An analysis of the fatigue test results of both the UKOSRP I and ECSC programmes has demonstrated that those joints which feature unsatisfactory weld profiles, as determined by lack of overall concavity and lack of smooth weld toe blending, do not produce significantly different fatigue endurances from those for nominally similar joints with satisfactory weld profiles. This is shown in Figure 1.17. which features the results of the 914 mm chord diameter series of joints where specimens with satisfactory and unsatisfactory weld profiles, as judged from the 'dime tests' (1976) criteria applied to weld/chord intersection, are presented. It is clear that there is no consistent indication that poor toe profiling results in below average fatigue performance. This suggests that for any measurable improvement of fatigue performance a more radical approach to the concept of 'profile controlled' welds needs to be adopted.

Marshall [1.38] suggested such an approach as an alternative to the 'profile control'. This requirement by Marshall called 'profile design' is shown in Figure 1.18. for different positions in the brace to chord connection. Firstly, flat profiles are laid down using a high deposition rate process followed by a definite size fillet at the chord weld toe. The new fillet had to have the following requirements:

i) to be large enough to transfer the position of peak SCF to a lower stress field.

ii) be made using electrodes with good wetting characteristics so as to provide generous toe radii.

iii) limit weld toe angle to approximately 45°.

iv) be hot enough to avoid the formation of hard heat affected zones.

Also a modified and stricter version of the dime test, where the radius of the disc was increased with increasing thickness thus requiring progressively flatter weld toe angles, was also recommended.

The work of deBack and Vaessen [1.39] who studied the effect of weld finishing techniques namely toe grinding and improved profiles on steel tubular T joints, could be considered as meeting the first requirement for Marshall's 'profile design' concept. The two profiles studied were called 'ordinary' and 'improved' profiles. A schematic of both types of profiles are presented in Figure 1.19. A small reduction in the SCNF for the improved weld profile was measured. The

greater extrapolated weld toe SCNF for the ordinary profile, was attributed to the fact that the SCNF are measured closer to the brace wall. The authors concluded that the extra stiffening effect of a larger weld metal and the shifting of the weld toe into a lower stress field contributed to lower SCNF values. This work is further discussed in Section 2.6.

Elliot *et al* [1.40] studied the effect of weld profile geometric parameters on the elastic SCFs at the weld toe using the frozen stress photoelastic technique and the FE method. Two types of weld profile were studied, the quality of each profile was judged against the API standard. The first type conformed to the minimum requirements of API and was considered as an unprofiled weld, whereas the second profile was fabricated with a specific butter and capping bead for the chord side. This was referred to as a controlled profile.

These profiles were produced for K and X joints which were studied under brace axial loading. The photoelastic models gave continuous stress distributions in the walls and the welds. Linear extrapolation of the surface stresses to the weld toe were compatible with the hot spot stress defined in the codes. The controlled weld profile gave a 15% reduction in the shell stress concentration factor at the position of maximum SCF (saddle position). At the crown position the stress gradients were small and no significant difference was observed. Notch stresses showed considerable scatter, and were influenced by the weld toe radius ρ, and the weld angle α. The 2D photoelastic and FE models gave surface stresses in weld toe fillets from which the depth of the through thickness notch zone was calculated. The range was 6-8% of the member thickness for a constant toe radius.

Niu and Glinka [1.35] carried out a series of studies on the weld profile effect on stress intensity factors in weldments. The work was based on FE analysis of 2D models of T-butt welded joints of uncracked geometries loaded in bending. The intersection was modelled using a very fine mesh, and a series of ρ and α values. The authors reported that the changes in weld toe radius ρ, mostly affects the stress concentration factor K_t and the stress field in the vicinity of the toe of the weld. The stress field was found to be influenced over a small region, some 2%, of the thickness. The weld angle α however, was found not only to affect K_t but also to greatly influence the stress field. The extent of the influence of α on the through thickness stress field, was about 10% of the thickness. Niu

concluded that the weld toe radius mainly affects the initiation period, whereas the weld angle α, may affect both crack initiation and propagation lives of a structure.

1.8 Scope of this Thesis

The research programmes reviewed in the previous sections provide the basis for the work undertaken in this study. The observations made from these programmes produced two conflicting conclusions as to the significance of the weld profile of tubular joints in terms of the fatigue life assessment of a structure. The two conclusions can be stated as the thickness effect and the weld profile approach.

This study has been conducted to evaluate the extent to which controlling the weld profile would affect the fatigue crack initiation and growth in welded tubular joints. Controlling the weld profile is based on the use of extra weld beads to alter the geometry of the weld profile. It was thought that this approach would result in an enhanced fatigue life.

To assess this possibilty a series of fatigue tests were conducted using out-of-plane bending loading on multi-planar joints. These nodes had a variety of weld profiles giving the desired change in the geometry of the weld profile. Finite element analysis, experimental stress analysis and fatigue crack monitoring was conducted to assisst in the interpretation of the fatigue data.

The total fatigue life of the tubular joints is calculated based on two predictive techniques, local strain approach and fracture mechanics. A fracture mechanics model is presented in conjunction with moment release models. The results are validated against the experimental data from this study and the effect of controlling the weld profile on the fatigue life of the tubular joints is considered.

1.9 References

1.1 Background to new fatigue guidance notes for steel welded joints in offshore structures, D.En HMSO 1984.

1.2 Cohesive programme of research and development in the fatigue of Offshore Structures 1983-85, Final report. Editors D.A. Topp and W.D. Dover

1.3 American Petroleum Institute - Recommended practice for planning, design and construction fixed offshore structures, API RP2A 11th edition 1980.

1.4 American Welding Society - Structural Welding code D1.1 - 1984.

1.5 British Standards Institution, code of practice for fixed offshore structures. BS 6235:1982

1.6 Irvine, N.M. Review of stress analysis techniques used in UKOSRPI. *Int. Conf. on Fatigue in Offshore Structural Steels.* Institution of Civil Engineers, London 1981, Paper 6.

1.7 Kuang, J.G., Potvin, A.B., and Leick, R.D., Stress concentration in tubular joints, paper, *Society of Petroleum engineers,* 1977

1.8 Gibstein, M.B., Parametric Stress analysis of T joints, Paper 26 *European Offshore Steels research Seminar.* Cambridge UK 1978

1.9 Wordsworth, A.C., and Smedley, G.P, Stress concentrations at unstiffened tubular joints, *Paper 31 European Offshore Steels Research Seminar,* Cambridge, November 1978.

1.10 Ahmad, S., Irons, B.M. & Zienkiewicz, O.C., Analysis of thick and thin shell structures by curved elements *IJNME 2.* pp 419-451, 1970.

1.11 Irons, B.M. The semiloof shell element. Chapter 11 in Finite elements for thin shells and curved membranes. Edited by D.G. Ashwell and R.H. Gallagher, Wiley 1976.

1.12 Irvine, N.M., Comparison of tubular joint stress analysis methods in the near weld region. *Steel in Marine Structures, Int. Conf.,* Oct 1981, Paris. Commission of the European Communities.

1.13 Koibuchi, K., Ohno, H., Local strain approach to fatigue life prediction of welded structures. *2nd Int. Conf. on Mechanical behaviour of materials*, Boston, USA, August 1976.

1.14 Itoh, Y., Fatigue life prediction for GMA welded butt joints in a C-Mn-Si Steel, *Welding Research Supplement* 51-S, February 1987.

1.15 Gibstein, M., Stress concentrations in tubular joints; Its definition, determination and applications. *Steel in Marine Structures, Int. Conf.*, Oct 1981, Paris. Commission of the European Communities.

1.16 Dover, W.D., Connolly, M.P., Fatigue fracture mechanics assessment of tubular welded Y and K-joints. *Int. Conf. on Fatigue and crack growth in offshore structures*, IMechE 1986.

1.17 Pappalettere, C., Stress concentration factors for cruciform welded joints. *Proc. SEM spring conference on experimental mechanics*, Las Vegas, 1985.

1.18 Atzori, B., Pappalettere, C., Stress concentration factors for cruciform welded joints with lack of penetration *5th ASME Failure Prevention and Reliability Conference*. Dearborn, Mi, 1983

1.19 Lawrence, F.V., HO. N.J., & Mazumdar, F.K., Predicting the fatigue resistance of welds. *Annual review Material Science*, No.11, 1981

1.20 Wohler, A., *Zeitschrift fur Bauwesen*, vol. 10, 1860

1.21 Morrow, J., Cyclic plastic strain energy and fatigue of metals. Internal Friction, Damping and Cyclic Plasticity, *ASTM* STP 378, pp 45-87

1.22 Landgraf, R.W., Cyclic deformation and fracture of hardened steels. *International Conference on Mechanical Behaviour of materials*, Koyoto, Japan 1972

1.23 Dowling, N.E.,Fatigue failure prediction for complicated stress-strain histories. *Journal of Materials, MJLSA*, Vol. 7 No. 1, pp 71-87

1.24 Palmgren, A., Ball and roller bearing engineering. Translated by G.Palmgren and B. Ruley, SKF Industries, Inc. Philadelphia, Pa. pp 82-83., 1945

1.25 Miner, M.A., Cumulative damage in fatigue. *Ins. of Applied Mechanics Trans ASME*, 12 pp 159-164 1945

1.26 Neuber, H., Theory of stress concentrations for shear-strained prismatical bodies with arbitary non-linear stress-strain law. *Transactions ASME Journal of Applied Mechanics*. Vol. 8, December, 1961

1.27 Dowling, N.E., Wilson, W.K., Analysis of notch strain for cyclic loading. *Proceedings of the 5th International Conference on Structural Mechanics in Reactor Technology*

1.28 Wetzel, R.M., (ed). Fatigue Under Complex Loading: Analyses and Experiments, Advances in Engineering, Vol. 6, *Society of Automative Engineers*, Warrendate, Pa. 1979.

1.29 Paris, P.C., and Erdogan, F., A critical analysis of crack propagation law. *J. Basic energy* Vol 85, pp 528, 1963

1.30 Rooke, D.P., *et al.*, Simple methods of determining stress intensity factors. *Engineering Fracture Mechanics*, 14, pp 397-426, 1981

1.31 Beuckner, H.F., *Zietschrift fur Angewandte Mathematik und Mechanik*, Vol. 50, 1970, pp 529-546

1.32 Rice, J.R., *Int. J. Solids Struct.*, Vol. 8, 1972, pp 751-758

1.33 Oore,M., Burns, D.J., Estimation of stress intensity factors for embedded irregular cracks subjected to arbitrary normal stress fields. *Journal of Pressure Vessel Technology, ASME*, Vol. 102, No. 2 1980.

1.34 Niu,X., Glinka, G., Stress intensity factors for semi-elliptical surface cracks in welded joints. *International Journal of Fatigue*, 1988. (To be published).

1.35 Niu, X., Glinka, G., The weld profile effect on stress intensity Factors in Weldments. *Int'l Journal of Fracture*, 1986

1.36 UKOSRPI Final Report, SRD UKAEA, Chesire 1986. To be published.

1.37 Steel in Marine Structures, *International conference October 1981*, Paris France. Commission of the European Communities.

1.38 Marshall, P., *The Houdremont Lecture*. Connections for Welded Tubular Structures, *Proc. 2nd Int. Conf. of Welding of Tubular Structures*. Boston, Mass., July 1984.

1.39 Back, J. de Vaessen, G.H.G. Effect of plate thickness temperature and weld profile on the fatigue and corrosion fatigue behaviour of welded offshore structures, *II ECSC convention,* Delft May 1984.

1.40 Elliot, K.S., Fessler, H., Stresses at weld toes in tubular joints in offshore structures. Final report, *Cohesive programme of research and development into the fatigue of offshore structures* 1985-87. To be published.

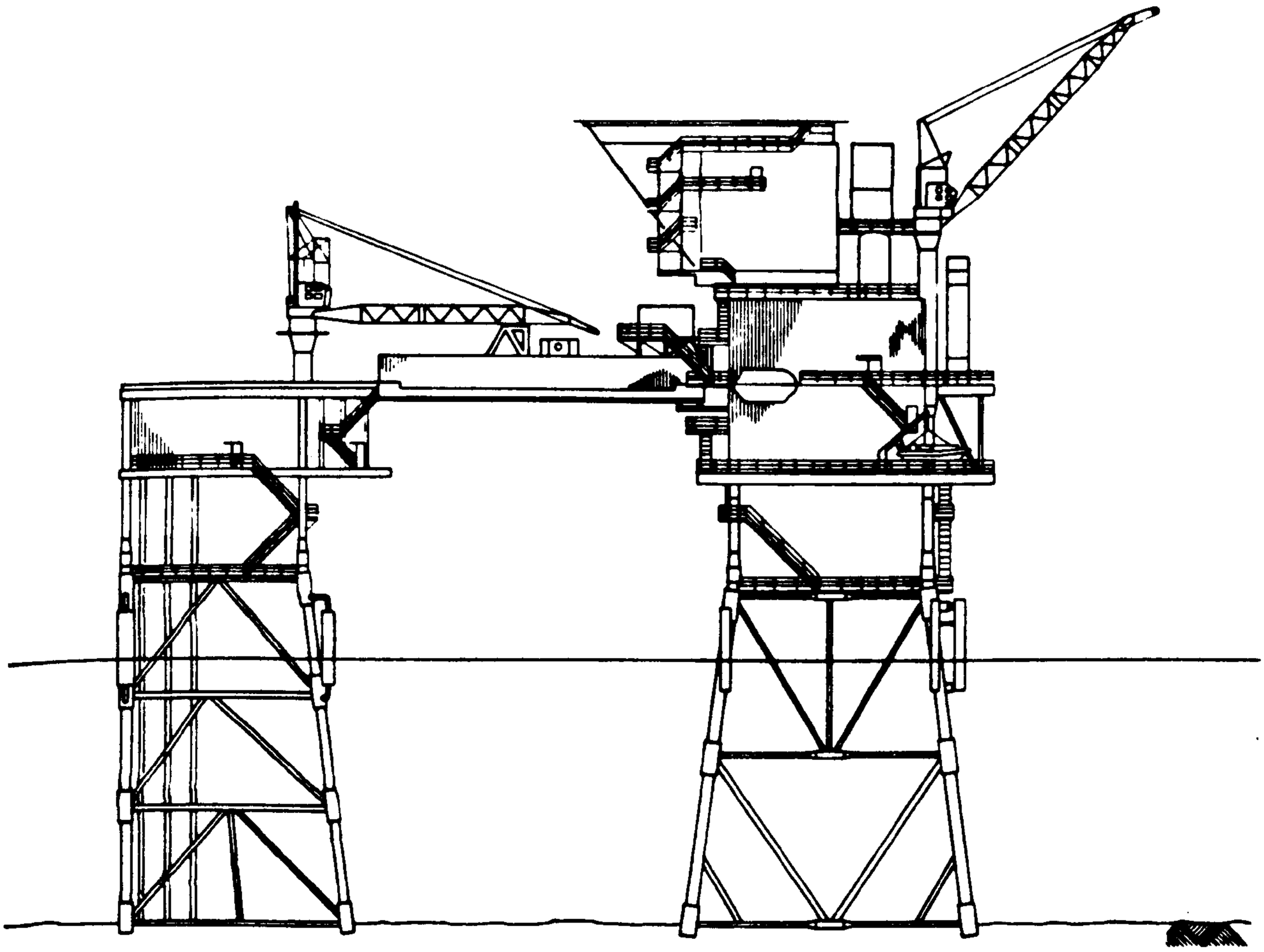

Figure 1.1 Schematic of a steel tubular structure used in offshore oil and gas production

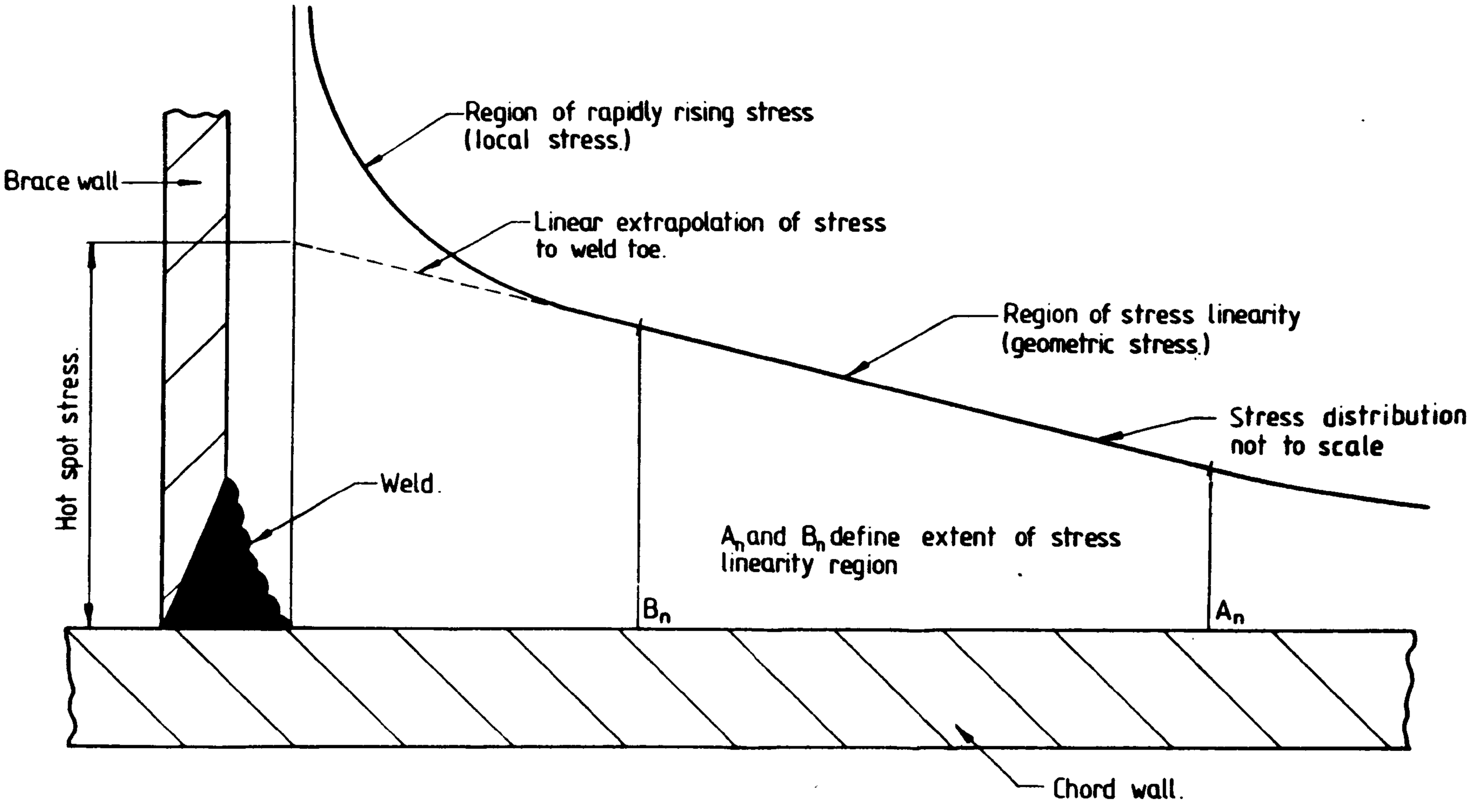

Figure 1.2 Hot spot stress definition given by the Department of Energy Guidance notes

$a = 0.2\sqrt{rt}$, but not smaller than 4mm.

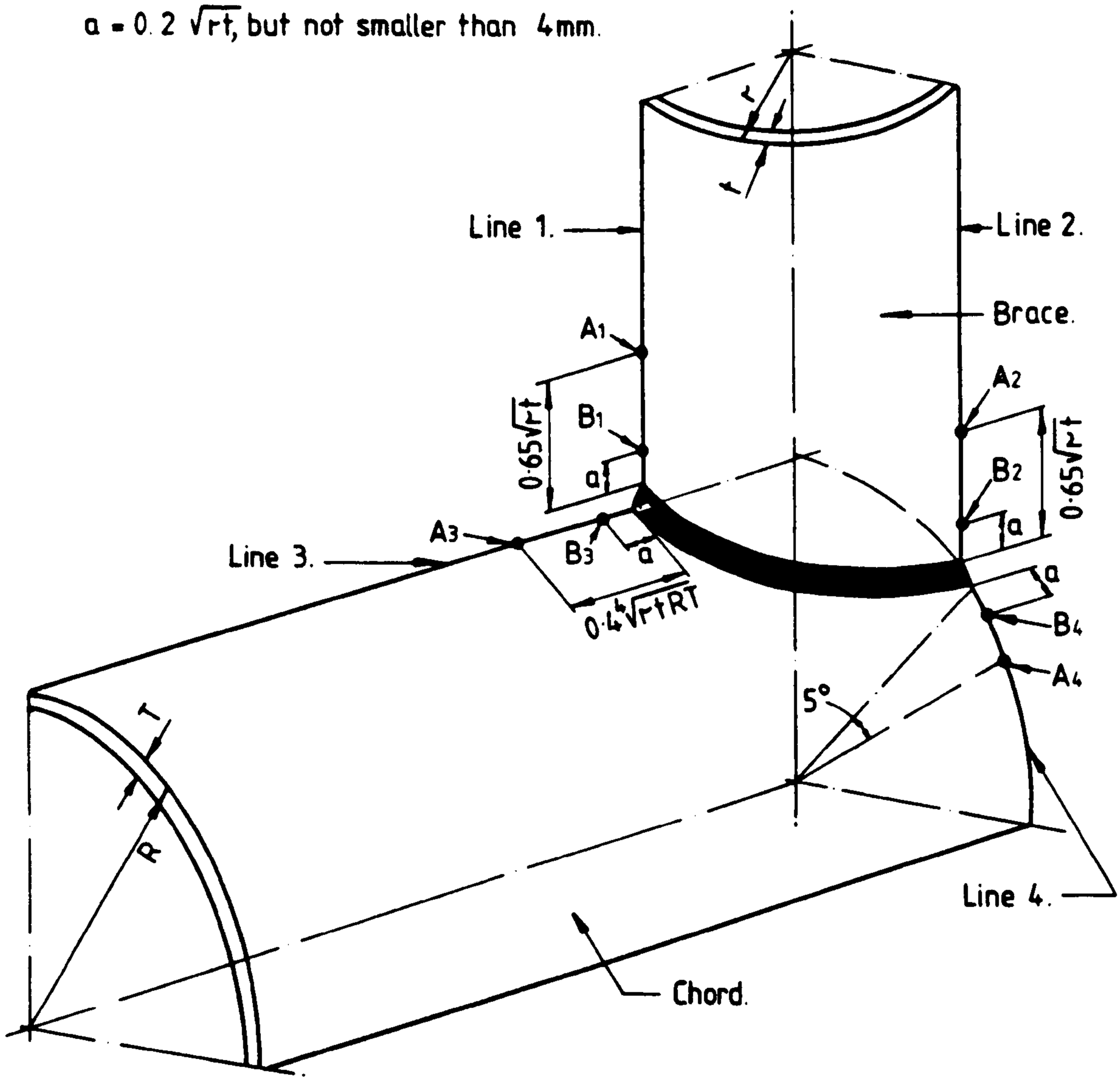

Figure 1.3 Definition of regions of strain linearity for welded tubular T and X joints

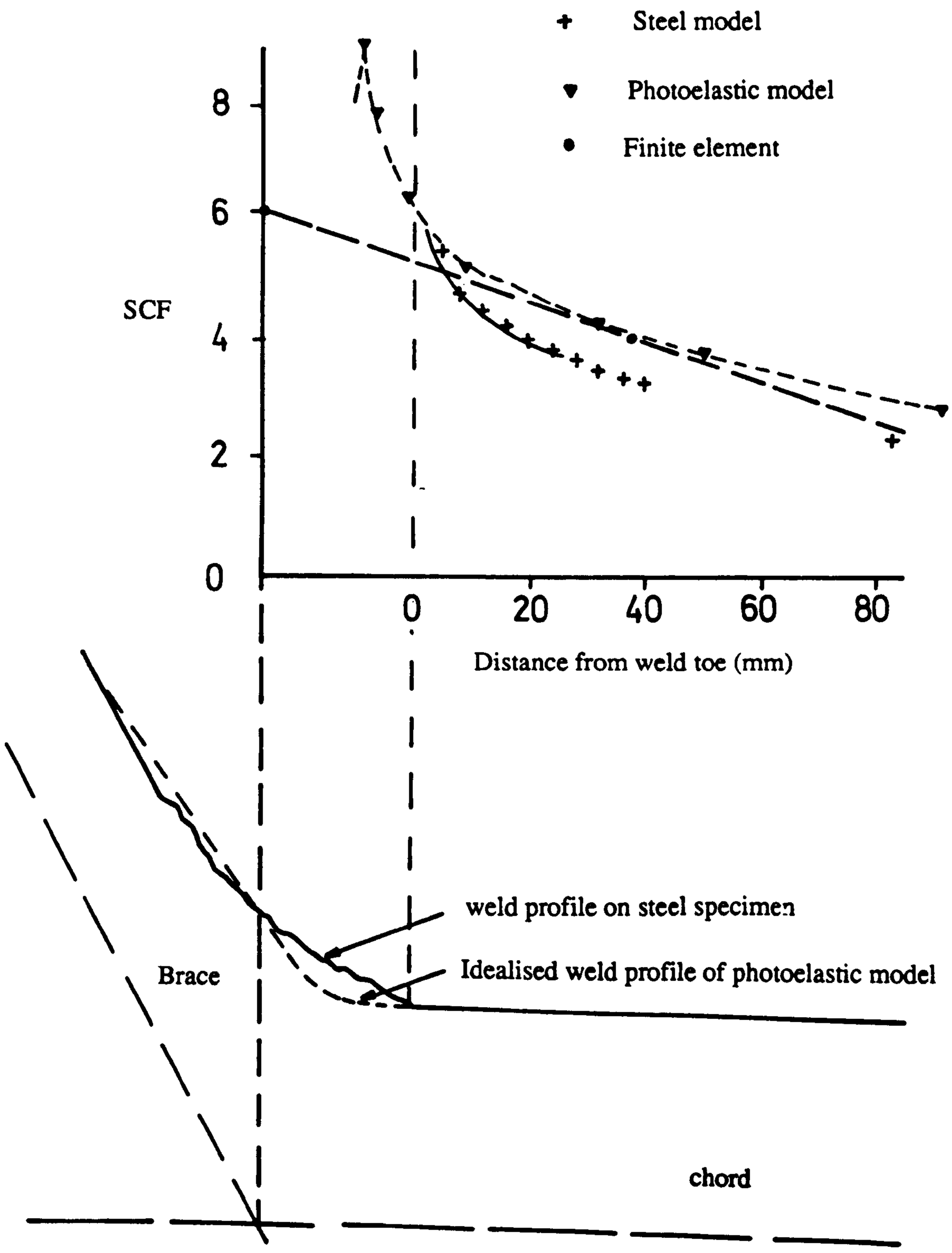

Figure 1.4 Comparison of Tubular joint stress analysis data in the near weld region (Irvine)

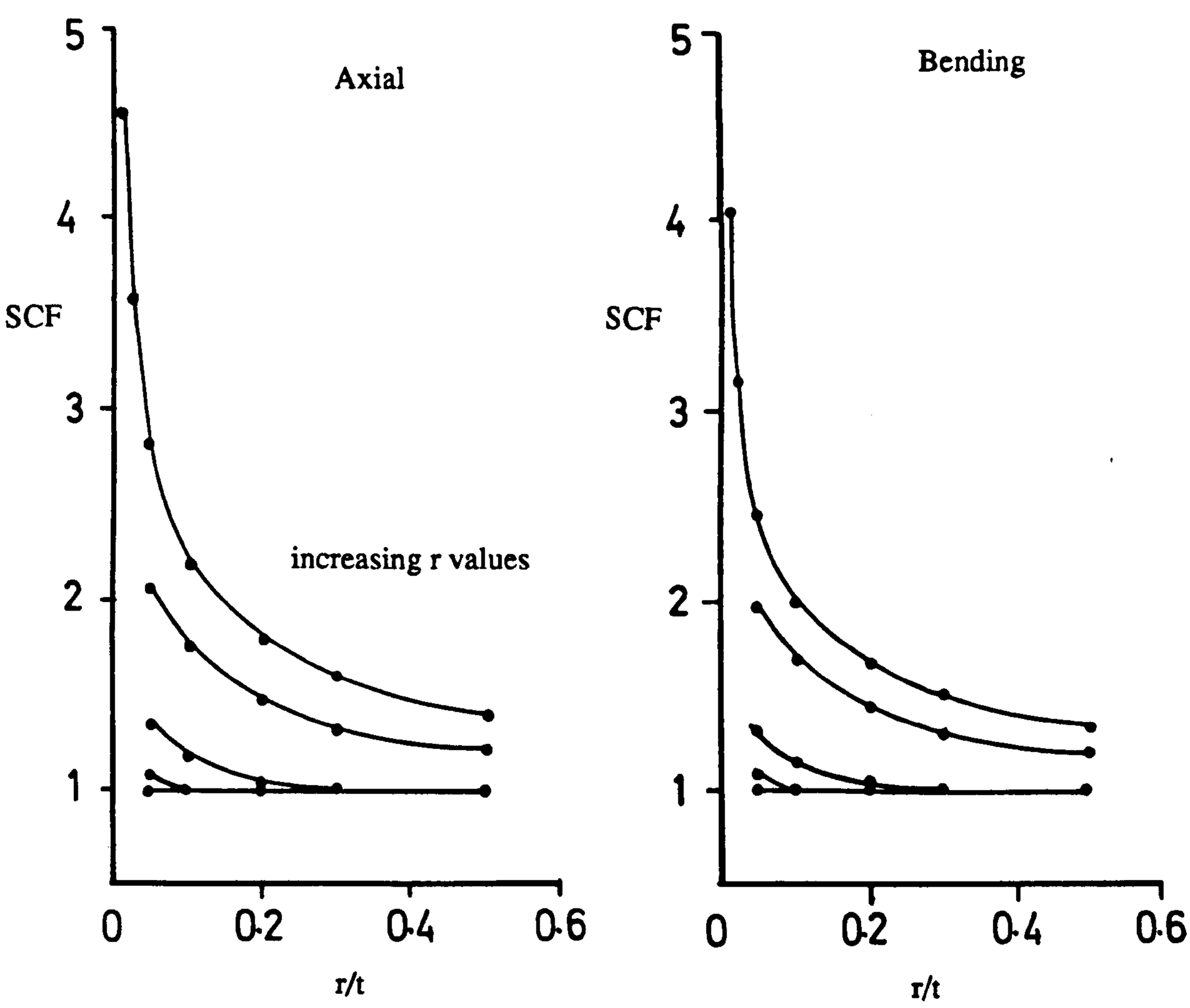

Figure 1.5 Variation in SCF values as a function of r/T (Atzori & Pappalettere 1.18)

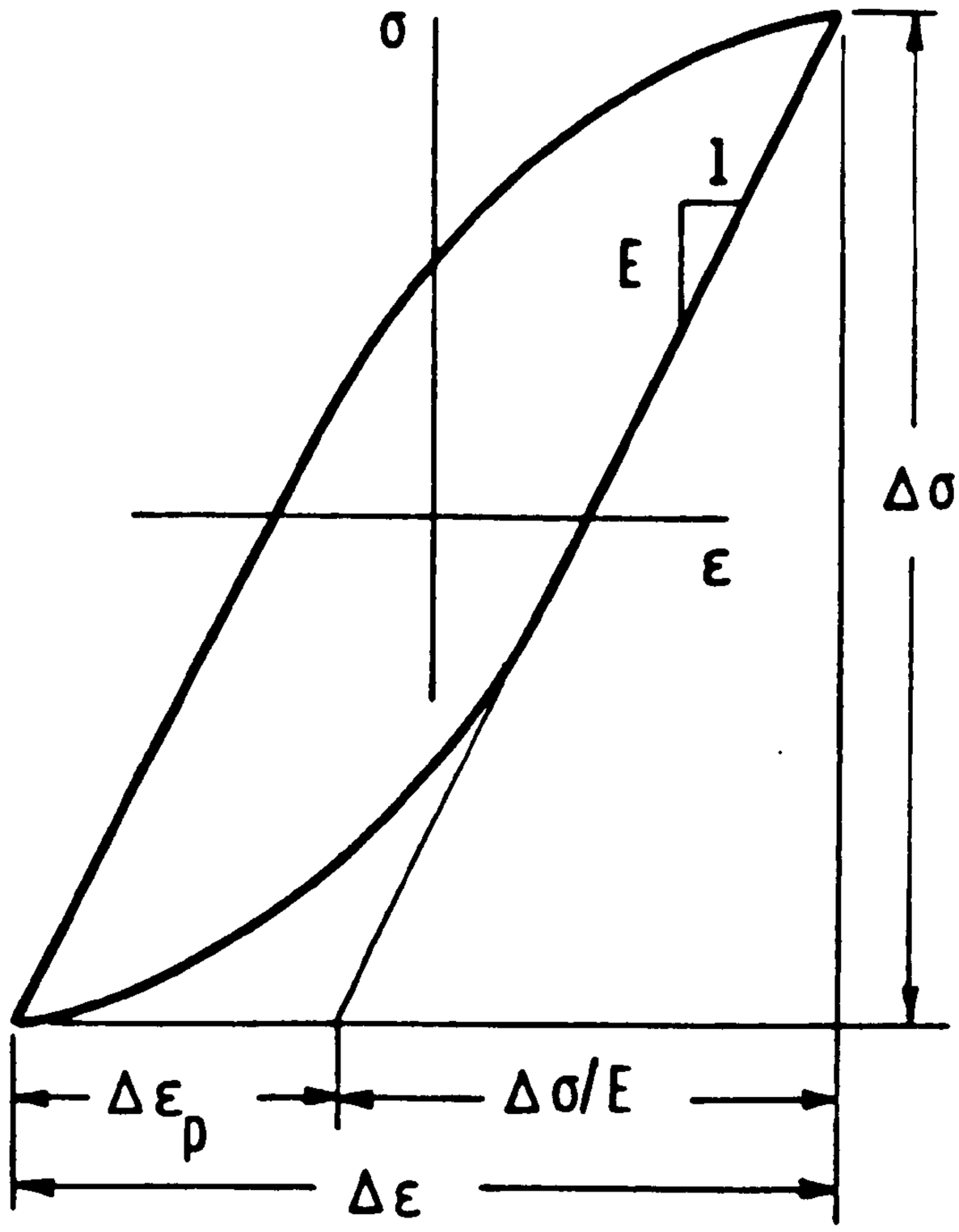

Figure 1.6 Stress-strain closed loop due to reversal cyclic loading

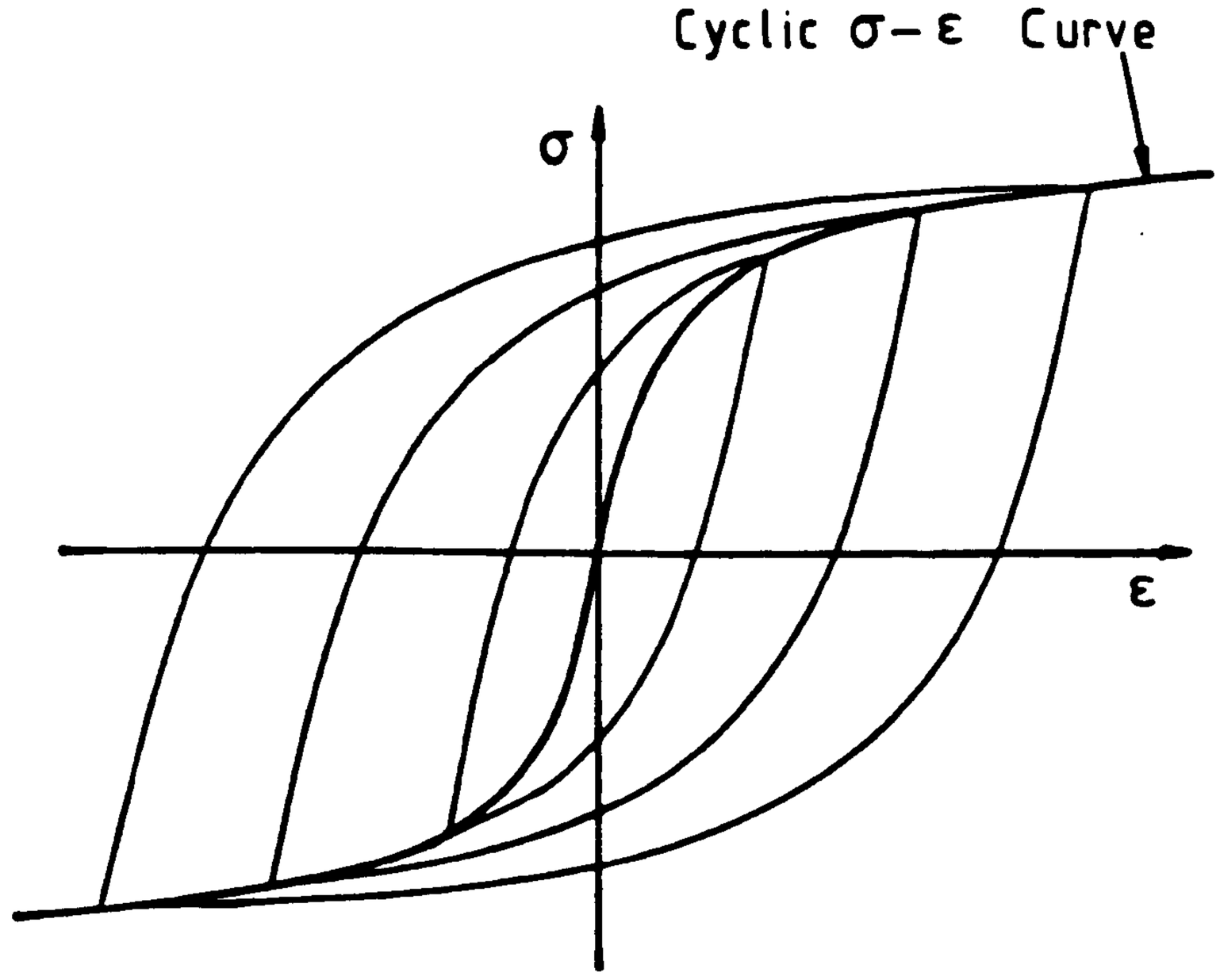

Figure 1.7 Definition of cyclic stress-strain σ - ε relation

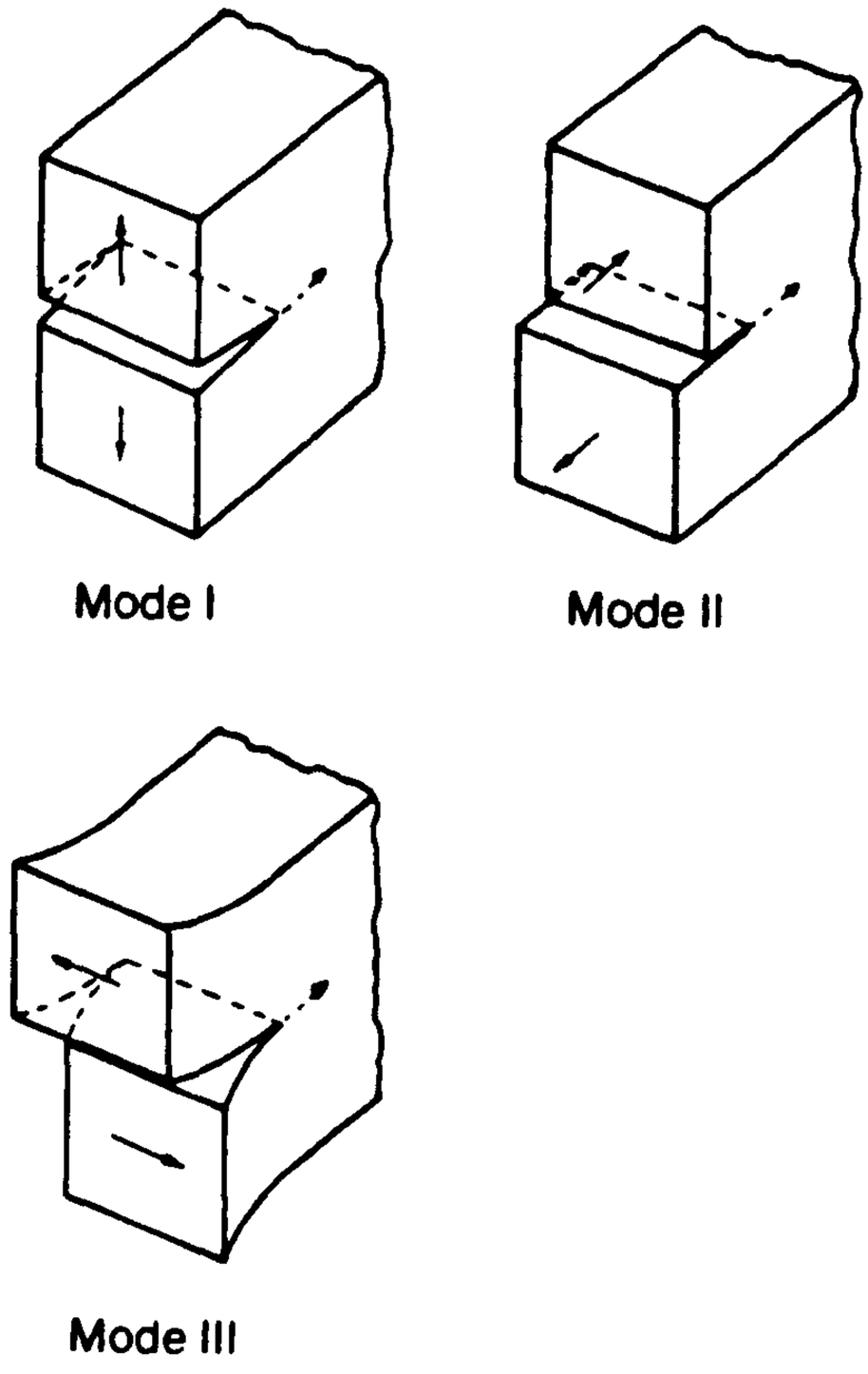

Figure 1.8 The modes of loading. Mode I opening mode. Mode II shear mode. Mode III tearing mode

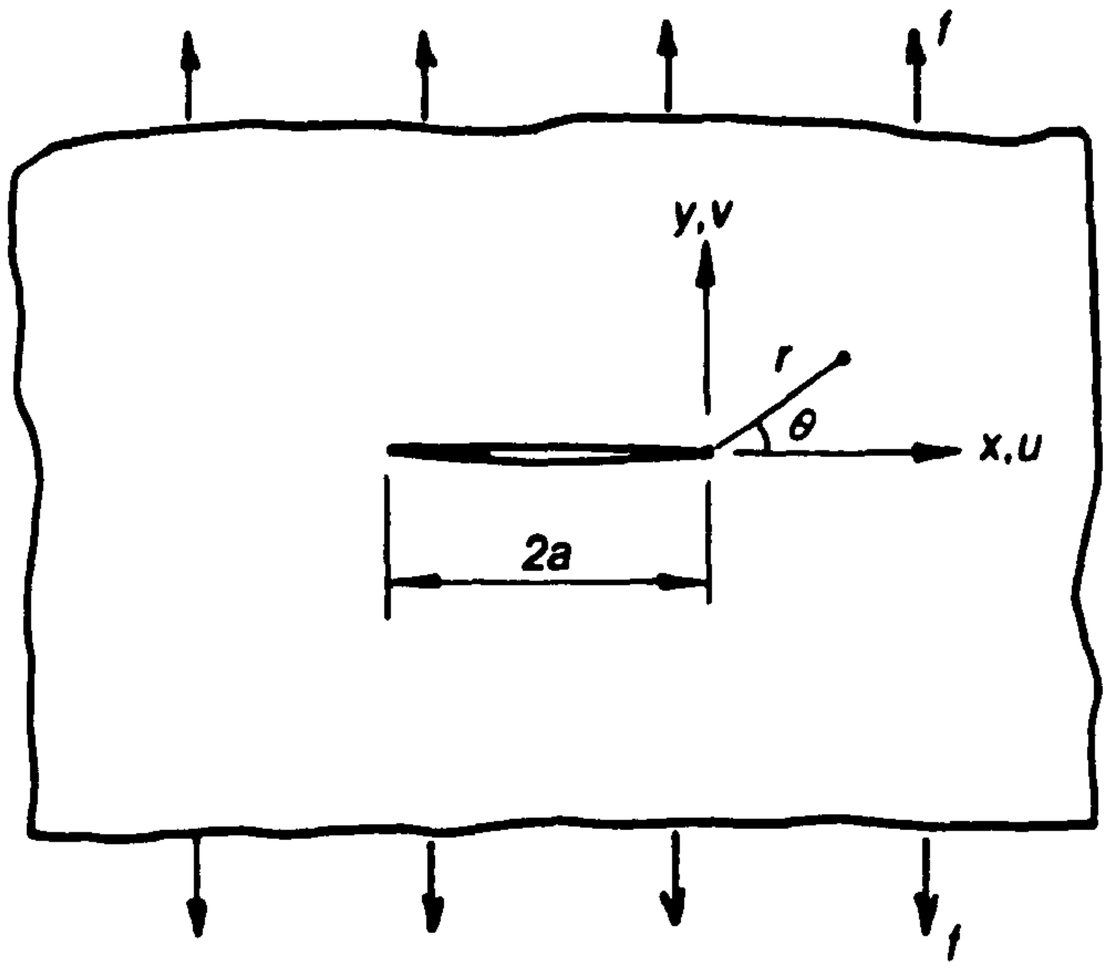

(a) Centre-cracked infinite panel

(b) Edge-cracked semi-infinite panel

Figure 1.9 Typical two dimensional crack problems

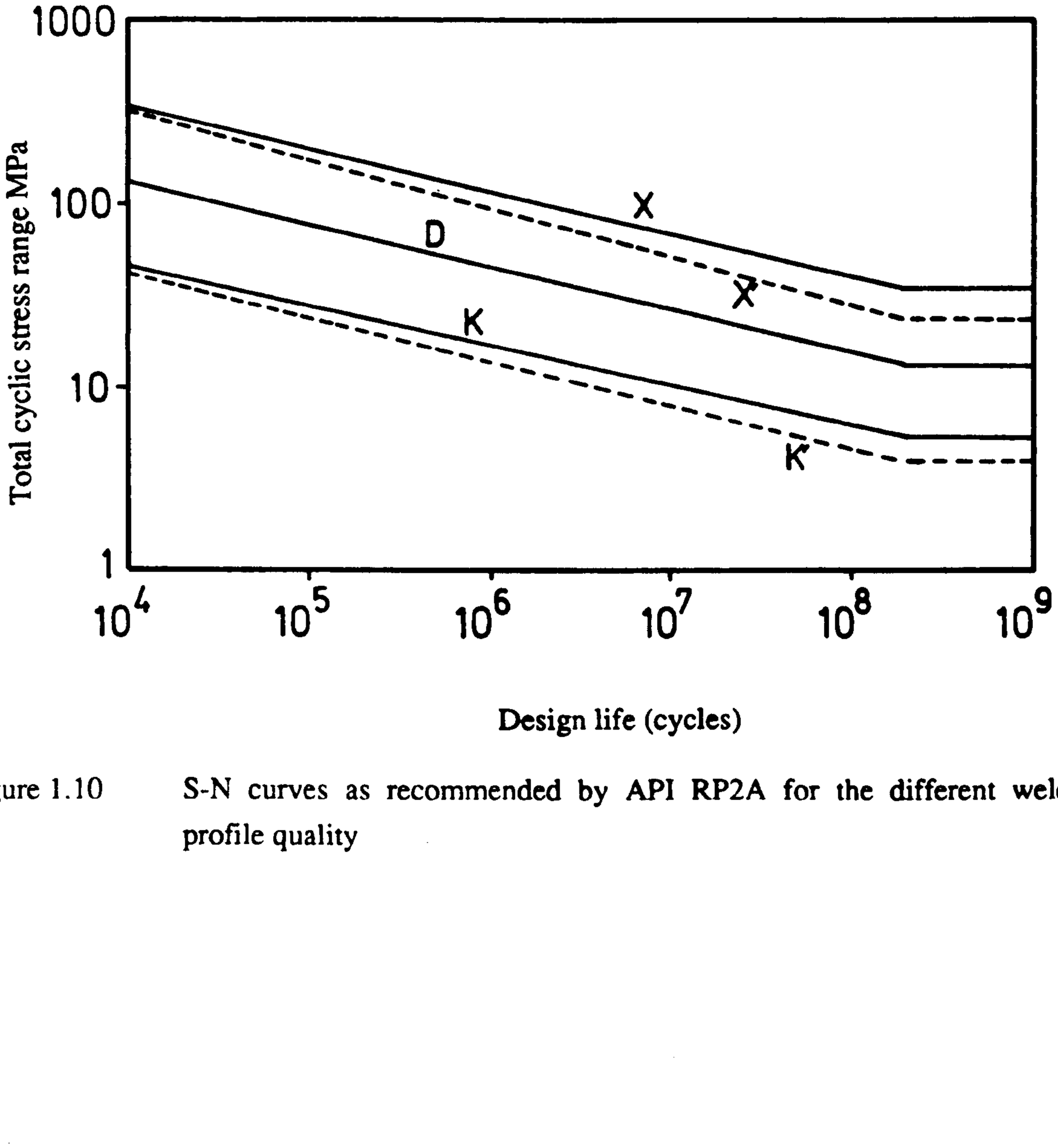

Figure 1.10 S-N curves as recommended by API RP2A for the different weld profile quality

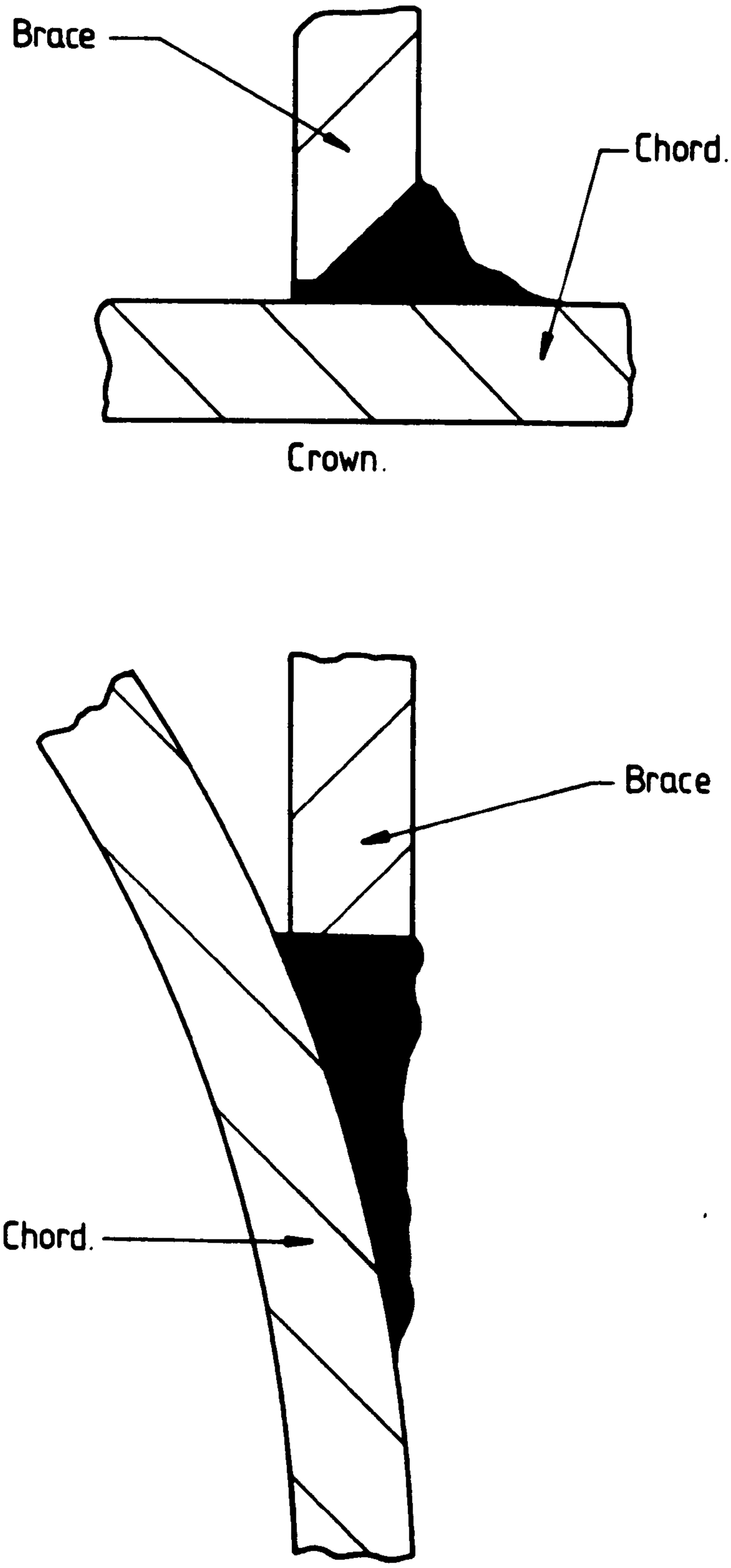

Figure 1.11 Idealised illustration of weld profile for a crown and saddle positions as was used in UKOSRP I

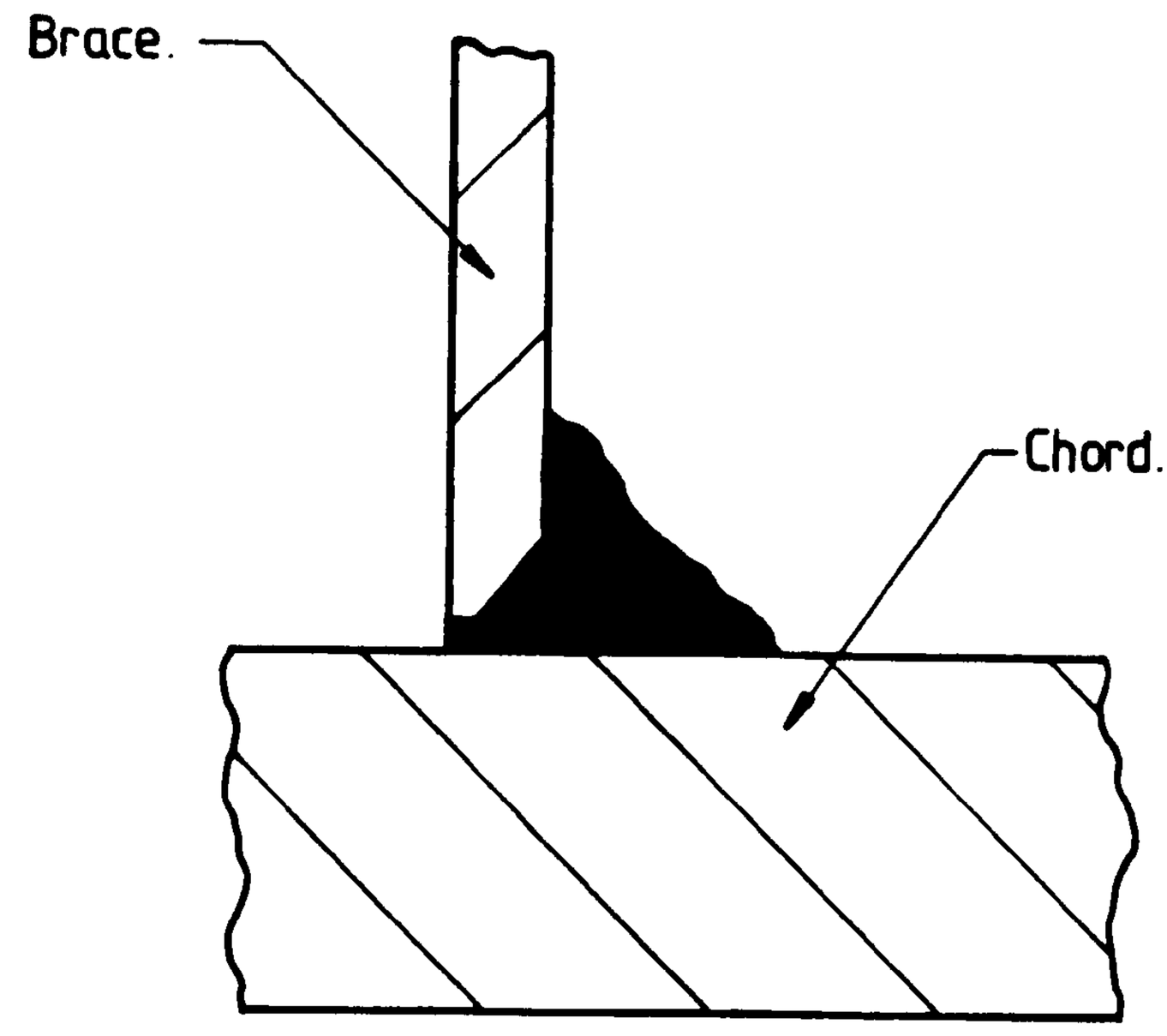

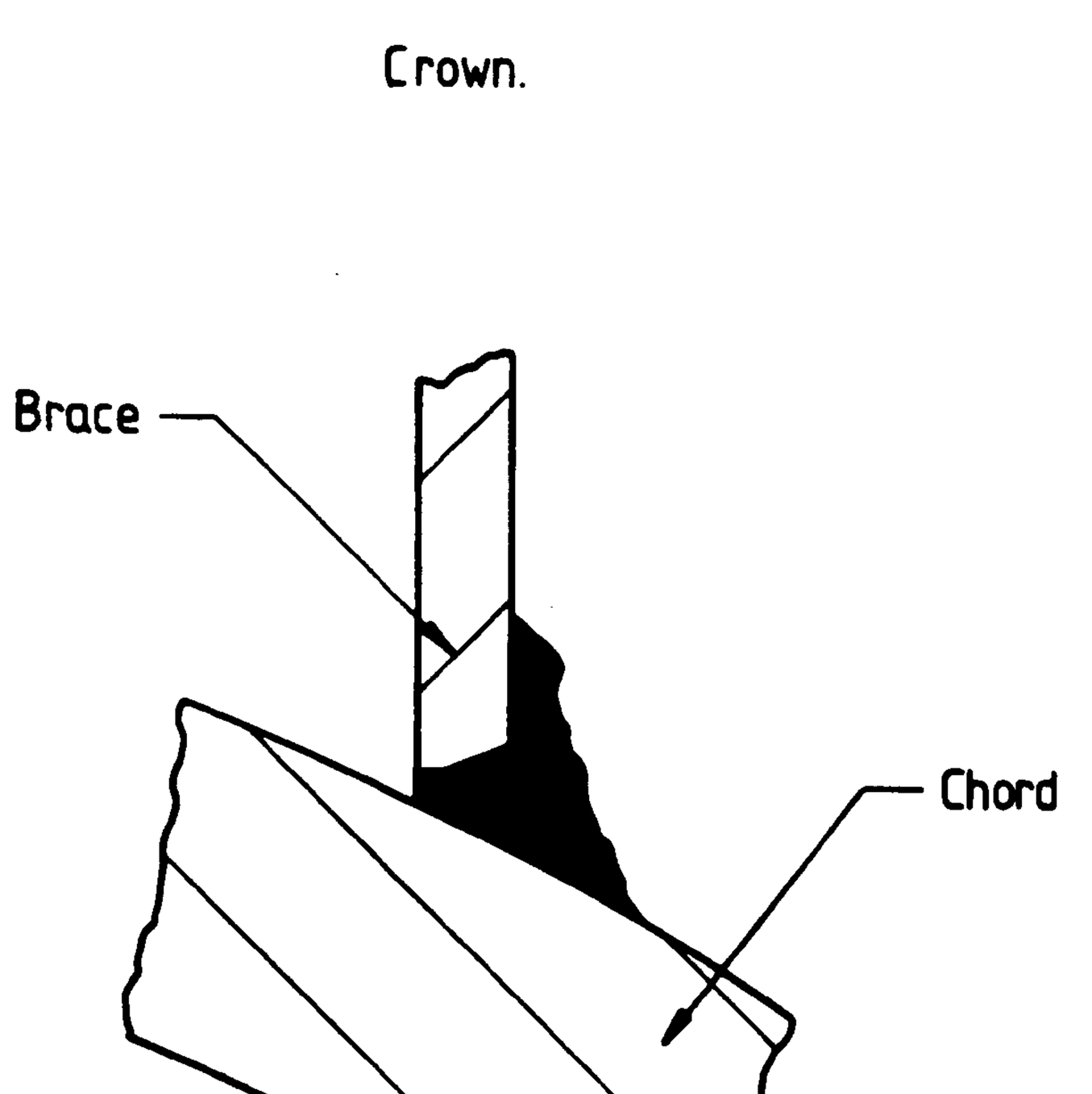

Figure 1.12 Illustration of weld profile where poor profiling is achieved due to the small number of weld runs used

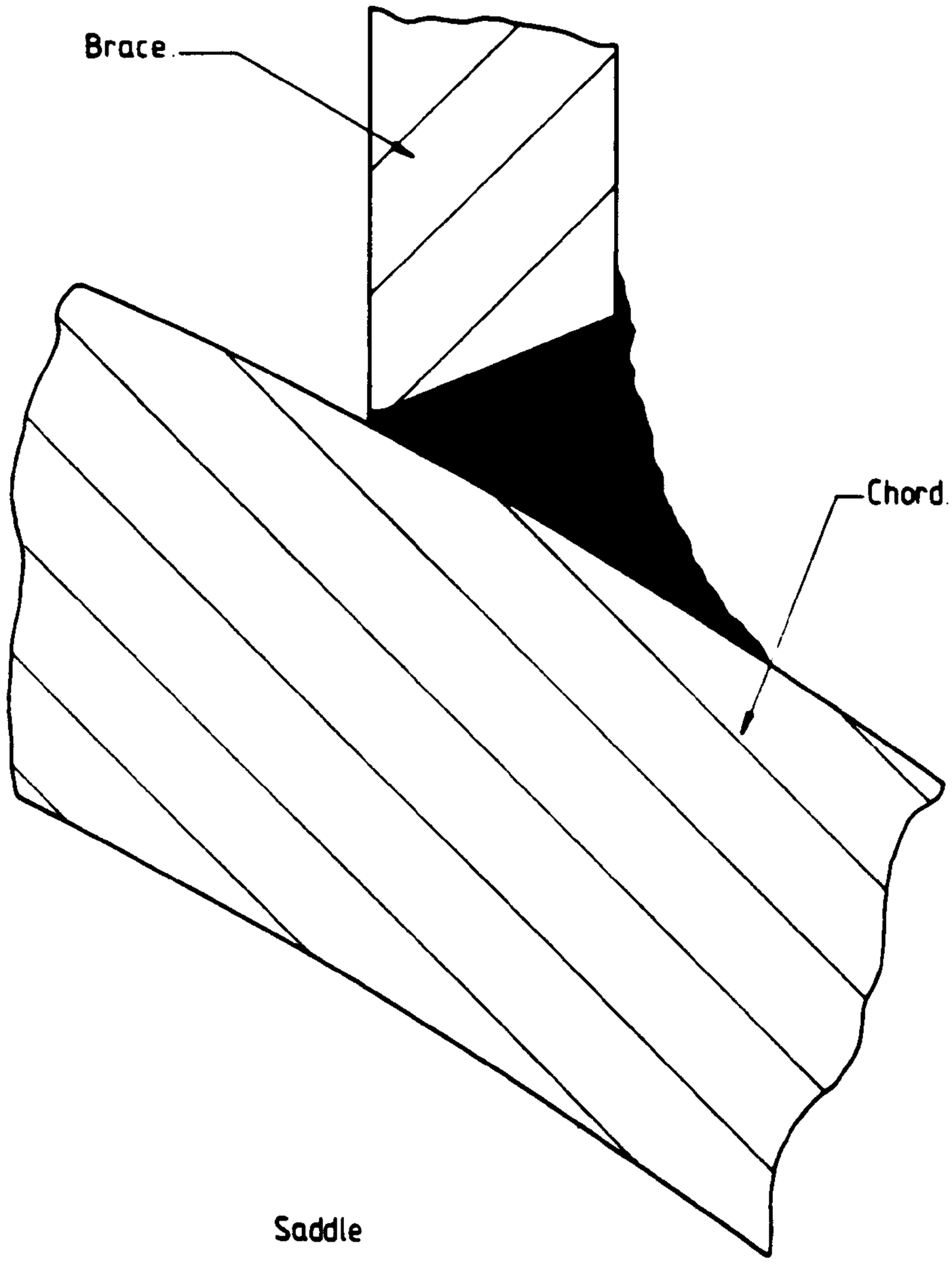

Figure 1.13 Schematic showing an ideal weld profile can be achieved, a minimum of 10-12 weld runs would be needed for such a profile

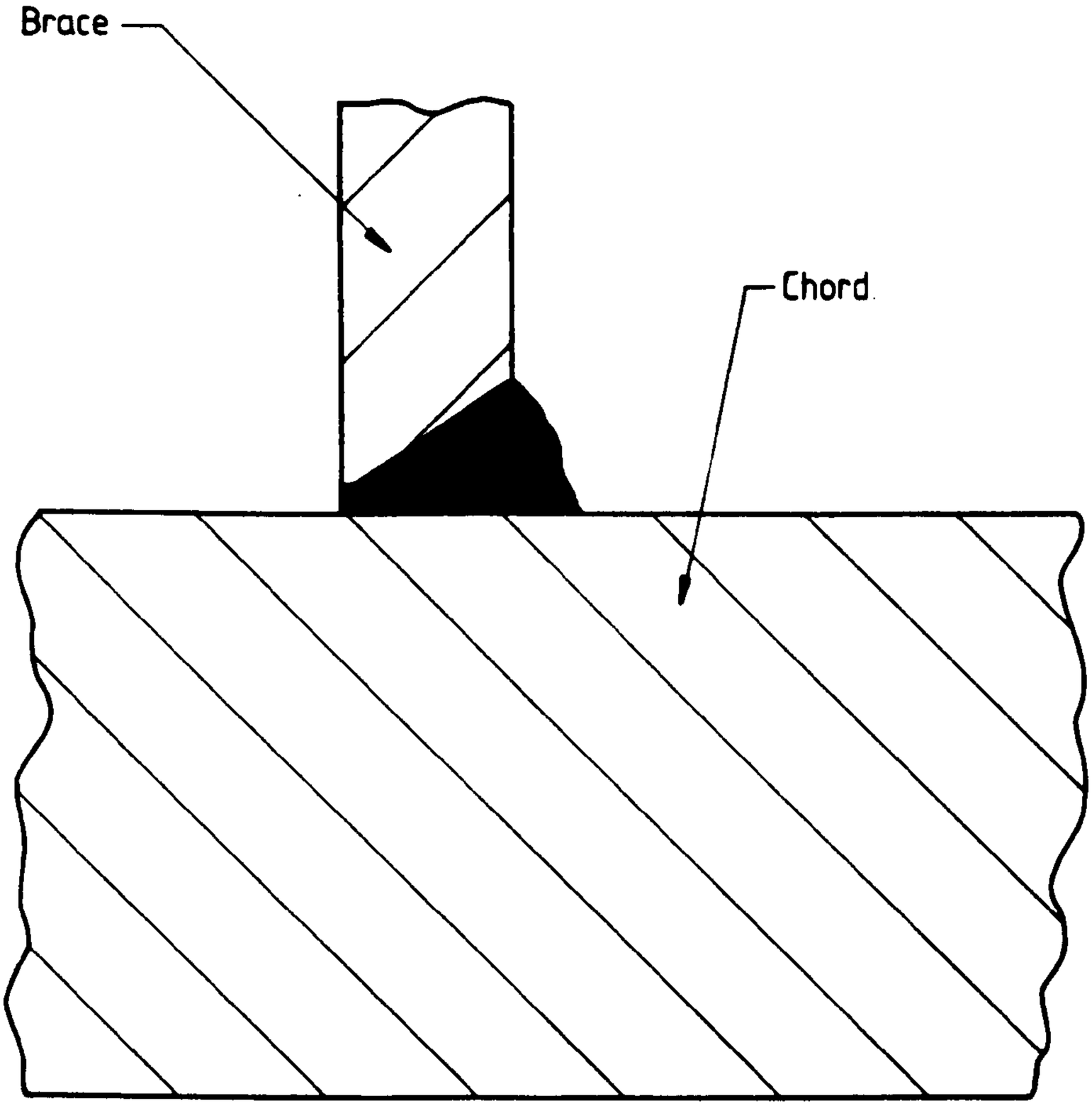

Figure 1.14 Schematic of a sharp weld toe/base metal intersection - French joint

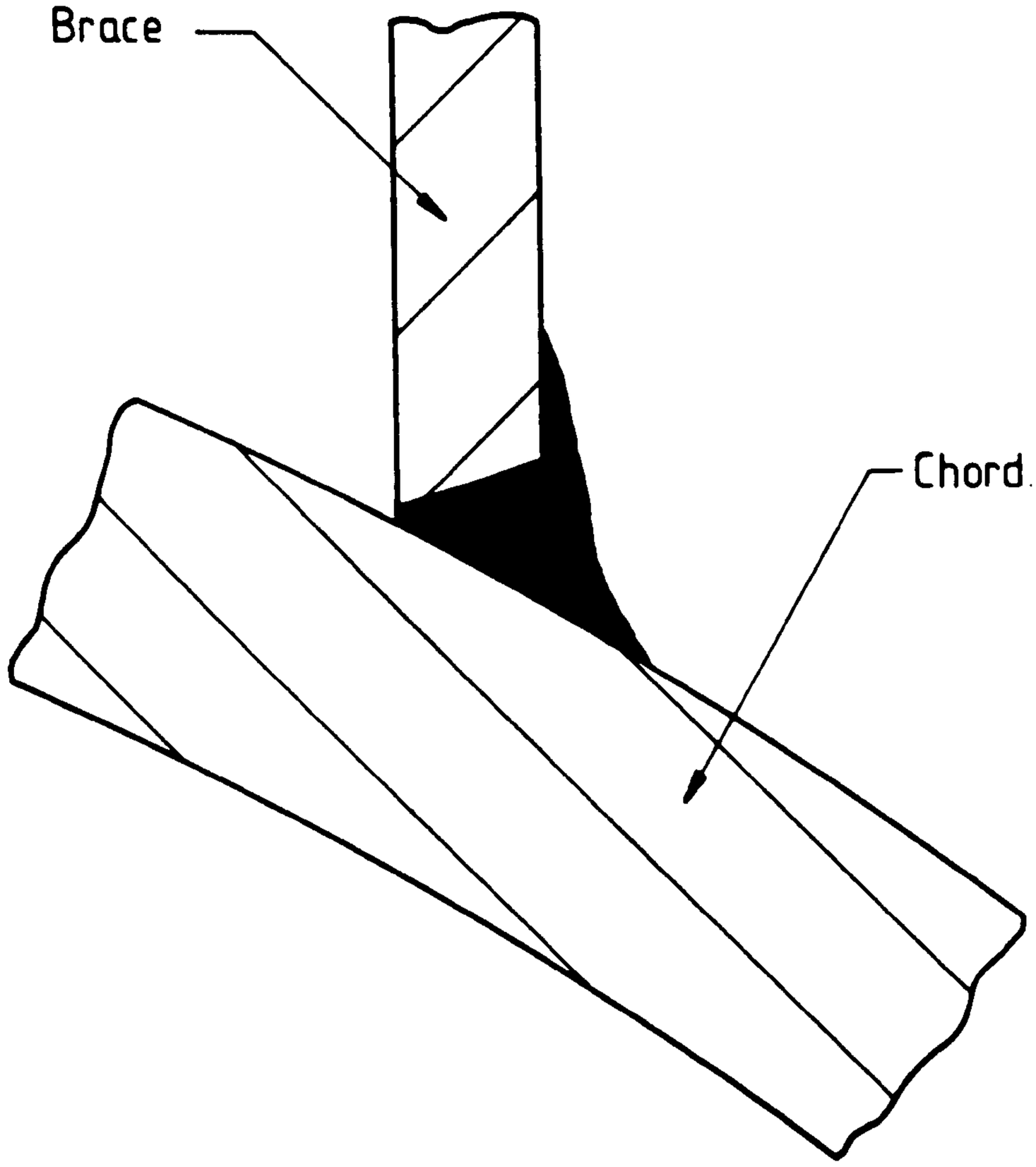

Figure 1.15 Schematic of weld quality achieved in Dutch programme

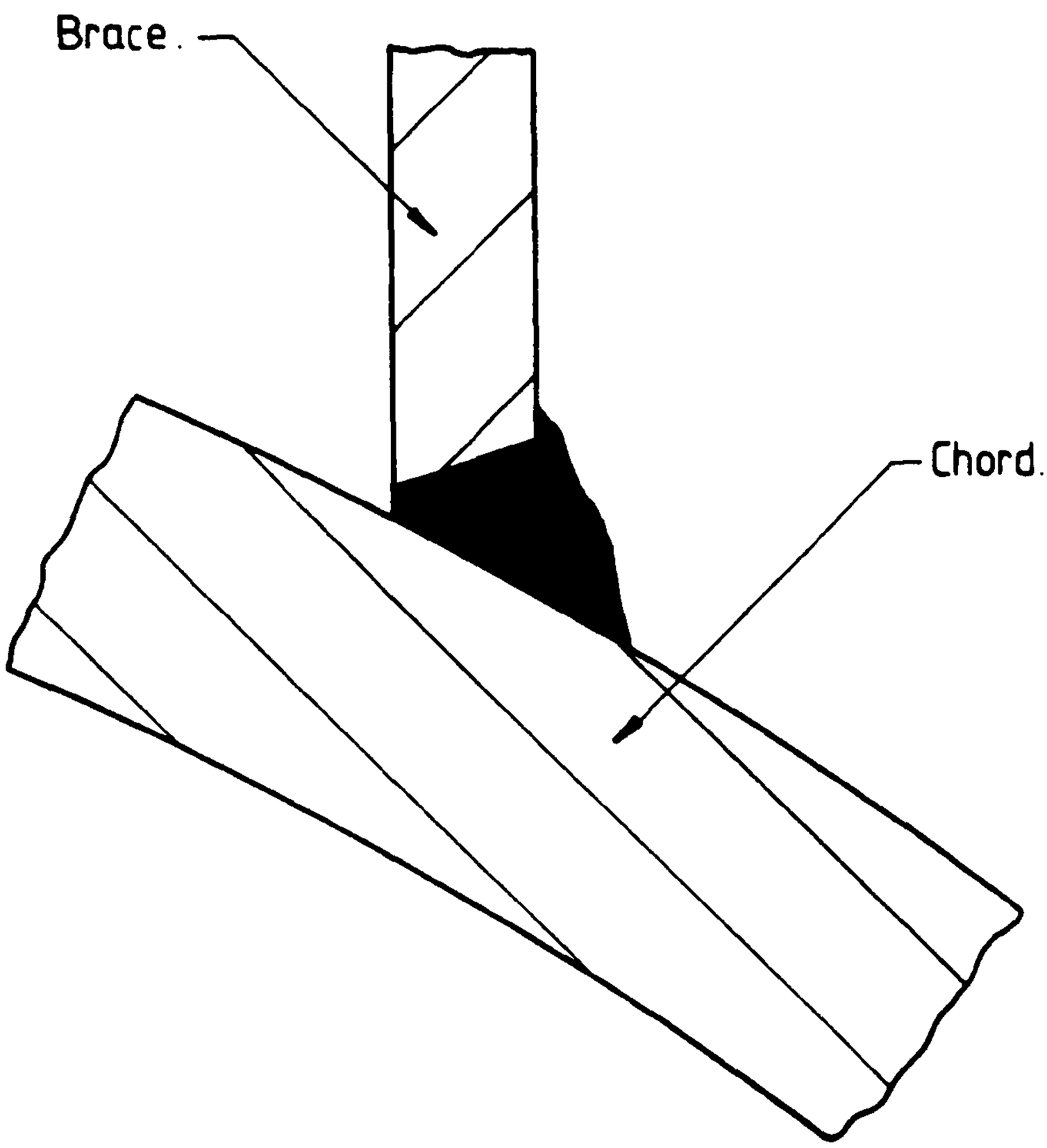

Figure 1.16 Schematic of a sharp weld toe/base metal intersection - Dutch joint (c.f. figure 1.15)

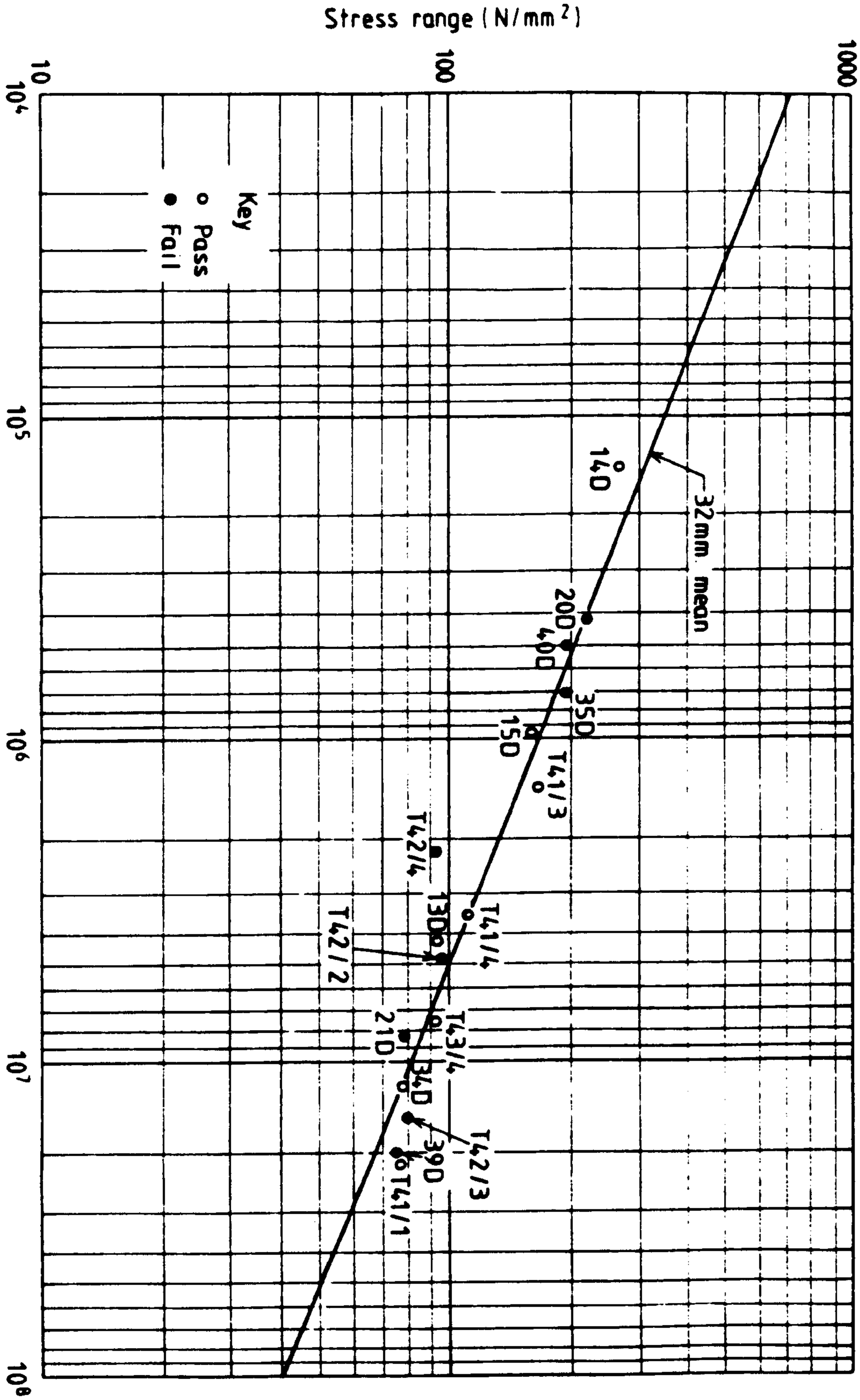

Figure 1.17 Influence of weld toe profile on endurance (N_2 failure)

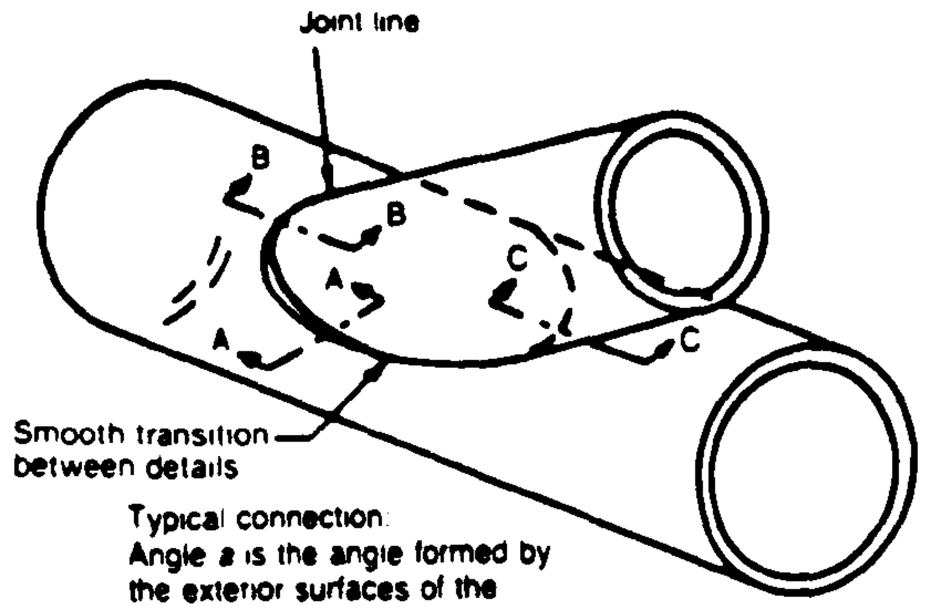

Typical connection.
Angle *a* is the angle formed by the exterior surfaces of the brace and chord at any point on their joint line (local dihedral angle)

Groove angle *b*	Root opening *G* (mm)
Over 90°	0–4.8
45–90°	1.6–4.8
Under 45°	3.2–6.4

Note: Includes tolerance

a	min. *T*
50–135°	1.25*t*
35–50°	1.50*t*
Under 35°	1.75*t*
Over 135°	See sec. B–B

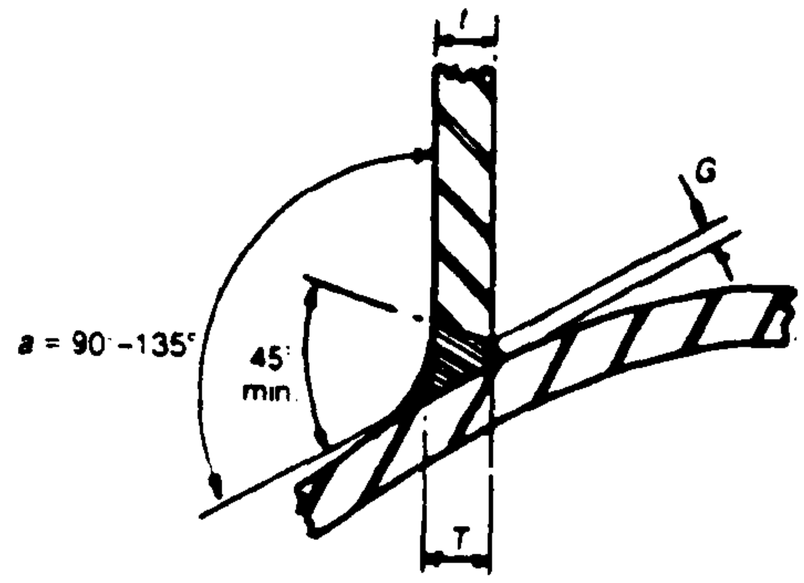

Section A–A

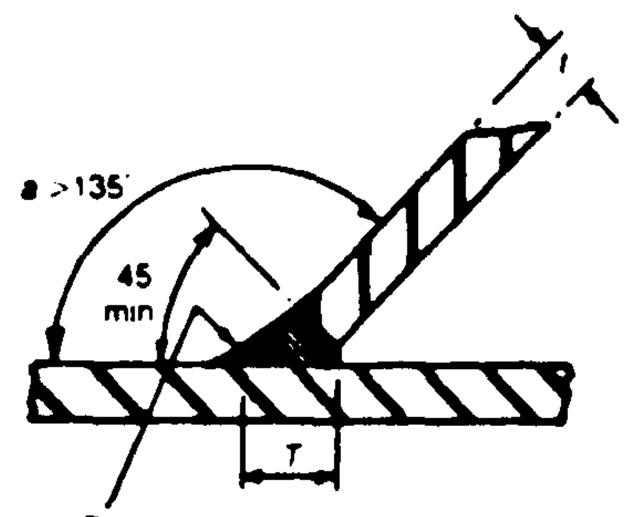

Build out to full thickness except *T* need not exceed 1.75*t*

Section B–B

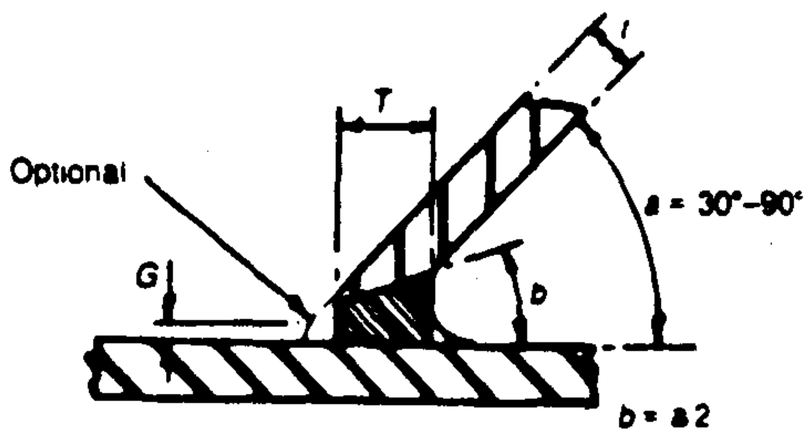

Section C–C

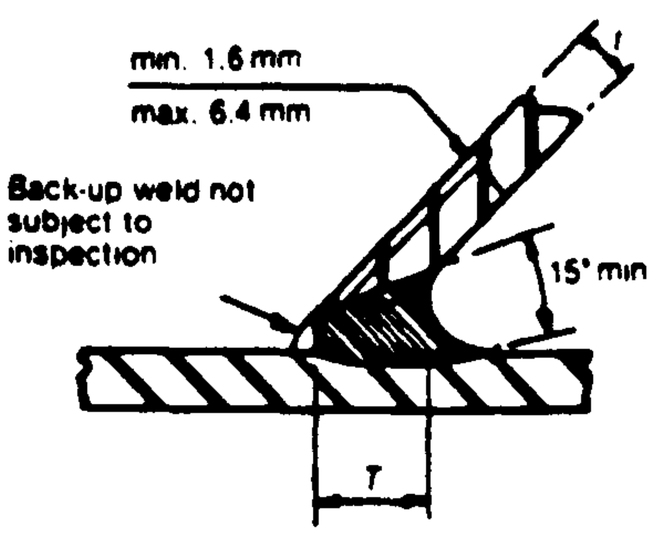

Section C–C (alternate)

Figure 1.18 Proposed AWS standard weld shapes with profile control at different positions in tubular joints (Marshall 138)

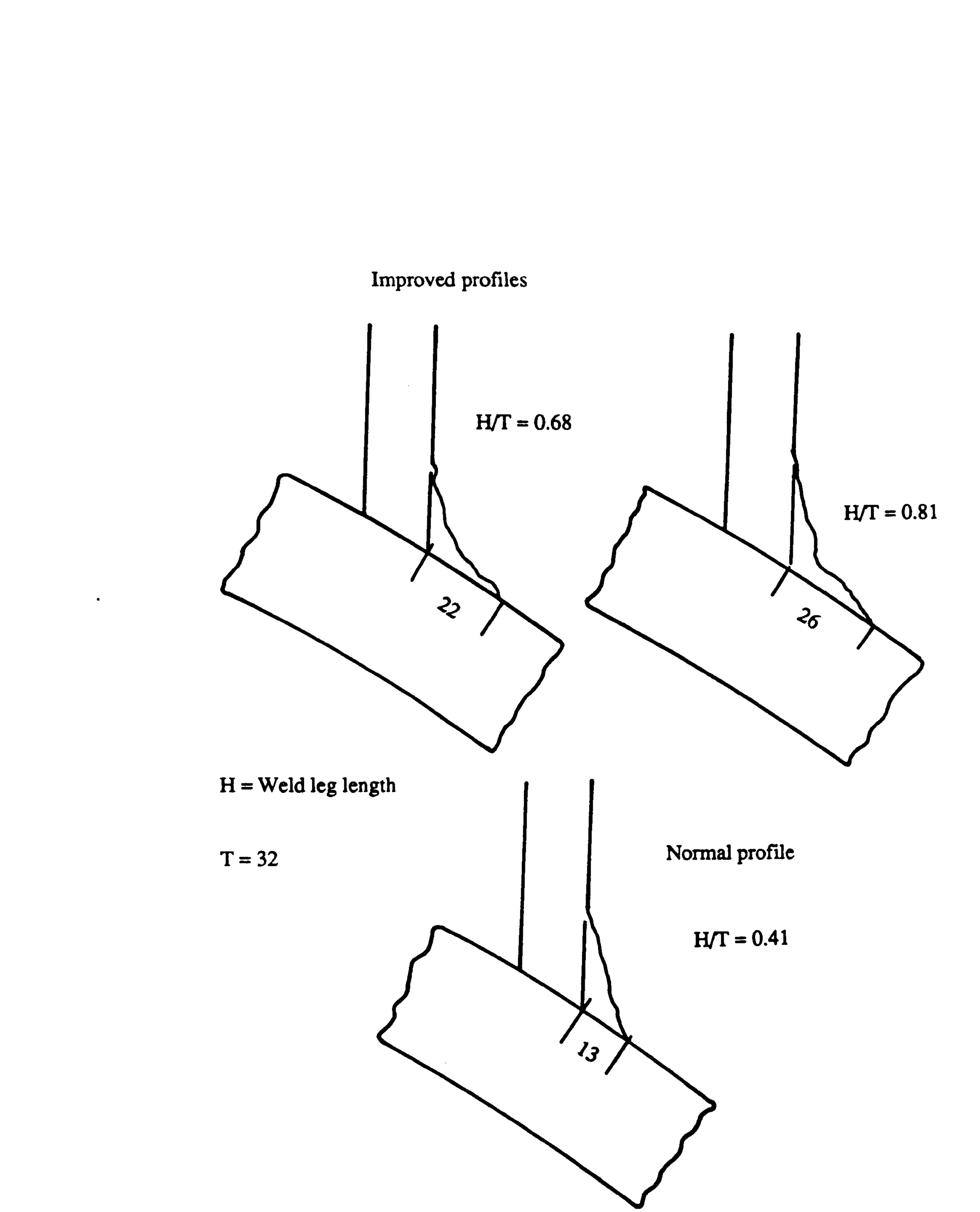

Figure 1.19 Ordinary and improved weld profiles used in the Dutch tests by deBack and Vaessen (1.9)

2 CHAPTER TWO

GLOBAL STRESS ANALYSIS

2.1 Scope of chapter

This chapter reports on the different stress analysis techniques used to determine the magnitude of the stress in the regions that are susceptible to fatigue damage. Two global analyses were conducted. Firstly an experimental strain measurement method where electrical resitance-strain gauges were used to measure the distribution of strain around the brace/chord intersection as well as at perpendicular distance from the weld toes of the loaded braces. The analysis was conducted in the OPB loading mode.

A second analysis was conducted using the finite element method. Thick shell elements were used to generate the full mesh of the tubular joint. The same joint configuration, for which the applied loads are reacted by a second brace, was analysed, and the results compared with the experimental strain analysis. For this load case, as well as for axial loading and in-plane bending, further finite element runs were made to investigate the differences in behaviour when the loads are reacted by torsion through the chord rather than through another brace. Although most studies of tubular joints are carried out with the chord ends fixed, brace-to-brace loading often occurs in offshore structures.

A review of the parametric equations for estimating the stress concentration factor at the crown and saddle positions for both brace side and chord side are presented. Also included, are the bending to membrane stress ratios calculated from this FE analysis, and compared with the values estimated using the recently developed UCL equations for predicting ratios of bending to membrane stresses.

A review of the development of the Controlled Weld profile CWP approach is presented along with the details of the fabrication of the steel tubular joints.

2.2 Stress analysis

A number of theoretical and experimental methods exist for analysing the stresses present in a body. Theoretical methods range from elementary strength of materials

approaches to mathematical theory approaches and numerical methods. Experimental methods make use of either direct measurements of strain on full size components and structures, or an analogue procedure using models in different materials. The simple strength of materials approach, involves the representation of the object being analysed in terms of simply-loaded tension or compression members, beams or shafts, under bending, and/or torsional loading. This approach leads to analytical solutions, which are only approximate. Precise analytical solutions based on the mathematical theories of elasticity or plasticity, are only possible for a limited range of problems, most of which are either two dimensional or rotationally symmetric.

Numerical methods, on the other hand, are in principle, capable of solving any stress analysis problem, to an accuracy which is limited only by the computing resources available. The principal numerical techniques are the finite difference method and the finite element method. These techniques differ in that the finite difference method leads to an approximate solution to the exact problem, while the finite element method gives an exact solution to an approximation of the original problem.

Experimental methods of stress analysis, rely on the measurement of strain, and the subsequent conversion of these to stress values. The most commonly used method employs electrical resistance strain gauges, based on either resistance wire or solid state devices. While strain gauging enables the strain distribution to be determined for a component under actual operating conditions, this is only possible on the surface of the component. An alternative experimental method is one which is based on the photoelastic properties of various transparent plastics.

Through methods of frozen stress photoelasticity, it is possible to determine stress conditions inside three dimensional bodies. The main disadvantages are that material properties are different, and it may not be possible to fully replicate all details of geometry and manufacture.

This project utilised two stress analysis techniques; the experimental strain gauge method for the steel welded tubular joints and the finite element method. For tubular joint analysis strain gauged steel models are considered the most accurate method of determining the strain distribution around the brace/chord intersection, because in this case a weld is present and a more realistic situation is tested.

The finite element method is capable of analysing complex geometries and once the mesh has been generated, further load cases can be tested. There are unfortunately inherent inaccuracies associated with this method regarding tubular joint analyses, especially in the regions where the stress varies sharply. This could be overcome by using very fine meshes, but this makes the analysis expensive because fine meshes require extensive computational facilities.

Normally FE analyses are conducted on a part of the component e.g. for a T-joint one quarter of the joint would be modelled and analysed. However, in this study the full multiplanar mesh was generated, and this allowed for the test conditions of the steel model to be fully reproduced in this analysis.

2.2.1 Strain gauged steel models

Three full scale steel models were strain gauged in accordance with the recommendations of the UKOSRP 1 [2.1] for stress analysis techniques. These recommendations state that the gauges are placed on a line perpendicular to the weld toe. The distance from the weld toe, a , to the first rosette; (for both brace and chord crown and saddle positions) should be the greater of 4mm or

$$a = 0.2\sqrt{rt} \qquad 2.1$$

r brace radius

t brace thickness

from the weld toe.

The second rosette for crown and saddle positions of the brace should be placed $0.65\ (rt)^{0.5}$. For the chord side, the distance for the crown position is designated by a as:-

$$a = 0.4\ rtRT^{0.25} \qquad 2.2$$

R chord radius

T chord thickness

For the saddle position on the chord side, it is the equivalent of 5° of the chord circumference. The two gauges for these steel models were placed in the linear region at 10 and 20mm from the weld toe. This ensures that the gauges are in

a region where the variation in strain is still linear, but far enough away from the intersection to be unaffected by the influence of the notch at the weld toe. The measured strain values were then extrapolated to the weld toe, and converted into stresses in order to calculate the extrapolated geometric stress. Four such pairs of gauges were placed around the intersection: one at the crown position, one at the saddle position, and two at intermediate locations, 30° and 60° away from the crown. The maximum value of extrapolated geometric stress is the 'hot-spot' stress, located at the saddle position in this case.

The test system used in this study was an Instron 250kN servohydraulic actuator. The strain analysis was carried out with the multi-planar joint in the OPB loading mode with a load range corresponding to 0-40% of the material yield stress. All strain gauges were connected to a 'Solatron' 192 channel integrated measurement system controlled by a DEC PDP 11/23 mini-computer. A schematic diagram of the test system is shown in Figure 2.1.

2.2.2 Finite element analysis

2.2.2.1 Introduction

A finite element (FE) analysis was conducted on the tubular joint. The whole joint was modelled, and analysis was conducted on all brace/chord intersections. Details of the mesh generator, type of elements, and loading conditions are given below.

2.2.2.2 Mesh generation

A mesh generator for tubular joints should be capable of producing relatively fine elements in the vicinity of any brace/chord intersection, where the stress gradients are large. Conversely, near the ends of the chord and braces, the program should generate coarse elements in order to avoid unnecessary computational effort. The mesh used in this analysis was generated by adapting an existing mesh generation program [2.2] for tubular Y and T-joints. The modified program was used to generate one- eighth part of the multi-planar joint mesh as shown in Figure 2.2.

The sequence of steps executed in the mesh generation procedure was as follows:- Firstly, the coordinates of the nodes at the intersection between the brace and chord were calculated and used to generate the brace nodes and elements. Secondly, the plug region was filled with a number of triangular elements. Thirdly, the remaining regions of the chord were generated.

Eight-noded quadrilateral elements were used in preference to triangular elements, since they are considerably more accurate, the latter were only used for reasons of geometric compatibility between adjoining regions.

By using the SIMILAR.NODES and GROUP.OF.SIMILAR.ELEMENTS options in PAFEC [2.3], the octant shown in Figure 2.2. was successively rotated and replicated until the full mesh for the multi-planar joint had been obtained Figure 2.3.

2.2.2.3 Element types

The element types used for this analysis were generally curved thick shell elements of the 'AHMAD 'type [2.4]. The first of these is a quadrilateral, with eight nodes which define the middle surface of the shell (type 4620 in PAFEC), while the other related element is a six-noded triangle (type 46110). These elements possess three translational and three rotational degrees of freedom at each node. They are only two-dimensional in nature, the element thickness being a mathematical entity which must be introduced in order to define the element stiffness matrix.

The thick shell elements are based upon a degenerate three-dimensional analysis to incorporate transverse shear effects. The effects of direct stresses through the thickness of the shell are neglected. A reduced integration technique is used with explicit integration through the element thickness. This allows these elements to perform well in some thin shell situations. They differ from semi-loof thin shell elements (PAFEC element type 4320 & 43215), in that the latter do not cater for shear deflection. This FE analysis does not model the weld leg length. It is an ordinary shell analysis, without any attempt to model the intersection using brick elements or even a fine mesh. It is intended to provide a global view of the stress distribution.

2.2.2.4 Boundary conditions

The FE model of the multi-planar joint was analysed in OPB. Accordingly, the lowest row of nodes on the bottom brace were completely fixed against any translation or rotation. In addition, since in OPB the model is symmetric about a plane passing through the centres of the braces, the nodes lying in this plane were constrained to enforce this symmetry. Eight equally spaced point loads of 2kN each, were applied to a ring of corner nodes at the end of one of the horizontal braces, resulting in a total downward force of 16kN. Two rows of elements on the chord side and plug side and one row of elements on the brace side of each intersection were stressed.

Two further load cases were studied, axial and in-plane-bending IPB. For each mode of loading, runs were performed with the chord ends both free and fixed. Figure 2.4 shows the fixities and direction of loading employed in each analysis. The analyses were run on a micro VAX II computer using the PAFEC finite element package, and results then examined by means of the PIGS interactive post-processor. With the aid of this, line drawings were made of the deformed mesh, superimposed on the unloaded mesh and contour plots of the numerically greatest principal stress value around the joint intersection.

2.3 Test rig design

This project utilised new servo-hydraulic equipment and part of a strong floor available at the Mechanical Engineering Department. This facility allowed the possibility of developing a different testing concept. The loading on most existing OPB test rigs was reacted by torsion through the chord, whereas in structures reaction of loads would most commonly be through a second brace.

Accordingly, a multi-brace, multi-planar arrangement was considered, and found to offer extra advantages in terms of savings of chord materials and test frame. Therefore multi-planar nodes were designed in such a way that each brace could have a steel ring welded on the end to provide for fixing and load application to the joint. Figure 2.5 is a schematic of the joint showing overall dimensions.

The tubular joints were fabricated from BS 4360 grade 50 D steel using the gas shielded continuous wire process. All the welds were received and tested in the as welded condition. Table 2.1 shows the mechanical and fatigue properties BS4360 50 D steel.

2.4 Controlled weld profile

The concept of controlling the weld profile of a tubular welded joint in order that the fatigue properties could be enhanced emerged from the findings of the research programmes, UKOSRP 1 [2.5] and ECSC [2.6].

The work produced basic S/N data for tubular welded connections and proposed a number of recommendations dealing with the fatigue properties of welded tubular joints. One significant recommendation, which was adopted by the Department of Energy Guidance Notes for Offshore Installation [2.7], was an emperical equation for thickness correction. The thickness effect is based on the observation that the fatigue strength gradually decreased as the connection size increased. The empirical equation attempts to mitigate this effect by allocating lower fatigue strength values at $2x10^6$ cycles, for thicknesses greater than 32mm in the case of tubular joints, and 22mm for welded plates. A number of experimental research programmes were conducted to study this effect, and a short review is presented.

2.4.1 Thickness effect

The earliest attempt to assess the effect of section thickness on the fatigue performance of welded plates and tubular test pieces was conducted by Gurney [2.8] and presented in BOSS 79. At the time there was limited data available and most of this data had been obtained from studies that had been conducted on relatively thin specimens, typically 12.7mm thick. It was concluded from these results, that a thickness effect existed, and that fatigue design lives based on this data could be unsafe for the thicker sections normally used in offshore structures. Consequently the fatigue design codes both in the UK and the USA noted this effect, and the UK Department of Energy, incorporated it in the Design Guidance Notes [2.7] in the form of an empirical equation

$$S = S_B\left(\frac{t_B}{t}\right)^{0.25} \qquad 2.3$$

S is the fatigue strength of the joint under consideration

S_B is the fatigue strength of the joint using the basic S-N curve

t is the actual thickness of member under consideration

t_B is the thickness relevant to the basic S-N curve (22mm for plate weldments and 32mm for tubular joints)

These findings prompted further examination of the available data, and in particular, interest was focused on the weld profiles of tubular joints used in the European fatigue tests. Analytical work conducted by Marshall [2.9] concluded that the thickness effect could be reduced by improvements in the overall chord-brace weld profile for thicker members. This also led the two American institutions API [2.10] and AWS [2.11], to introduce specific S-N curves for tubular joints with typical weld profiles, Figure 1.10 shows an example of the X′ curve adopted by API.

A number of attempts were made to analyse the thickness effect in terms of fracture mechanics models. Berge [2.12] postulated that an increase in the thickness of a plate, will cause that member to develop relatively higher local stress concentration factors, and from simple beam theory, a thick joint subjected to a given surface stress will possess a shallower stress gradient in the through-thickness direction. Consider a given size of initial defect in a comparatively thicker section, the tip of this defect will be subjected to a significantly higher stress and therefore higher ΔK, resulting in more rapid crack growth in the crucial low ΔK region, which controls a large fraction of life. Conversely for a thinner section, the steeper stress gradient and the smaller initial weld defects, result in the ΔK levels being below the threshold for growth, and would therefore exhibit better fatigue properties.

Modifications to the geometry of the weld toe by Eide *et al* [2.13] were attempted, and the results show that a high consistency of weld angle can be obtained if a controlled weld process is used. Larger weld toes are predicted, to reduce stress concentrations at the weld toe. Similarly for weld toe grinding to specific radii, these contribute to a decreasing thickness effect.

Improvements to the weld shape by Elliot *et al* [2.14] conducted on photoelastic models, resulted in an increase in the observed fatigue lives. It was noted that this was caused by increased weld leg length, which effectively shifted the weld

toe into a region of lower strain range, hence, the same nominal load produced lower hot spot stress range. This has obviously an important consideration for the concept of 'profile control' approach.

The work by Webster [2.15] and deBack [2.16] concluded that two aspects govern the observed fatigue lives, the local weld toe SCF, and the overall stress gradient.

Weld toe SCF effects reduce the apparent fatigue crack growth threshold for geometrically similar joints for increasing plate thickness. For cast joints, virtually no influence or threshold was observed, but the effect on the established crack growth, the linear region of the curve, was similar to that of the welded joints. The measured SCF for cast fillets was therefore essentially governed by the change in stress gradient.

Bignonnet *et al* [2.17] conducted a study on welded connections, where improvement in fatigue lives of offshore structures was observed for joints with controlled weld profile. The improvements were achieved by increasing the average measured weld toe radius ρ from 0.9mm to 1.7mm and also in the reduction of the weld angle α from 60° to 36°. These modifications reflected a 30% reduction in the weld toe stress measurement.

Therefore it would appear that the effect of material thickness on the fatigue life of geometrically scaled welded joints has been confirmed, but it is very possible that this includes the effect of an interaction between thickness and weld profile. Weld shape control can more easily be achieved in the larger joints, it is therefore possible to lessen the thickness effect by attention to weld profile. The analytical work by Marshall confirms these views and the fact that both API and AWS have designated specific S-N fatigue life curves appropriate to the quality of the weld, clearly demonstrates the importance of the concept of controlled weld profile.

This CWP approach, proposed for this work, emerged in response to these recommendations. The use of extra weld beads and capping runs, to achieve a flatter weld angle and a profile, which merged smoothly with the base plate, would be easier to enforce in the field and be commercially more viable than the use of weld toe grinding in order to meet the Dime test requirements. Also, it was considered that the use of extra weld beads to increase the weld leg length

and subsequently reduce the weld angle α, would cause the area of high stress at the toe of the weld to be moved further away from the brace/chord intersection. This implies that the region of high local stress at the site of potential crack initiation has effectively been moved into a region of lower stress concentration. The result could therefore be a longer crack initiation time, and subsequently a longer total fatigue life, and could therefore compensate for the adverse effect of using a thicker member. Two profiles were studied, a standard profile and a CWP.

The standard profile adopted for this study, is that, which is designated by the specifications of the AWS D1.1-1984 [2.18] for offshore structures. The CWP is a modification of the welding procedure of the AWS profile.

2.4.2 Welding procedure for CWP

The initial suggestion for CWP, consisted of simply adding one extra weld bead to the AWS profile after fabrication was completed. The addition of the extra weld bead should be for the chord side, and would had to have been applied over an arc of 180° starting and finishing at the crown positions. Thus each brace would have a CWP finish on one half of its intersection with the chord, (i.e. modifying one saddle position) whilst leaving the other half with the AWS profile.

Since testing was to be conducted under OPB, each brace could have two major crack initiation sites. This approach could therefore have provided a direct comparison of the two weld profiles. This suggestion was rejected on the basis that the addition of one, or even two, extra weld beads was not thought to provide sufficient deviation from the AWS profile to cause measurable changes on the near weld toe stresses. It was therefore decided that the emphasis should be directed towards the reduction in the weld angle α to approximately $\alpha/2$ to cause the area of high stress at the toe of the weld to move away from the brace/chord intersection.

Clearly one or two extra weld beads would not affect the weld angle α significantly as these extra beads may not blend in smoothly with the existing AWS profile, thus leading to a weld finish that may not pass the dime test, and could create an area of high notch stresses at the toe of the weld. Therefore a substantial

increase in the weld leg length was considered necessary, in order to meet the requirements needed to reduce α and provide for a weld profile that merges smoothly with the base metal at the weld toe. It was thus decided that a minimum of three weld beads should be used.

Since testing of the tubular joints was to be conducted in OPB, initiation and growth of fatigue cracks would be more likely to occur on the chord side rather than the brace side [2.19]. Therefore the weld profile modification should only be applied to the chord side of the tubular connection. The proposed weld profile was discussed with Highlands Fabricators of Ross-shire, Scotland, an offshore fabrication yard with whom the contract to fabricate the steel joints was placed. It was decided that trials would be necessary to demonstrate that the CWP could be achieved. The specification for fabricating the joint was as follows:

i) manufacture the joint to AWS D1.1-84

ii) deposit three weld beads starting from the chord side and moving towards the brace. This should achieve the desired CWP and provide the benefit of a weld bead temper heat treatment.

Figure 2.6 shows the results of these trials.

It would seem that a degree of improvement in the hardness test results is shown, due to the effect of the weld bead temper heat treatment. This could contribute to a reduction in the brittleness of the heat affected zone, in the vicinity of the weld toe where fatigue cracks are likely to initiate. These results were accepted but on condition that the tubular joint also passed either the Irish penny test or the Dime test. Figure 2.7 (a) shows the AWS weld profile, designated profile A, for a saddle position, and Figure 2.7 (b) the CWP profile, designated C1, for a similar saddle position.

The schematic diagram of C1 clearly shows that the weld angle α was reduced and the weld leg length increased. However, the sequence of fabrication resulted in a 'canyon' type effect occurring between the original AWS weld profile and the three extra weld beads, leading to a site of potential fatigue crack initiation.

It was clear that the geometric changes required in the profile could be achieved using three extra weld beads, but the fabrication sequence needed to be reappraised. This resulted in Highlands Fabricators, conducting further small scale

trials to try to improve the weld shape finish. The sequence eventually adopted is shown in Table 2.2 and Figure 2.7 (c) and shows a schematic of this CWP designated C2. The welding procedure qualification records (as supplied by the fabricators) for profile A and profile C2 are shown in Table 2.3.

It can be seen from the sequence of fabrication that both the AWS and the CWP were manufactured to the requirements of 'weld profile control' as defined by the structural welding code. This necessitated that capping layers had to be applied so that the welded surface merged smoothly with the adjoining base metal and approximated a concave profile. Also the finished profile should not have deviations in the profile deeper than 1mm relative to a thin disc with a diameter equal to, or greater, than the brace thickness at the weld (dime test). As a further requirement the manufacturers were instructed that no part of the weld outer surface, should be subjected to any form of grinding.

A 100% inspection of all welds was carried out using the Magnetic Particle Inspection (MPI) technique. A second NDT test was carried out, ultrasonic testing (UT) of all the welds. The Fabricators test reports show that the welds did comply with the standard for MPI and UT testing.

These procedures were then used to manufacture the three tubular joints that were tested for this project. Joint one was manufactured with weld profile C1. For joints 2 & 3, each had two braces with AWS, and two braces with C2 profiles. It must be noted that whereas the AWS profile needed 3 capping runs to complete the weld, the CWP (C2) required 5 capping runs to complete the weld. This means that the joints with CWP had approximately 40% extra weld metal thus providing for a stiffer connection.

2.4.3 Numbering system for the welds

Weld Profile			Test Position				Test Number		Joint Number		
UCL Spec CWP	HF CWP	AWS	Four Crack Growth Sites with Different SCF's				1st Test	2nd Test	Three Specimens		
C1	C2	A	A	B	C	D	1	2	X	Y	Z

2.5 Stress analysis results

The stresses measured from this analysis, are referred to as the geometric stresses. These are global stresses, and arise due to the need for the brace and chord to maintain geometric compatibility, as they deform under applied loading. The distribution of stress along a perpendicular distance from the weld toe, could be divided into three regions as shown in Figure 1.5. Close to the weld toe high stresses are produced, due to the effect of the local weld geometry. Further away from the intersection these high stresses decrease to a region where the increase in stress is linear. This region is dominated by the deformation of the brace and the chord under applied loading. Further away, remote from the intersection, the stresses decrease to the value of the applied nominal stress.

This analysis was conducted to measure the stress at two locations at a specific perpendicular distance from the weld as shown in Figure 1.3, and then the values were extrapolated to the weld toe according to the recommendations of UKOSRP 1 [2.1]. This extrapolated value of stress is known as the 'hot-spot stress' and in terms of the fatigue life of a structure is known as the stress which controls the fatigue endurance of a tubular joint. The hot spot stress is normally expressed in the form of the Stress Concentration Factor, where the SCF is defined as;

SCF = extrapolated geometric stress/nominal stress

The nominal stress in the above equation is the stress at the intersection calculated from the beam theory. For this test set-up nominal stresses are presented in Appendix I.

2.5.1 Experimental strain analysis

Figure 2.8 shows the stress distribution around the brace/chord intersection, brace side and chord side for tubular joint C1-X tested in OPB. The maximum value of stress, shown in this figure in terms of SCF, lies at the saddle position. At the crown position (neutral axis of the brace) the value of the SCF is zero. For the brace side and chord side the four saddle positions A, B, C and D exhibit a range of SCF values. Positions A and C lie on the same brace and have the same nominal stress value.

Despite this, the SCF values are markedly different; A exhibits the highest value and C the lowest of the four saddle positions. Positions B and D lie on the second brace and their nominal stress values are different. (See Appendix I for nominal stress definition and calculations). The difference in their SCF values are less marked though Position B, consistently has a higher value than position D. In terms of strain or stress values the highest to lowest sequence would be A B D C. The brace SCF distributions are flatter with a sharper peak at the saddle than those at the chord, and are at all points lower than the corresponding chord values. This is consistent with the experimental observations that fatigue cracks grow in the chord rather than the brace [2.20].

Figure 2.9 shows the distribution of stress around the brace/chord intersection chord side and brace side for tubular joint A-Y. The test conditions and nominal stress calculations are the same as those of tubular joint C1-X. Figure 2.9 shows the same variation in SCF values for the four saddle positions as those shown in Figure 2.8, the only difference being that all four A-Y results exhibit higher SCF values than their equivalent C1-X braces.

Figures 2.10 & 2.11 show the stress values at the 90° position, which is the peak stress site, expressed as a function of the perpendicular distance from the weld toe. The extrapolated value of SCF shown, is known as the geometric stress concentration factor K_G. Included in these results are the stress values at the two saddle positions tested for profile C2. These values are 5.2 for position A and 4.5 for position B. The range of SCF values for C1-X braces is 3.2-5.6 with an average of 4.4. However, the A-Y braces show a higher range of values, 3.8-6.3 with an average of 4.93, representing a difference of 11% as measured on the chord side. On the brace side of the intersection the trend is the same, although

the stress distributions are 40% and 32% lower for A-Y and C1-X braces respectively. The difference between the two braces is 6%. It must be noted here that no modification to the weld profile was undertaken on the brace side of the intersection. The SCF values brace side and chord side for C1-X and A-Y as well as the two SCF values for C2 profile are presented in Table 2.4.

2.5.2 Finite element analysis

2.5.2.1 OPB loading

The FE analysis, provided information on the stress distributions at the outer and inner tube surfaces, for both the chord and brace sides of all the intersections. The results of the analysis were also examined using the PIGS interactive post-processor. Line drawings were made showing the deformed mesh superimposed upon the unloaded mesh. Figures 2.12 & 2.13 show this effect at different angular locations for the OPB case.

Stress values, normalised with respect to the nominal stress, were plotted between the crown (neutral axis) position and the saddle point and are symmetrical about the saddle. The differences in SCF between the four saddle positions on the loaded braces are confirmed by the FE analysis, the highest SCF occurring at A and the smallest at position C. Positions B and D again display a less marked difference in SCF values. The SCF values for the chord saddle location range from 2.57 - 3.9 with an average of 3.32 while the brace values range from 2.73 - 4.16 with an average of 3.38, as shown in Tables 2.5 and 2.6.

It is interesting to note, that, whereas the brace side values of the steel results exhibited flatter distributions with a sharper peak at the saddle position for both types of profiles, the FE results are overall higher with a similar value at the peak position. The trend in the SCF distributions between the saddle positions of highest value at A and lowest at site C as measured for the steel results emerges for the FE predictions as well.

Figure 2.14 & 2.15 shows the AWS, CWP and FE analysis results for the SCF distribution between the chord crown and saddle positions A, B, C and D. These plots show similar trends to the strain gauge measurements for SCF distributions, and also confirm the SCF value at the saddle position A is the

highest, and at C, is the lowest. This implies that although two braces were unloaded, they act to stiffen the chord wall, and may contribute to a varied distribution in the SCF values measured.

It is apparent from Tables 2.5 and 2.6 that while the brace SCF values from the FE analysis are similar to the steel model results, the FE predictions for the chord SCFs, consistently underestimate the measured values. This is presumably due to the errors involved in modelling the brace/chord intersections using shell elements and in omitting the welds.

Figures 2.16 - 2.19 show the variation of outer and inner surface stresses about the saddle positions A, B, C and D for both brace and chord. The stress distribution curves at the outer surface of brace and chord are all fairly similar in shape, and in general show a greater change between crown and saddle sites, than those for the inner surface stresses. The inner surface stresses at the saddle positions are numerically less than, and of opposite sign to, those on the outer surface. It is apparent that a considerable portion of the stresses around the intersection is due to local bending, made evident by the change from tensile to compressive stress, in going from the outer to inner surface. The ratio of bending to membrane stresses for the four saddle positions ranges from 5.08:1 to 7.63:1 on the chord and from 3.11:1 to 3.72:1 on the brace, as shown in Tables 2.7 and 2.8.

A further FE analysis, was conducted with the chord ends rigidly fixed in order to investigate how the SCF values differed between this case and the brace-to-brace type of loading considered so far in this project. Figure 2.20 shows the stress distribution curves for both brace and chord in the vicinity of saddle position A (where the maximum SCF occurs) with chord ends fixed (c.f. Figure 2.16), Tables 2.7 and 2.8 give the ratio of bending to membrane stress.

It can be seen that the curves exhibit similar trends in both cases, but that fixing the chord ends leads to a reduction in saddle SCF (from 3.90 to 3.00 on the chord and from 4.16 to 3.38 on the brace (see Tables 2.5 and 2.6). This is probably because restraining the chord ends, causes torsional moments to be induced, which tend to act symmetrically and give lower ratios of bending to membrane stress.

For comparison purposes the SCF predictions obtained using various parametric equations for T-joints, are also contained in Tables 2.5 and 2.6. The formulae taken are those due to Kuang, [2.21] Gibstein, [2.22] Wordsworth and Smedley, [2.23] as well as a set of equations recently derived at UCL [2.24] and considered to be conservative.

The average results from the thick shell analysis was 3.32 for the chord SCFs. This shows fairly good agreement with the results predicted from Kuang's equation, as the difference between the results presented here is only 5%. However, both cases are about 30% less than the steel model results (joints with AWS profile).

A second comparison with parametric equations is made with that of Wordsworth; the values predicted show an average of 20% difference between the two values. It should be noted that all of these formulae were obtained from studies in which the chord ends were fixed. These were all finite element studies, except for ref. [2.23] which was based on acrylic model tests. Since they apply to a T-joint, strictly speaking, none of them is directly comparable with the results from the multi-planar X-joint used in the present study. However, Wordsworth and Smedley [2.25] have also presented equations for X-joints which lie in one plane only, and use of this equation leads to a small reduction in the predicted SCF (from 4.02 to 3.91 on the chord and from 3.53 to 3.46 on the brace). Set against this, however, is the increase in SCF which occurs when the restraint is removed from the chord ends, and the applied load is instead reacted by a second brace. From the FE analysis of the multi-planar joint, this suggests that the SCF at site A increases by about 20% on both the chord and brace. This phenomenon could be relevant to situations where additional support or restraint is applied to a multiplanar joint on one brace at a site near to the intersection. This would seem to be a design situation that should be avoided.

The ratios of bending, to membrane stress obtained from the FE analysis of the multi-planar joint are compared in Tables 2.7 and 2.8 with the predictions of parametric equations [2.26] at the saddle and hot-spot positions on both

the chord and brace of a T-joint. It can be seen that there is quite good agreement between these predicted ratios and the FE values from the analysis with chord ends fixed.

One interesting observation for this OPB loading case is the low value of SCF measured at position C, irrespective of the method of analysis used. This feature may be explained in terms of the deformation of the the whole chord wall and in particular region CD. Figure 2.21 shows line drawings of the deformed chord wall, superimposed upon the undeformed section. Consider the region between braces 1 and 4 and braces 3 and 2 i.e. the region between site A and the unloaded brace 4 and site B and the unloaded brace 3. Chord wall deformation, and evidence of bending can be seen in those two regions, but chord ovalising is not significant. However, the section of the chord CD where the deformation experienced, is governed by the behaviour of braces 1 and 2, (brace 2 being fixed and has a low length to depth ratio), and can therefore be considered as structurally rigid. Brace 1 through which the load is applied can travel in the direction of the applied load.

The premise that brace 1 behaves as a cantilever fixed to a rigid body is not wholly correct, the chord rotates under load.The deformation at site D is primarily due to the bending resistance of brace 2 to the chord wall rotation. At position C the deformation is due to the bending resistance of region CD. This region experiences the maximum deformation, and the least bending resistance of all the sections of the chord that lie between the four braces. In general the preferred load path would be through the stiffer section of a body and in this case would be in the sequence sites A B D and C which is consistent with the SCF values measured. In the case of the chord ends being rigidly fixed, then brace 1 can be considered as a cantilever fixed to a rigid body, and as observed, stress distributions at A and C are symmetrical. It therefore appears that the stress value measured at position C is peculiar to the fixities and end condition of the chord wall

A more significant comparison of the steel model results, is between the values obtained for the two different weld profiles. In the case of the CWP the addition of three extra weld beads and the subsequent reduction of the weld angle α from 48° to approximately $\alpha/2$, caused a reduction in the

measured stress at all the saddle positions. Expressed in terms of SCFs the average stress value was reduced by 11%. This is a small but not negligible decrease in SCF and hence greater resistance to fatigue.

The possible explanation for such a reduction may be due to the addition of approximately 40% extra weld metal thus producing a stiffer connection which could influence the distribution of stress. More significant is the increase in the weld leg length which occurs when α is reduced to $\alpha/2$, this effectively moves the area of high stress at the weld toe further away from the intersection, and into a region of lower stress field.

Morgan [2.27] studied the effect of changing weld leg lengths on the weld toe stress concentration factors for a range of L/T of 0.4-0.53 where L represents the weld leg length and T, the member thickness for welded plates. The results show a reduction of approximately 10% on the SCF values. In the same study, weld toe grinding to totally remove the singularity at the weld toe, reduces the peak SCFs significantly. The author concludes that increasing weld leg length moves the region of high stress into a lower stress field.

2.5.2.2 Axial loading FE results

Figures 2.4 c and d, are schematics of the applied loads and fixities for the two finite element analyses of the multi-planar joint, performed under axial loading. The distribution of stresses, for case 2.4 c, expressed in terms of SCF, (see Appendix I for nominal stress calculations) is shown in Figures 2.22 - 2.25 for the four saddle positions A, B, C and D. A state of symmetry was found to exist about the neutral axis of brace 1, so that a single curve represents both positions A and C. For brace 2, however, positions B and D exhibit markedly different SCF distributions, even though the nominal stress is identical. At position D the principal stress at the outer surface is compressive, whereas for position B it is tensile with a numerical value 31% lower than at D.

This indicates that the load on brace 1 causes the chord to deform, thereby imposing a bending moment on brace 2 in the out-of-plane direction. Figures 2.26 and 2.27 show line drawings of the deformed mesh under axial loading superimposed upon the unloaded mesh. The deformation of the mesh clearly

shows that brace 1 undergoes both axial and OPB types of loading. All four distributions of stress exhibit a minimum, though not zero value, at the crown positions (neutral axis of the brace) with the maximun SCF values occuring at the saddle positions.

The second axial load analysis was conducted with the chord ends fixed, as shown in Figure 2.4 d, in order to provide the torsional restraints usually present in studies of tubular joints i.e. with brace 2 free. Brace 1 exhibits behaviour consistent with that of an ordinary T-joint, as shown in Figure 2.28 and by the SCF comparisons with parametric equations given in Tables 2.5 and 2.6.

Tables 2.7 and 2.8 show the bending to membrane stress ratios for both types of chord end conditions. For the analysis, with the chord ends free, it is apparent that there is a high bending component of the through-thickness stress leading to very high SCFs at sites A and C. For the chord ends fixed, the ratio of bending to membrane stress, is significantly lower and the SCF values agree closely with values predicted by parametric equations for an ordinary T-joint. It would therefore appear that brace-to-brace loading or local restraint represents a much more severe type of loading, leading to an increase in chord hot-spot SCF.

2.5.2.3 In-plane bending FE results

Figure 2.4 (e & f) shows the loads and fixities that were used to conduct the analysis for the IPB mode. This loading configuration was analysed in order to provide a basis for comparison with the axial and OPB results. It should be emphasised that in a real structure, such a loading condition would be unlikely to occur, especially for the bottom fixed brace. The calculated SCF distributions confirm this observation.

Figure 2.29 shows the four crown positions identified as E, F, G, and H in relation to braces 1 and 2. The nominal stress calculation for the IPB case is shown in Appendix I. Figure 2.30 - 2.32 show the stress distribution expressed in terms of SCF around the brace/chord intersection. The hot-spot SCF occurs approximately 22° from the crown position, and the whole region either side

of the crown is under a high positive SCF for position E, and a high negative SCF for G. The ratio of bending to membrane stresses appears to be consistent with other IPB results.

For positions F and H on brace 2, the stress distribution calculated, is of the same magnitude as that measured at E and G. However, the significant difference between the behaviour of the brace through which the load is applied, and brace 2, which is fixed, is the direction of the principal stress. For E and G this principal stress is in the plane of a potential fatigue crack, and would lead to a Mode I type crack, which is consistent with tubular fatigue crack behaviour. However, the maximum principal stress direction at brace 2, is parallel to the plane of the crack, and a fatigue crack initiating at the intersection would grow under Mode III loading, a situation that is not typically associated with tubular joints. The bending to membrane stress ratio at H, is similar to E and G. However, the result at F suggests a pure bending situation, the ratio of bending to membrane stress being very large.

A comparison of the results for IPB, with chord ends free and fixed, show similar SCF distributions both for the brace and chord (see Fig. 2.30 - 2.33). There is a small decrease in SCF when the load is reacted by a second brace, rather than the chord ends, amounting to 10% on the chord and 3% on the brace. The ratio of bending to membrane stresses is not significantly affected.

2.6 Summary

Three stress analysis methods were used to estimate the magnitude and distribution of stresses around the brace/chord intersections of the tubular joints. The loading conditions investigated were the OPB, IPB and axial loading. For the OPB case all three methods of stress analysis were used; experimental strain measurement conducted on the steel models, global thick shell finite element analysis of the whole mesh of the tubular joint and finally the use of different parametric equations to estimate the non-dimensional stress concentration factor at the crown and saddle positions. The OPB case provided one further set of results; a comparison between the results of the two different weld profiles used to manufacture the braces of the tubular joints.

For the IPB and axial loading cases two stress analysis methods were used; thick shell finite element analysis of the whole of the multiplanar joint and the parametric equations to predict the SCF values at crown and saddle positions. The thick shell finite element analysis of the three load cases, OPB, IPB and axial loading did not attempt to model the brace/chord intersection and therefore no comparison of different weld profiles could be made. However, the effect of brace to brace loading was investigated and compared with results of analysis where the chord ends are fixed thus providing the necessary torsional restraint as is the case in most laboratory test rigs.

Experimental strain analysis results conducted on steel models are generally considered to provide the most realistic distributions of stress at brace/chord intersections. The steel model results are only available for OPB loading case, thus this forms the basis of comparing all three methods of stress analysis and should provide a measure of the accuracy of the finite element and parametric equations values for the IPB and axial loading cases.

Figure 2.1 shows the experimental testing arrangement for the OPB loading case of the steel models. The four saddle positions A,B,C,and D loacted at the two loaded braces represent the sites of maximum SCF values. In view of the fact that all braces have the same geometric dimensions and that the nominal stress value at sites A and C is the same the four saddle positions exhibited different values of SCF. This was noted irrespective of the particular weld profile studied. Site A is that of the greatest SCF and site C is the lowest. The sequence of SCF values is A, B, D and C. The fact that the loading is reacted through an adjacent brace rather than through the chord ends and the stiffening effect on the chord wall due to the presence of the unloaded braces suggests that the load path is from site A through the unloaded braces to B, D and C.

Therefore, during subsequent testing of the multi-planar joints four different 'hot spot' stresses would exist during each test. This will give rise to different initiation periods, crack growth rates and potentially four different endurances.

The second conclusion to emerge from this study is that using a different welding procedure, where the geometry of the weld profile could be controlled, produced a measured reduction in the average value of K_G, of some 11%. This should give improved fatigue resistance and must be taken into account together with any

improved fatigue life measured on the basis of a common hot spot stress. Note that fatigue tests are conducted on the basis of a chosen value of hot spot stress. A lower SCF means that the CWP brace would require a higher force i.e a higher nominal stress in the brace to give the same hot spot stress as for the AWS brace. In assessing the benefit of the CWP the different forces used and the differences in S/N should be taken into account.

This conclusion is supported by the work of deBack *et al* [2.16] who conducted stress analysis studies on welded plates, with, and without, profile control, with the result that the controlled (concave) profile recorded a reduced SCF value of approximately 10%.

Subsequent fatigue tests in air and sea water, with cathodic protection, indicated that improved weld profiles had no primary effect on the fatigue performance. In these tests the welded attachment is non-load carrying and is therefore significantly different from the case of a tubular joint where the brace to chord joint of a tubular structure, the brace would usually be loaded. The paper [2.16] suggests, that with a load carrying attachment in a tubular joint, a weld with a controlled concave profile will develop a lower hot spot stress, than a weld with a less blended profile. The authors further suggest that the test results plotted in terms of brace load rather than hot spot stress might provide for a three fold life improvement when a blended profile is used. The idea of comparing fatigue results on the basis of brace load rather than hot spot stress for steel joints studied in this project is reported in chapter four.

The SCF values predicted for the four saddle positions A,B,C and D using the thick shell finite element analysis exhibited the same range of values as for the steel model results. This confirms the essential correctness of the distributions and establishes that the trend for SCF values at the saddle positions to be genuine. However, the FE analysis underestimates the magnitude of the SCF at all four sites. The values fall within an error band of -20/-40% of the steel values.

A second significant point noted from the FE SCF study, showed that reacting forces through an adjacent brace, rather than at the chord ends, leads to increases of 30% in the SCF values predicted. This is an important observation especially when considering SCF values estimated using parametric equations.

Tables 2.5 and 2.6 show the SCF predictions using various parametric equations. On the whole the FE results show fairly good agreement with the predictions of the parametric equations but compared with the steel model results they all appear to underestimate the SCF values. It must be noted that Kuang [2.21] Gibstein [2.22] UCL [2.24] parametric equations were derived from FE analyses conducted with the chord ends fixed. Wordsworth/Smedley [2.23] derived their equations from acrylic model testing with the chord ends also fixed to provide the necessary torsional restraint. As shown from this study, fixing the chord ends leads to a reduction in the SCF at the brace/chord intersection.

It is therefore not unreasonable to conclude that the FE predictions and parametric eqution estimation of SCF values for the IPB and axial loading cases could be considered as generally representative of what steel models tested under the same loading conditions might produce. For the chord ends fixed a comparison between the parametric equations and the FE results show reasonable agreement for both axial and IPB loading. However, brace to brace loading exhibts a significant increase in the value of SCF, 79% for axial loading and a 10% decrease in hot-spot SCF for IPB. These findings are not consistent with Gibstein's results. Gibstein [2.22] investigated the effect of chord wall boundary conditions for all load cases, OPB, IPB and axial loading with both chord ends rigidly fixed and simply supported.

In assessing the effect of chord boundary conditions Gibstein concludes that a difference of 5% in the case of axial load was observed and no difference in either of the two bending cases.

The observations from this study confirms that the important condition is not whether the chord ends are fixed or free, (in a platform all brace and chord connections would be made). The important point to consider is the influence on the local restraint, as there will invariably be differences in the level of restraint between braces especially where a repair has been conducted and an additional support is placed. The distance of this additional support or restraint, would be the important parameter controlling the changes in SCF and therefore this situation could be important in multi-mode multi-node studies.

2.7 Conclusions

1. The average value of geometric SCF K_G for the four saddle positions on the loaded braces of the multi-planar joint was 11% lower for profile C1 than for profile A. The limited number of results for C2 profile suggest a further drop in SCF values.
2. Use of a CWP is expected to enhance the fatigue life as a reduction in K_G implies slower growth of a fatigue crack once it has initiated.
3. The carryover effect of the unloaded braces results in a characteristic variation in SCF between the four saddle positions of the loaded braces. This effect was evident in both the steel model results and the FE analysis.
4. From thick shell FE analysis of the multi-planar joint, reacting loads via a second brace rather than through the chord ends leads to increases in SCF of 30% for out-of-plane bending, 79% for axial loading and a 10% decrease in hot spot SCF for in-plane-bending. The implications of such an observation could be significant for a situation where additional support is required on a multinode structure.

2.8 References

2.1 Irvine, N.M. Review of stress analysis techniques used in UKOSRP I, Paper 6, *Int. Conf. on Fatigue in Offshore Structural Steels*, Inst. of Civil Engineers, London, 1981

2.2 Dharmavasan, S. Fatigue fracture mechanics analysis of welded tubular joints, PhD Thesis, University of London, 1983

2.3 PAFEC Data Preparation User Manual, Pafec Ltd, Nottingham, UK, 1984, Version 6.1, Section 4.22

2.4 Ahmad, s., Irons,B.M. and Zienkiewicz, O.C. Analysis of thick and thin shell structures by curved elements, *IJNME 2, pp.419-451, 1970*

2.5 UKOSRP 1 Final report, SRD UKAEA, Cheshire 1986. To be published

2.6 *International Conference on Steel in Marine Structures*, Paris, October 1981. European Coal and Steel Community

2.7 Background to new fatigue design guidance for steel welded joints in offshore structures, Report of the Department of Energy Guidance Notes Revision Drafting Panel, HMSO, London, 1984

2.8 Gurney, T.R., The influence of thickness on the fatigue strength of welded joints , paper 41,. *BOSS Conference,* London, August 1979

2.9 Marshall, P.W., Size effects in tubular welded joints. *Proc. ASCE Structures Congress 1983*, 17 October 1983, Houston, Texas

2.10 American Petroleum Institute (1984), Recommended practice for planning, designing, and constructing fixed offshore platforms, API RP2A, 14th ed., Dallas

2.11 American Welding Society Structural Welding Code, D1.1-82 ANSI/AWS, Miami

2.12 Berge, S., On the effect of plate thickness in finite welds. *Engineering Fracture Mechanics*. Vol. 21 No. 2 pp 423-435. 1985

2.13 Eide, O.I, *et al* Size effects in fatigue of large scale girders, *Paper 5309 18th Annual Offshore Technology Conference*, Houston, May 1986

2.14 Elliot, K.S., Fessler, H., Stresses at weld toes in non-overlapped tubular joints. *Fatigue and Crack Growth in Offshore Structures,* IMech E London 1986

2.15 Webster, S.E., Walker, E.F, The effect of section thickness upon the fatigue properties of welded and cast steel nodes. *Proc. of Int. Conf. on Fatigue and Fatigue Thresholds*, september 1984. EMAS

2.16 de Back, J., Vaessen, G.M.G., Effect of plate thickness, temperature and weld toe profile on the fatigue and corrosion fatigue. Behaviour of Welded Offshore Structures. *Foundation for Materials Research in the Sea*, Netherlands. ECSC 7210-KG/601. April 1984.

2.17 Bignonnet, A., Lieurade, H.P., Picout, L., Improvement of the fatigue life for offshore welded connections. IIW - IIS pp 271-278, Pergamon Press 1984

2.18 American Welding Society Structural Welding Code, Section 10.13 D1.1-84. Section 10.13

2.19 Gibstein, M.B. Stress concentration in tubular joints. Its definition, determination and applications, Paper 1.4, *Int. Conf. on Steel in Marine Structures,* Commission of the European Communities, Paris, France, October 1981

2.20 Dover, W.D., McDiarmid, D.L. and Kare, R.F. Influence of weld profile on fatigue in tubular welded joints. Fatigue in Offshore Structures, Editors W.D.Dover & G. Glinka. *Proc. of EMAS Conf.* London September 1988

2.21 Kuang, J.G., Potvin, A.B. and Leick, R.D. Stress concentration in tubular joints, Paper, *Society of Petroleum Engineers*, 1977

2.22 Gibstein, M.B. Parametric stress analysis of T-joints, Paper 26, *European Offshore Steels Research Seminar,* Cambridge, UK, November 1978

2.23 Wordsworth, A.C. and Smedley, G.P. Stress concentration factors at K and KT tubular joints, *Conference on Fatigue in Offshore Structural Steel.* Institution of Civil Engineers London February 1981

2.24 Hellier, A.K., Connolly, M.P. and Dover, W.D. Stress concentration factors for tubular Y and T-joints, submitted for publication in *Journal of Strain Analysis for Engineering Design*

2.25 Wordsworth, A.C. and Smedley, G.P. Stress concentrations at unstiffened tubular joints, Paper 31, *European Offshore Steels Research Seminar,* Cambridge, UK, November 1978

2.26 Connolly, M.P., Hellier, A.K., Dover, W.D. and Sutomo, J. A parametric study of the ratio of bending to membrane stress in tubular Y and T-joints, submitted for publication in *Journal of Strain Analysis for Engineering Design*

2.27 Morgan, H.G., The effect of section thickness on the fatigue performance of simple welded joints. Springfields Nuclear Power Development Laboratories. UKAEA Northern Division HMSO 1983

Yield stress σ_y	370 MPa
Ultimate tensile stress UTS	538 MPa
Elongation (%)	32
Charpy impact value	119 at -20°

Table 2.1 Mechanical properties of BS4360 50D steel

Weld run	Weld type	Description
1-9	——	The same for all AWS and CWP braces
10-12	AWS	Capping runs to complete weld
10-12	CWP	Runs to achieve desired change in weld profile
13-17	CWP	Capping runs to complete weld

Table 2.2 Fabrication steps used in manufacture of the tubular joints

Table 2.3

HIGHLANDS FABRICATORS LTD.

WELDING PROCEDURE QUALIFICATION RECORD

FOR U.C.L.

QUALIFIED IN ACCORDANCE WITH SPECIFICATION
CLIENT INSTRUCTIONS

WELDING PROCEDURE NO DP32/4 POSITIONS 2G
REVISION
THICKNESS TESTED 16/32mm DATE 31.8.87

MATERIAL USED FOR QUALIFICATION API 5L X52/BS.4360 - 50D
MATERIAL CERTIFICATION REF NOS 9898/10628

CONSUMABLE BATCH CERT NOS
3.00mm - 036096
3.25mm - 132344

WELDING CONSUMABLES
MAKE OERLIKON
TYPE TENACITO 38R
CLASSIFICATION AWS 7018-G

SHIELDING GAS N/A
COMPOSITION OF GAS N/A
FLOW RATE OF GAS N/A
TYPE OF FLUX N/A

PROCESS AND ELECTRODE POLARITY MMA DC-ve ROOT, DC+ve FILL
WELDING PROCESS 1ST SIDE MMA
PREPARATION OF 2ND SIDE N/A
WELDING PROCESS 2ND SIDE N/A

MIN PREHEAT (°C) 50°C
METHOD GAS
MAX INTERPASS (°C) 250°C

POST HEAT TREATMENT CYCLE

NONE

WELDERS NAME AND NUMBER P. J. STONE (1052)

JOINT DETAILS —

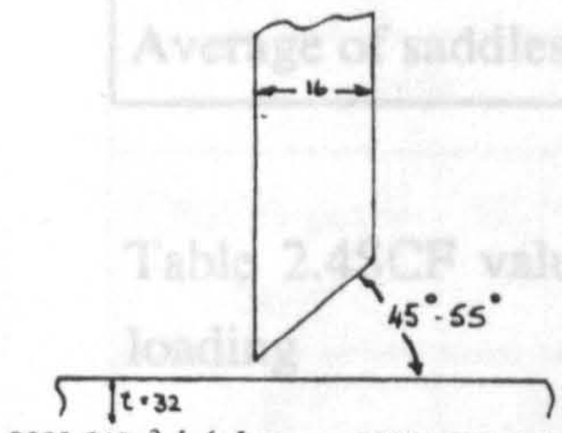

ROOT GAP 3.5-6.5mm ROOT LAND 0-2mm
PREPARATION METHOD FLAME CUT & GRIND

RUN SEQUENCE

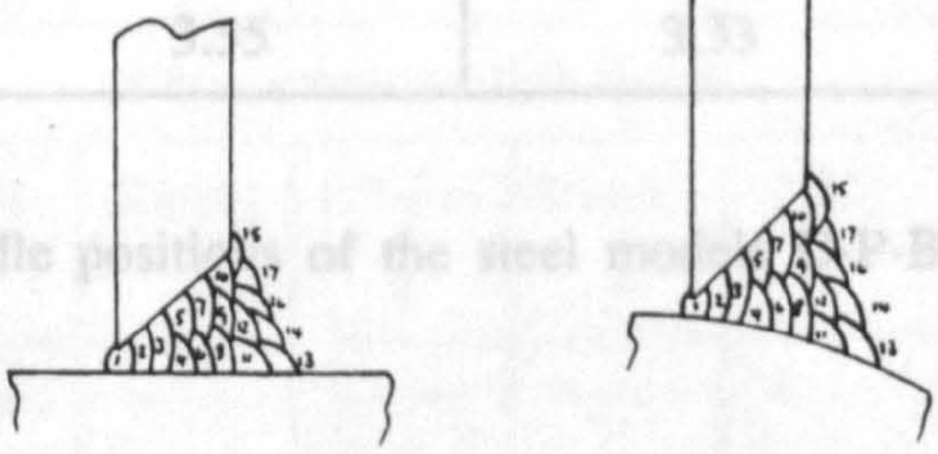

PASS NO	ELECTRODE SIZE (mm)	CURRENT AMPS	VOLTAGE VOLTS	W.F.S.	TRAVEL SPEED (cm/min)	R.O.L. (cm)	HEAT INPUT (KJ/mm)	INTER-PASS °C	SPECIAL NOTES
1	3.00	65	20			4-6		50	
2-3	3.25	125	21			12-13		50	
4-14	3.25	130	21			11-16		50+	
15	3.25	115	21			15		50+	
16-17	3.25	130	21			12-14		50+	

JOINT DETAILS —

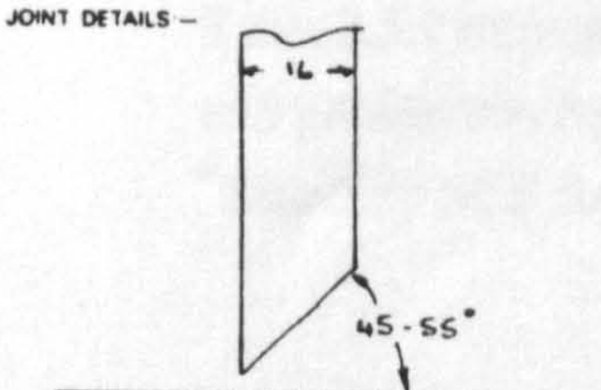

ROOT GAP 3.5-6.5mm ROOT LAND 0-2mm
PREPARATION METHOD FLAME CUT & GRIND

RUN SEQUENCE

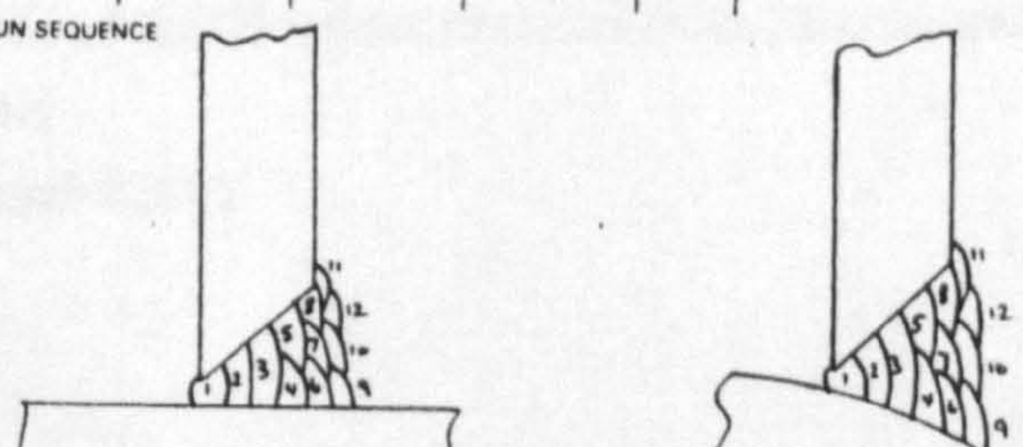

Chord		Stress concentration factor		
	σ_n	AWS	C1	C2
Saddle position	(MPa)	K_G	K_G	
A	0.823	6.30	5.60	5.2
B	1.103	5.30	4.80	4.5
C	0.823	3.80	3.20	
D	1.220	4.33	4.00	
Average of saddles		4.93	4.40	

Brace		Stress concentration factor	
	σ_n	AWS	C1
Saddle position	(MPa)	K_G	K_G
A	0.823	4.55	4.40
B	1.103	3.65	3.50
C	0.823	2.60	2.30
D	1.220	3.40	3.10
Average of saddles		3.55	3.33

Table 2.4SCF values at saddle positions of the steel models O-P-B loading

OPB		Stress concentration factor				
Saddle position	σ_n (MPa)	FE	Kuang	Gibstein	Smedley	UCL
A	0.660	3.90	3.50	4.01	4.02*	4.85
B	0.954	3.31	3.50	4.01	4.02*	4.85
C	0.660	2.57	3.50	4.01	4.02*	4.85
D	1.072	3.48	3.50	4.01	4.02*	4.85
Average	———	3.32	3.50	4.01	4.02*	4.85
Chord fixed	0.660	3.00	3.50	4.01	4.02*	4.85
Axial		Stress concentration factor				
Saddle position	σ_n (MPa)	FE	Kuang	Gibstein	Smedley	UCL
A	0.065	10.90	———	———	———	———
B	0.310	3.10	———	———	———	———
C	0.065	10.90	———	———	———	———
D	0.310	4.50	———	———	———	———
Chord fixed	0.065	6.10	6.13	5.46	6.82	6.63
IPB		Stress concentration factor				
Crown position	σ_n (MPa)	FE	Kuang	Gibstein	Smedley	UCL
E	0.660	2.44	———	———	———	———
F	0.310	2.10	———	———	———	———
G	0.660	2.44	———	———	———	———
H	0.310	2.60	———	———	———	———
Chord fixed	0.660	2.70	1.83	2.08	2.28	2.64

Table 2.5. Comparison of chord SCF values obtained from FE analyses and parametric equations

* Smedley SCF for X-joint = 3.91

OPB		Stress concentration factor				
Saddle position	σ_n (MPa)	FE	Kuang	Gibstein	Smedley	UCL
A	0.660	4.16	4.36	3.89	3.53*	5.03
B	0.954	3.23	4.36	3.89	3.53*	5.03
C	0.660	2.73	4.36	3.89	3.53*	5.03
D	1.072	3.39	4.36	3.89	3.53*	5.03
Average	——	3.38	4.36	3.89	3.53*	5.03
Chord fixed	0.660	3.38	4.36	3.89	3.53*	5.03
Axial		Stress concentration factor				
Saddle position	σ_n (MPa)	FE	Kuang	Gibstein	Smedley	UCL
A	0.065	11.80	——	——	——	——
B	0.310	2.60	——	——	——	——
C	0.065	11.80	——	——	——	——
D	0.310	4.00	——	——	——	——
Chord fixed	0.065	6.40	8.34	5.48	5.30	7.53
IPB		Stress concentration factor				
Crown position	σ_n (MPa)	FE	Kuang	Gibstein	Smedley	UCL
E	0.660	3.30	——	——	——	——
F	0.310	3.20	——	——	——	——
G	0.660	3.30	——	——	——	——
H	0.310	3.60	——	——	——	——
Chord fixed	0.660	3.40	2.52	2.08	2.44	2.89

Table 2.6. Comparison of brace SCF values obtained from FE analyses and parametric equations

* Smedley SCF for X-joint = 3.46

OPB	Ratio of bending to membrane stress		
Saddle position	FE	UCL eqn (saddle)	UCL eqn (hot-spot)
A	7.63	6.22	6.84
B	7.04	6.22	6.84
C	6.25	6.22	6.84
D	5.08	6.22	6.84
Chord ends fixed	6.34	6.22	6.84
Axial	Ratio of bending to membrane stress		
Saddle position	FE	UCL eqn (saddle)	UCL eqn (hot-spot)
A	6.80	——	——
B	7.40	——	——
C	6.80	——	——
D	8.50	——	——
Chord ends fixed	3.69	4.34	4.10
IPB	Ratio of bending to membrane stress		
Crown position	FE	UCL eqn (crown)	UCL eqn (hot-spot)
E	4.63	——	——
F	20.00	——	——
G	4.63	——	——
H	4.80	——	——
Chord ends fixed	4.40	6.20	6.23

Table 2.7 Comparison of chord bending/membrane stresses obtained from FE analyses and parametric equations

OPB	Ratio of bending to membrane stress		
Saddle position	FE	UCL eqn (saddle)	UCL eqn (hot-spot)
A	3.71	3.10	2.68
B	3.72	3.10	2.68
C	3.13	3.10	2.68
D	3.11	3.10	2.68
Chord ends fixed	3.47	3.10	2.68
Axial	Ratio of bending to membrane stress		
Saddle position	FE	UCL eqn (saddle)	UCL eqn (hot-spot)
A	3.47	——	——
B	3.47	——	——
C	3.75	——	——
D	3.30	——	——
Chord ends fixed	2.88	2.70	2.64
IPB	Ratio of bending to membrane stress		
Crown position	FE	UCL eqn (crown)	UCL eqn (hot-spot)
E	4.53	——	——
F	4.53	——	——
G	5.35	——	——
H	3.60	——	——
Chord ends fixed	3.86	3.97	2.88

Table 2.8 Comparison of brace bending/membrane stresses obtained from FE analyses and parametric equations

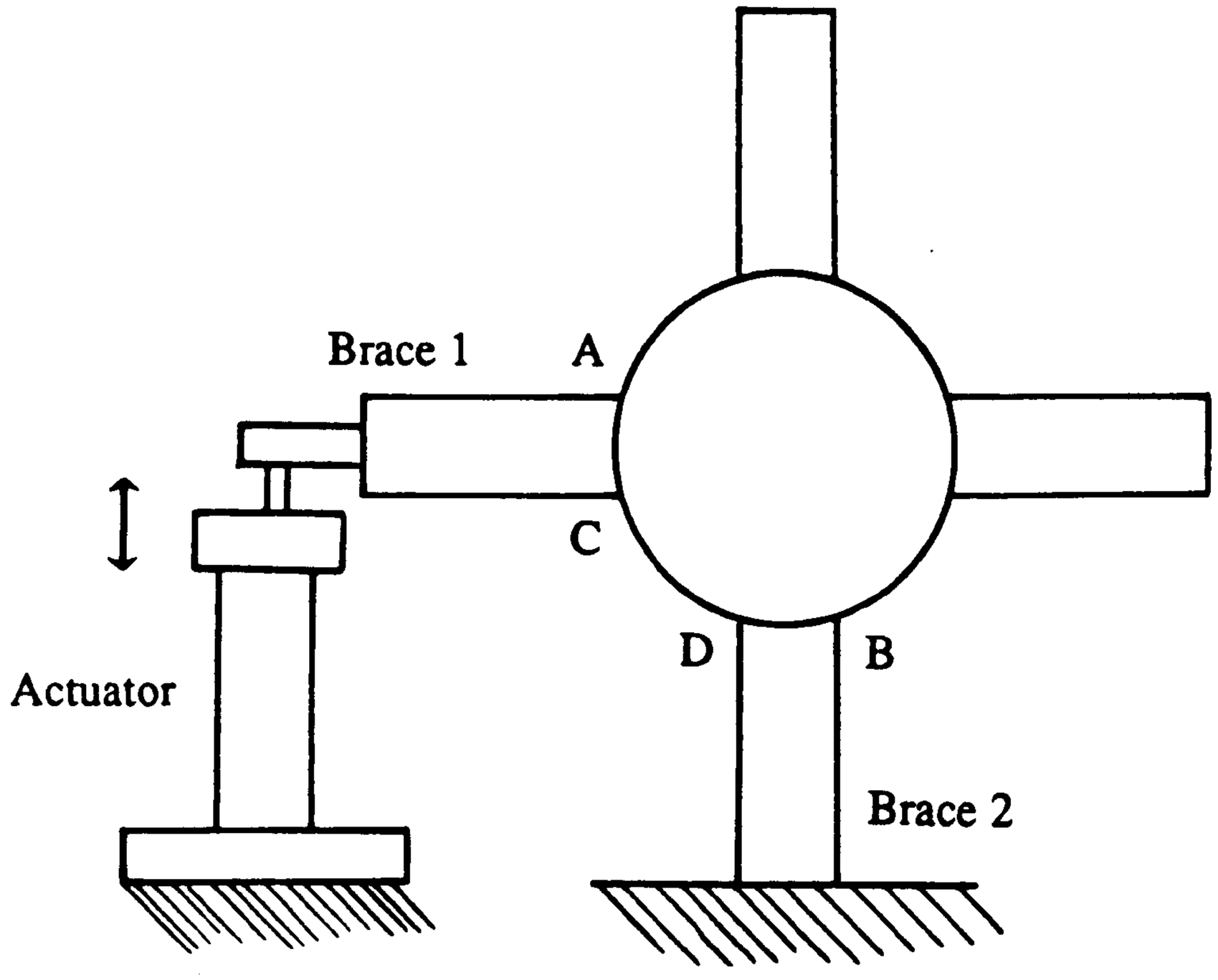

Figure 2.1 Schematic of experimental testing arrangement of the steel joints. A B C and D are the four saddle positions

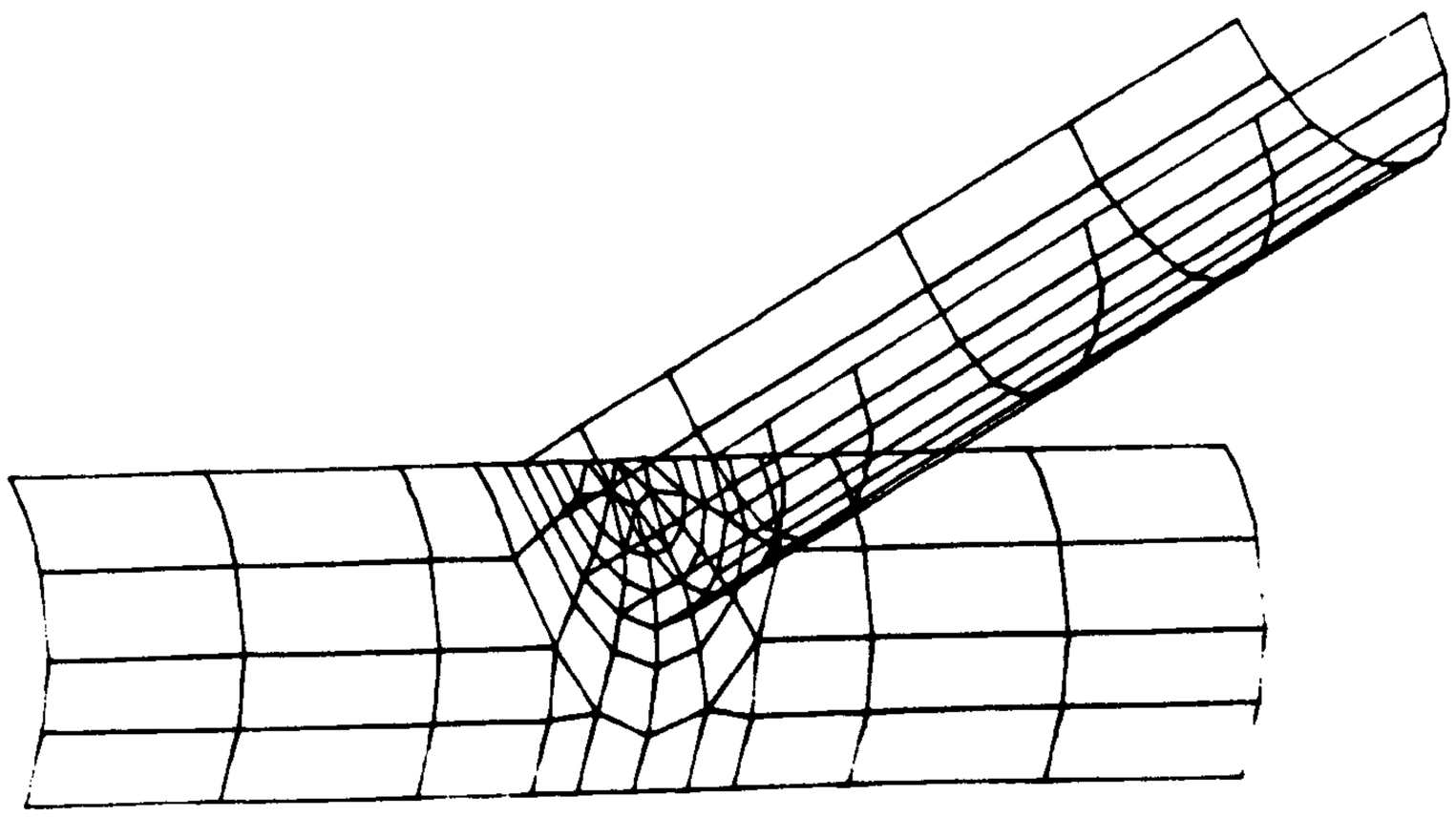

Figure 2.2 One-eighth part of the tubular joint mesh

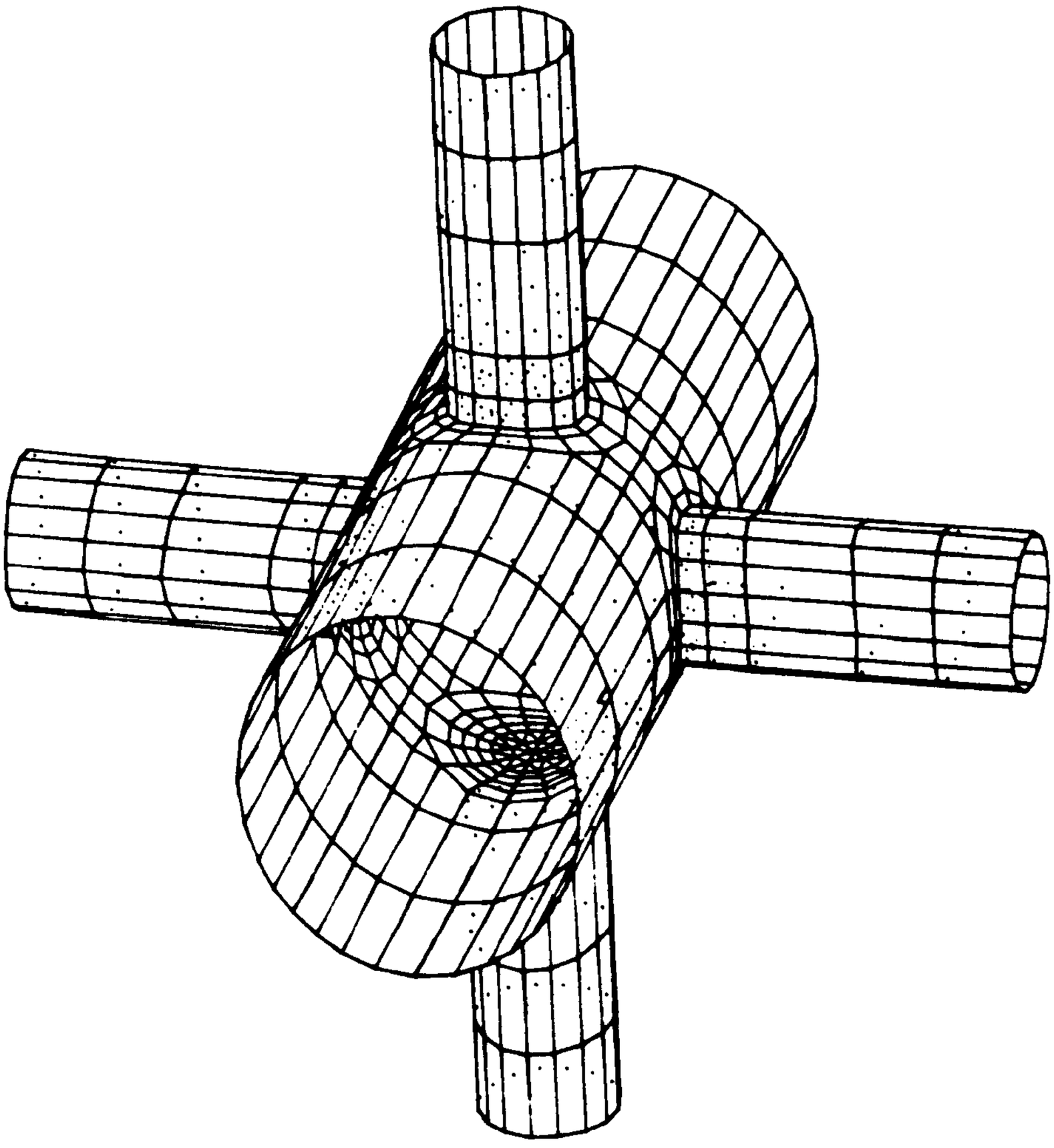

Figure 2.3 **Finite element mesh used for analysis of multi-planar joint**

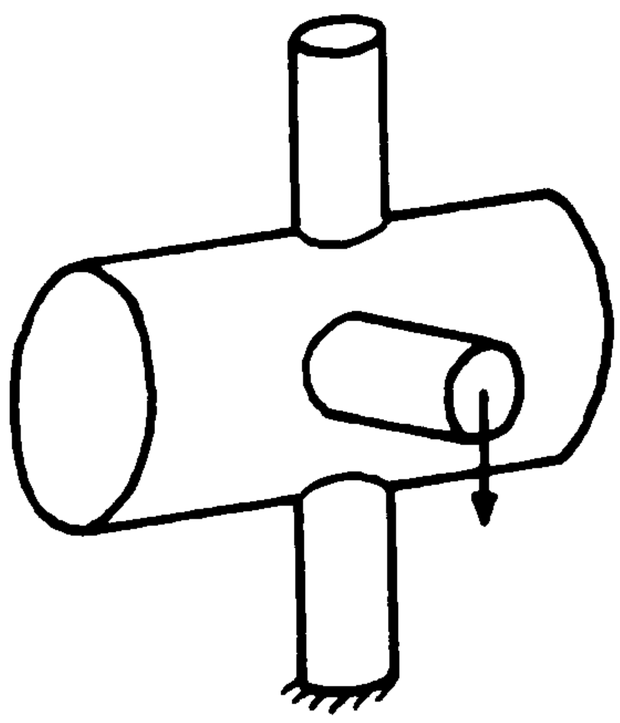

OPB

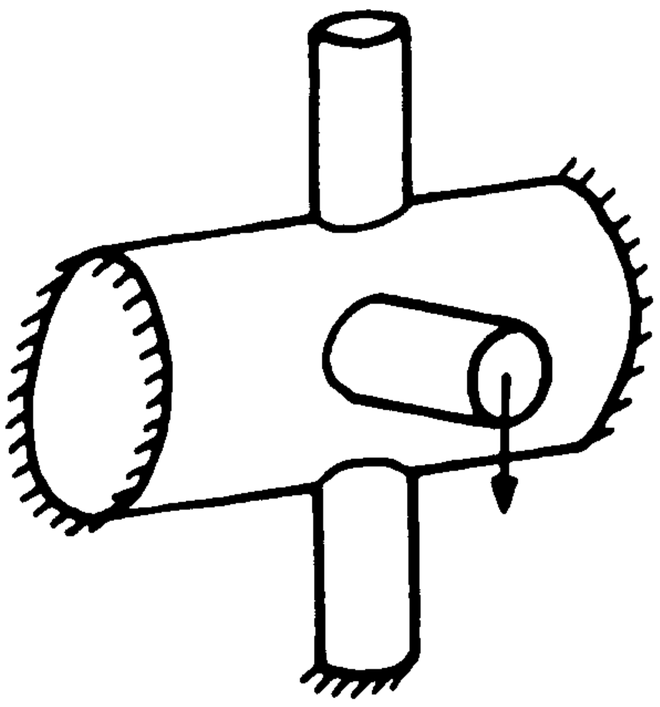

(a)

(b)

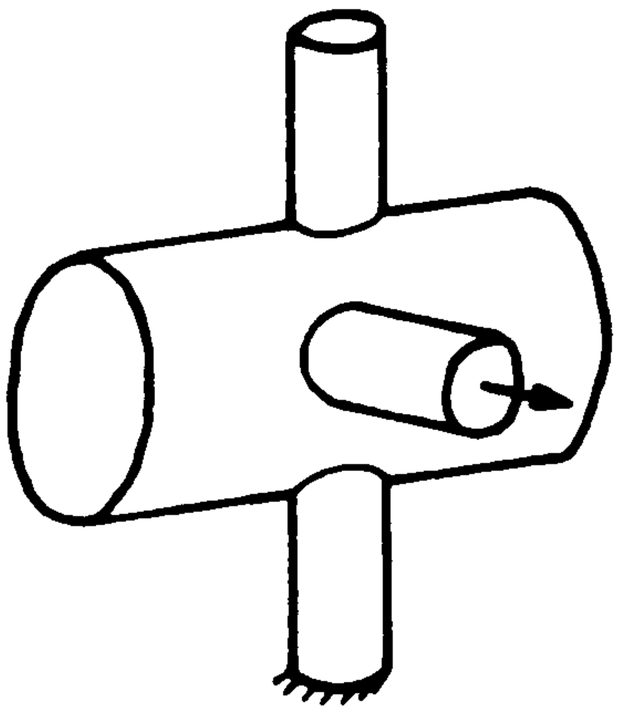

Axial

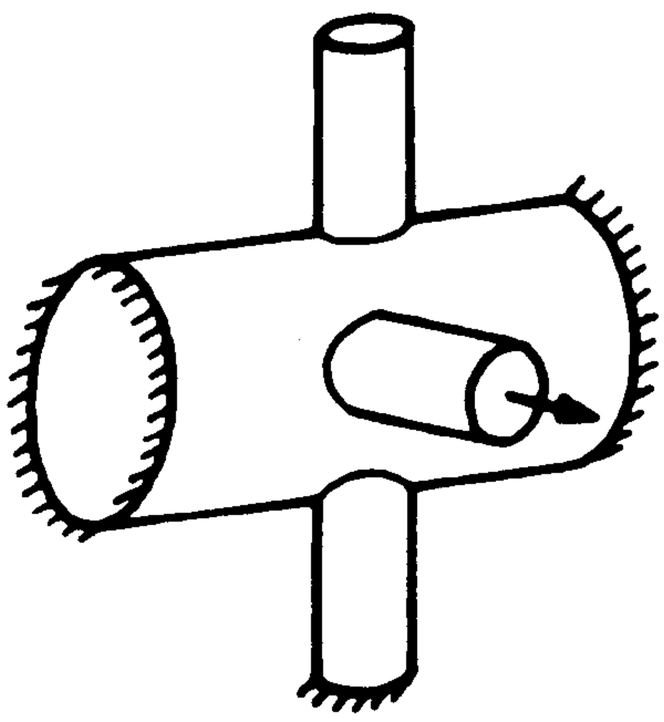

(c)

(d)

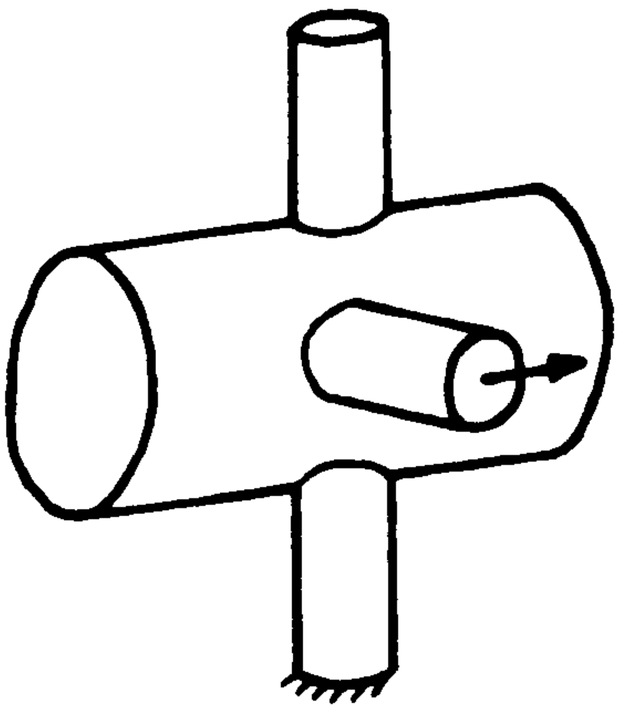

IPB

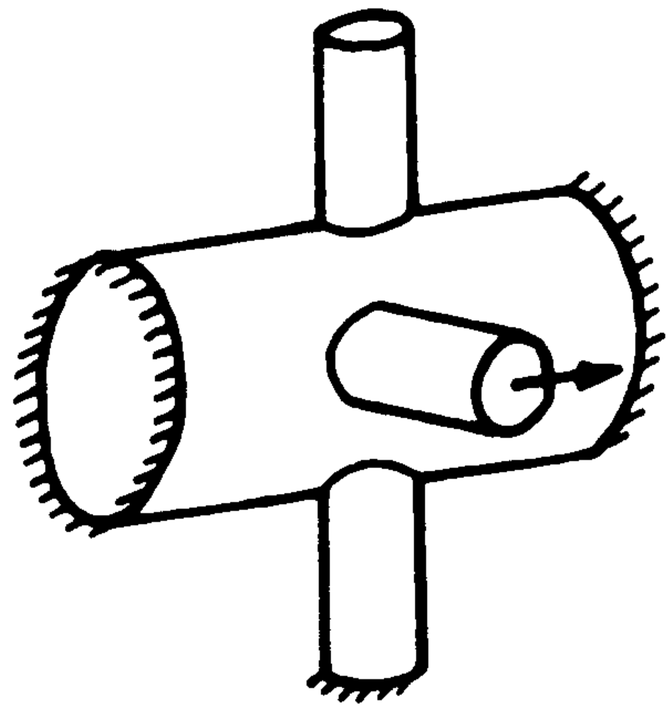

(e)

(f)

Figure 2.4 Applied loads and fixities for FE analyses. (a) OPB (Chord ends free); (b) OPB (Chord ends fixed); (c) Axial (Free); (d) Axial (Fixed); (e) IPB (Free); (f) IPB (Fixed)

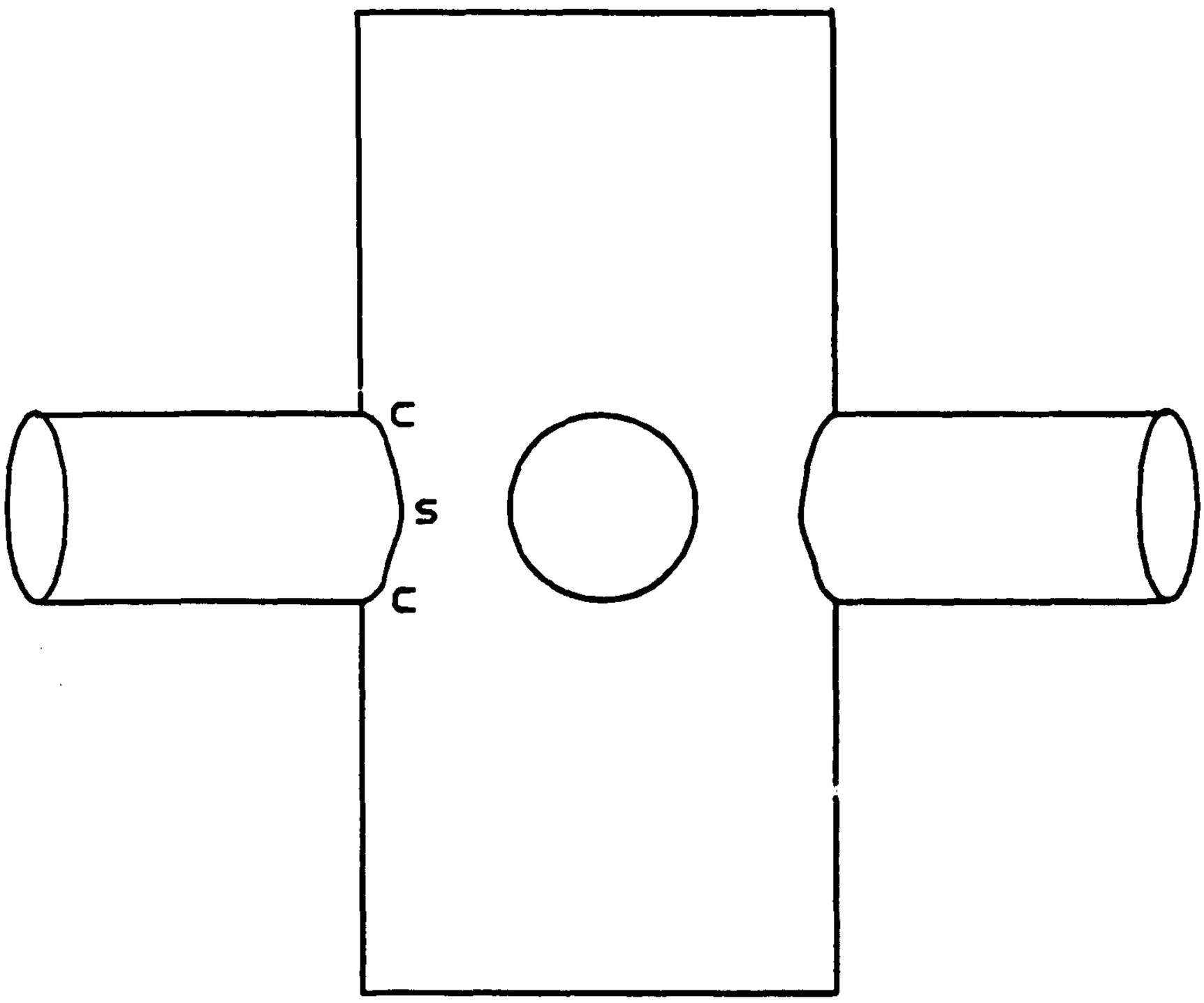

c=crown
s=saddle

JOINT DIMENSIONS

Chord dia. = 800mm
Chord length = 2000mm
Brace dia. = 324mm
Brace length = 750mm

Figure 2.5 Schematic of tubular joint (dimensions in mm)

Highlands Fabricators Ltd

MACROGRAPH AND HARDNESS SURVEY REPORT

Procedure No. DP 16/1B	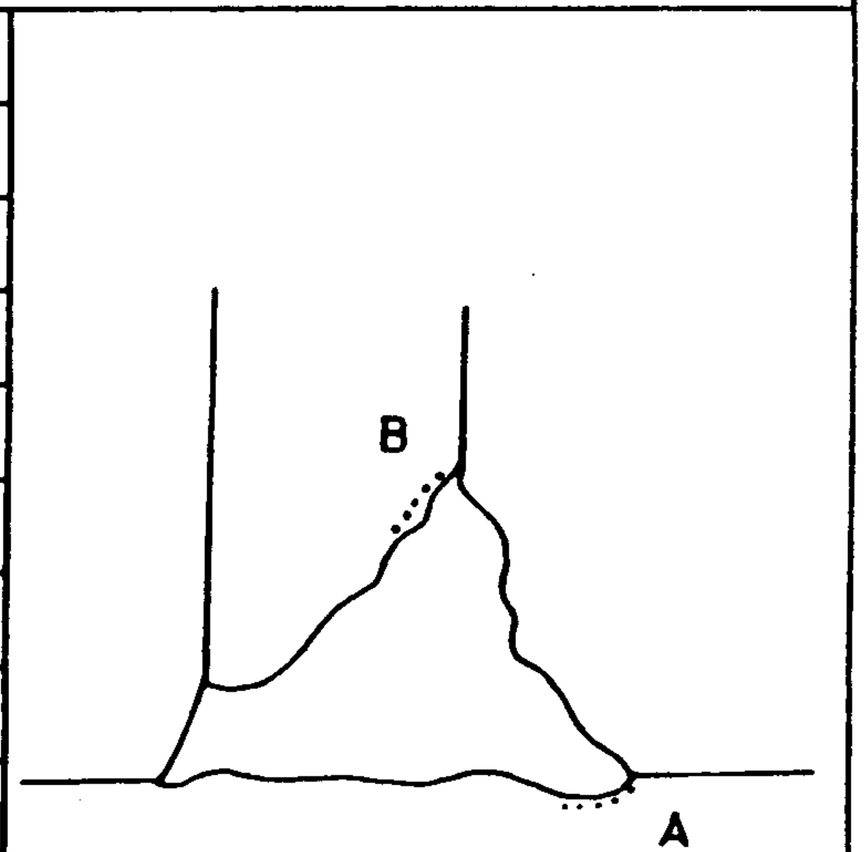
Date 11.6.86	
Indenter Avery-Denison	
Welding Process M.M.A	
Test Code B.S 427 Part 1	
Lab Number 231	
Contract UCL	
Test Load Kg 10	
Max. Hardness Weld	
Max. Hardness Haz 287 Hv	

Location	Hardness	Location	Hardness
1mm	287		
2mm	247		
3mm	264		
4mm	249		
5mm	247		
1mm	281		
2mm	287		
3mm	237		
4mm	243		
5mm	242		

Tested by: G Graham	Witnessed by:	Witnessed by:

Highlands Fabricators Ltd

MACROGRAPH AND HARDNESS SURVEY REPORT

Procedure No. DP 16/2	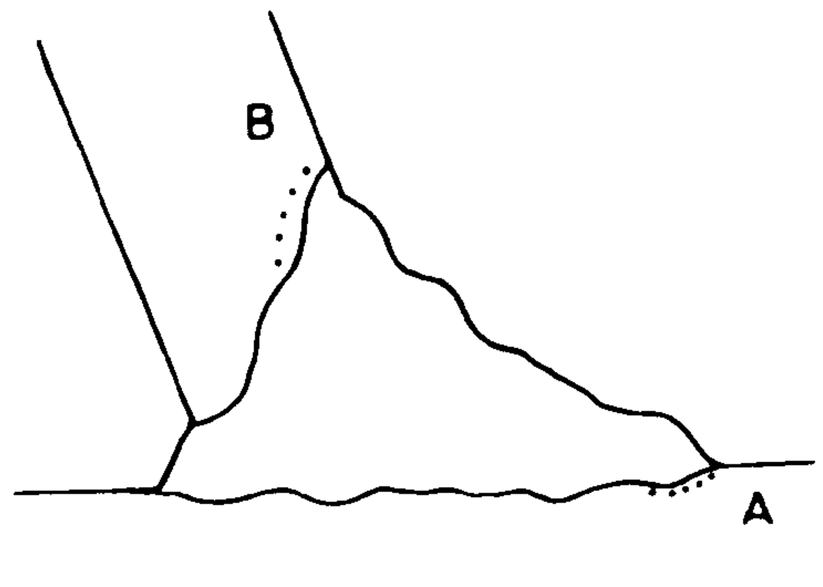
Date 10.6.86	
Indenter Avery-Denison	
Welding Process M.M.A	
Test Code B.S 427 Part 1	
Lab Number 231	
Contract UCL	
Test Load Kg 10	
Max. Hardness Weld	
Max. Hardness Haz 311 Hv	

Location	Hardness	Location	Hardness
1mm	281		
2mm	270		
3mm	279		
4mm	272		
5mm	268		
1mm	302		
2mm	311		
3mm	287		
4mm	240		
5mm	245		

Tested by: G Graham	Witnessed by:	Witnessed by:

Figure 2.6 Schematics of weld profiles and hardness results from trials for CWP conducted by the fabricators

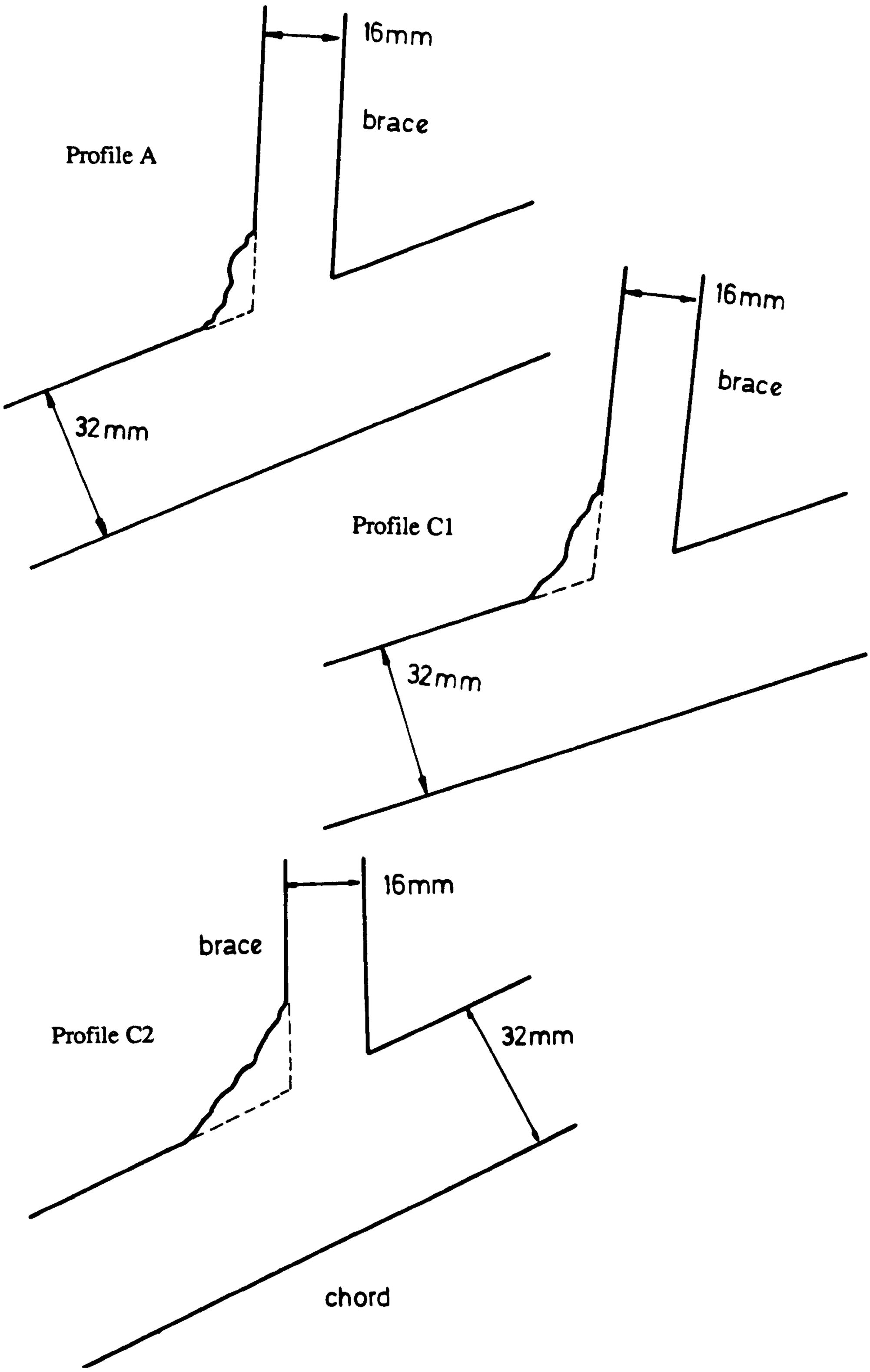

Figure 2.7 Schematic of weld profiles. (a) AWS (Joint 2); (b) CWP C1 (Joint 1) and (c) CWP C2 (joint 2)

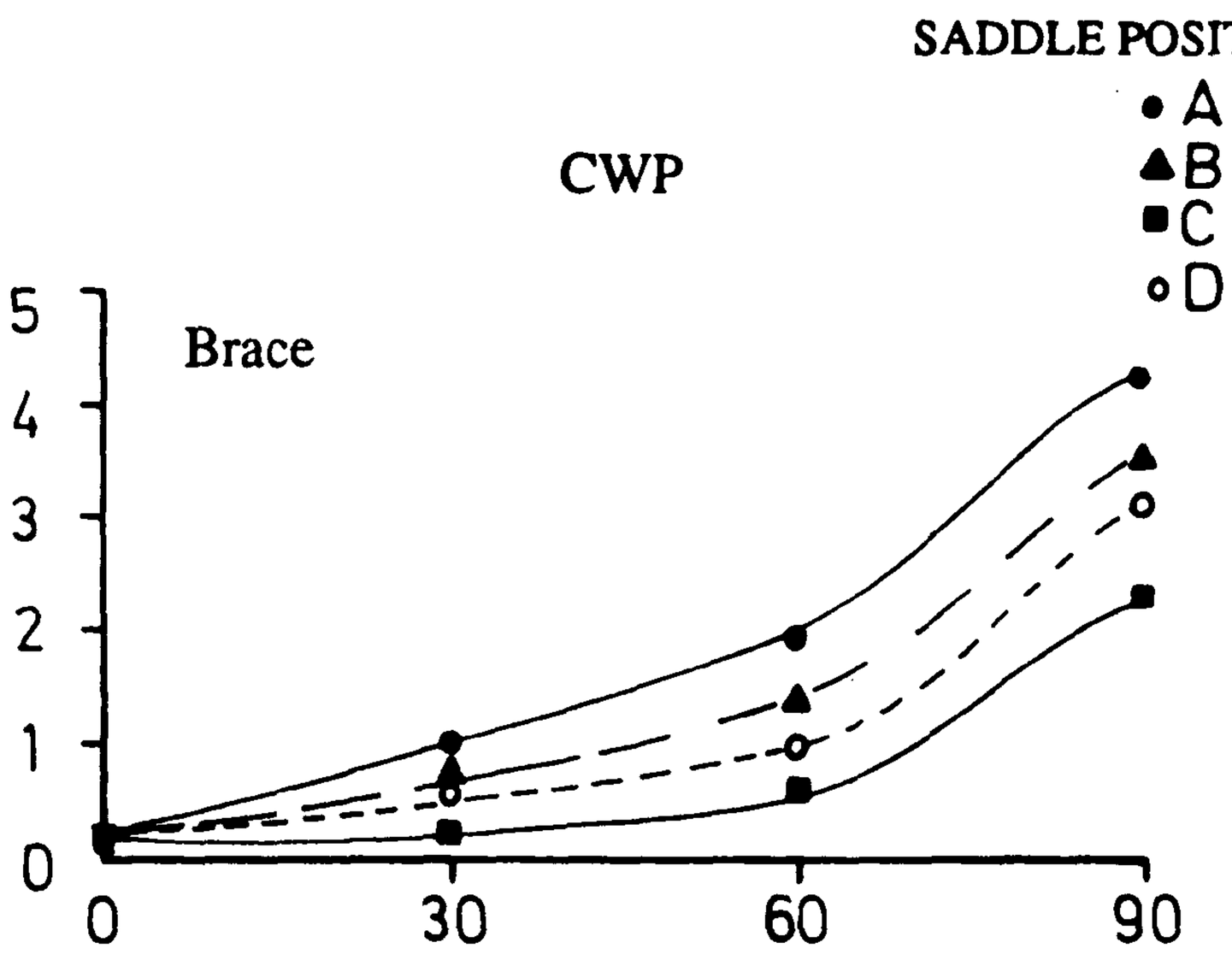

Figure 2.8 Stress distributions around brace/chord intersection from steel model tests. CWP (C1-X)

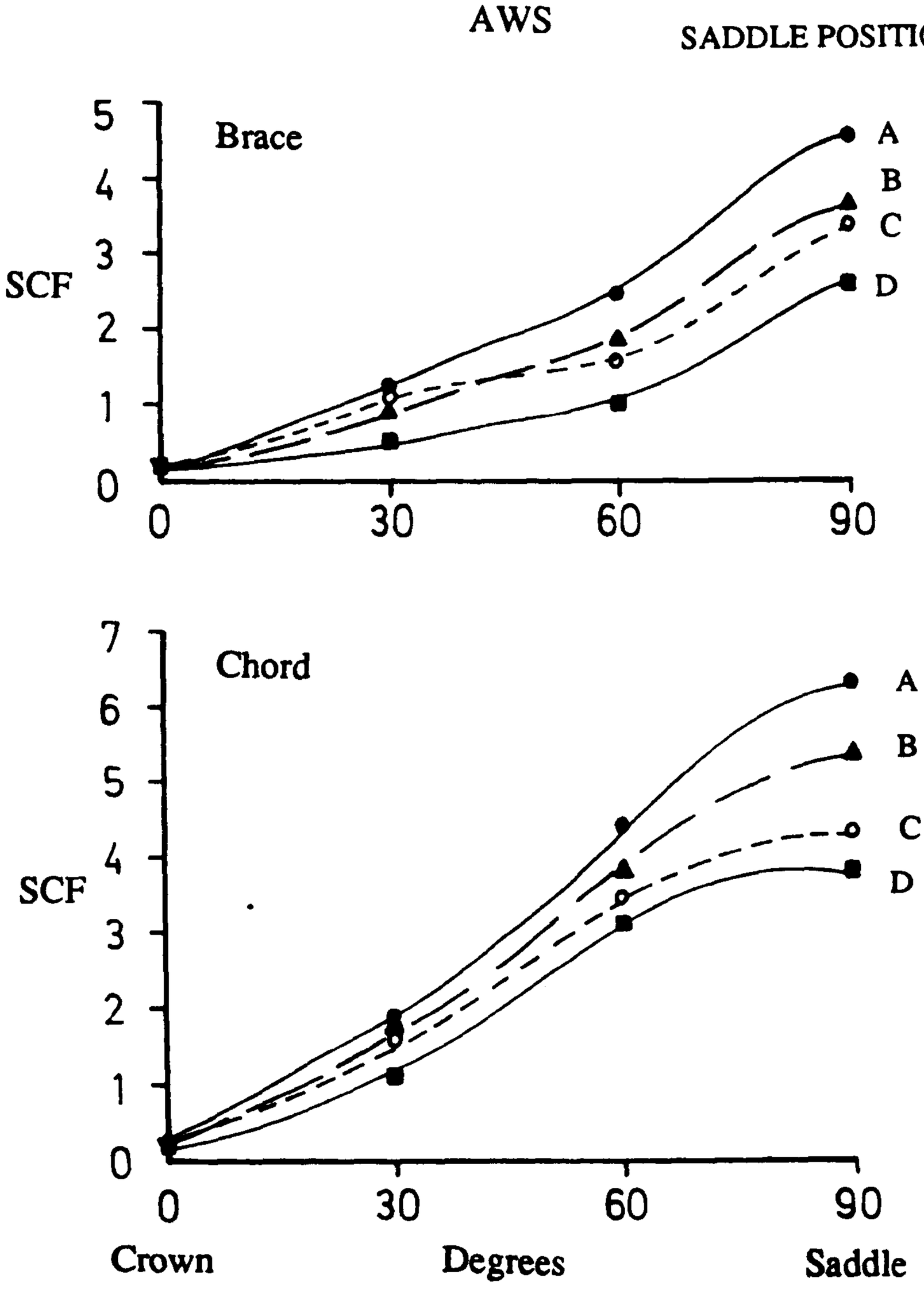

Figure 2.9 Stress distributions around brace/chord intersection from steel model tests. AWS (A-Y)

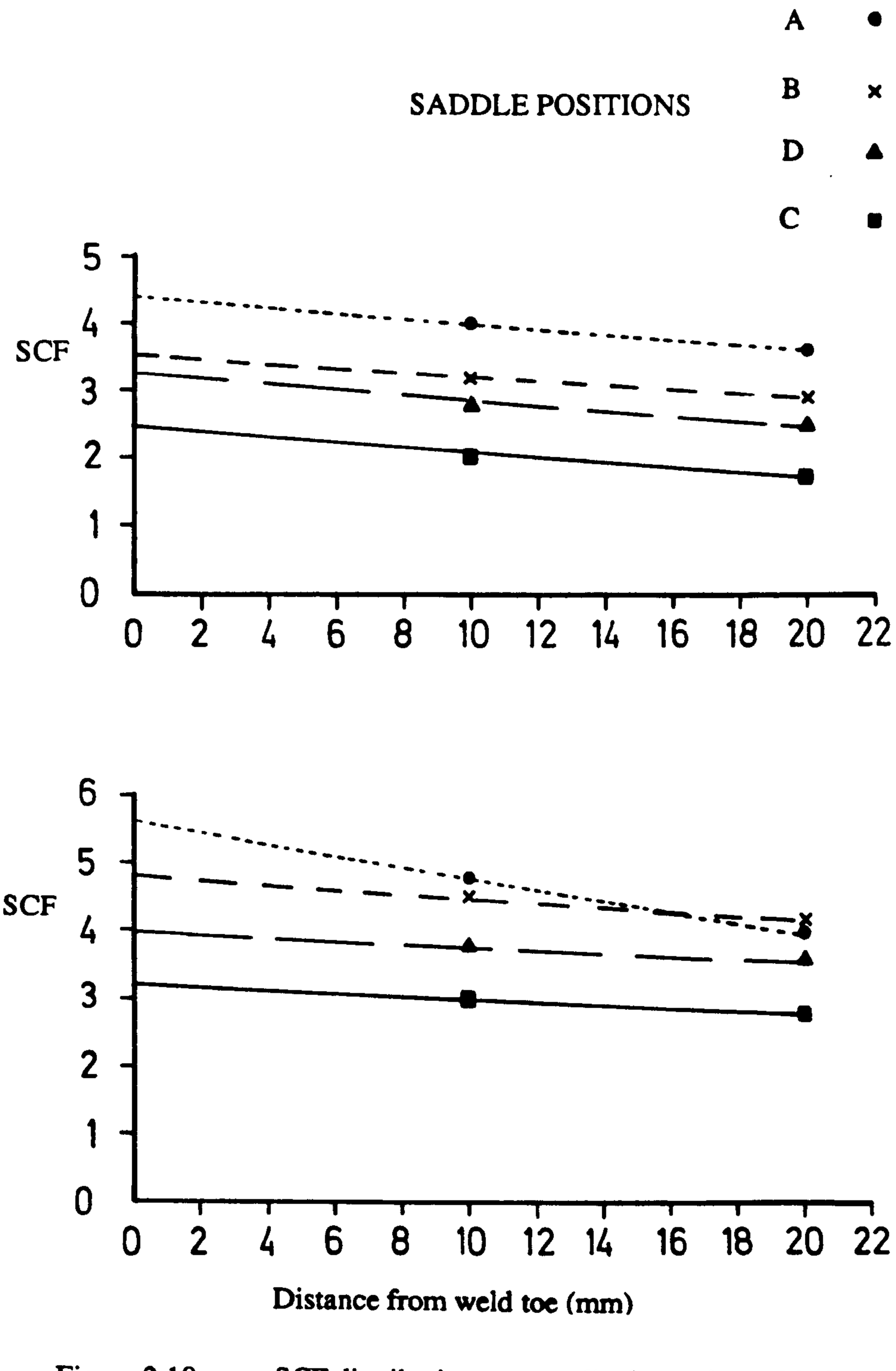

Figure 2.10 SCF distributions perpendicular to the weld. C1-X

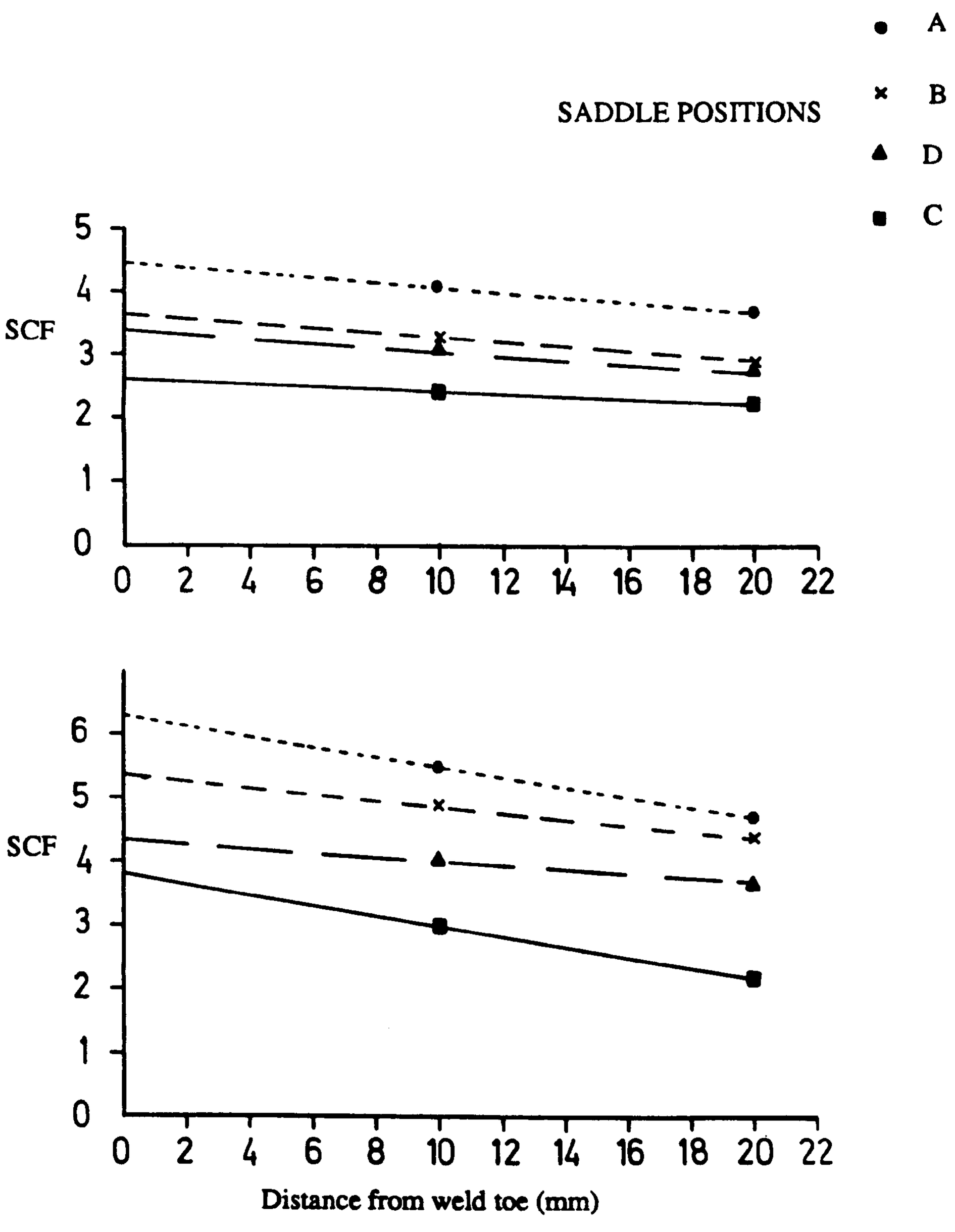

Figure 2.11 SCF distributions perpendicular to the weld. A-Y

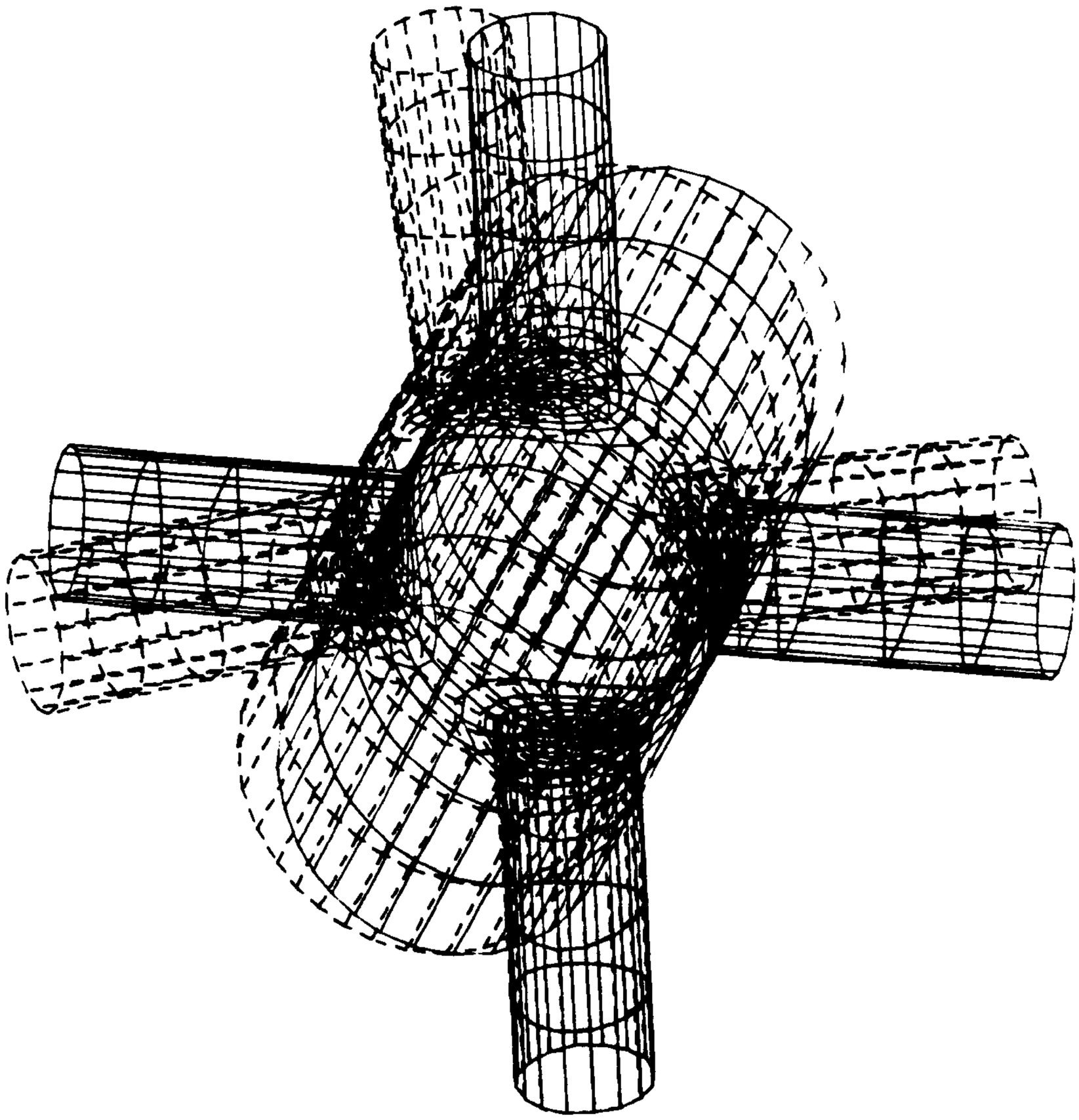

Figure 2.12 Line drawings showing the deformed mesh superimposed upon the unloaded mesh (rotation 60 ° , 60 ° , 60 °). OPB loading

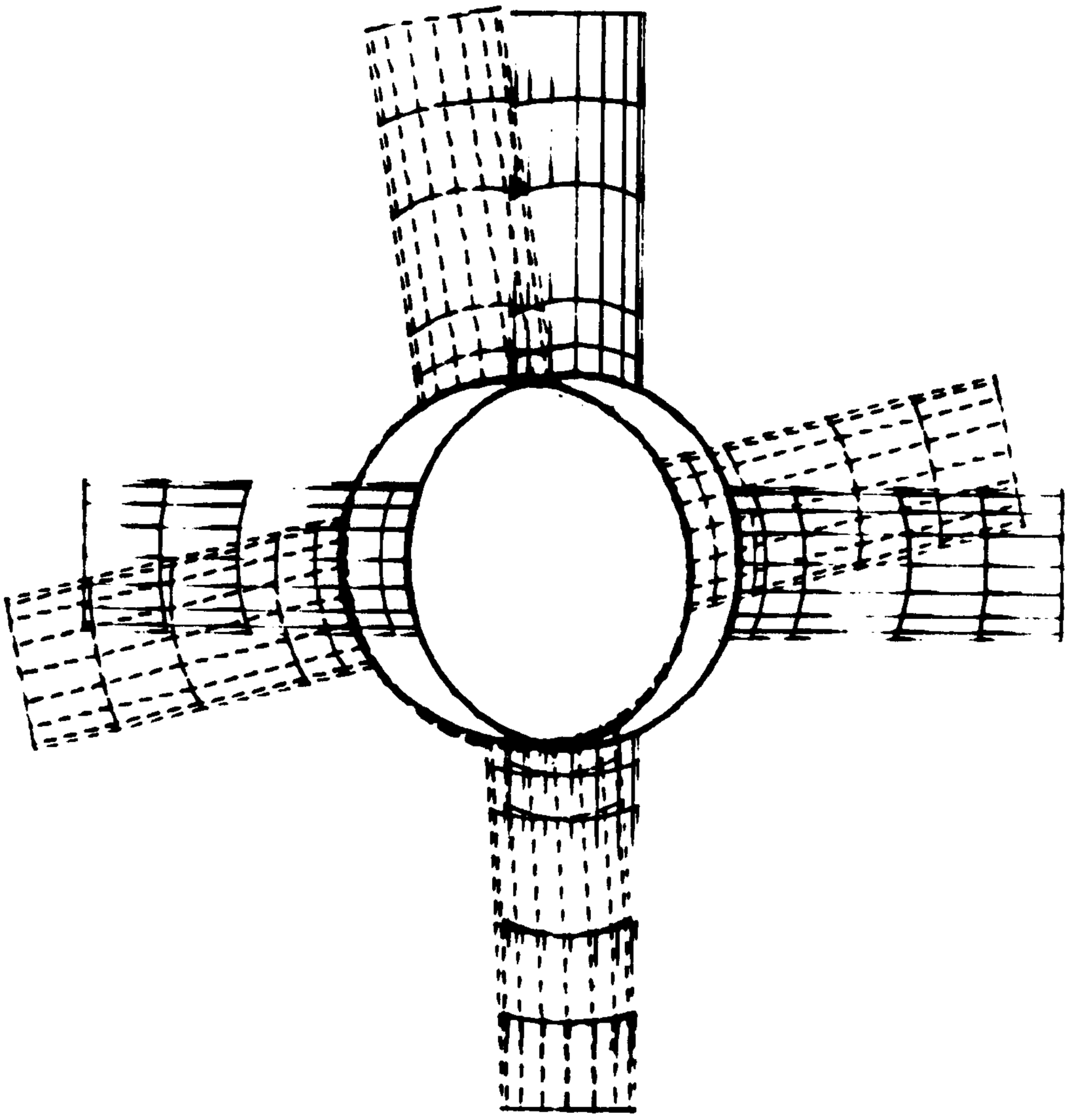

Figure 2.13 Line drawings showing the deformed mesh superimposed upon the unloaded mesh (rotation 0 ° , 90 ° , 0 °). OPB loading

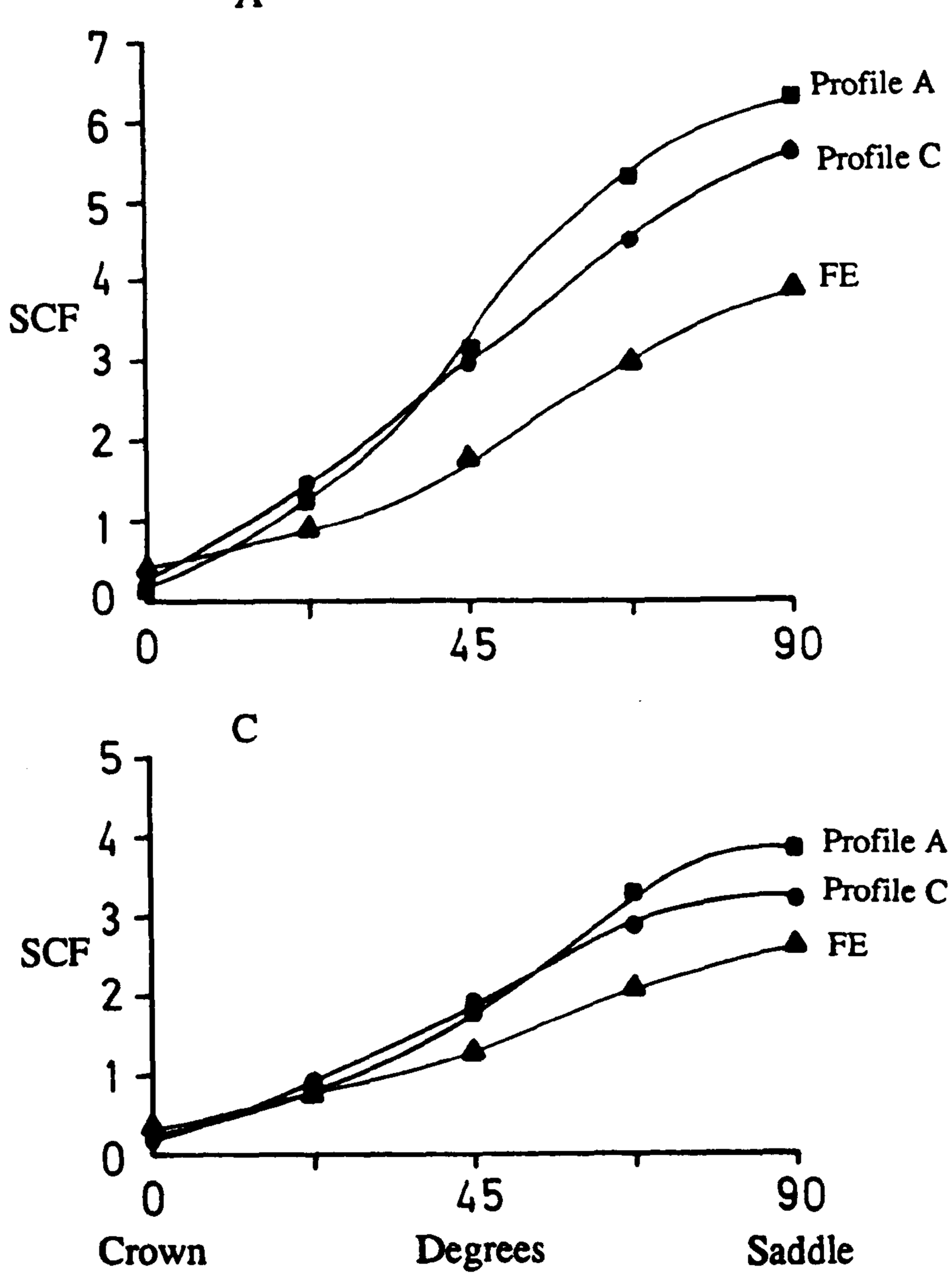

Figure 2.14 Comparison of AWS, CWP and FE results for stress around the intersection (Position A & C)

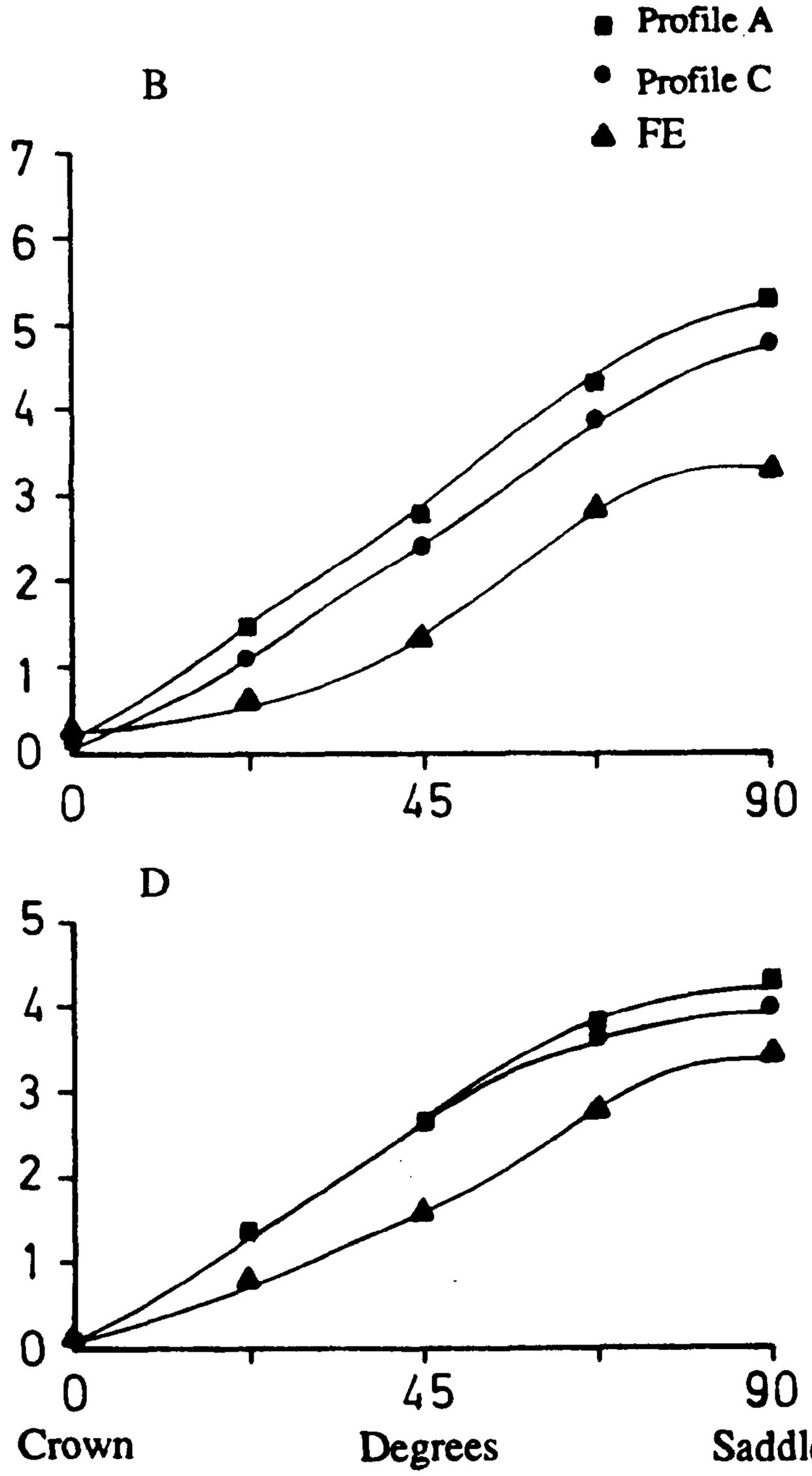

Figure 2.15 Comparison of AWS, CWP and FE results for stress around the intersection (Position B & D)

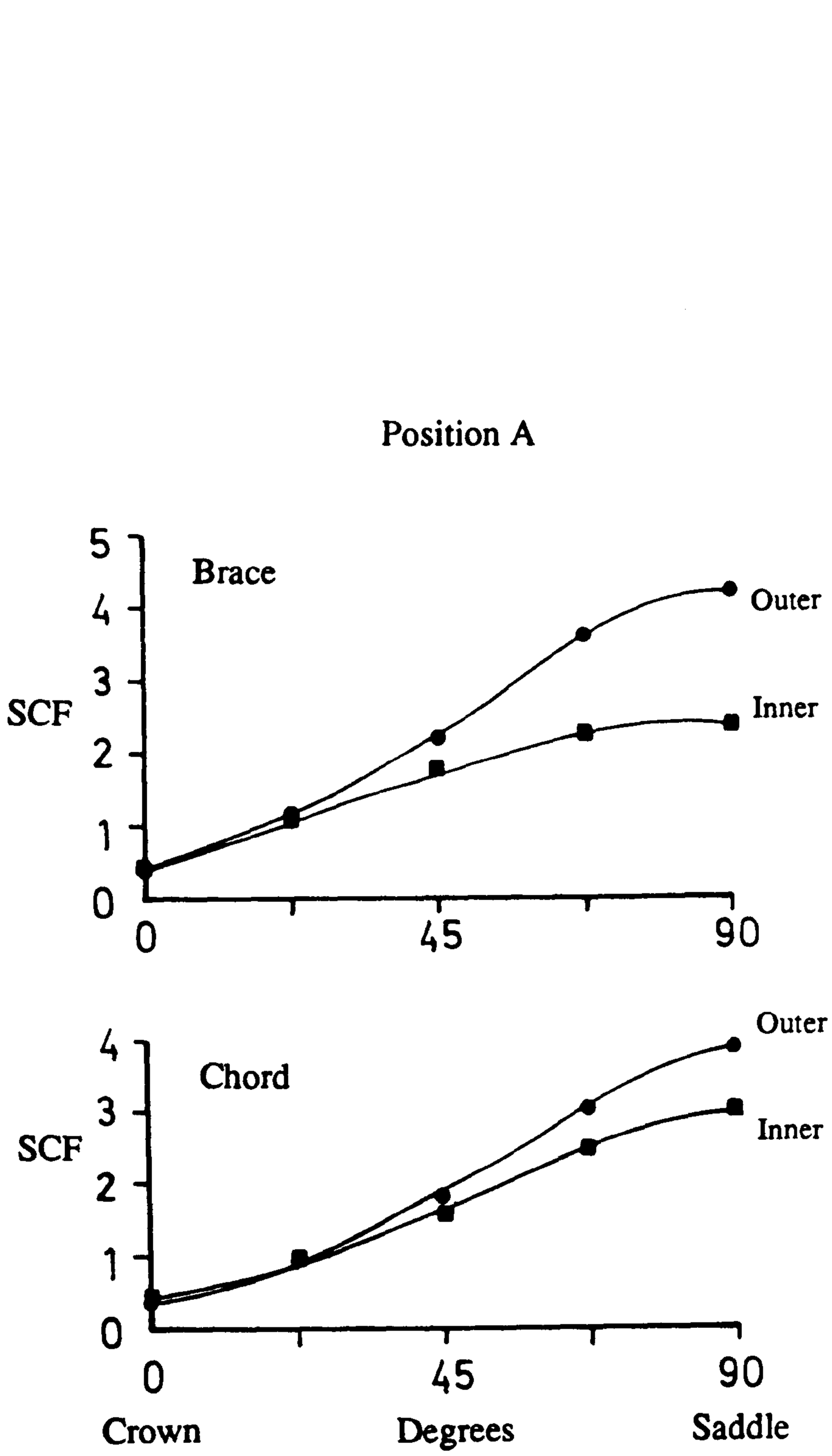

Figure 2.16 Stresses at the outer and inner surfaces of brace and chord predicted by FE analysis for OPB. Position A

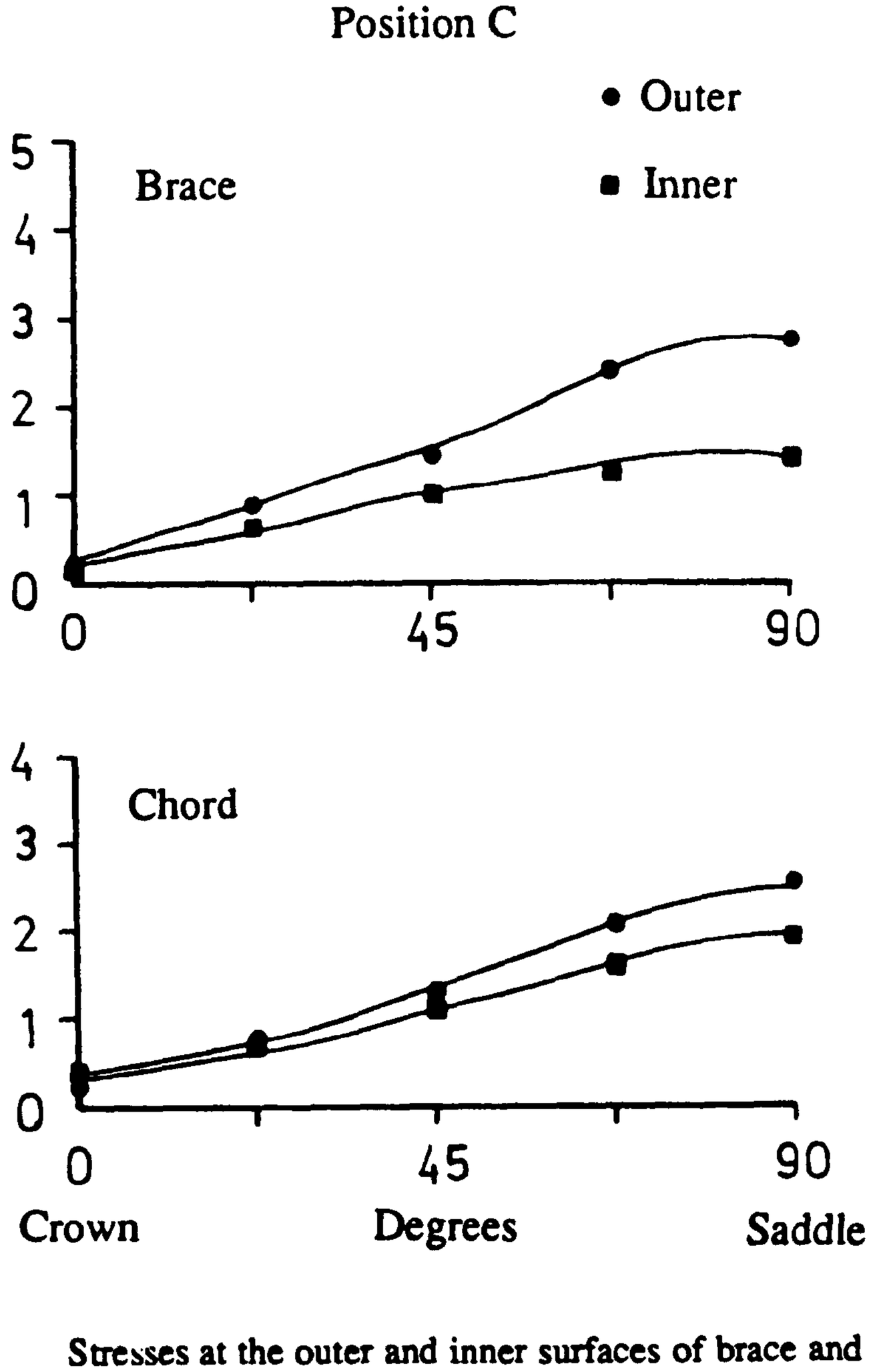

Figure 2.17 Stresses at the outer and inner surfaces of brace and chord predicted by FE analysis for OPB. Position C

D

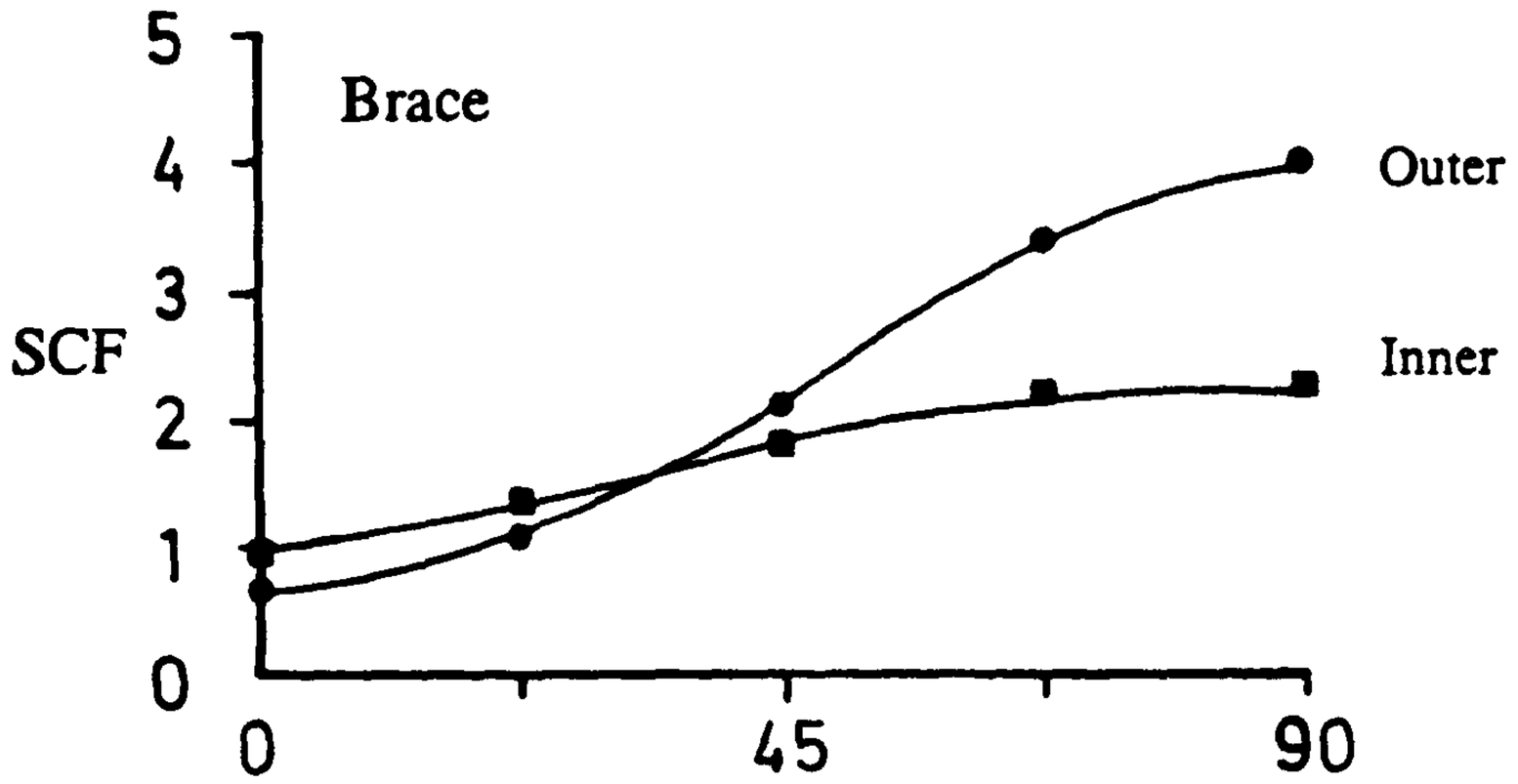

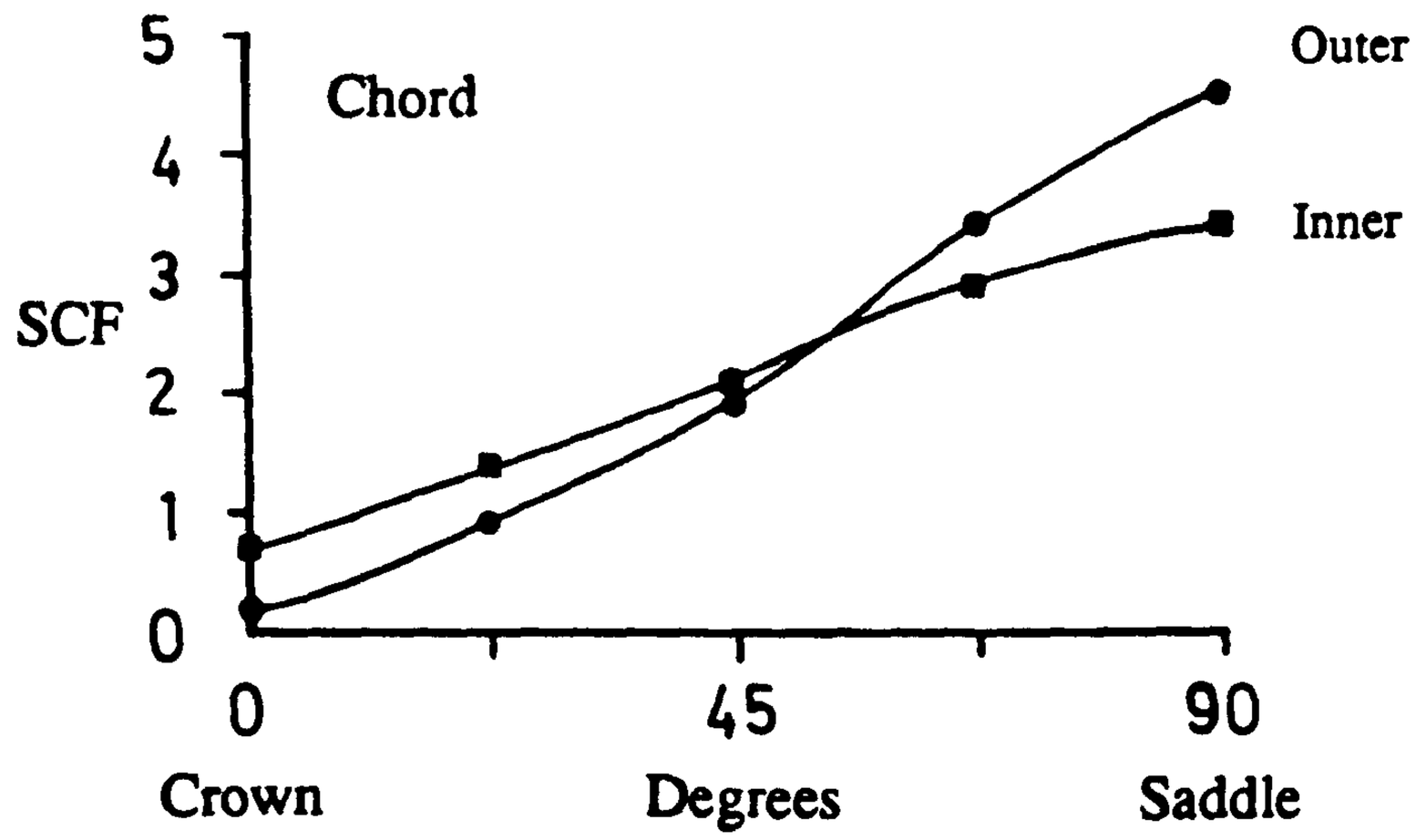

Figure 2.18 Stresses at the outer and inner surfaces of brace and chord predicted by FE analysis for OPB. Position D

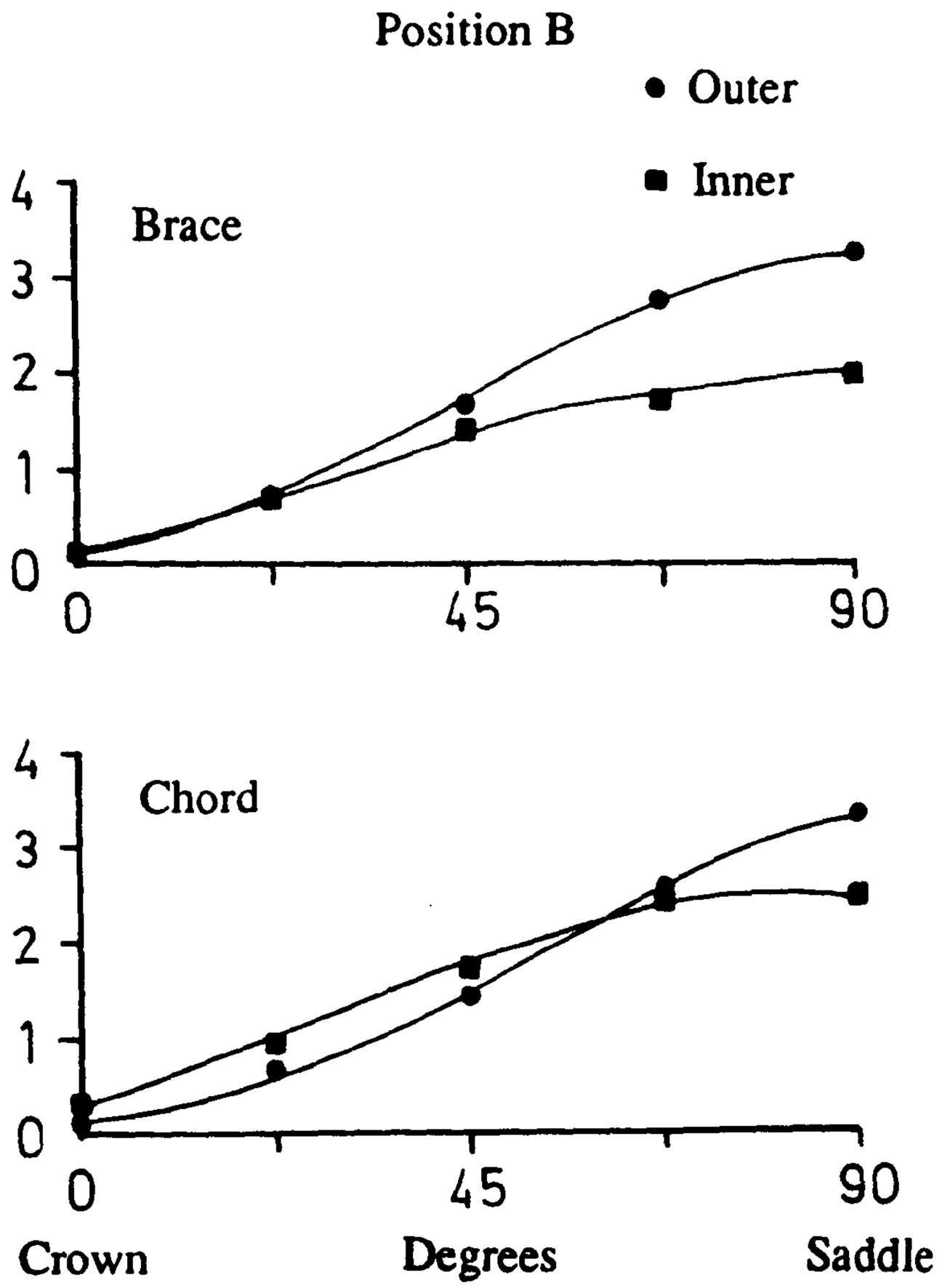

Figure 2.19 Stresses at the outer and inner surfaces of brace and chord predicted by FE analysis for OPB. Position B

Position A - Chord ends fixed

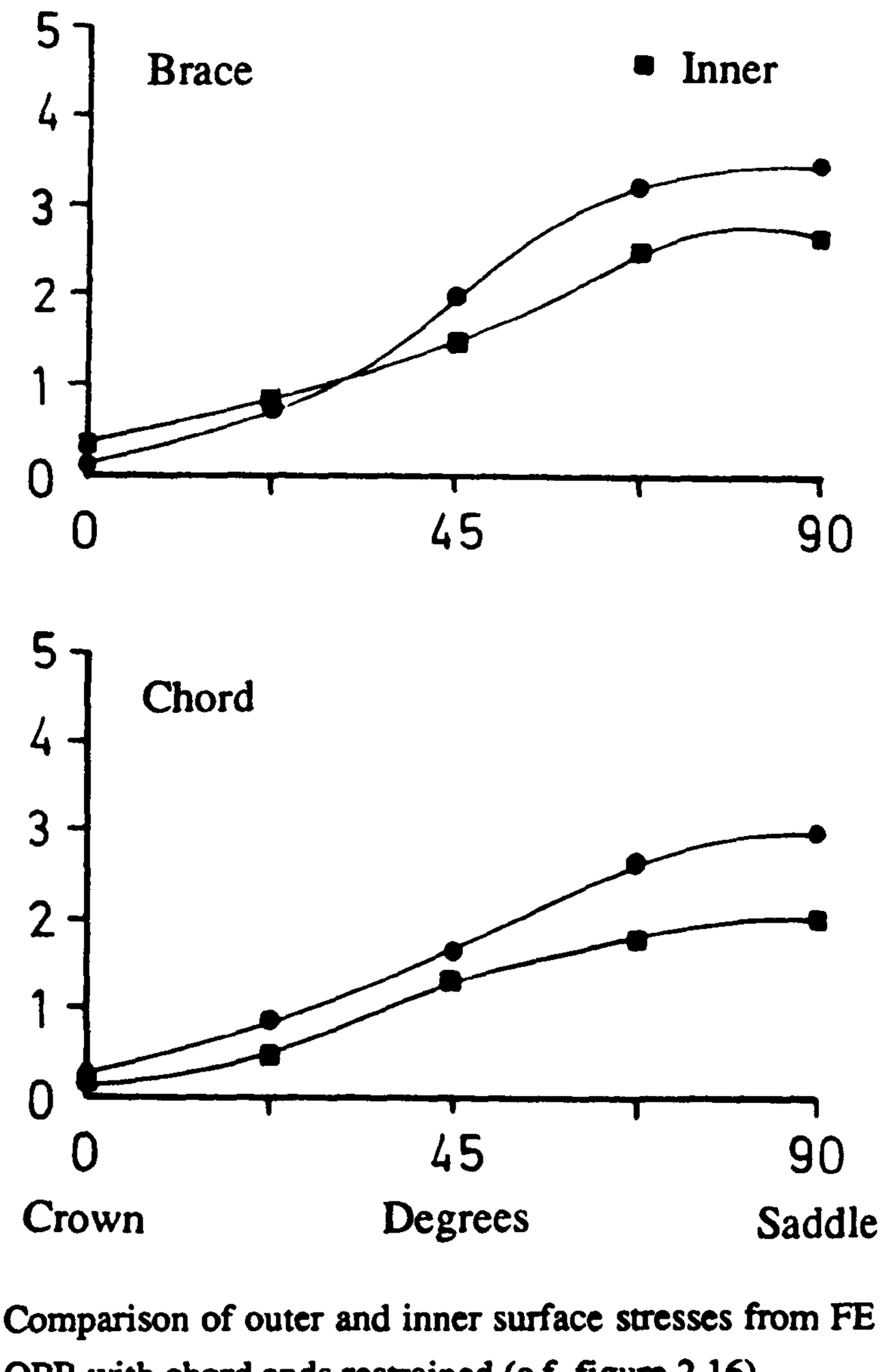

Figure 2.20 Comparison of outer and inner surface stresses from FE analysis for OPB with chord ends restrained (c.f. figure 2.16)

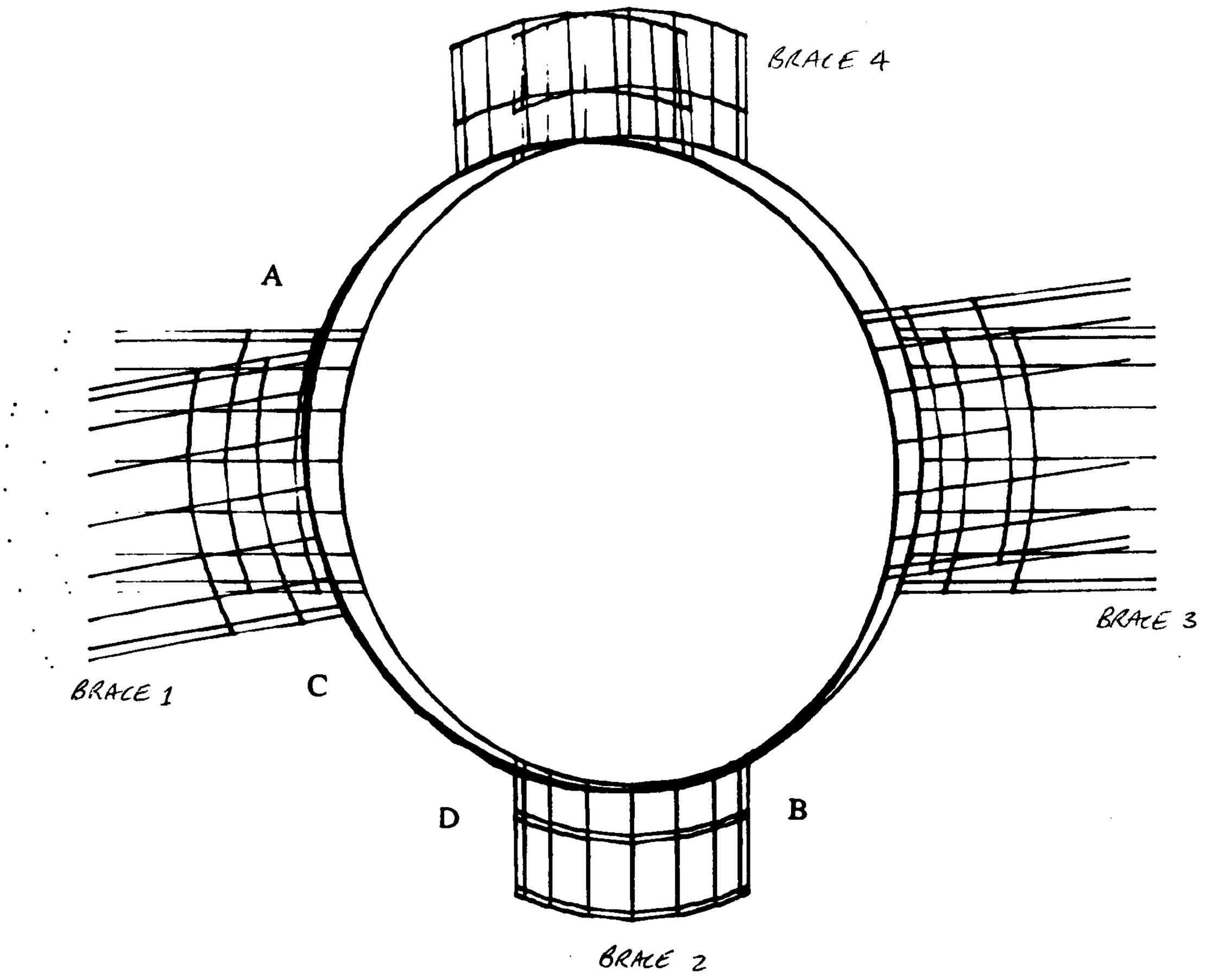

Figure 2.21 Line drawings of the deformed chord wall superimposed upon the undeformed wall (rotation 0°, 90°, 0°) OPB

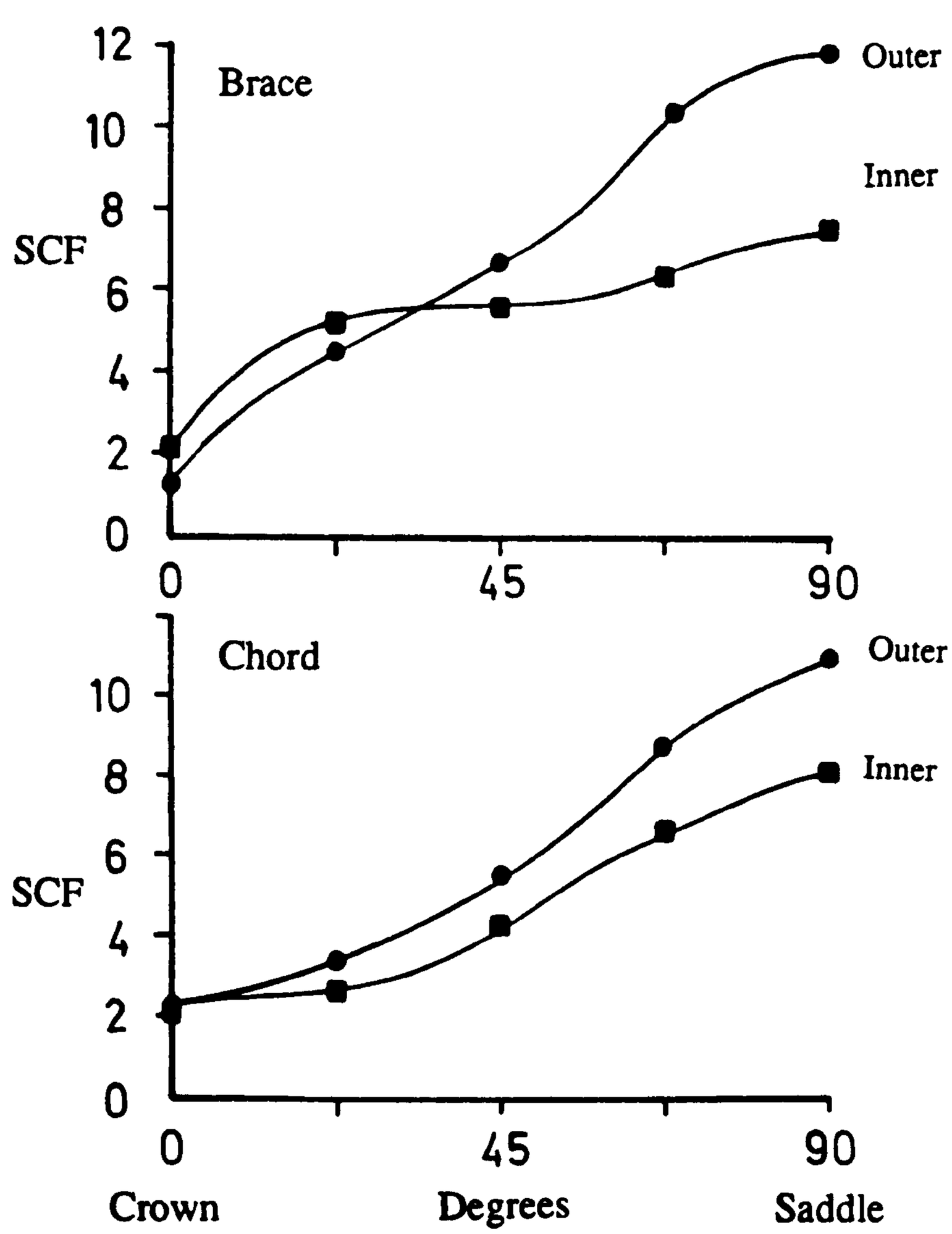

Figure 2.22 Stresses at the outer and inner surfaces of brace and chord predicted by FE analysis for axial loading. Distribution around Positions A and C (Symmetry)

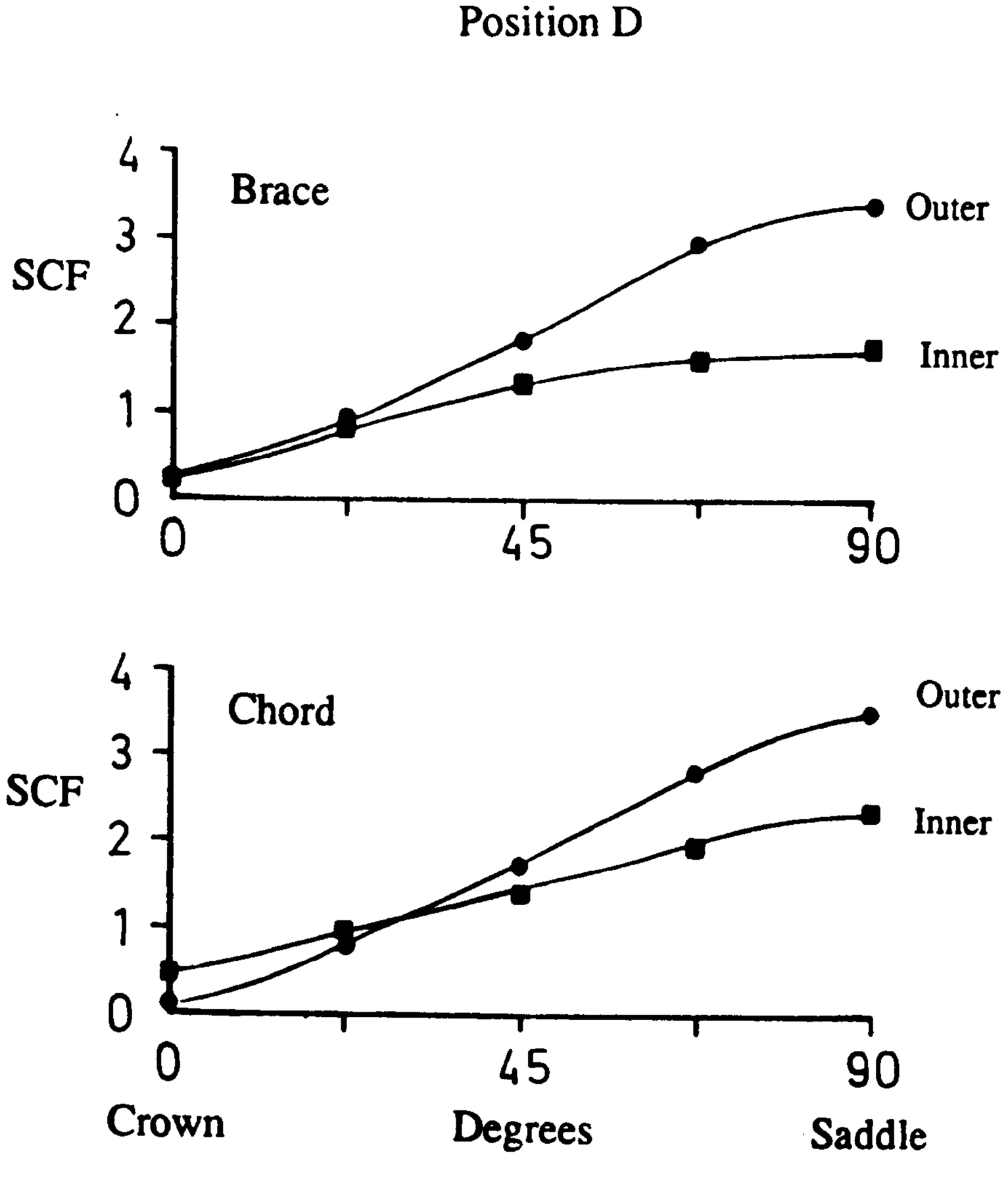

Figure 2.23 Stresses at the outer and inner surfaces of brace and chord predicted by FE analysis for axial loading. Distribution around Position D

B

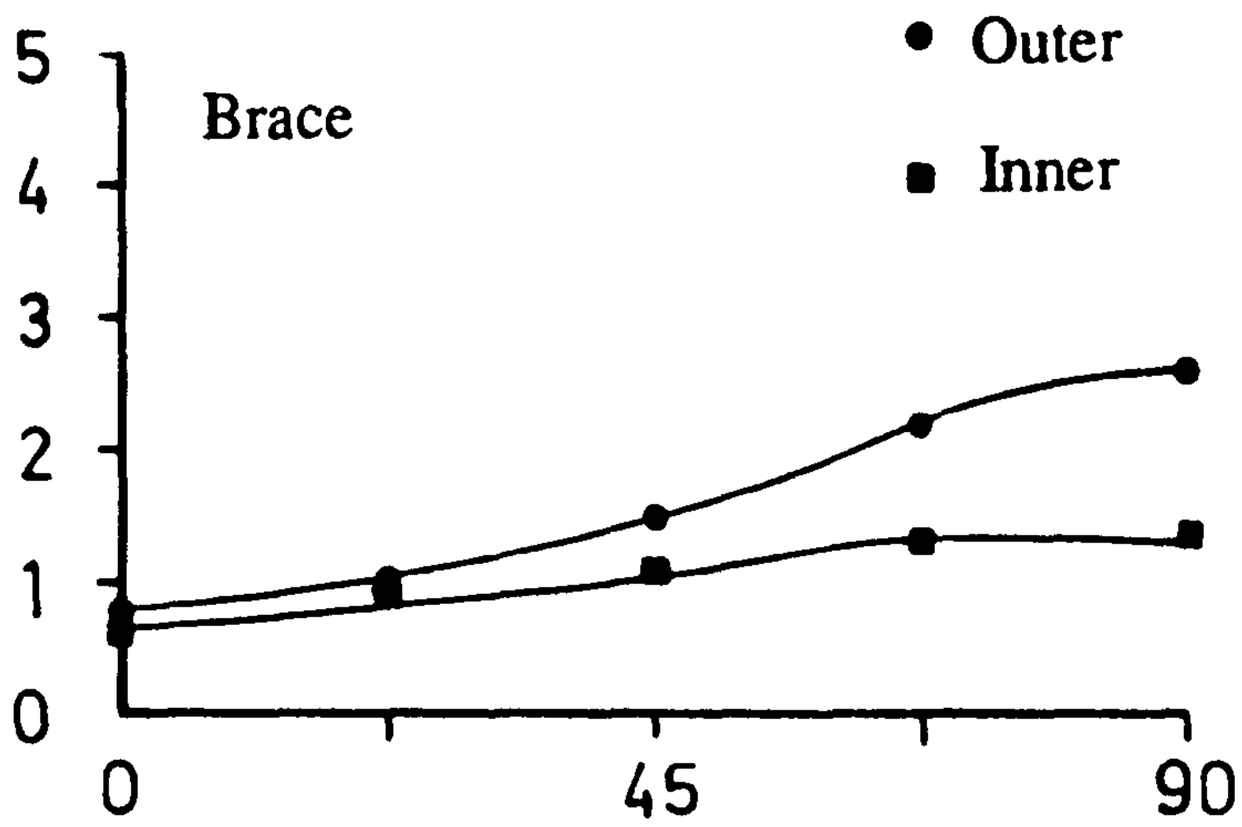

Figure 2.24 Stresses at the outer and inner surfaces of brace and chord predicted by FE analysis for axial loading. Distribution around Position B

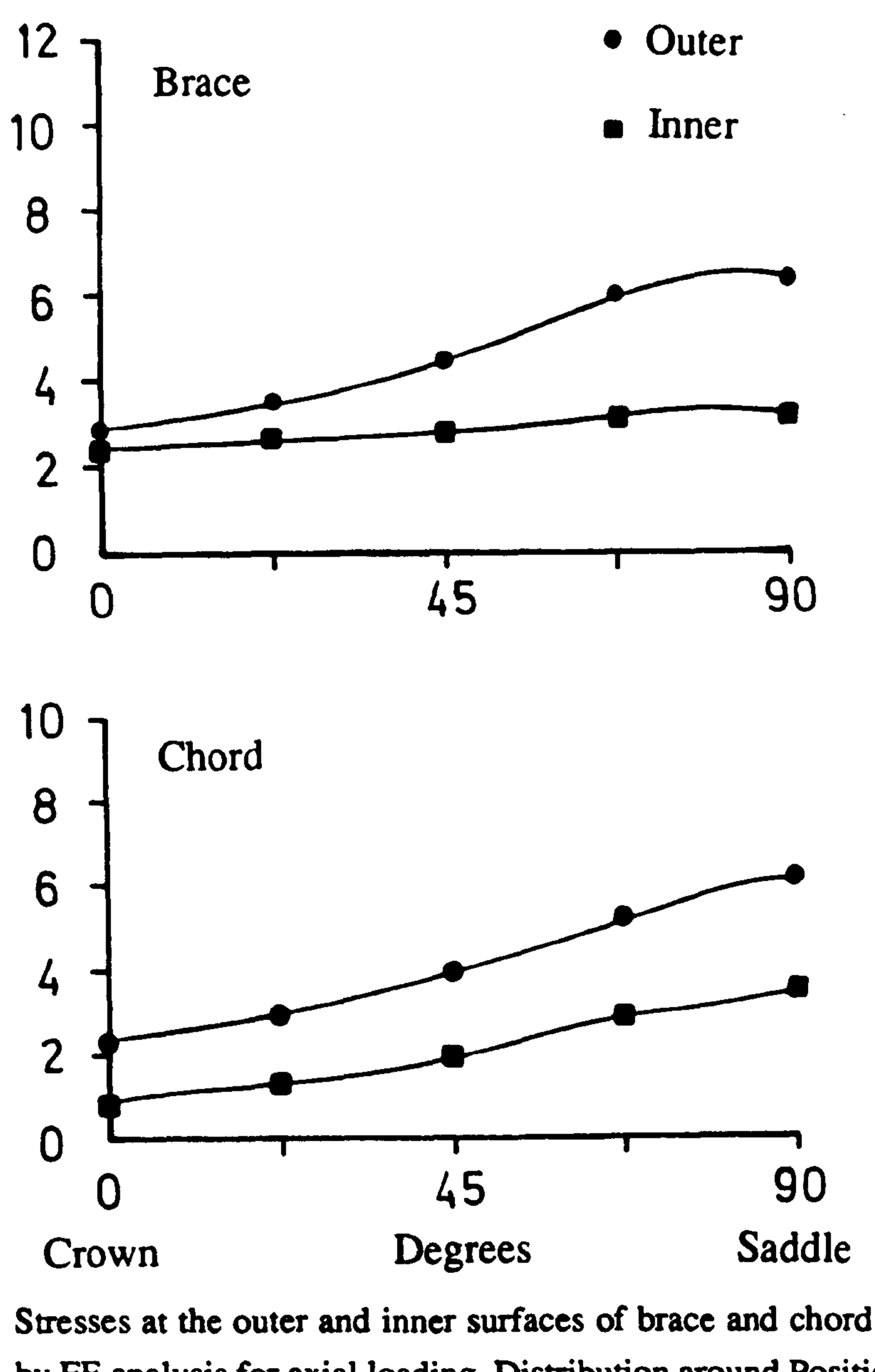

Figure 2.25 Stresses at the outer and inner surfaces of brace and chord predicted by FE analysis for axial loading. Distribution around Positions A and C (Chord ends restrained)

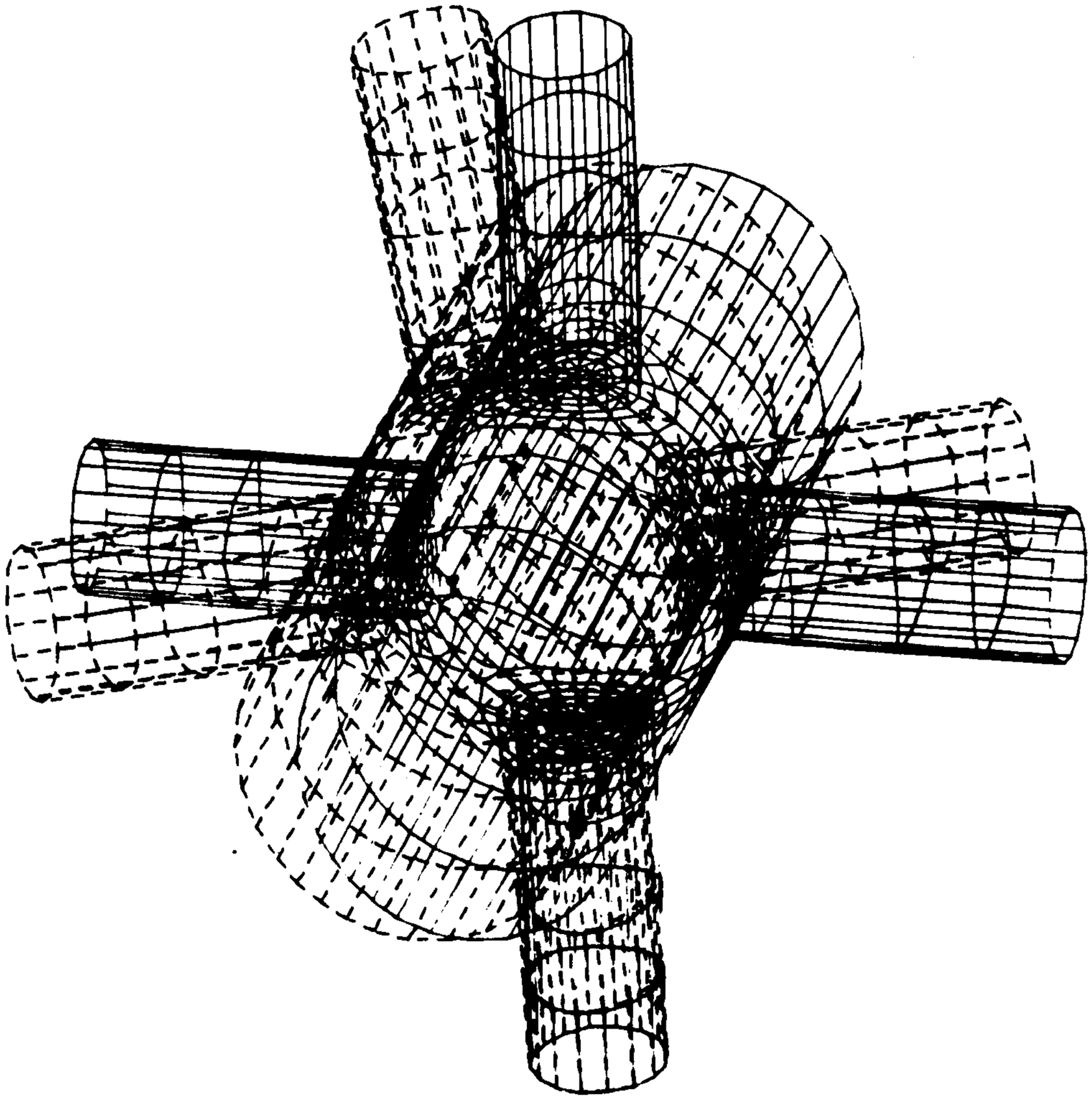

Figure 2.26 Line drawings showing the deformed mesh superimposed upon the unloaded mesh (rotation 60 ° , 60 ° , 60 °). Axial loading

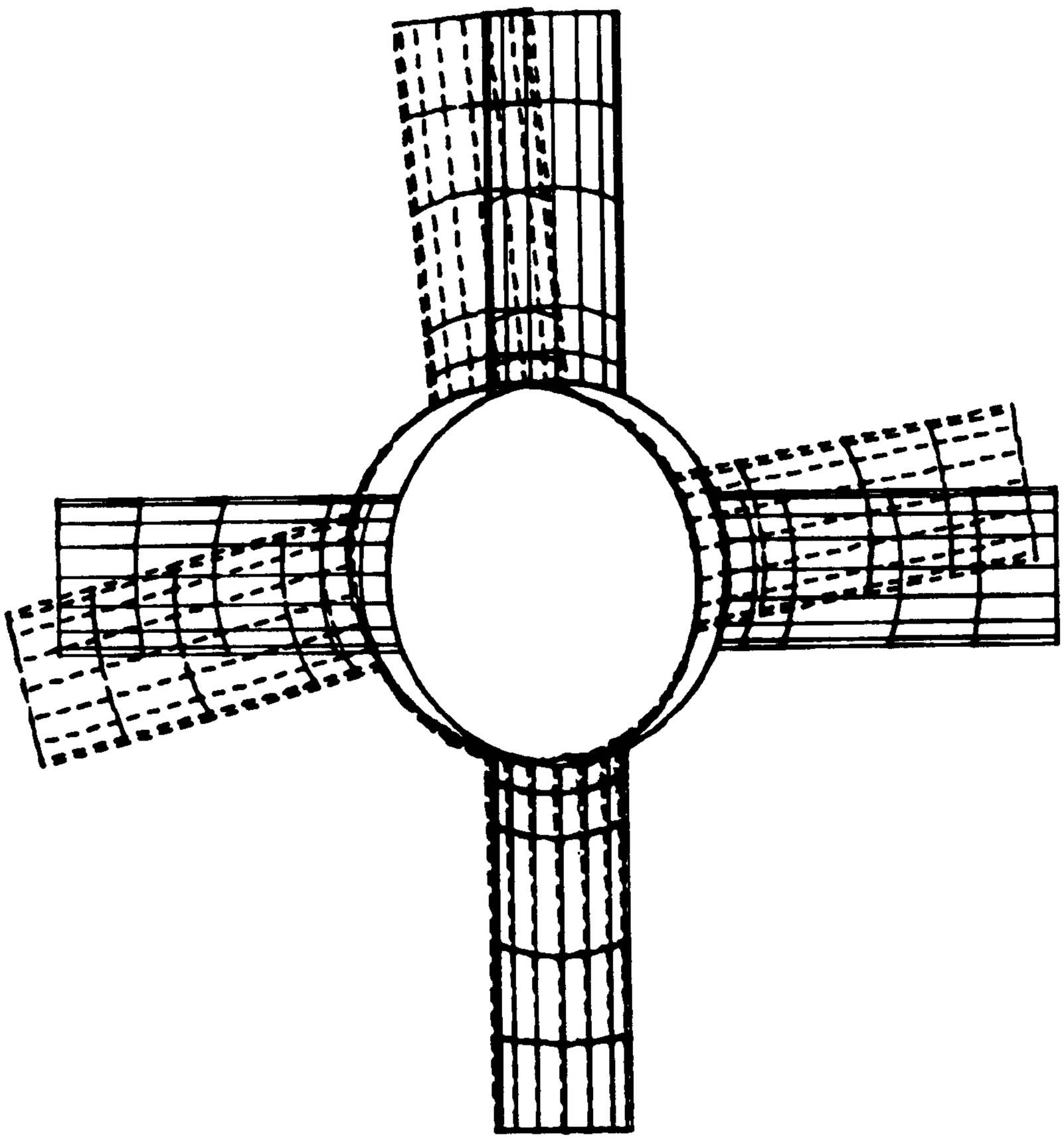

Figure 2.27 Line drawings showing the deformed mesh superimposed upon the unloaded mesh (rotation 0 ° , 90 ° , 0 °). **Axial loading**

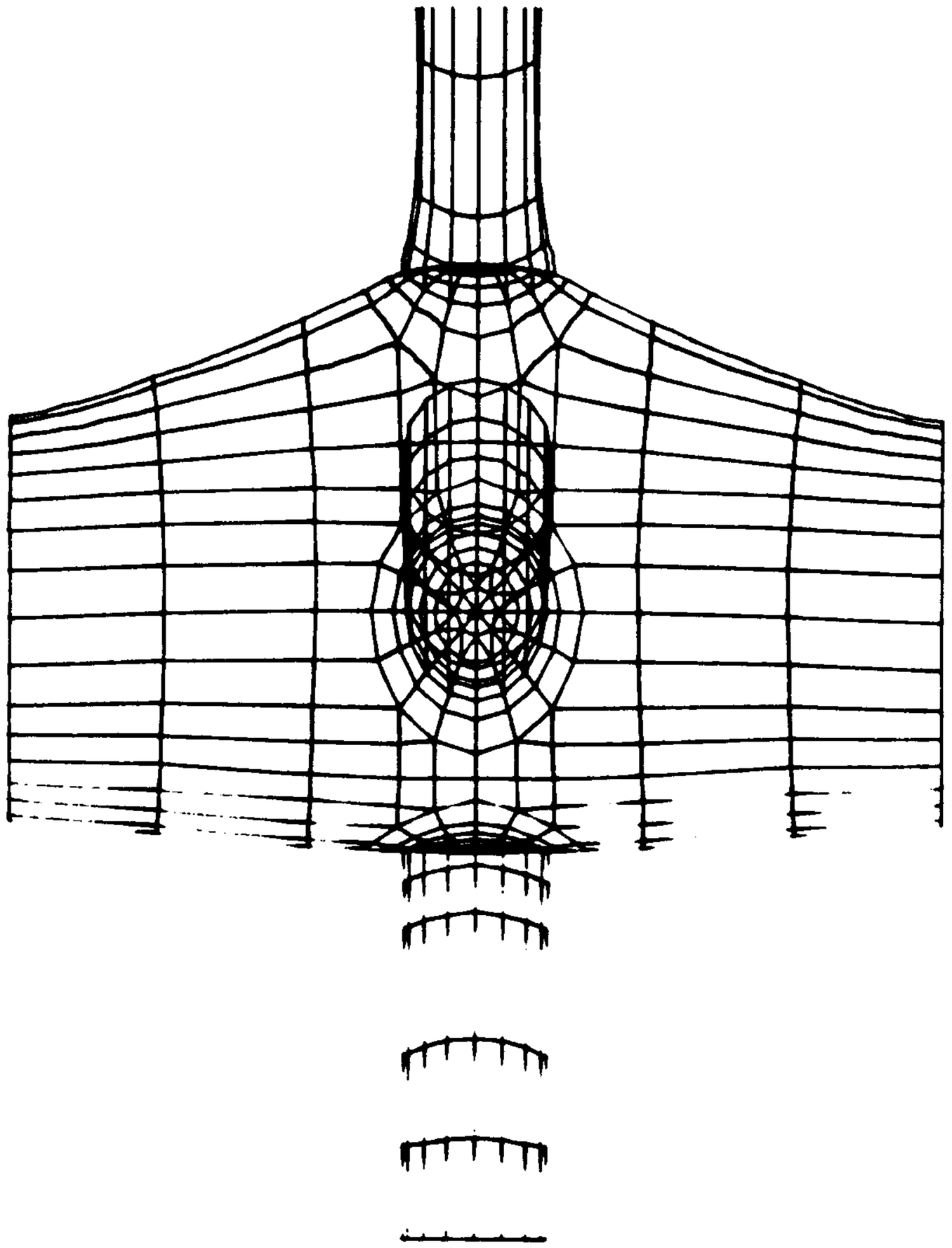

Figure 2.28 **Line drawings showing the deformed mesh for axial loading with ends restrained (c.f. normal T-joint test)**

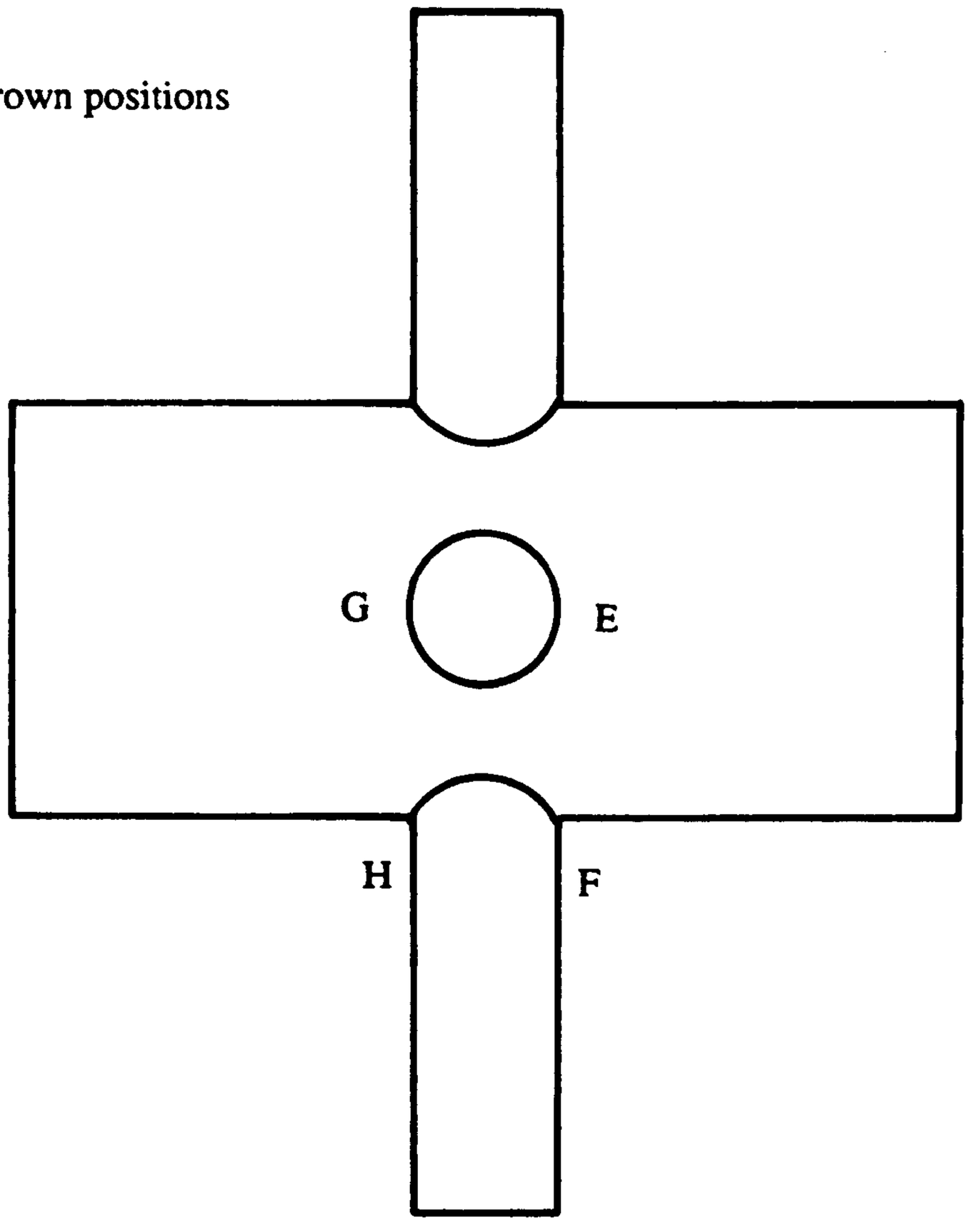

Figure 2.29 The four crown position identified as E F G H

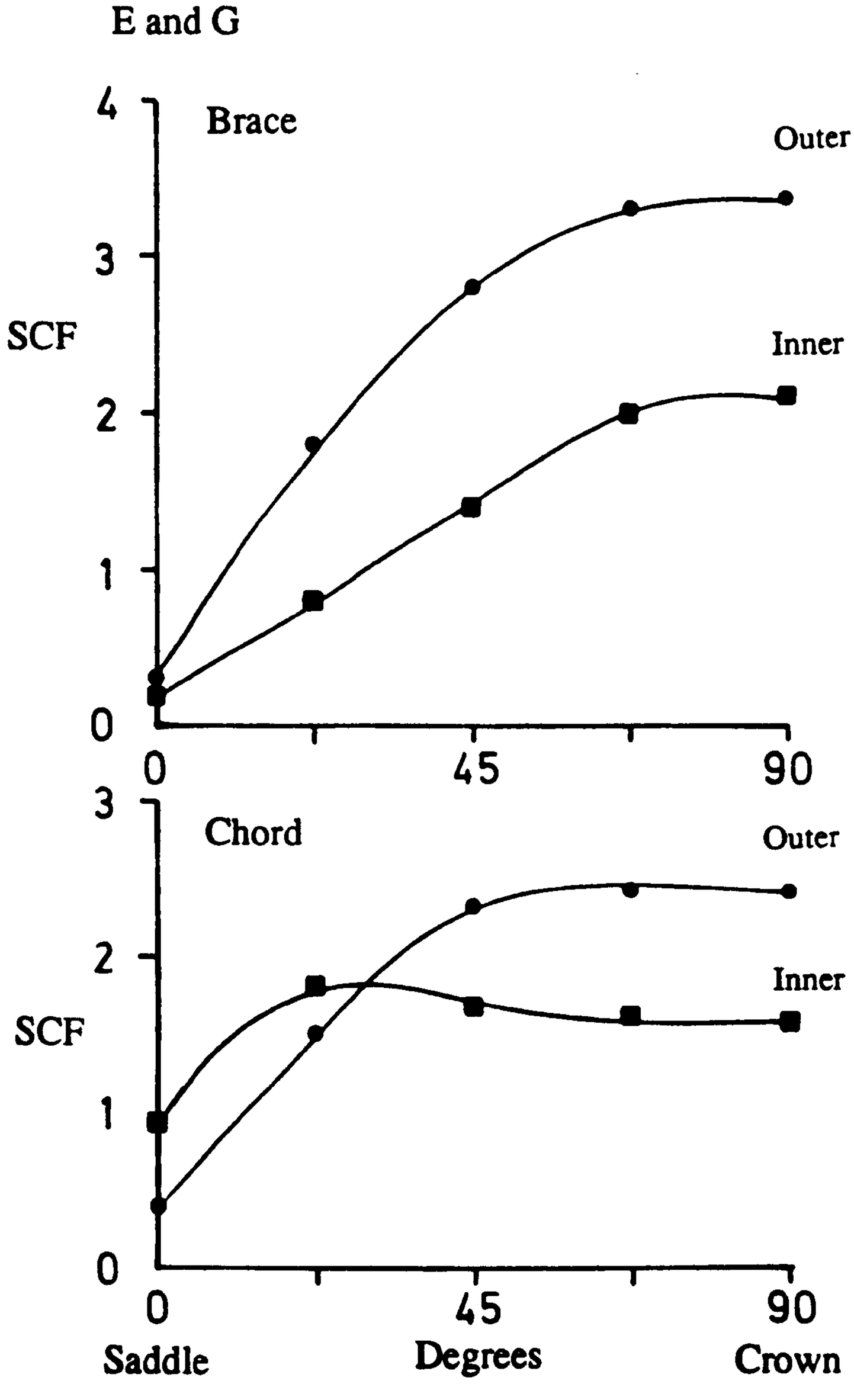

Figure 2.30 Stresses at the outer and inner surfaces of brace and chord predicted by FE analysis for IPB. Distribution around Positions E and G (symmetry)

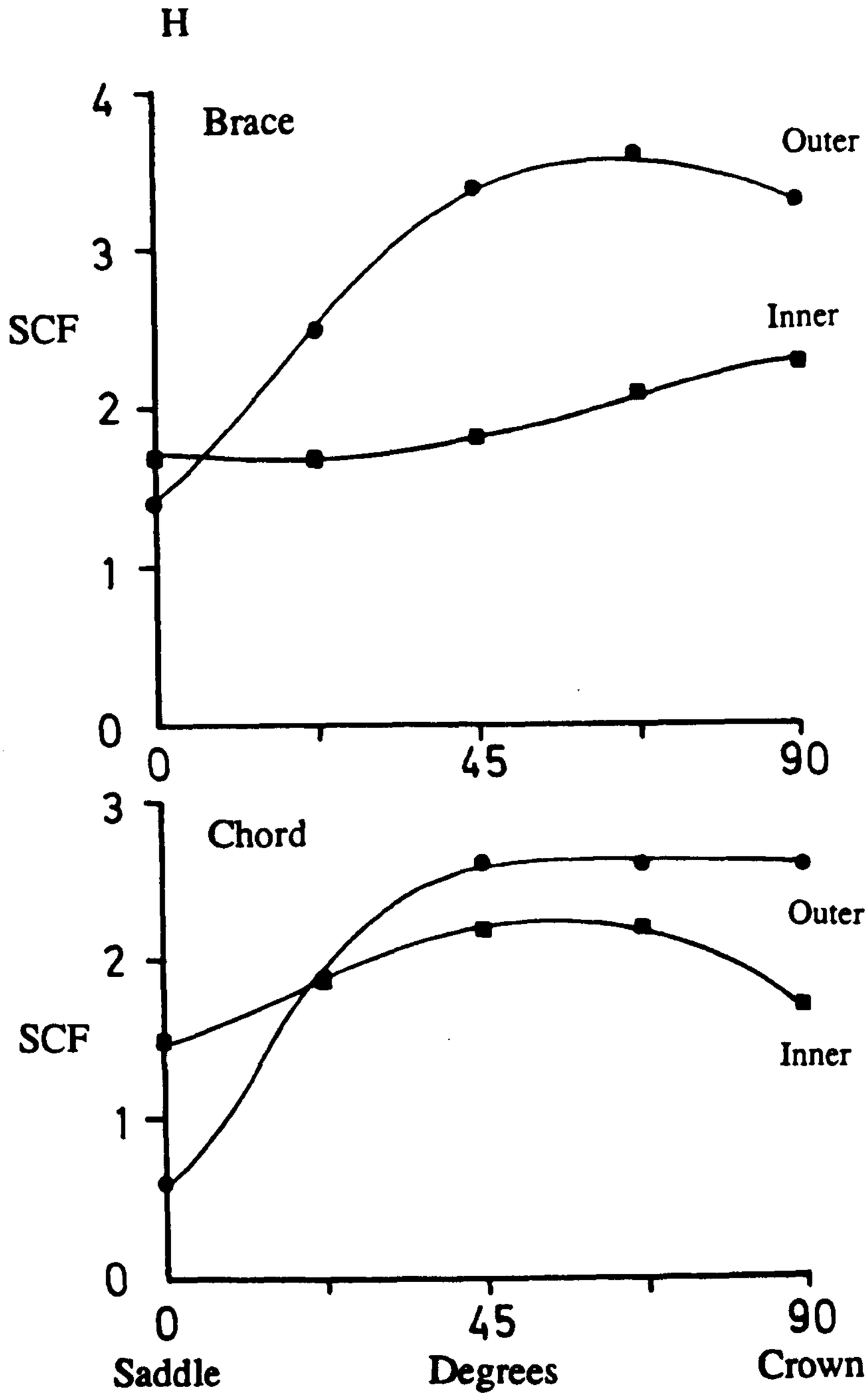

Figure 2.31 Stresses at the outer and inner surfaces of brace and chord predicted by FE analysis for IPB. Distribution around Position H

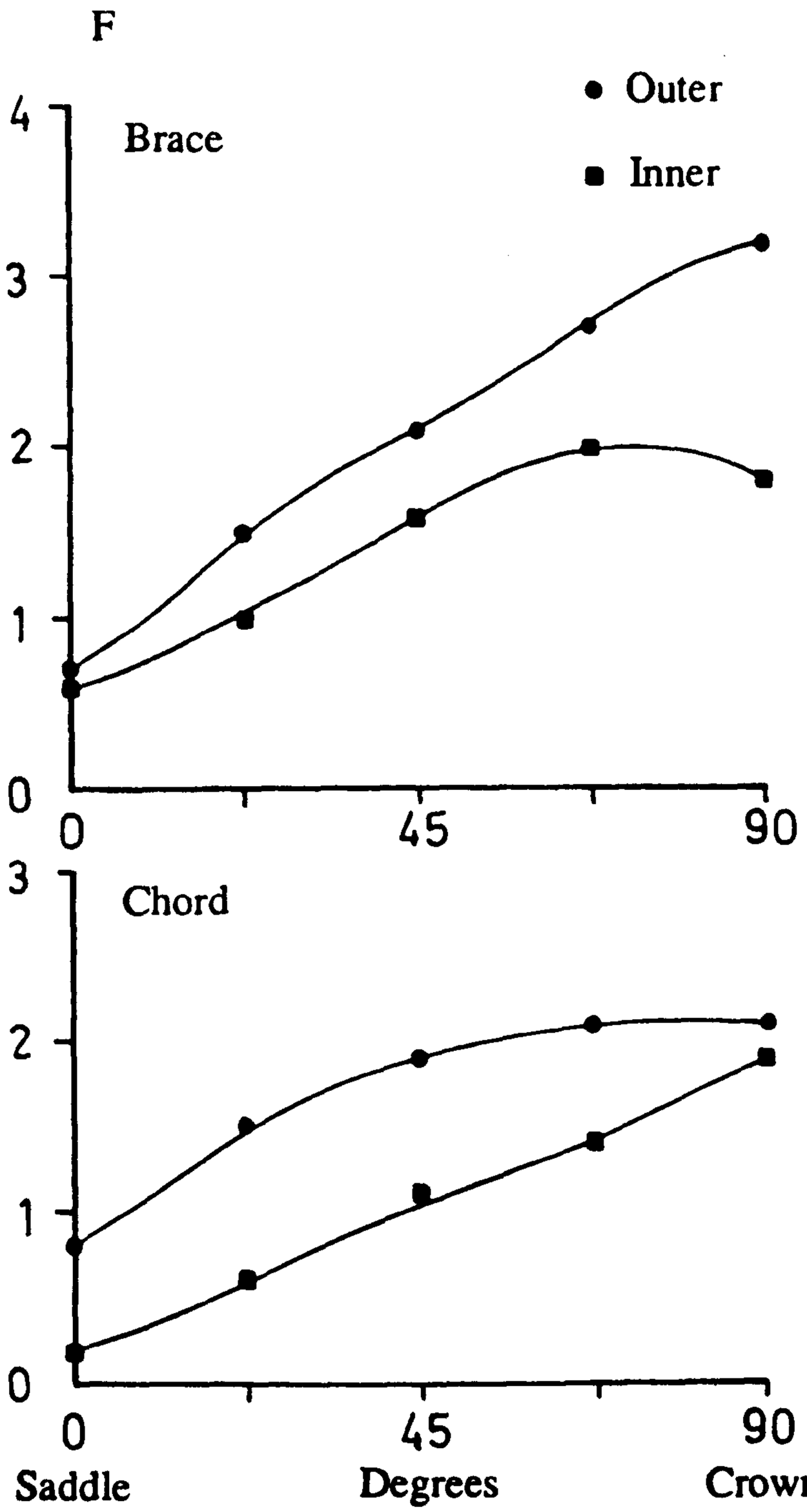

Figure 2.32 Stresses at the outer and inner surfaces of brace and chord predicted by FE analysis for IPB. Distribution around Position F

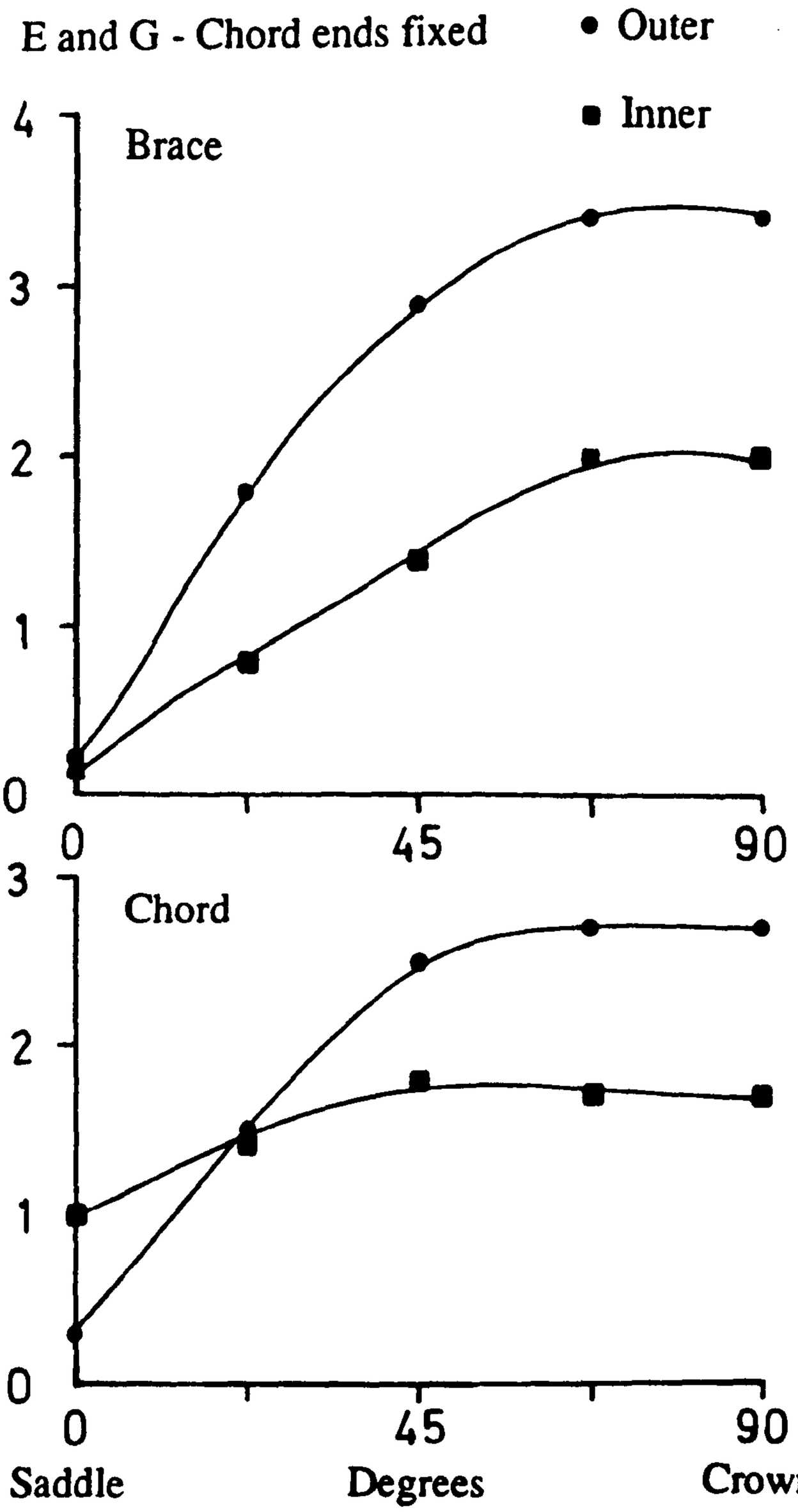

Figure 2.33 Stresses at the outer and inner surfaces of brace and chord predicted by FE analysis for IPB. Distribution around Positions E and G (Chord ends restrained)

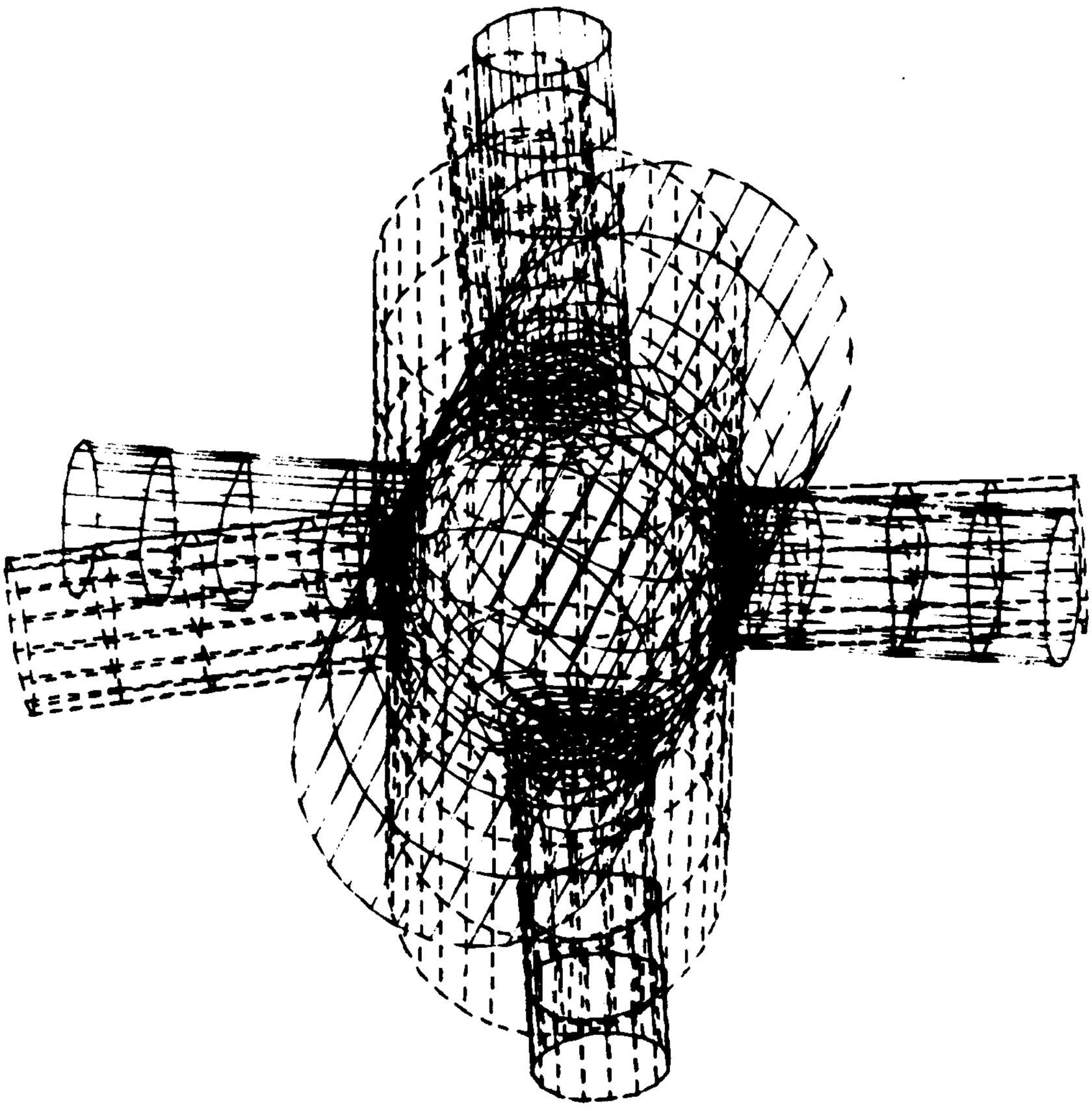

Figure 2.34 Line drawings of deformed mesh superimposed upon the undeformed mesh IPB loading (rotation 60°, 60°, 60°)

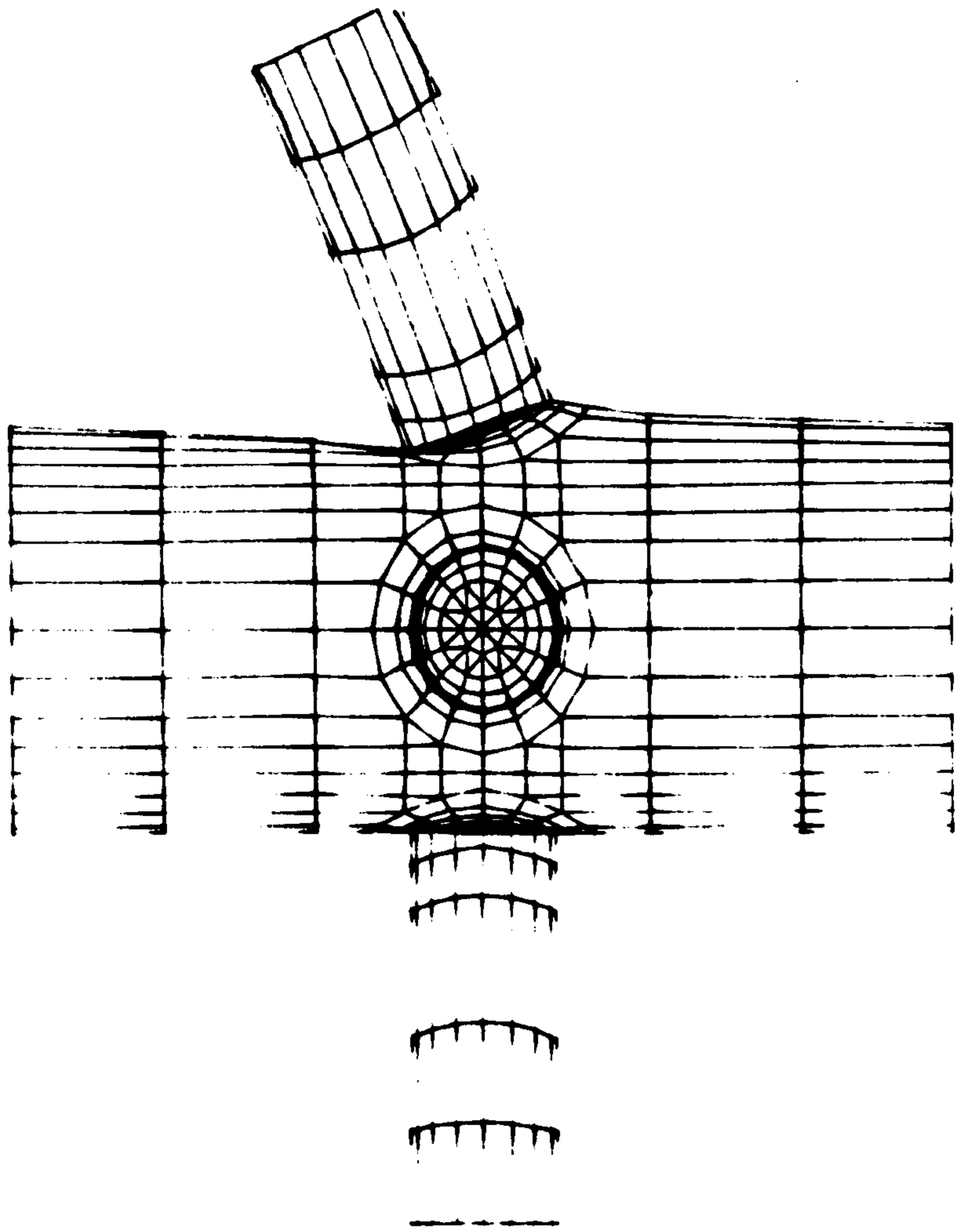

Figure 2.35 Line drawings of deformed mesh IPB (chord ends restrained)

3 CHAPTER THREE

LINEAR ELASTIC STRESS ANALYSIS AT THE WELD TOE

3.1 Scope of chapter

This chapter reports on the measurement of the geometric parameters of the steel tubular joints for the weld profiles studied. A series of measurements were taken for the weld angle α and weld toe radius ρ. The distribution of weld toe radii values is presented for both saddle and crown positions.

Experimental strain measurements were conducted at the outer surface of the chord wall and an attempt was made to measure the variation in strain values at the toe of the weld. These measurements enabled the component of stress due to the weld toe notch for both the AWS weld profile and the CWP braces of the steel models to be calculated.

The values of the weld geometric parameters α and ρ were used to develop a number of two-dimensional models of a saddle position. Using the substructuring technique displacement values calculated from the global shell analysis were used to calculate the boundary conditions of the two-dimensional models. These models were analysed under plane strain conditions.

The results reported in this chapter include the variation of through thickness stress in relation to the geometric parameters; weld angle and weld toe radius. Also the distribution of stress along the surfaces is reported. The through thickness stress distributions are compared with the results for T-butt welded joints.

3.2 Introduction

Tubular welded joints are often used to form the three-dimensional load carrying space frame of steel offshore structures. Such a structure is susceptible to localised fatigue failure at the welded intersections due to high stress concentrations in these regions and cyclic loadings experienced in service. In order to ensure that the joints are adequately designed against fatigue it is necessary to know the stress fields around welded intersections where cracks are likely to initiate and grow.

It is known [3.1-3.3] that under simple in-plane or out-of-plane bending loading the so called crown or saddle positions, shown in Figure 2.29, experience the highest local stresses at the weld toe. The maximum crown or saddle stresses depend on the global joint geometry, and the mode of loading [3.4]. Therefore several experimental studies and theoretical studies were carried out in the past [3.1-3.4] to determine the maximum stresses at the crown or saddle position. However, it is also known that the dominant period in fatigue life of welded tubular joints is the through thickness fatigue crack growth which initiates in the region of maximum stress. Thus, the estimation of fatigue lives of welded tubular joints in offshore structures has to be based on the analysis of fatigue crack growth. Therefore, the knowledge of the maximum stress of the saddle or crown position is not sufficient because fatigue crack growth depends on both the stress magnitude and the through thickness stress distribution in the critical region. Consequently, the maximum stress at the critical location and the through thickness stress distribution depend on the global joint geometry, mode of loading and on the local geometry of the weld. It is also felt that changes in weld geometry such as the weld toe radius, weld angle and weld leg length can significantly alter the through thickness stress distribution affecting finally the fatigue life of the joint.

The study presented in this chapter deals with through thickness stress calculation in tubular welded multiplanar joints under out-of-plane bending loading. The studies were carried out for two series of joints with two different weld profiles. The analysis includes experimental strain measurements, finite element shell analysis and through thickness stress calculations using a small part of the joint substructured from the full scale node.

It must be noted at this point that the majority of the analyses and measurements taken for the controlled weld profile refer to profile C1. Some measurements were taken for C2 but these are included with profile C1 and are not distinguished separately. This only applies to the work in this particular chapter.

3.3 Measurement of weld geometric parameters

3.3.1 Measurement of weld toe radius

The measurement of the weld toe radii was conducted on the chord side saddle and crown positions for both the AWS [3.5] and CWP intersections. A high

resolution replicating material, microset [3.6] was used to produce impressions of the weld area. It is a specially formulated two-part liquid polymer which cures rapidly to produce a firm but flexible rubber. The area to be replicated was cleaned using solvent cleaner and a wire brush. A mixture of oil and alcohol was sprayed on the surface as a lubricant. The two parts of the liquid polymer were mixed and applied on the surface using a special pneumatic mixing and injection gun. Once the polymer cured it was then lifted from the surface and on it were imprinted all the details of that particular surface area. Impressions of 16 crown and 16 saddle positions for AWS and CWP profiles were taken. These were then systematically sliced every 2mm using a scalpel knife. The pieces were placed on a shadow graph at a magnification of 25 times. The weld toe radii were identified and a trace taken of each radius. The radii were measured using a pair of dividers. The high magnification was used in an attempt to reduce experimental error. Appriximately 200 radii were measured on the saddle positions of each type of profile.

Figure 3.1 shows the distribution of radii measured at the saddle positions for each type of weld profile. These distributions show clearly that the peak of the curve for profile A occurs between 0.5-0.7mm which is in reasonable agreement with the values by Mondina *et al* [3.7] and Koibuchi *et al* [3.8]. Profile C however, produces a broader distribution with the peak occuring closer to 1.00mm. The differences between the two types of weld profiles is highlighted in the average value of weld toe radius and also in the difference in the magnitude of their respective standard deviation. These values are presented in Table 3.1. Two further sets of measurements were taken for the crown positions, 90 for profile C and 70 for profile A. The weld radii distributions are shown in Figure 3.2. The trend exhibited for the saddle positions is clearly evident for the crown values though it appears that the weld toe at the crown position of profiles A and C measure significantly larger radii than either value for the saddle positions. This suggests that the welding process is easier to conduct in the vicinity of the crown position, the weld beads blend in smoothly and a more generous average weld toe radius emerges.

3.3.1.1 Measurement of weld angle

The average value of the weld angle α was calculated from schematics of the weld profile taken across the saddle regions of profiles A and C at all brace chord intersections. A very fine steel weld profile gauge was used to take an image of the whole weld profile from chord to brace. This profile was then constructed on a scaled schematic of a brace/chord intersection. Figure 3.3 is one such schematic with the weld angle and weld toe radius identified. The values of the weld angle α shown are the two averages calculated from impressions of profiles A and C. These values are 47° for A and 27° for C. The use of profile C produced an increase in the weld leg length from 11.5mm for profile A to 25.5mm for profile C. Also the welding procedure used to produce profile C contributed to a reduction in the weld angle α. These modifications to the weld geometric parameters could provide for a twofold increase in the fatigue life of a structure in terms of extended initiation periods arising from a reduced notch effect and a slower crack growth in the linear region of the crack growth curve.

3.4 Definition of weld toe SCF in tubular joints

The stress analysis so far conducted and reported in chapter two has concentrated on the global stress distribution at the brace chord intersection of a tubular joint. This measured stress is known as the hot spot stress. Specific experimental guidelines exist to conduct the measurement of this stress so that the results are experimentally reproducible and could be compared with other hot spot stress values measured at different laboratories. This characteristic stress is often used to compare fatigue lives of tubular structures. However, in terms of fatigue crack initiation the imporatant stresses are those associated with the region near the weld toe where the local variations of overall weld geometry and weld bead size can have influence. There are no guidelines available to help characterise the stress field at the weld toe. Research work is currently being undertaken to achieve this and to develop elasto-plastic fracture mechanics models for the early crack growth part of the fatigue life.

The nominal stress σ_{nom} is calculated on the basis of simple beam theory using the following equation:

$$\sigma_{nom} = \frac{\Delta F L}{Z} \qquad 3.1$$

where ΔF is the load range between highest (most tensile) and lowest (most compressive) loads.

L is the distance from actuator pin to chord surface

$$Z = \frac{\pi}{4 r_o}(r_o^4 - r_i^4)$$

where r_o and r_i are brace outer and inner radii as measured nearest to brace/chord intersection.

The 'hot spot stress', σ_{HS}, is defined as the greatest value around the brace/chord intersection of the extrapolation to the weld toe of the linear stress distribution away from the weld toe shown in Figure 1.2 Section 1.3. The rules for determining σ_{HS} are given in the United Kingdom Offshore Steels Research Programme 1 (UKOSRP 1) [3.9]. This stress is the most often used parameter in designing for offshore platforms. However, this is not the actual stress experienced by a structure at the hot spot location. The actual stress at the hot spot location is known as the local stress, σ_L, and arises due to the influence of the weld discontinuity adjacent to the weld toe. It is experimentally and numerically difficult to quantify and it is superimposed upon the geometric stress.

These stress values are generally normalized with respect to the nominal stress σ_{nom}, and are expressed in terms of the stress concentration factor SCF, thus

$$K = \frac{\sigma_L}{\sigma_{nom}} \qquad 3.2$$

$$K_G = \frac{\sigma_{HS}}{\sigma_{nom}} \qquad 3.3$$

The component of stress arising due to the influence of the weld discontiuity adjacent to the weld toe may be calculated in terms of the stress concentration factor K_w from the relation proposed by Gibstein [3.10]. This relation to estimate K_w was derived from experimental strain measurement study conducted on T and Y joints as part of

the DnV [3.11] programme of research. Strain distributions on the chord side and brace side of the tubular joints were analysed with the aim of characterising this region close to the intersection as 'notch free' or 'notch active'.

Gibstein observed that strain values along the surface perpendicular to the weld, in the case of most brace and some chord ends of welds, increased linearly up to a distance 1.6mm from the weld toe. Thus, the extrapolated weld toe values for such cases could be considered as 'notch free'. However, some welds did not blend smoothly with tube walls resulting in rapid non-linear increase in strain values. This increase commenced at a distance 4mm from the weld toe. The 4mm distance was found to be independent of weld, wall thickness, position and loading. This region was designated as 'notch active'. Consequently the component of stress concentration due to the weld toe notch, K_w, can be estimated by placing small gauges in the 'notch active' region to measure the strain values and corresponding gauges along the same perpendicular line, but placed in the linear stress region.Therefore using this data Gibstein proposed a numerical definition of the stress concentration factor K_w as the ratio between the stress concentration factor at the weld toe (notch active SCF) divided by the stress concentration factor at the same position which corresponds to a 'notch free' condition (the extrapolated value from the rosette gauges). This equation therefore provides the numerical definition:

$$K_w = \frac{K}{K_G} \qquad 3.5$$

3.4.1 Experimental strain measurement in tubular joints

The experimental strain measurement is conducted on the outer surface of the chord wall in the vicinity of the four saddle positions A, B, C and D for both types of steel models. In view of the fact that the use of the controlled weld profile was restricted to the chord side of the tubular joint and that the investigation by Gibstein [3.10] concluded that the majority of the brace side weld toe regions are considered 'notch free' zones, the measurement of strain at the weld toe was restricted to the chord side of the tubular joint. As well as the four saddle positions A, B, C and D a number of other locations at the intersection were also studied. These areas were strain gauged in accordance with the recommendations of the UKOSRP 1 [3.9] for stress analysis techniques.

Figure 3.4 shows a schematic of one saddle position indicating the location of rosette gauges, gauge length 2 mm placed at 10 and 20mm distance from the weld toe. Also shown are additional strain gauges of gauge length 0.3mm; one gauge is placed at the toe of the weld and the second displaced 1mm from the weld toe. The backing of the small gauges was cut away so that the gauge element could be positioned as close to the weld toe as physically possible.

Kerr [3.12] investigated the effect of gauge trimming on the accuracy of the strain gauges and concluded that there was no measurable effect recorded. The analysis was conducted under an out-of-plane OPB bending loading using a static load of 5.0 kN. For the steel model with profile C three extra rosette gauges were placed at 80, 115 and 155mm from the weld toe in order to measure the strain values remote from the intersection.

The strain values measured by the rosette gauges were converted into principal stresses σ_1 and σ_2 using the relation

$$\sigma_1, \sigma_2 = \frac{E}{2}\left(\frac{\varepsilon_A + \varepsilon_c}{1-\nu} \pm \frac{1}{1+\nu}\sqrt{(\varepsilon_A - \varepsilon_c)^2 + 2(2\varepsilon_B - \varepsilon_A - \varepsilon_c)^2}\right) \qquad 3.5$$

The UKOSRP 1 procedure recommended in reference [3.9] was used to determine the 'hot spot stress' σ_{HS} perpendicular to the weld toe.

The strain values from the small strain gauges placed in the vicinity of the weld toe were converted into stresses, these represent the local stress value σ_L which is in the perpendicular direction of the weld toe.

3.4.1.1 Results

Figures 3.5 and 3.6 show the distribution of stresses on the outer chord surface, normalised with respect to the nominal stress, as a function of the perpendicular distance from the weld toe. Both sets of curves representing profiles A and C exhibit a sharp decay in the SCF values close to the weld toe, but further away from the intersection the effect is greatly reduced and the distribution is almost linear confirming the results presented in reference [3.9]. Profile A exhibits consistently higher values of stress than profile C for all notch effective regions of the four saddle positions. Typical examples of the differences between the two profiles is demonstrated by position A where the average overall stress concentration factor K, is 13 for profile A and and 10 for profile C. The

corresponding K_G values were 6.3 and 5.6 for profile A and profile C respectively. Consequently, the contribution of the weld notch, K_w, to the total stress concentration factor was calculated.

Table 3.2 shows the SCF values K, K_G and K_w at the four saddle positions. The notch stress concentration factor K_w for the saddle positions fell within the range 1.19-3.02 with an average of 1.82 for profile A and 1.13-1.79 with an average of 1.43 for profile C. A more extensive survey of K, K_G and K_w for all positions around the intersections of both types of profiles showed that profile A values of K_w ranged from 1.18-3.04 with an average of 1.85, while those for profile C ranged from 1.07-2.90 with an average of 1.57 (see Table 3.3). This illustrates the fact that high K_w values do not necessarily have to occur at the hot spot SCF position; K_w appears to be a function of the local weld geometry i.e. the last weld bead.

3.4.1.2 Discussion

The results are discussed in terms of the differences in weld profile properties as well as with other data and techniques previously used. Some values of K, K_G and K_w from previous tests on tubular joints described in the literature are given for comparison purposes in Table 3.4 ref.[3.13, 3.10, 3.14 & 3.5]. All joints had chord wall thicknesses of 16mm. The weld toe SCF values reported in ref.[3.14] were recalculated assuming $K_w = K/K_G$. It is apparent that the K_w values are very similar, lying between 1.24 and 1.59 with an average of 1.39, irrespective of the joint type (T, Y or K) or the mode of loading employed.

A study of simple T-butt welded specimens which do not possess a K_G has been made by Iida *et al* [3.15] in an attempt to isolate the stress concentration contribution due to the local weld geometry. By casting epoxy resin models of a cruciform specimen and employing a photo-elastic stress freezing technique, they found that the weld toe SCF varied from 2 to 6 with an average of 3.2.

The average K_w values measured in the present study lie in between the average value from other tubular joints and that obtained by Iida. That the weld toe SCF's are generally greater than those from previous tests on tubular joints is probably due to the considerable care taken in cutting away the backing of the

gauges in order that they could be positioned as close as possible to the weld toe. As shown in Figures 3.5 and 3.6 the stress gradient is very sharp in the vicinity of the weld toe. A small error in positioning the strain gauges can therefore lead to substantial underestimation of the extrapolated stress value. However, no matter how close the strain gauges are to the weld toe they merely measure an average strain over the gauge length. It is therefore to be expected that the photoelastic method might result in higher weld toe SCF values. Nevertheless, although the absolute values are dependent on the method of measurement, since the same technique was used for both profiles A and profile C it might be stated that the use of a controlled weld profile leads to a reduction in K_W.

Therefore the change in the weld procedure to produce profile C resulted in reductions for the average geometric stress concentration factor, K_G, by 11% for all saddle positions and the weld notch stress concentration factor, K_W, by 15%. The total reduction for the overall stress concentration factor K, was 30%.

The reductions in stress concentration factors due to the modifications of the weld profile were attributed to two main factors:

(i) a decrease in the weld angle α by a factor of two

(ii) an increase in the overall distribution of weld toe radius ρ values.

The distributions of weld toe radii shown in Figures 3.1 and 3.2 clearly demonstrate that the use of profile C leads to larger radii at the toe of the weld which contribute to a reduced notch effect. However, the distribution of the weld toe radii does show that radius values of 0.2mm were found in the vicinity of the saddle positions. This value is even less than the notch radius considered as a worst case by Lawerence [3.16] and Dover *et al* [3.17]. To initiate a crack would only require the occurance of one such notch in the region of maximum hot spot stress. Thus, the fact that the most frequent and the average weld toe radii were significantly larger than 0.25mm may prove to be not important as far as the initiation part of the fatigue life is concerned.

It should also be noted that the change in the welding procedure to produce profile C resulted in shifting the weld toe further away from the notional point of intersection of the brace and chord. In the case of profile A the weld toe was 19.5mm from the mid-plane of the brace wall while in the case of profile C the distance was 33.5mm. This fact is probably responsible for the differences between the K_G stress concentration factors which should be the same because the global geometry of both joints was identical.

It is apparent, therefore, that a twofold benefit may be derived from the use of the controlled weld profile. For early fatigue crack growth studies the weld toe SCF (K_w) is important. Any significant reduction in this value could contribute to an increase in crack initiation time. Once a crack begins to grow, however, the influence of K_w rapidly diminishes and the parameter which governs further crack growth is the geometric SCF (K_G). A lower value of K_G should give improved fatigue resistance and life, measured on the basis of a common hot spot stress.

3.5 Finite element stress analysis

It is well known that calculating the near notch tip stress fields requires fine 3-D finite element meshes. These are cumbersome to generate and require significant computational facilities. Therefore, in order to avoid large 3-D computations the analysis was divided in two stages; a global stress analysis using thick shell finite element analysis to provide a validation for the steel model experimental results and secondly a through thickness analysis using the substructuring technique.

3.5.1 Thick shell analysis

The finite element mesh used in this section is the same as that analysed in chapter two for the global stress analysis study. The analysis was conducted under OPB loading mode with the same restraints and fixities shown in Figure 2.4 (a) i.e. the bottom brace was fixed and the load was applied via a second brace at 90° to the fixed brace. The chord ends are not restrained.

3.5.2 Results

Figure 3.7 shows the FE predictions of values of stress expressed in terms of SCF for the four saddle positions A, B, C and D. The distributions represent the values

along the chord outer surface as a function of the distance from the mid-plane of the brace wall. All four distributions exhibit lower SCF values than either of the two steel model results.

Figure 3.8 shows the results from the FE analysis compared with the steel model results for saddle position A. Two observations are noted; firstly, the steel model results are extrapolated to the Y-axis on the graph which represents the weld toe. For the FE analysis the first node is at the mid-plane of the brace and if plotted on the same graph is actually -8mm distance on the X-axis. Secondly the FE thick shell analysis does not model the weld at the intersection and consequently the notch effect due to the geometry of the last weld bead is not modelled. The significance of this notch effect is demonstrated in the sharp decay of the stress value in the vicinity of the weld toe for the steel model results as demonstrated by both types of weld profiles in Figures 3.5 and 3.6. One further observation is the fact that the mesh along the outer surface of the chord is fairly coarse. The element size at the intersection is 63x50mm.

3.5.3 Discussion

It is important to consider the implications of using such a large element at the brace/chord intersection. Figure 1.3 shows the extent of the region over which the notch is considered to be active as well as that part of the stress distribution where the stress gradient is linear. Consequently for this particular tubular joint geometry the notch active region extends from the weld toe up to 10.5mm and the linear region is between 10.5-30.5mm. Beyond 30.5mm the stress is constant and corresponds to the brace nominal stress.

The first element at the brace/chord intersection is 50mm long. Therefore the stress values predicted at the nodes within this element are an average of the distribution of stress in the notch active region, the linear stress region as well as the area where the brace stress is dominant. Thus, it is not unreasonable that the FE thick shell analysis underpredicts the hot spot stress value compared with the steel model results. Clearly the results obtained from this analysis provide a global view of the stress distribution with no attempt to accurately predict the stress values. Remote from the intersection these FE predictions exhibit reasonable agreement with the steel model results of both types of weld profiles.

These above results were predicted from the analysis of the full mesh of the multi-planar joint which comprised of 944 elements and 3064 nodes. This mesh was generated from an octant shown in Figure 2.2. The octant shows that the perpendicular distance from the chord side saddle position was dicretised into 3 elements. This was chosen so as to reduce the computational expense of analysing a very large mesh. But the underestimate of stress values predicted are significantly large and since it is intended that these results would be used for the substructuring studies in the following section a finer mesh was therefore required. Consequently, modifications to the octant shown in Figure 2.2 were made to increase the number of elements around the intersection and at perpendicular distance from the weld toe.

An increase in the number of elements around the intersection from 8 to 10 resulted in an element size of 50x50mm (which in terms of the FE method is considered as the optimum width to length ratio) but the results showed little influence on the distribution of stress. However, an increase in the number of elements in the perpendicular direction alone from three to five elements resulted in a significantly higher value of SCF being predicted at the mid-plane of the brace. Increasing the number of elements in both directions would produce the best results but this would have resulted in a large and expensive analysis.

Therefore, the mesh adopted was a compromise in order to improve the FE predictions without creating a large and expensive mesh. The mesh used comprised of 1072 elements and 3480 nodes. The element size was 63x32mm. It must also be noted that no further reduction in element size could be achieved, the limiting factor being the element thickness. In spite of the fact that thick shell elements do not model the thickness this parameter is a mathematical entity and is required for subsequent calculation when predicting stress distributions. Consequently if the thickness dimension is larger than either of the two other dimensions this would result in an ill-posed mathematical problem and PAFEC cannot solve for displacements nor compute stresses.

Figure 3.9 shows a comparison between the two sets of non-dimensional stress distributions using two different element sizes at the brace/chord intersection. Clearly a smaller size element predicts a higher hot spot stress value, but still well below the corresponding steel model results.

3.6 The weld profile effect on stresses in the vicinity of the weld toe

The stresses in the through thickness direction and along the outer chord surface near the saddle position A were analyzed using the "so called" substructuring technique. In the present study the analysis was limited to the plane of symmetry i.e. the saddle position. Given that the chord wall is a long cylindrical body in which the saddle position lies on a plane passing through the centre of the chord, it is reasonable to assume that the strains in the vicinity of the saddle position are plane. Therefore, the analysis of the brace/chord intersection near the saddle position was reduced to the two-dimensional plane strain analysis.

The finite element models of the brace/chord intersection for the weld profiles studied are shown in Figures 3.10-12. The size of the substructured section was chosen such that the stresses at each end of the section were beyond the local influence of the weld. The analysis was conducted under prescribed displacements. The displacement values applied at the boundary of the substructured section were calculated from the rotation and translations of the boundary nodes obtained from the global analysis based on the thick shell finite element calculations.

The weld geometry parameters used in this study were:

	α	ρ
Profile A	47°	0.75mm
Profile C	27°	0.92mm

For both types of profiles the weld toe radius was modelled using the average value calculated and not the most frequently occuring radius value. Also the smallest radius measured, 0.2mm corresponding to the worst case for this study was also ignored. An additional artificial model without any weld was generated and analyzed.

Typical through thickness stress distributions in the substructured model with weld profile A and C are shown in Figure 3.13 & 3.14. It is apparent that the near weld toe stress field was not affected by the boundary conditions of the models. The contours denote the lines of constant maximum principal stresses of different levels. The stress distributions along the outer chord surface obtained from the 2-D models are shown in Figure 3.15. For comparison the experimental and shell analysis results have also been included.

The stresses measured and predicted were normalised with respect to the nominal stress σ_{nom}. The data shown represents non-dimensional stress distributions as a function of the perpendicular distance from the weld toe. The data are presented according to the convention adopted in the offshore industry, i.e. all stress distributions have the same origin of coordinates. However, as noted earlier for the FE shell analysis the origin of coordinates is at the mid-plane of the brace whereas the two steel models the origin is at the weld toe of each profile thus the steel model results at the origin do not coincide due to the different weld leg lengths between profiles A and C.

It is interesting to note that the shell analysis predicted the lowest distribution of stress over the distance of $0 < x < 3T$. It was also found that away from the weld toe($x >$ 80mm) all stresses converge to approximately one line as should be expected from stress values beyond the notch affected region.

The stress analysis data shown in Figure 3.15 was replotted and presented in a new form in Figure 3.16 showing the true location of the origion of each coordinate system. This method of presenting the results would appear to be more appropriate because it shows the actual position of the hot spot stress relative to the brace wall. Using the shell finite element data plotted in Figure 3.16 it is possible to read the stress concentration factor K_G at each weld toe position. These values are 3.5 for profile A and 2.5 for profile C. The stress concentration factors K_G determined in this way are different for each weld profile and the lower K_G value i.e 2.5 occured for profile C which is markedly different from the experimentally measured data.

The stress concentration factors determined by linear extrapolation of the stress in the linear region of each of the 2-D stress distributions were 4.9 and 5.0 for profiles A and C respectively. These values suggest that the stress at the brace/chord mid-plane intersection obtained from the shell FE analysis does not seem to be a very accurate estimation of the hot spot stress, σ_{HS}, and the stress concentration factor, K_G. It is felt that the differences between the stress concentration factors for profiles A and C are due to different weld leg lengths between the two profiles studied. Therefore, in tubular joint analyses, the weld profile should be characterised by at least three parameters; the weld angle α, the weld toe radius ρ and the weld leg length L.

The 2-D model generated with no weld, just a sharp intersection produced comparitively lower value of hot spot stress. This is because the element sizes at the intersection were large compared with those of the other 2-D models, finer elements produced progressively higher stress values. This excersize illustrates the importance of the size of the element particularly when comparisons are made with other techniques or even with FE results where the mesh was discretised into smaller regions. It is felt that guidelines should be set for discretising a mesh e.g. a weld toe radius should be modelled using a specific number of elements irrespective of it's size. This then provides a base for comparing the results.

It is also apparent that the shell FE analysis gave the lowest stress estimation over the entire region $0 < x < 160$mm as shown in Figure 16. However, it must be restated that the shell FE data is taken at the mid-plane of the chord while all experimental and 2-D FE stress predictions were extrapolated to the brace outer surface. Therefore, the shell FE data should be treated with caution especially for thick wall strucures.

The stress distributions obtained from the 2-D substructured elements indicate that the non-linear region of stress distribution on the chord surface which was affected by the weld was up to approximately 20mm (see Figures 3.15 & 3.16). This therefore suggests that the rosette strain gauge placed at 10mm from the weld toe (as per UKOSRP 1 recommendations [3.9]) was actually inside the region where the stress increases non-linearly. This is contrary to the basic assumptions of [3.9] which state that both gauges should be inside the region where stress is linearly decreasing, but outside the weld notch affected zone.

The fact that one of the rosette strain gauges was placed within the non-linear stress field region resulted in the linear extrapolation of the two strain gauge data to the weld toe to produce higher 'hot spot' stress estimation as compared with the result from the extrapolation of the true linearly changing stress region. In spite of the fact that the UKOSRP 1 recommendations were observed for the hot spot stress estimation, one gauge was too close to the weld toe. Also all the predicted and experimentally estimated stress distributions, except the shell FE data, merged for distances $x >$ 90mm indicating that the size of the substructured model was sufficient.

Finally, the through thickness stress distributions, the primary objective of the study in this chapter, were determined. The non-dimensional through thickness stress distributions in the chord beneath the saddle position are shown in Figure 3.17. The

stress distributions were normalised with respect to the nominal stress σ_{nom}. It is apparent that all stress distributions were linear beyond $0 < x/T > 0.25$. Thus the intersection and geometry did not affect the through thickness stresses over more than one quarter (0.25T) of the chord thickness. Extrapolation of the linear section of the stress distribution to the outer chord surface made it possible to determine the hot spot stresses and the stress concentration factor K_G shown in Figure 3.17. These values were 13.0 for profile A and 7.6 for profile C. These are very close to the values determined from the chord outer surface stress distribution (see Figure 3.15). The 2-D analysis presented in Figures 3.15 and 3.16 suggests that the hypothetical linear stress distribution shown in Figure 3.17 was predominantly due to bending with the ratio of bending to membrane stress of 5:1. The finite element shell analysis predicted a higher ratio of 6.5:1

The effect of the weld profile on the through thickness stress distribution is shown more distinctly in Figure 3.18. It is apparent that noticeable differences occured over approximately 10% of the chord wall thickness. Higher stresses were predicted for profile A over the distance of < 0.1T. The stress concentration factors in the weld toe were 7.6 and 13.0 for profiles C and A respectively which are close to the experimentally obtained values using the small single element gauges placed at the weld toe.

3.7 Discussion

The analysis of stresses in tubular welded structures is very difficult due to the complex three-dimensional geometry of these joints and the presence of high stress concentrations around the welds. Detailed examination of stress distribution around critical locations would require three-dimensional stress analysis using complex boundary conditions. Analytical solutions even for the simple cases are not available. The generally used data regarding stresses in tubular connections have been obtained experimentally, or numerically using the finite element method.

Experimental analysis of stresses in tubular joints is time consuming and expensive. In the case of full scale steel models or acrylic models the strains can only be measured on the surface of the model. Therefore, with the exception of photoelasticity experimental methods are not capable of measuring through thickness stress distributions. The FE method can be used to predict through thickness stress distribution but this requires three-dimensional analysis using 20 noded brick elements which are

expensive and require extensive computational facilities. Furthermore the regions around the weld would need to be modelled using a very fine 3-D mesh. Therefore, for this reason shell FE analysis are often performed.

The shell FE stress predictions provides an estimation of the global stress distributions as this type of analysis does not model the weld at the intersection nor the chord or brace wall thicknesses. However, it is generally assumed that the shell analysis provides a reasonable estimation of the hot spot stress at the brace/chord intersection. Figure 3.19 shows a comparison of measured and predicted SCF values for data available in the literature. The accuracy of the FE method appears to fall in a band of -20%+20% of the steel model results. But the hot spot stress value for a steel joint is that measured in the weld toe whereas the predicted hot spot stress value using shell FE analysis is that value predicted at the mid-plane of the brace wall some distance away from where the weld toe would be had it been modelled. It is therefore correct to suggest that FE shell analysis should be treated as a general approximation of stress distributions.

The shell FE data presented and discussed above yielded the lowest estimate of SCF values compared with the experimental strain measurement results. On the other hand the experimental hot spot stress value appears to be comparitively high. This is because the recommended locations of the strain gauges were not wholly in the region of linear stress gradient but incorporated part of the notch region thus causing an overestimation of the stress.

The hot spot stress values obtained using the experimental method and the thick shell FE analysis compared the results predicted using a detailed 2-dimensional model shows that by incorporating the weld geometry and the weld toe notch in the FE model the predicted distribution of stress approximates those of the steel model results. An improvement in these FE predictions was achieved in spite of the fact that the boundary conditions for the 2-D models were taken from specific nodes in the multiplanar joint which exhibited significant underestimation of the hot spot SCF values. The translation and rotation values of these nodes were used to calculate the boundary conditions for the 2-D mesh.

The study presented in this chapter provided specific information on through thickness stress distribution in tubular welded multi-planar joints tested under out-of-plane bending loading. The changes in weld geometry namely, weld toe radius ρ, weld

angle α and weld leg length L have been shown to significantly influence the through thickness stress distribution. It is predicted that such changes will ultimately affect the fatigue life of a structure through their influence on the behaviuor of the stress intensity factor. These effects have already been demonstrated for T-butt welded joints by the work of Niu[3.18].

Niu conducted a comprehensive stress analysis study on T-butt welded joints where the effect of the weld geometry was characterised. This information was then used along with the Niu-Glinka [3.19] weight function to assess the effects of the weld geometry on the stress intensity factors. The Niu-Glinka weight function method allows one to calculate the stress intensity factors for fatigue cracks in T-butt welded joints subjected to any loading mode. It also provides the means to assess the effects of the weld angle and weld toe radius on the stress intensity factors for T-butt jonts. The authors concluded that the stress intensity factor is both a geometry and stress dependent quantity.

The results also revealed that the influence of the geometric parameters weld angle α and weld toe radius ρ on the stress intensity factor were significantly greater than their influence on the distribution of through thickness stress values. Further the weld angle effects on the stress distribution were evident over a greater distance than those of the weld toe radius. Therefore, given that the analyses conducted on T-butt welded joints resulted in conclusions that are similar to the results obtained for this stress analysis study, an attempt was made to investigate both these results.

The parametric equations of Niu to predict the stress concentration factors for T-butt welded joints and the through thickness stress distributions were used to compare with the results of the tubular section modelled.

3.7.1 Comparison of T-butt and tubular joint results

3.7.1.1 Niu FE model

The FE model used in the study of the stress fields for T-butt welded joints is shown in Figure 3.20. The irregular weld surface was simplified as a flat surface and the weld toe geometry was idealised as a blunt notch of radius ρ at an angular corner of α. It was assumed in this study that the stress fields were dominated by the plane strain state. This therefore allowed for the construction

of the model to be made using two-dimensional elements. Conventional eight-noded isoparametric elements were used in the analysis. The values of α and ρ used in this study were:

	30°		1/15
α	45°	ρ/T	1/25
	60°		1/30
			1/50

The geometric parameter for the ratio of weld leg length to joint thickness was a constant L/T=0.5. Photoelastic studies have shown that the effcet of varying this parameter on the local stress field is of secondary importance for the case of pure bending loading. The actual geometry of the mesh Figure 3.20 shows the weld toe region modelled using a very fine mesh so as to accurately model the high stress gradients. The study was conducted for both bending and tension loading.

3.7.1.2 Results

Figures 3.21 - 3.24 show the through thickness stress distributions for bending and tension conducted on T-butt welded joints with weld angle α 45° and 30° corresponding to the two steel models with profile A and weld angle α of 47° and profile C, weld angle α 27°. A comparison of these T-butt joint results with the stress distributions for the tubular joints is only possible provided that the basic parameters are defined on a common basis. Two problems arise namely:

(i) nominal stress definition for T-butt joints is different to that of the tubular joints.

(ii) the stress distributions for T-butt joints are for tension and bending separately whereas for tubular joints the distribution is a combined tension and bending.

Therefore, in order to make a comparison between the tubular joint results for through thickness stress distributions and the T-butt welded joint results one initial assumption needs to be made i.e. the concept of hot spot stress applicable to tubular joint analysis should be exter.ded to T-butt joints. The equivalent hot spot stress could be expressed as:

$$\sigma_* = \sigma_B + \sigma_T \qquad 3.6$$

The aim in this section is to show that the stress predicted through the thickness of a tubular joint is of the same magnitude and distribution as the through thickness stress for a T-butt welded joint subjected to pure bending and tension i.e.

$$\sigma = (SCF)_B\sigma_B + (SCF)_T\sigma_T \qquad 3.7$$

σ_*	Equivalent hot spot stress for T-butt joint
σ_T	Stress in T-butt joint under pure tension
$(SCF)_T$	SCF for T-butt joint under pure tension
σ_B	Stress in T-butt joint under pure bending
$(SCF)_B$	SCF for T-butt joint under pure bending

Consider only the R.H.S. of equation 3.7 i.e. T-butt joint analysis. Using the assumption that the hot spot stress concept can be extended to T-butt joints this part of the equation can be normalised with respect to the hot spot stress giving:

$$\sigma = \frac{(SCF)_B\sigma_B + (SCF)_T\sigma_T}{\sigma_B + \sigma_T} \qquad 3.8$$

The ratio of bending to tension is defined as:

$$R = \frac{\sigma_B}{\sigma_T} \qquad 3.9$$

Substituting equation 3.9 into equation 3.8 thus:

$$\sigma_* = (SCF)_B\left(\frac{R}{1+R}\right) + (SCF)_T\left(\frac{1}{1+R}\right) \qquad 3.10$$

Using equation 3.10 the values of through thickness stress distribution for pure bending and tension could now be combined for T-butt joints assuming that the R ratio for T-butt joints is known.

It must be noted that so far it is not claimed that the stress distribution for tubular joints is equivalent to the combined tension and bending stresses of the T-butt joints. In order to establish if equation 3.10 is valid and confirm or otherwise wether T-butt joint data could be used for tubular joints the stress distributions for T-butt joints for tension and bending can be combined using equation 3.10. However, the value of the ratio of bending to tension R, is that

value calculated for the particular tubular joint under consideration. The stress distribution σ for the tubular joint is normalised with respect to the nominal stress value. Therefore, equation 3.10 could be represented as:

$$\frac{\sigma}{(\sigma_B + \sigma_T)} = (SCF)_B\left(\frac{R}{1+R}\right) + (SCF)_T\left(\frac{1}{1+R}\right) \qquad 3.11$$

Figures 3.25 and 3.26 show a comparison of the stress distributions through the thickness for a saddle position substructured from a tubular joint and analysed using boundary conditions from the multi-planar thick shell analysis and the T-butt results calculated from pure tension and pure bending separately and combined using equation 3.10. It appears that even though the two methods studied used two significantly different approaches to predict the through thickness stress distributions, if compared on a common basis the results provide excellent agreement. This suggests that the L.H.S. of equation 3.11 is equivalent to the R.H.S. and that it is reasonable to use the T-butt joint data for tubular joint analysis.

It also suggests that it is no longer necessary to use complex boundary conditions or substructuring methods in order to calculate through thickness stress distributions for tubular joints.

3.8 Conclusions

1) The average weld toe SCF K_w value for the controlled weld profile was 15% lower than for the AWS type.

2) The changes in weld geometry namely, weld angle α, weld toe radius ρ and weld leg length L have been shown tc significantly influence the through thickness stress distribution.

3) Possible inaccuracies exist in the equations recommended by UKOSRP 1 for calculating the extent of the linear region on the outer surface of a tubular joint.

4) The substructured technique was successfully validated against experimental stress analysis results.

5) Through thickness stress distributions for T-butt welded joints for pure bending and tension can be combined to represent the through thickness stress distribution of a tubular joint.

3.9 References

3.1 Design of Tubular Joints for Offshore Structures Volume 2 UEG Publication UEG/CIRICA UR 33 1985

3.2 *European Offshore Steels Research Seminar* . Cambridge, UK 27-29 November 1978.

3.3 Connolly M. P., Hellier A. K., Dover W. D., Sutumo J., A Parametric study of the ratio of bending to membrane stress in tubular Y and T-joints. *Journal of Strain Analysis for Engineering Design*, 1989 (To be published).

3.4 Hellier A. K., connolly M. P., Dover W. D., Stress concentration factor for tubular Y and T-joints. *Journal of Strain analysis for Engineering Design*, 1989 (To be published).

3.5 American Welding Society Structural Welding Code D1.1-1984.

3.6 Microset Replica System, Applied Metallurgical Services Ltd Hawley Rd, Hinckley Leics England.

3.7 Mondina A., Pappalettere C., Sangirardi M., Polycarbonate photoelastic coatings for curved specimens. *Journal of Experimental Mechanics. SESA* December 1985.

3.8 Koibuchi k.,Ohno H.,Local Strain approach to life prediction of welded structures. *2nd International conference on mechanical behaviour of materials*. Boston, USA August, 16-20,1976.

3.9 Irvine N. M., Review of stress analysis techniques in UKOSRP1. *Int. Conf. on Fatigue in Offshore Structural Steels*. Institution of Civil Engineers London 1981 paper 6.

3.10 Gibstein, M.G., Stress concentration in tubular joints. Its definition, determination and applications. *Steel in Marine Structures. Int. Conf.* Oct 1981, Paris. Commission of The European Communities.

3.11 Fatigue Handbook Offshore Steel Structures, ed.A. Almar-Naess Published Tapir 1985.

3.12 Kerr,J., The effect of strain gauge trimming. *Strain* 17, 1981. pp 147-150.

3.13 Holdbrook, S.J., The application of linear elastic fracture mechanics to fatigue crack growth in welded tubular joints, PhD Thesis, University of London, 1980.

3.14 Dover, W.D., Connolly, M.P.M., Fatigue fracture mechanics assessment of tubular welded Y and K-joints, *Int. Conf. on Fatigue and Crack Growth in Offshore Structures,* Inst. of Mechanical Engineers, London, 1986.

3.15 Iida, K., Asano, K., Toyofuku, T., and Ishikawa, K., A fatigue design procedure for offshore tubular connections, Paper II, *Int. symposium on Integrity of Offshore Structures* (ed. Faulkner), Glasgow, 1981.

3.16 Lawrence, F.V., Mazumdar, F.K., Predicting the fatigue resistance of welds. *Annual Review of Materials Science,* No. 11, 1981.

3.17 Dover, W.D., Dharmavasan,S. Fatigue fracture mechanics analysis of T and Y joints. OTC 4404. Offshore Technology Conference. Houston, Texas May 1982.

3.18 Niu, X., Effects of local stresses on fatigue of tubular welded joints. PhD Thesis, University of London, 1987.

3.19 Niu, X., Glinka, G., The weld profile effects on the stress intensity factors in weldments. *Intl. Journal of Fracture,* 1986.

	Average value of α	Average value of ρ	Most frequent value of ρ
Profile A (s)	47°	0.75mm	0.62mm
Profile C (s)	27°	0.92mm	0.82mm
Profile A (c)	_____	0.96mm	0.86mm
Profile C (c)	_____	1.23mm	1.08mm

Table 3.1 Geometric parameters of weld profiles
(s) saddle position (c) crown position

Chord	Stress concentration factor					
	Profile A			Profile C		
Saddle position	K	K_G	K_w	K	K_G	K_w
A	18.88	6.30	3.02	6.42	5.60	1.15
B	6.33	5.30	1.19	5.41	4.80	1.13
C	5.45	3.80	1.70	6.10	3.20	1.79
D	5.90	4.33	1.36	6.50	4.00	1.63
Average		4.93	1.82		4.40	1.43

Table 3.2 SCF values at saddle positions of steel joints OPB case

Stress concentration factor					
Profile A			Profile C		
K	K_G	K_w	K	K_G	K_w
6.17	5.23	1.18	5.77	5.4	1.07
6.27	5.31	1.18	6.42	5.6	1.15
5.92	4.23	1.40	4.45	2.8	1.59
5.90	4.20	1.41	0.11	0.1	1.10
4.33	1.54	2.82	1.13	0.9	1.26
5.53	3.79	1.46	2.10	2.14	1.45
14.44	5.82	2.48	6.90	2.66	1.90
17.69	5.92	3.04	6.76	3.10	2.18
5.90	4.33	1.36	7.29	3.40	2.14
5.45	3.80	1.70	6.21	4.05	1.53
6.33	5.30	1.19	5.89	3.80	1.55
18.88	6.30	3.02	8.96	3.09	2.90
			2.82	2.49	1.13
			1.43	1.10	1.30
			0.09	0.08	1.13
			3.57	2.55	1.40
			5.41	4.80	1.13
			7.31	4.30	1.70
			6.50	4.00	1.63
			6.10	3.20	1.79
			8.50	4.80	1.77
			9.82	5.60	1.75
Total	22.24		Total		34.55
Average	1.85		Average		1.57

Table 3.3 SCF values for a number of positions around brace/chord intersection-chordside. OPB loading case

Joint type	Mode of loading	K	K_G	K_W
T^{13} (UCL)	Axial	12.00	8.96	1.33
T^{13} (UCL)	Axial	8.00	5.80	1.38
T^{10} (DnV)	Axial	——	——	1.36
T^{10} (DnV)	Axial	——	——	1.26
Y^{10} (DnV)	Axial	——	——	1.24
K^{14} (UCL)	IPB	3.46	2.17	1.59
K^{14} (UCL)	IPB	3.20	2.10	1.52
K^{14} (UCL)	IPB	3.04	2.15	1.41
K^{14} (UCL)	IPB	3.05	2.16	1.41
Average	——	——	——	1.39
Iida[15]	Axial	——	——	3.20

Table 3.4 Comparison of geometric (K_G) and weld toe (K_W) stress concentration factors for a number of other tubular joints

References in Table should have a prefix 3.

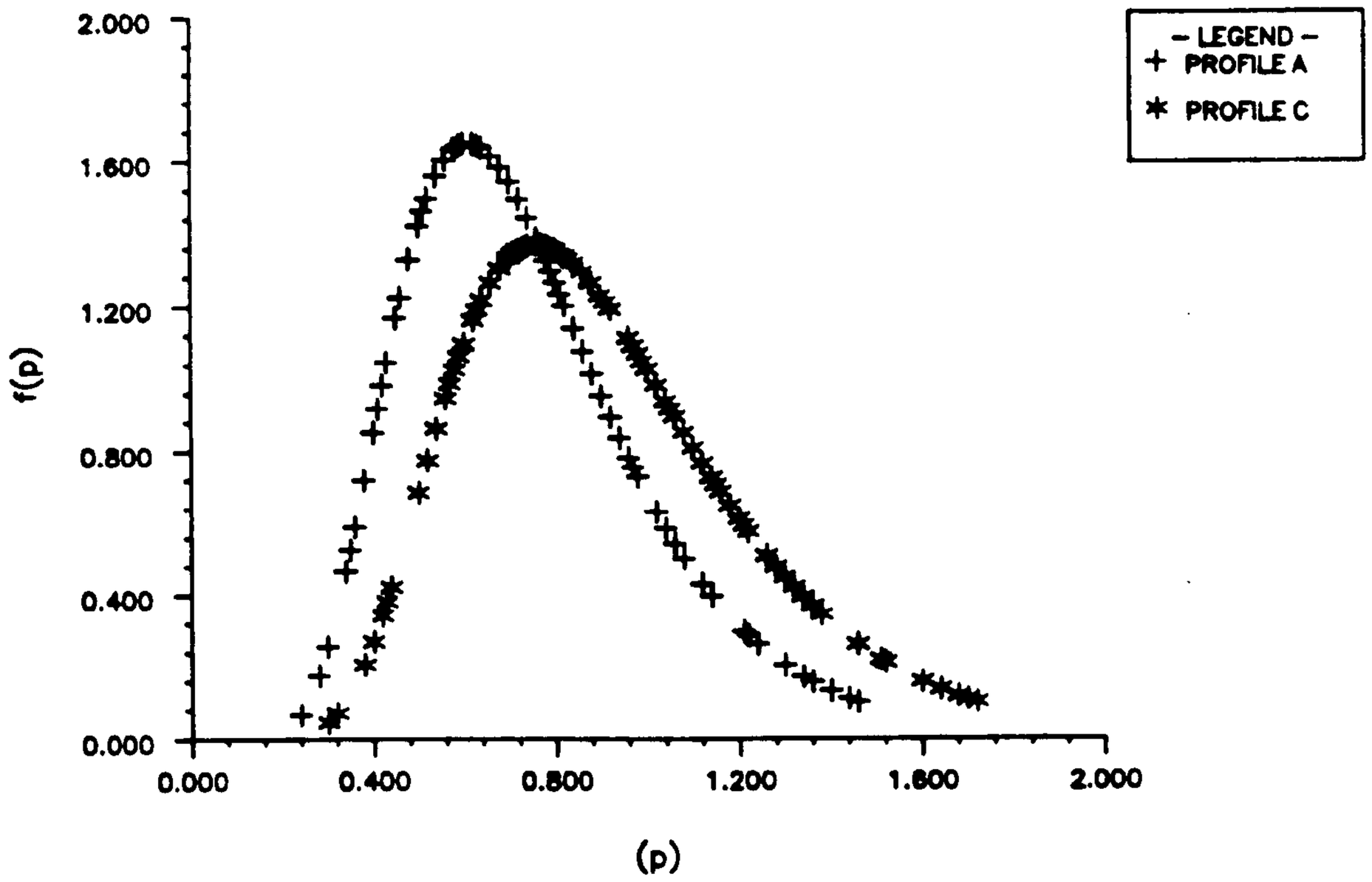

FIGURE 3.1 DISTRIBUTION OF WELD TOE RADII – SADDLE POSITION

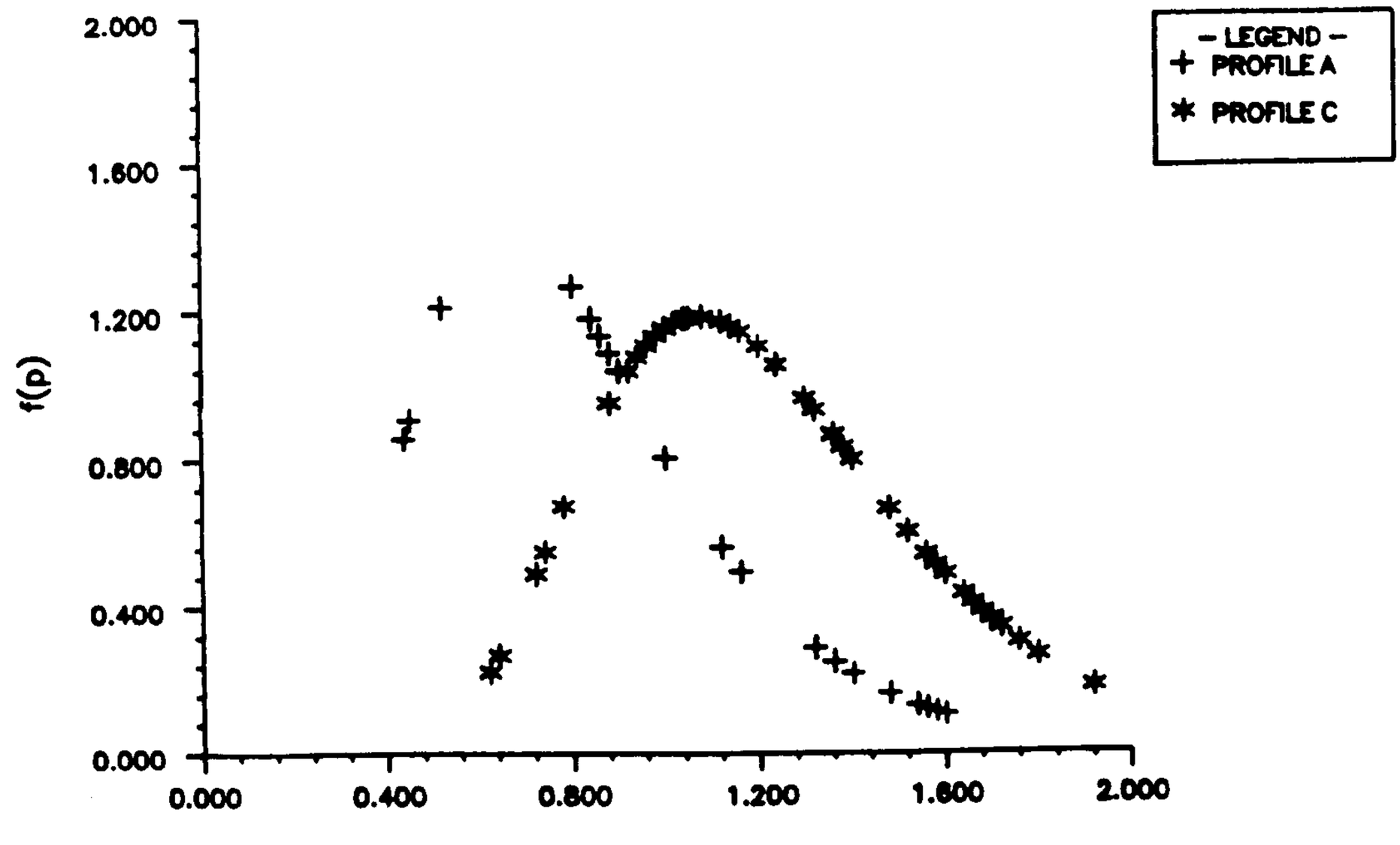

FIGURE 3.2 DISTRIBUTION OF WELD TOE RADII – CROWN POSITON

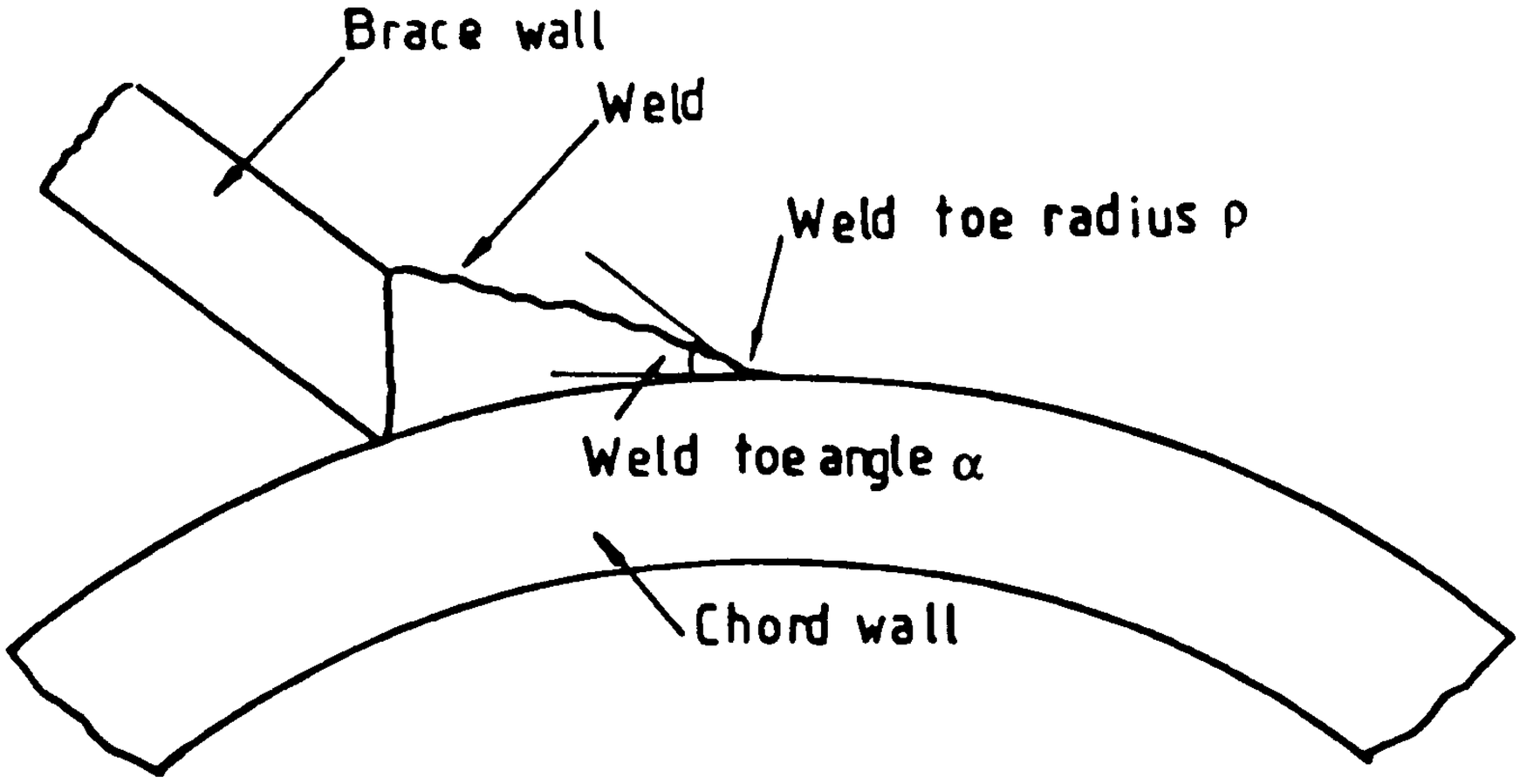

Figure 3.3 Schematic of weld profile showing weld toe angle α and weld toe radius ρ

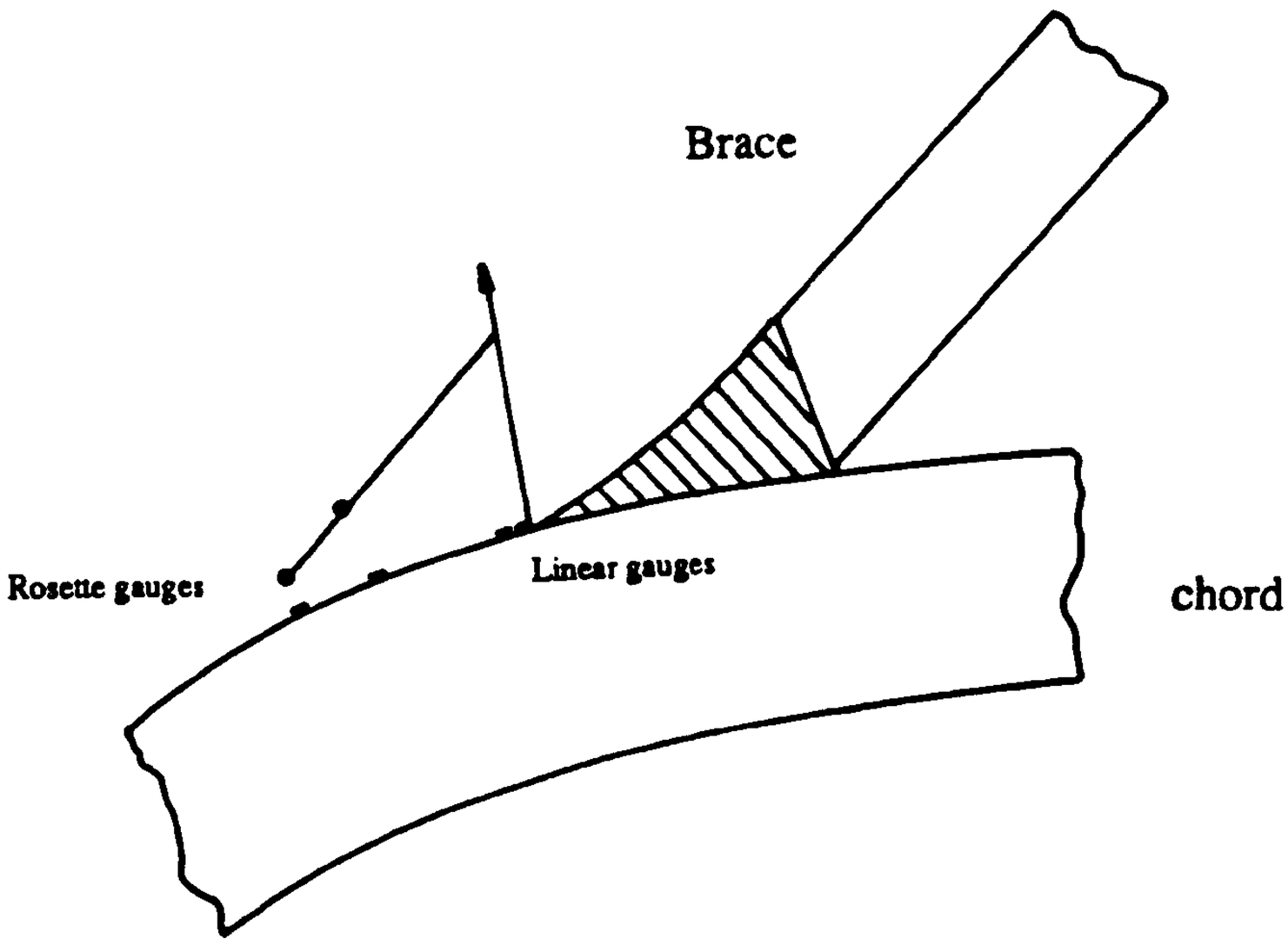

Figure 3.4 Schematic of brace/chord intersection showing locations of strain gauges

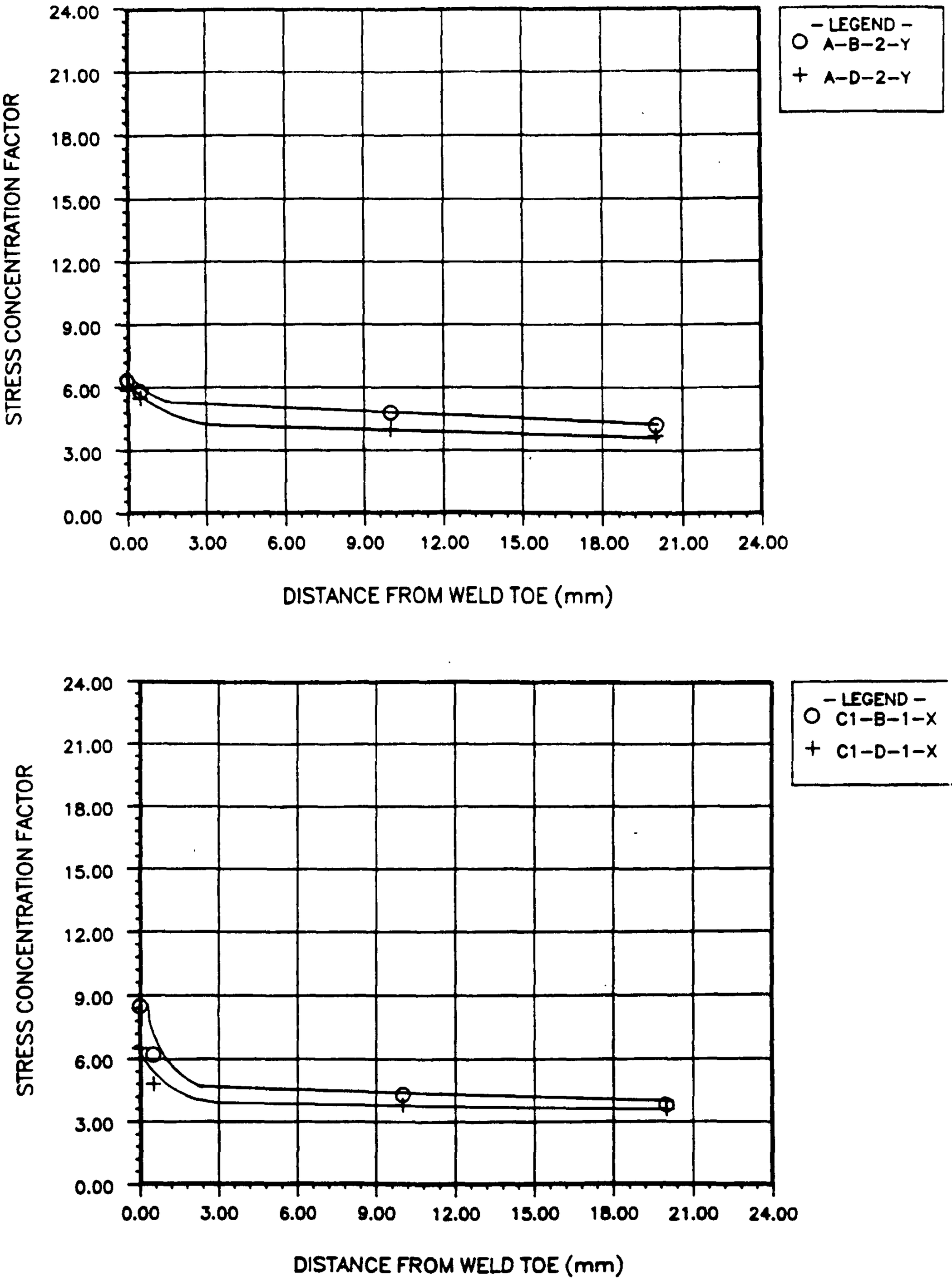

Figure 3.5 Distributions of SCF values on the outer chord surface as a function of distance from weld toe for profiles A and C. Saddle position B and D

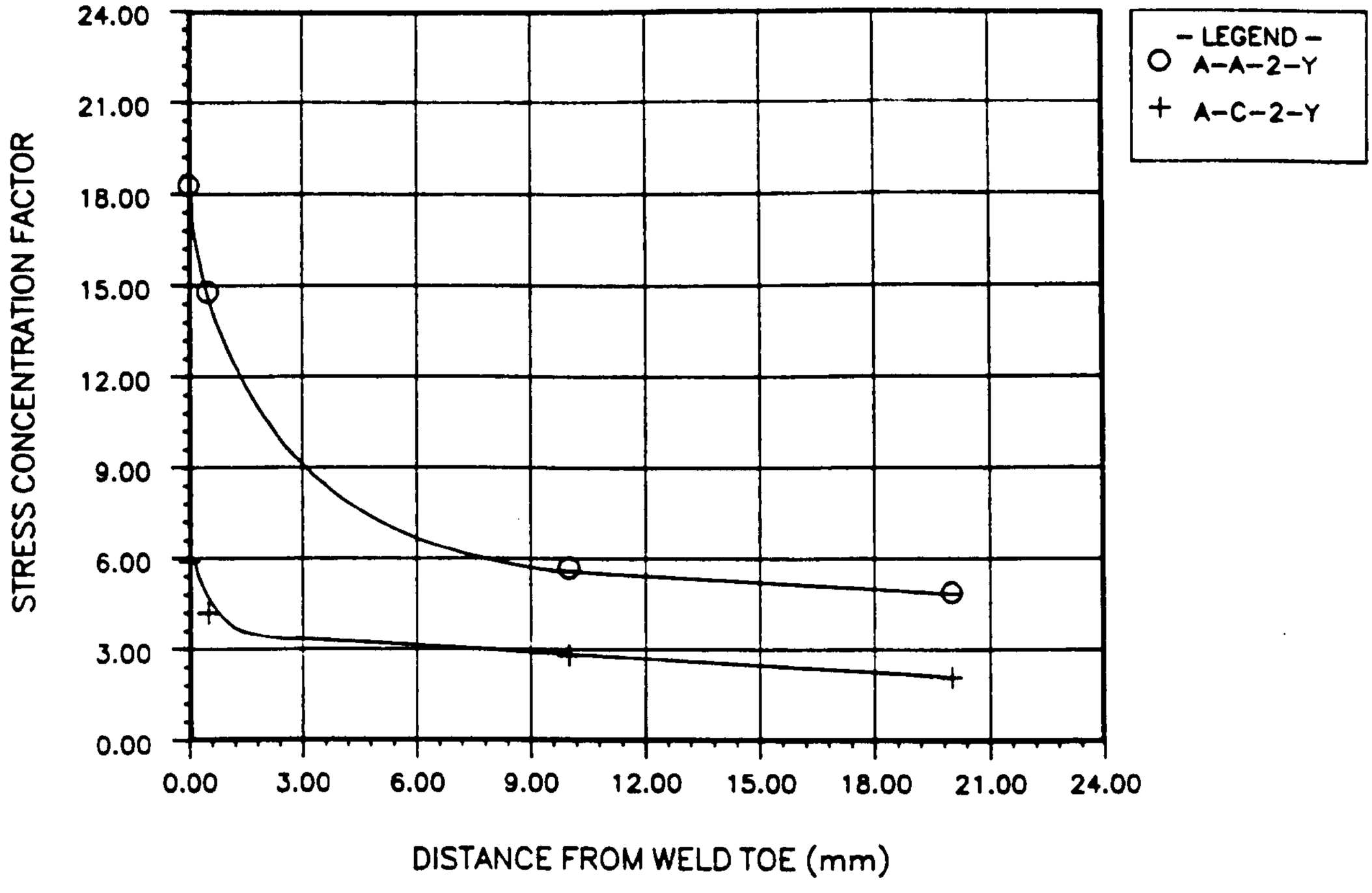

Figure 3.6 Distributions of SCF values on the outer chord surface as a function of distance from weld toe for profiles A and C. Saddle position A and C

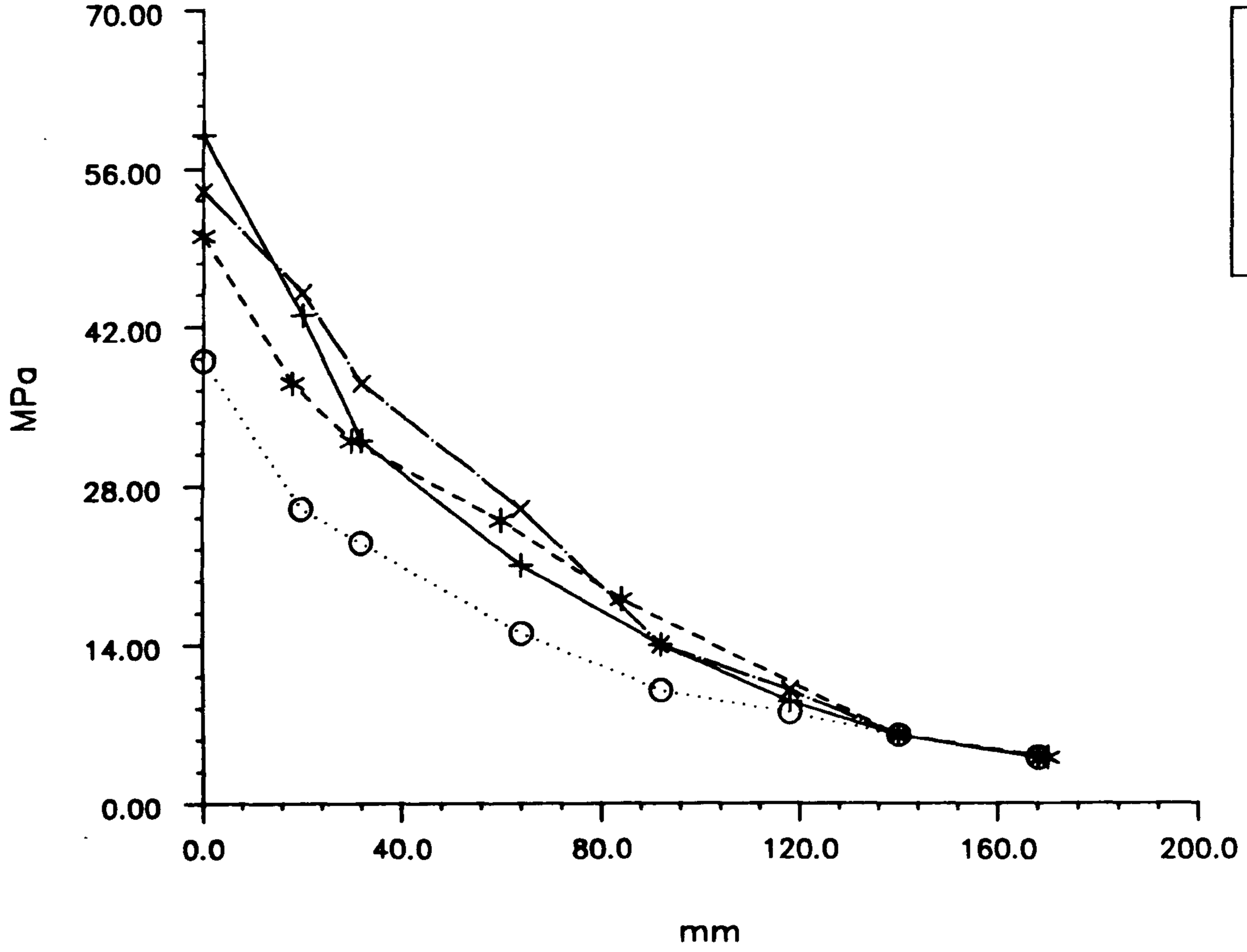

FIGURE 3.7 FE SCF PREDICTIONS SADDLE POSITIONS

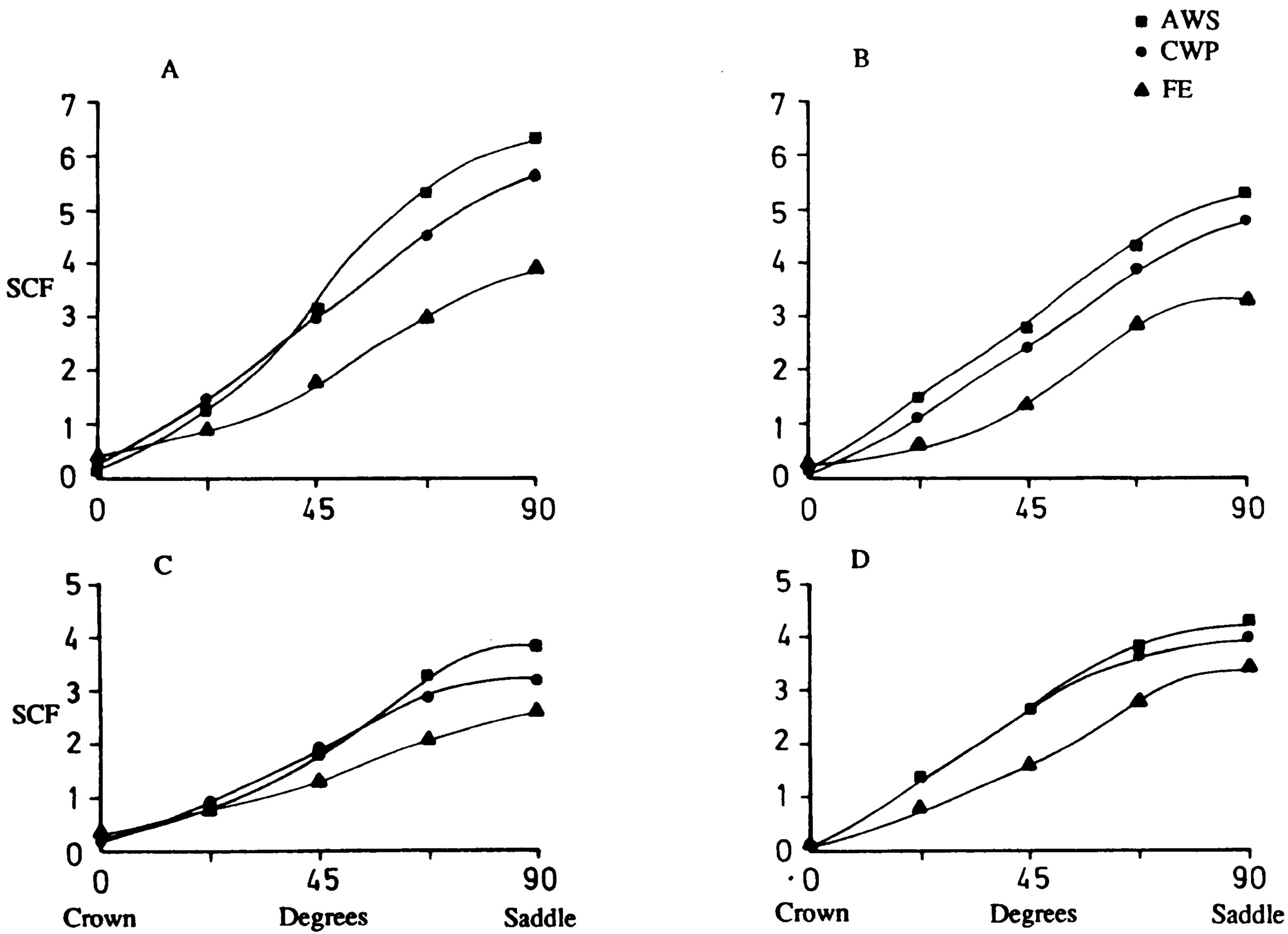

Figure 3.8 Comparison of steel model results with FE analysis predictions for saddle positions A B C and D

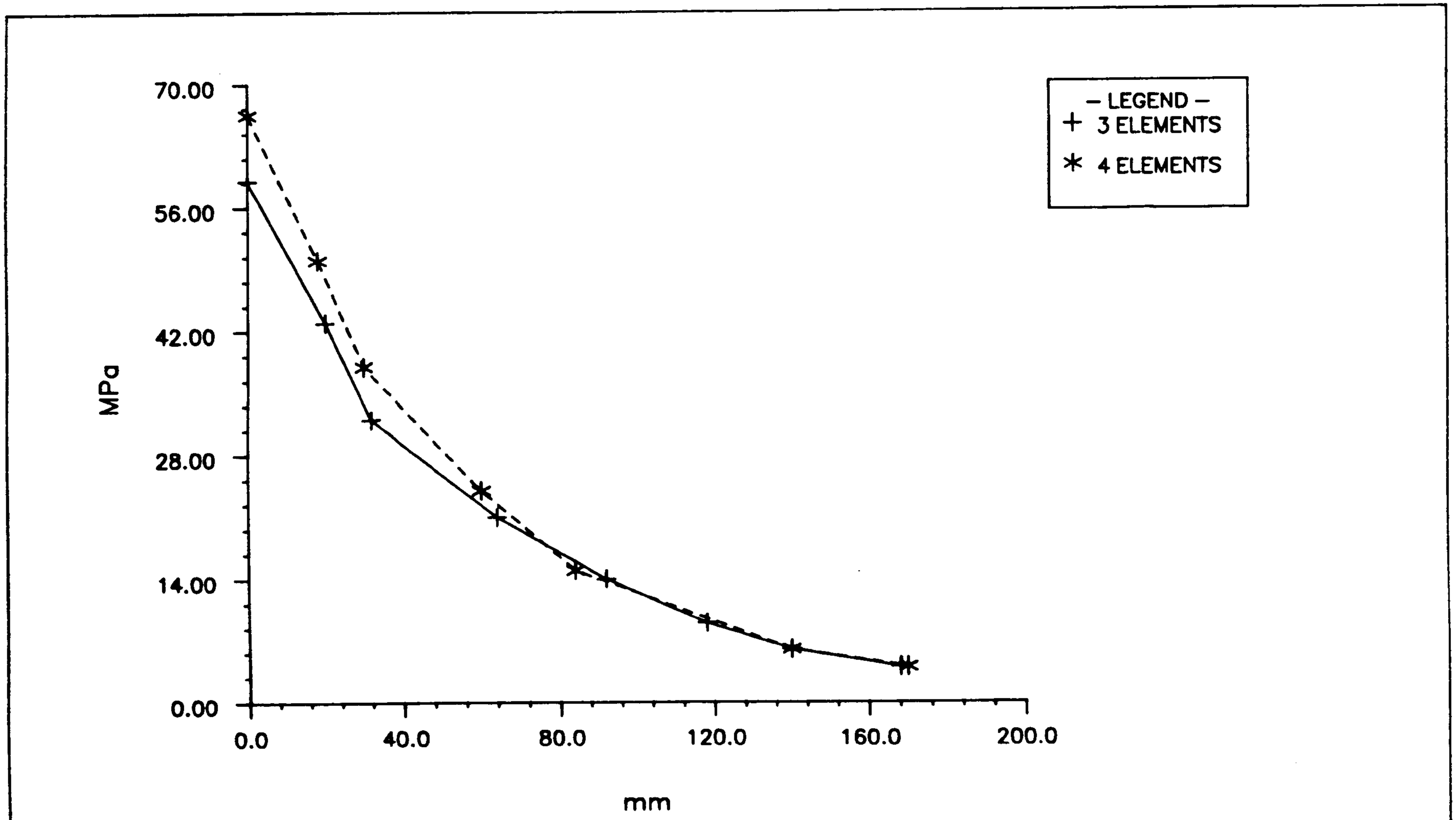

FIGURE 3.9 EFFECT OF ELEMENT SIZE ON SCF AT WELD TOE

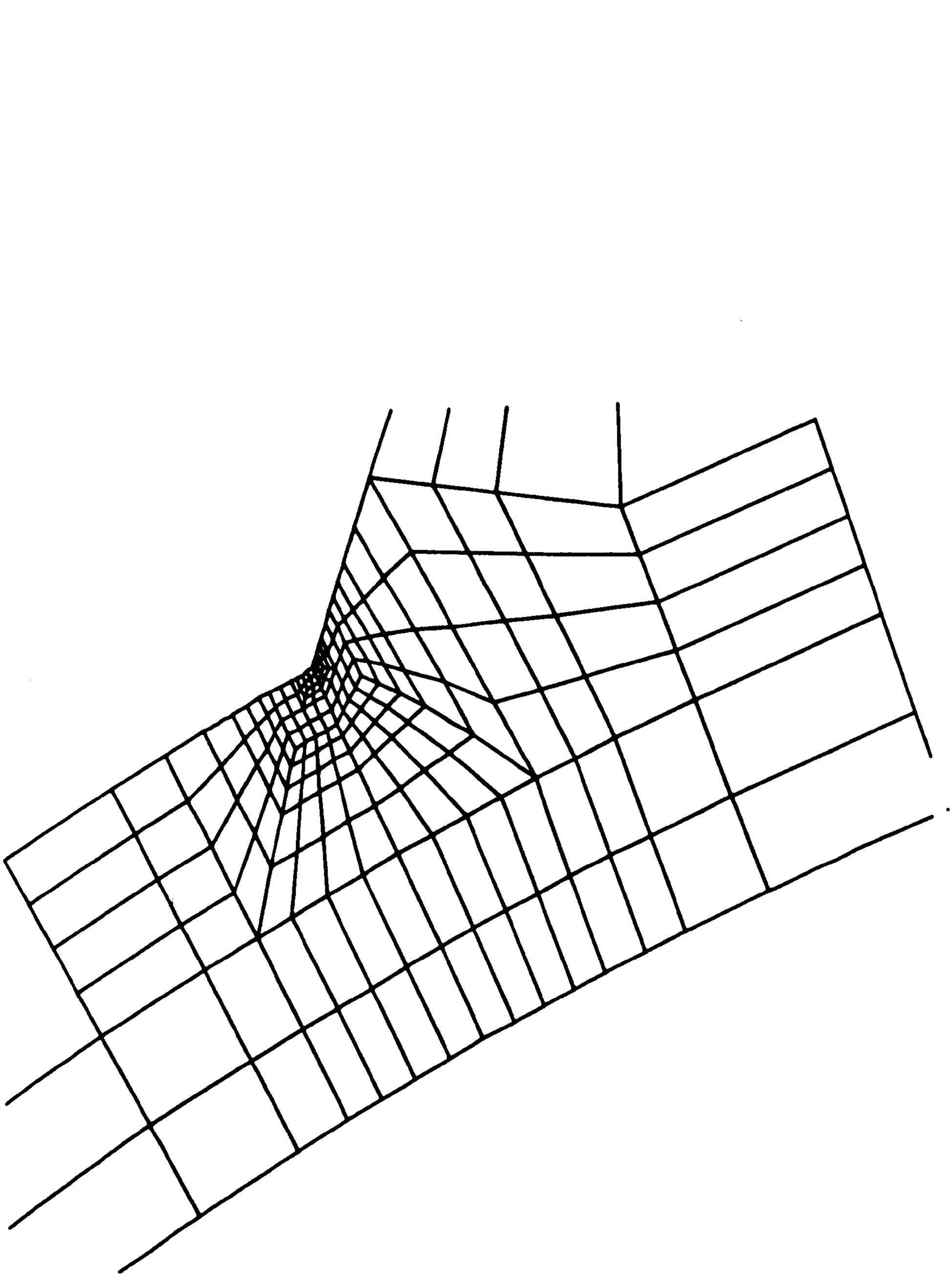

Figure 3.10 2-D FE mesh of the substructured saddle position Profile A

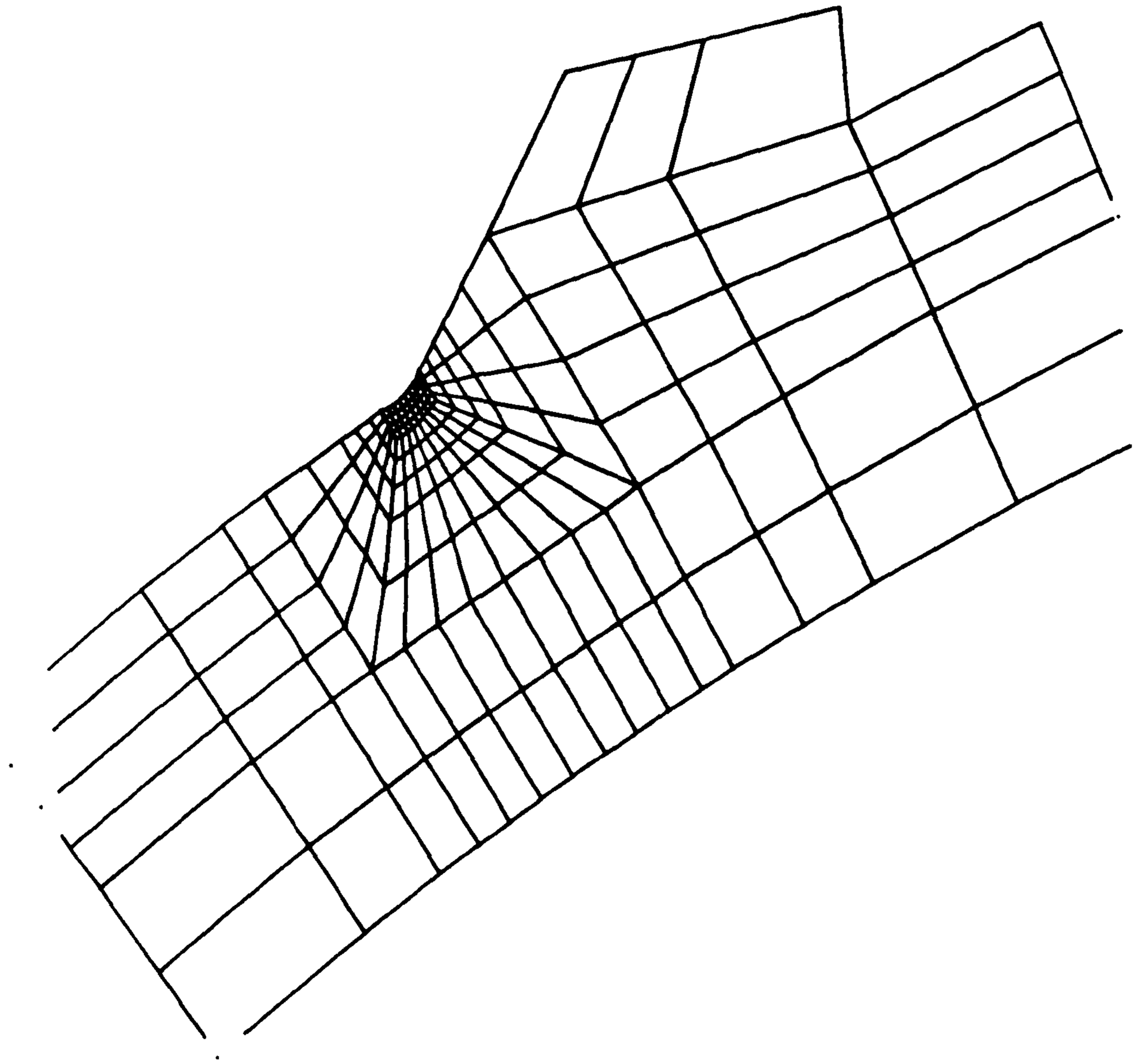

Figure 3.11 2-D FE mesh of the substructured saddle position Profile C

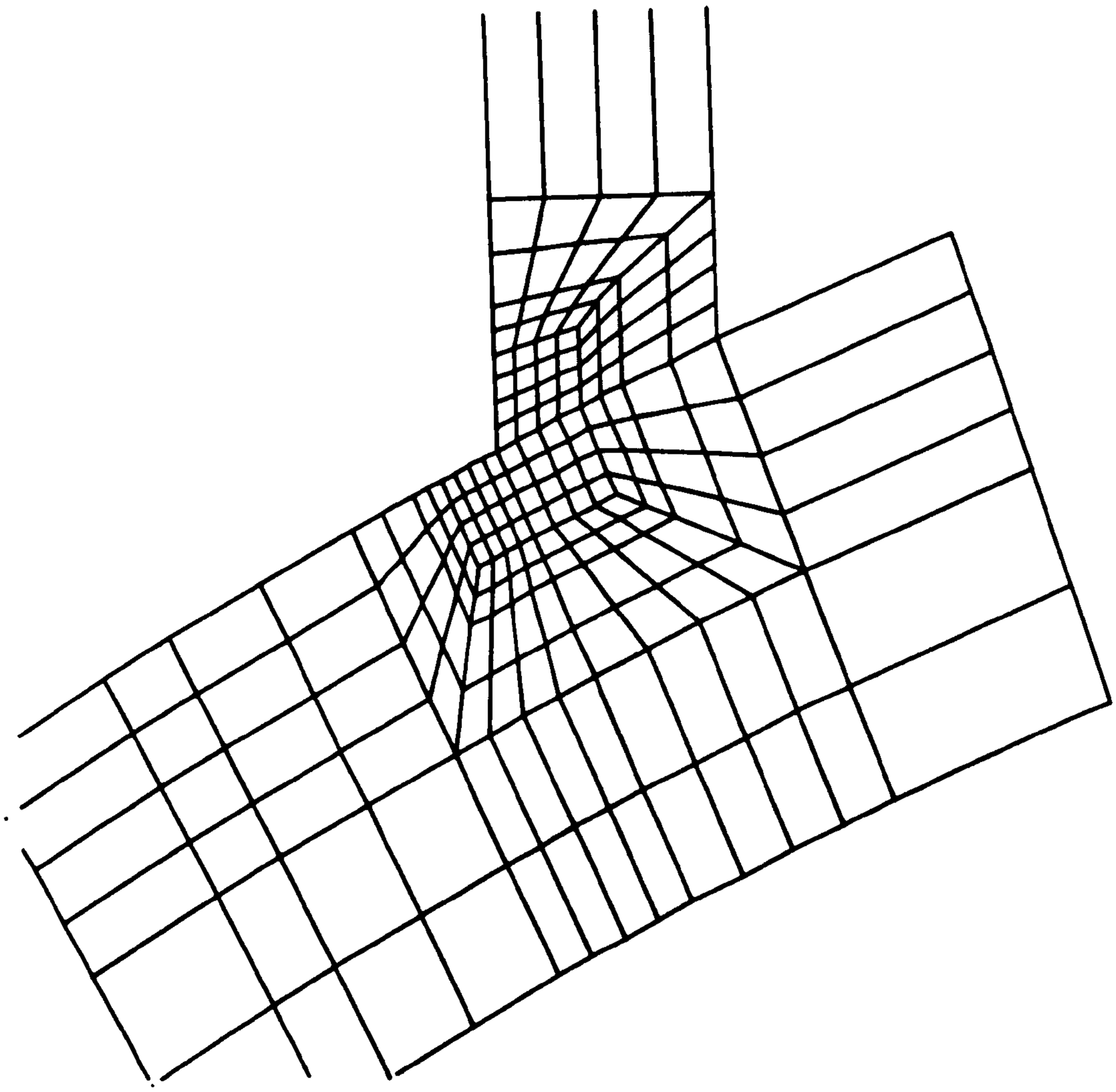

Figure 3.12 2-D FE mesh of the substructured saddle position No weld

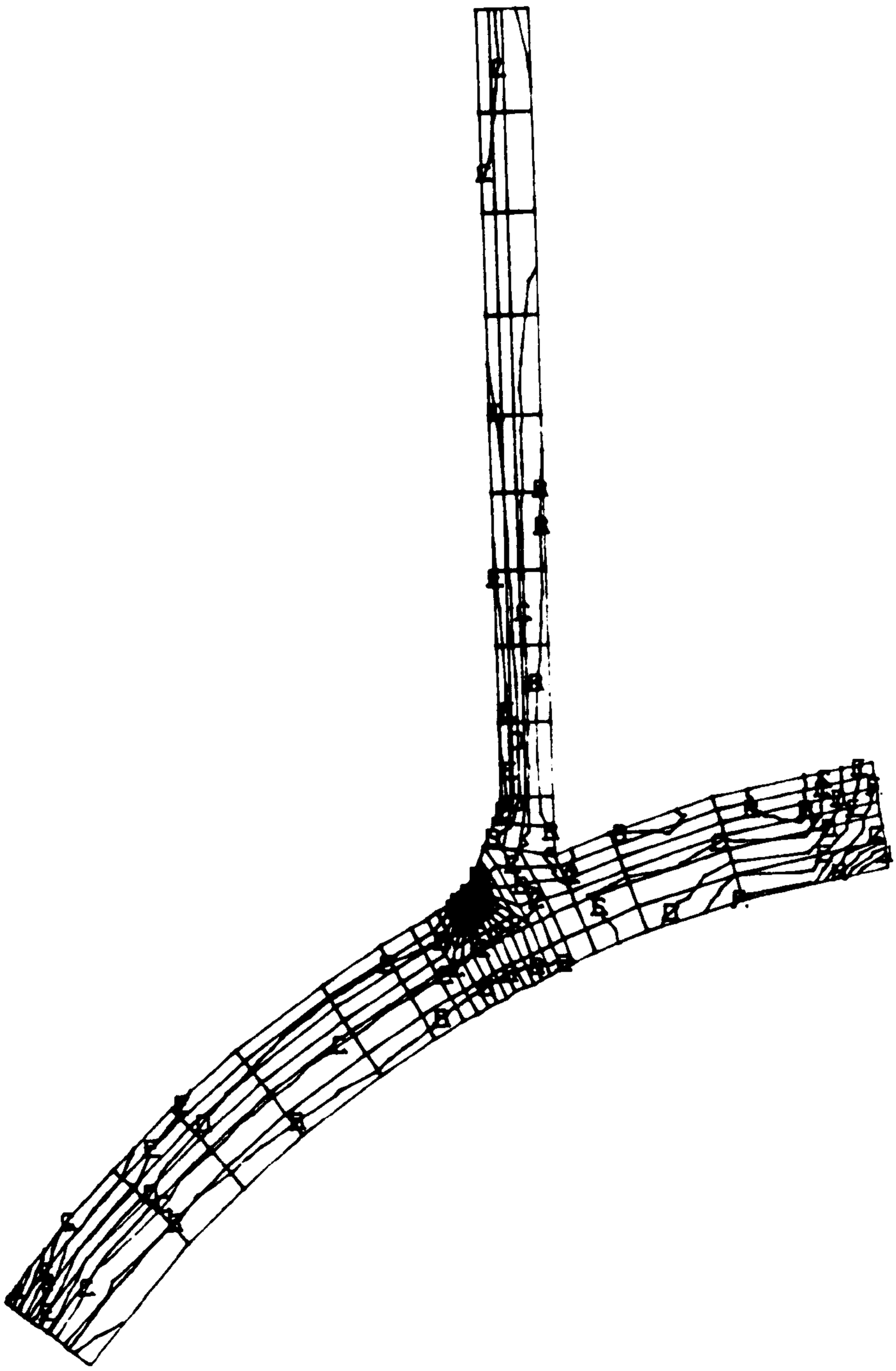

Figure 3.13 Line contours showing through thickness stress distributions at the weld toe. Profile A

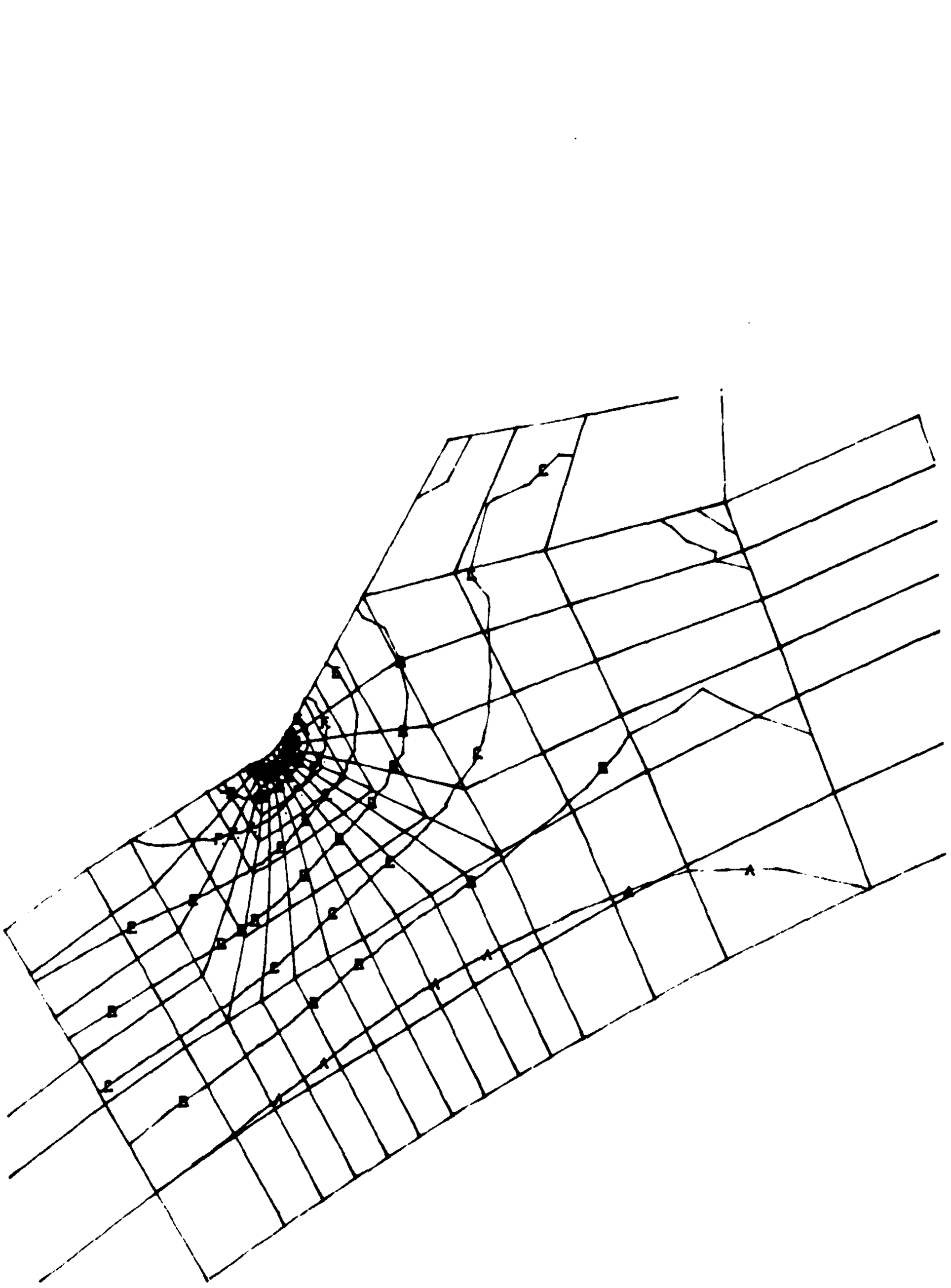

Figure 3.14 Line contours showing through thickness stress distributions at the weld toe. Profile C

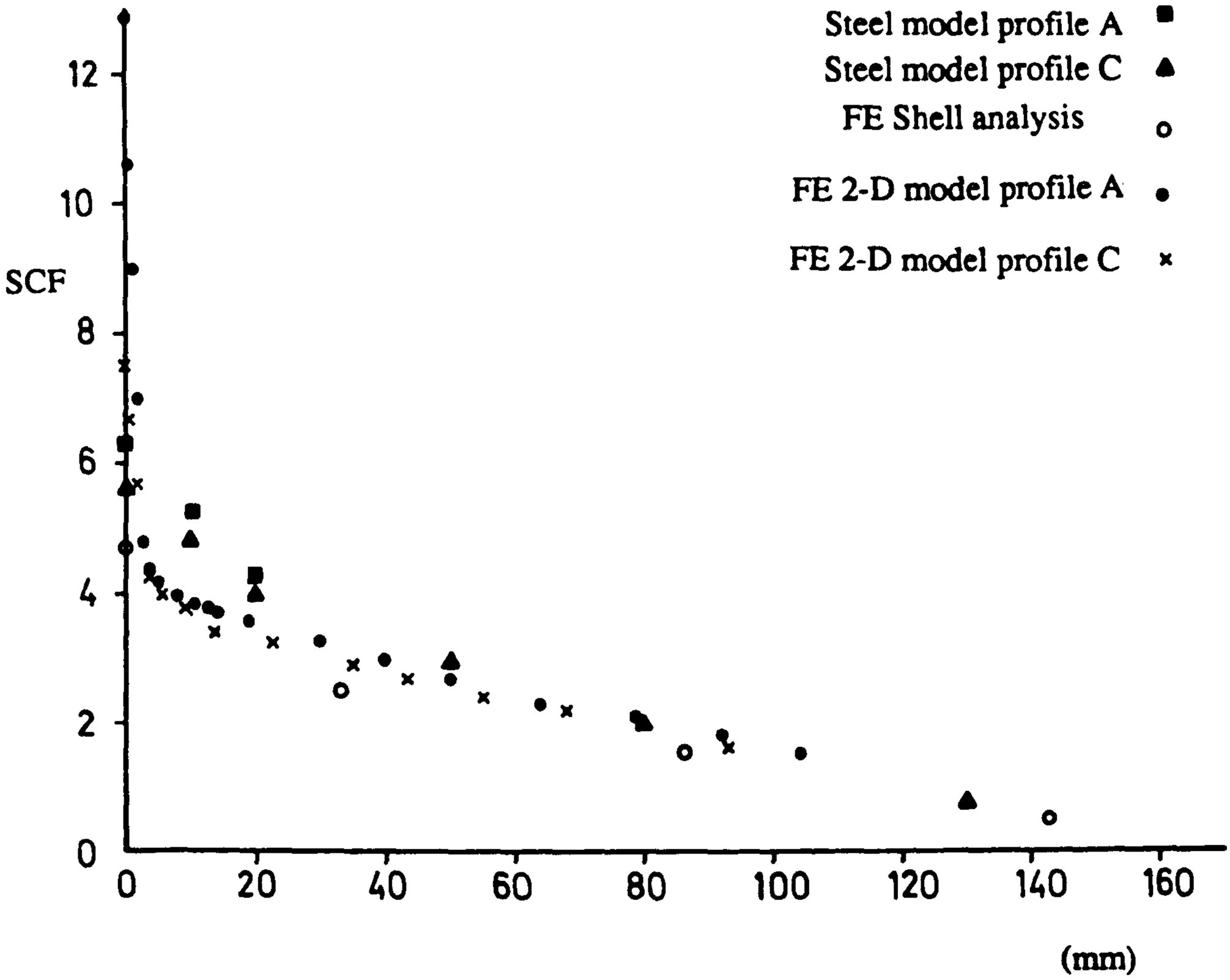

Figure 3.15 Comparison of stress distributions on the outer surface of the chord using the common origin for all coordinate systems: Experimental data, FE data and 2-D FE results

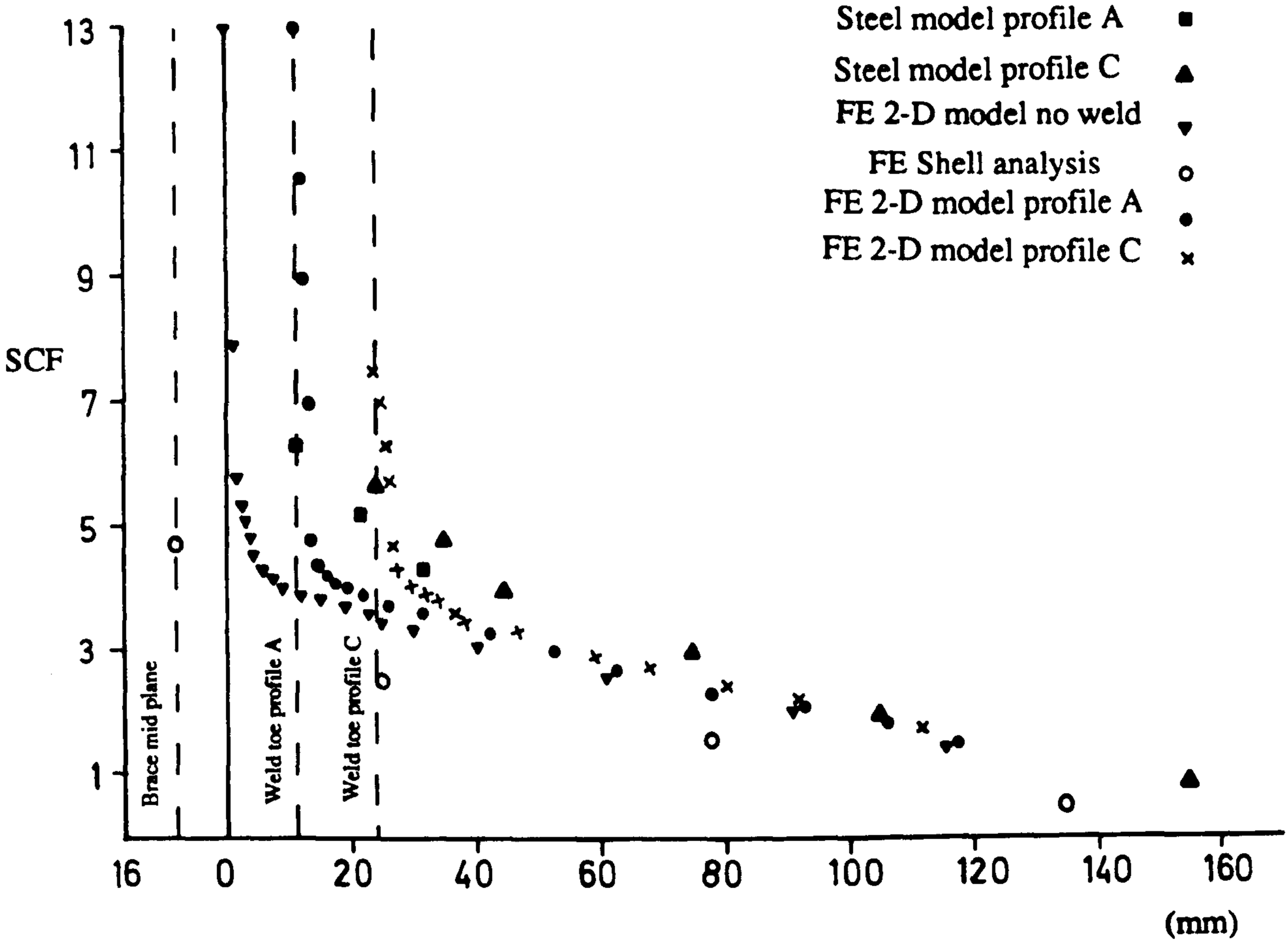

Figure 3.16 Comparison of stress distributions on the outer surface of the chord using the true positions of coordinate systems in relation to the brace/chord intersection

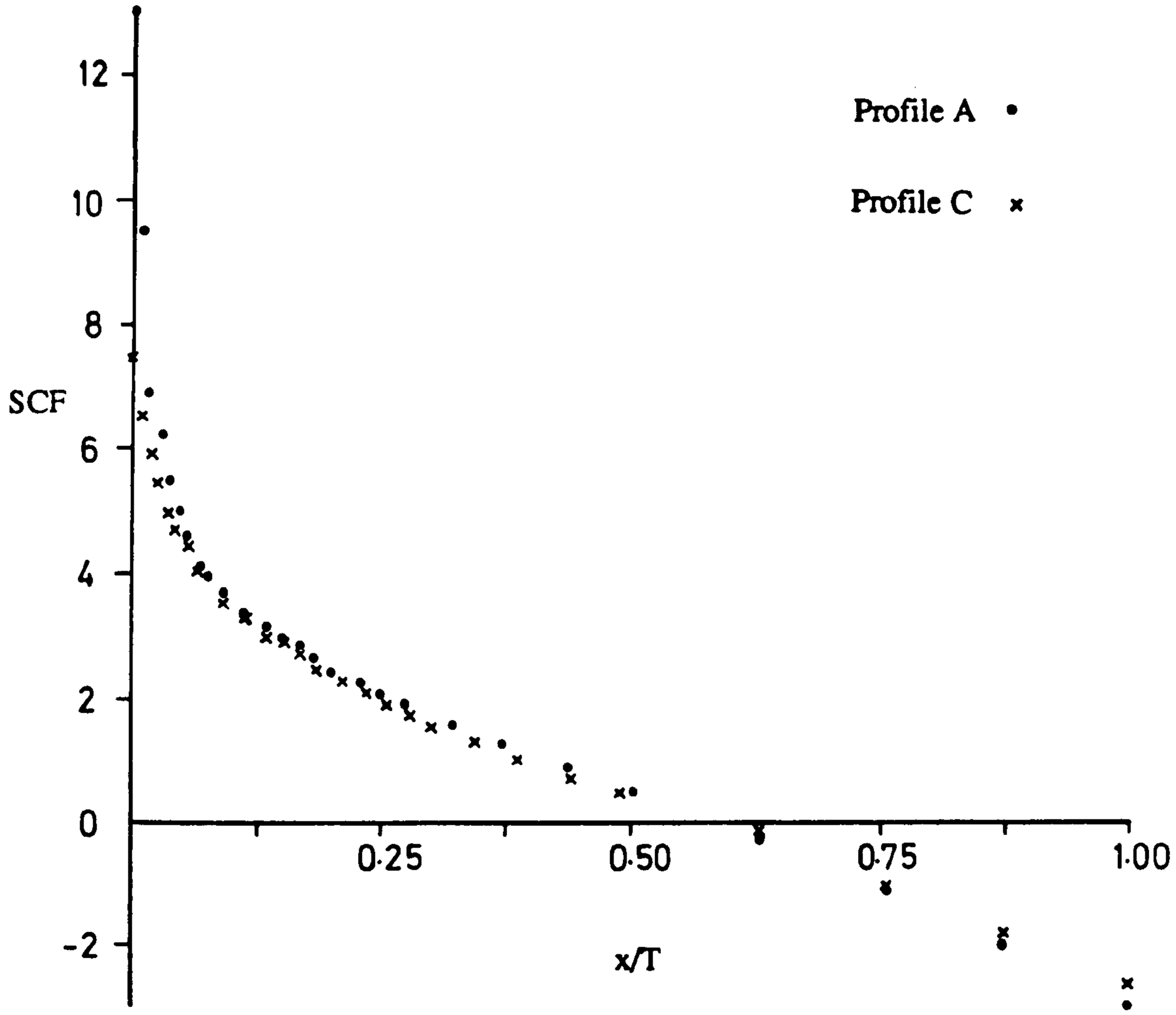

Figure 3.17 Through thickness stress distributions for profiles A and C obtained from the FE analyses of 2-D substructured element

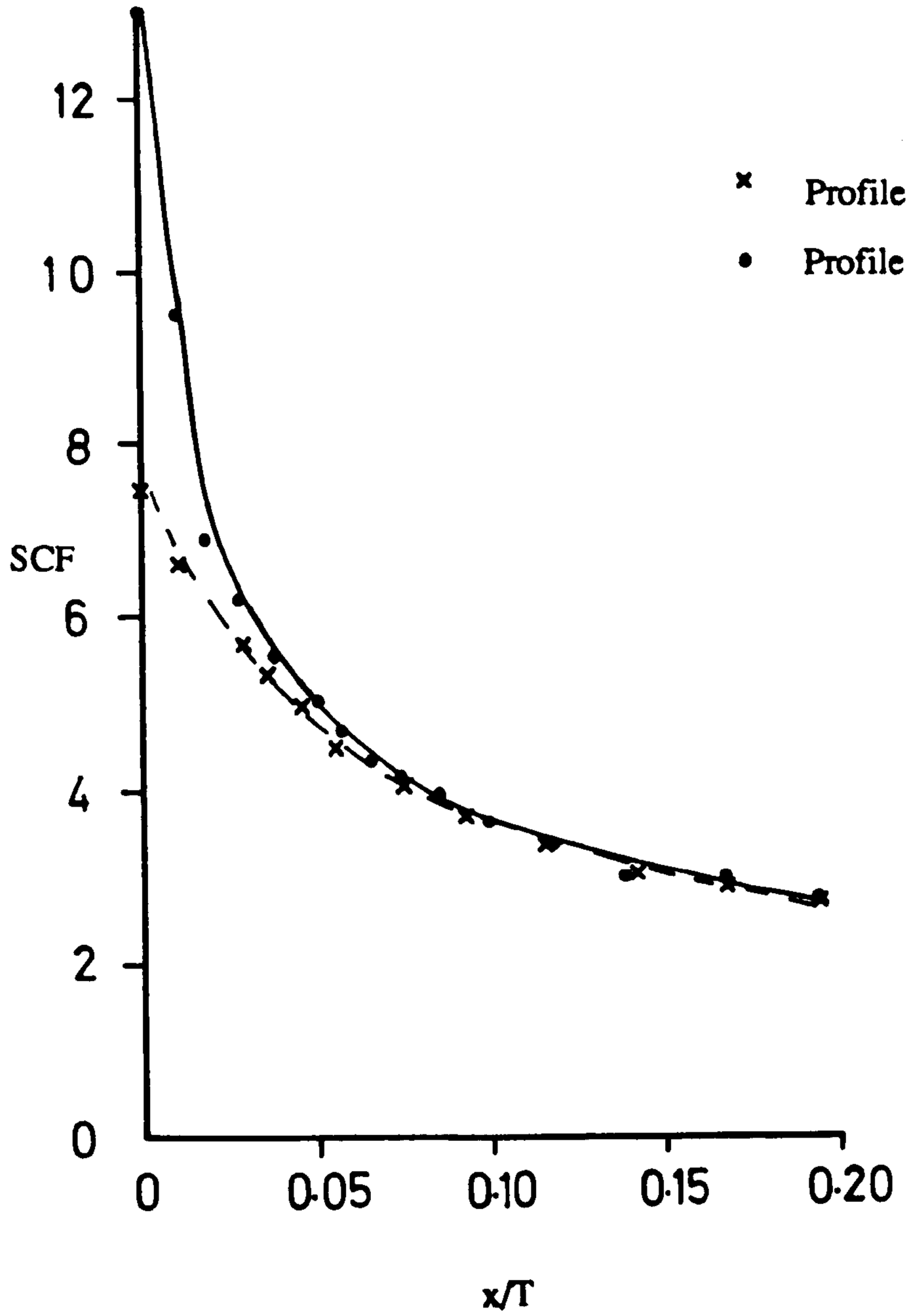

Figure 3.18 Effect of geometry of weld profile on through thickness stress distribution

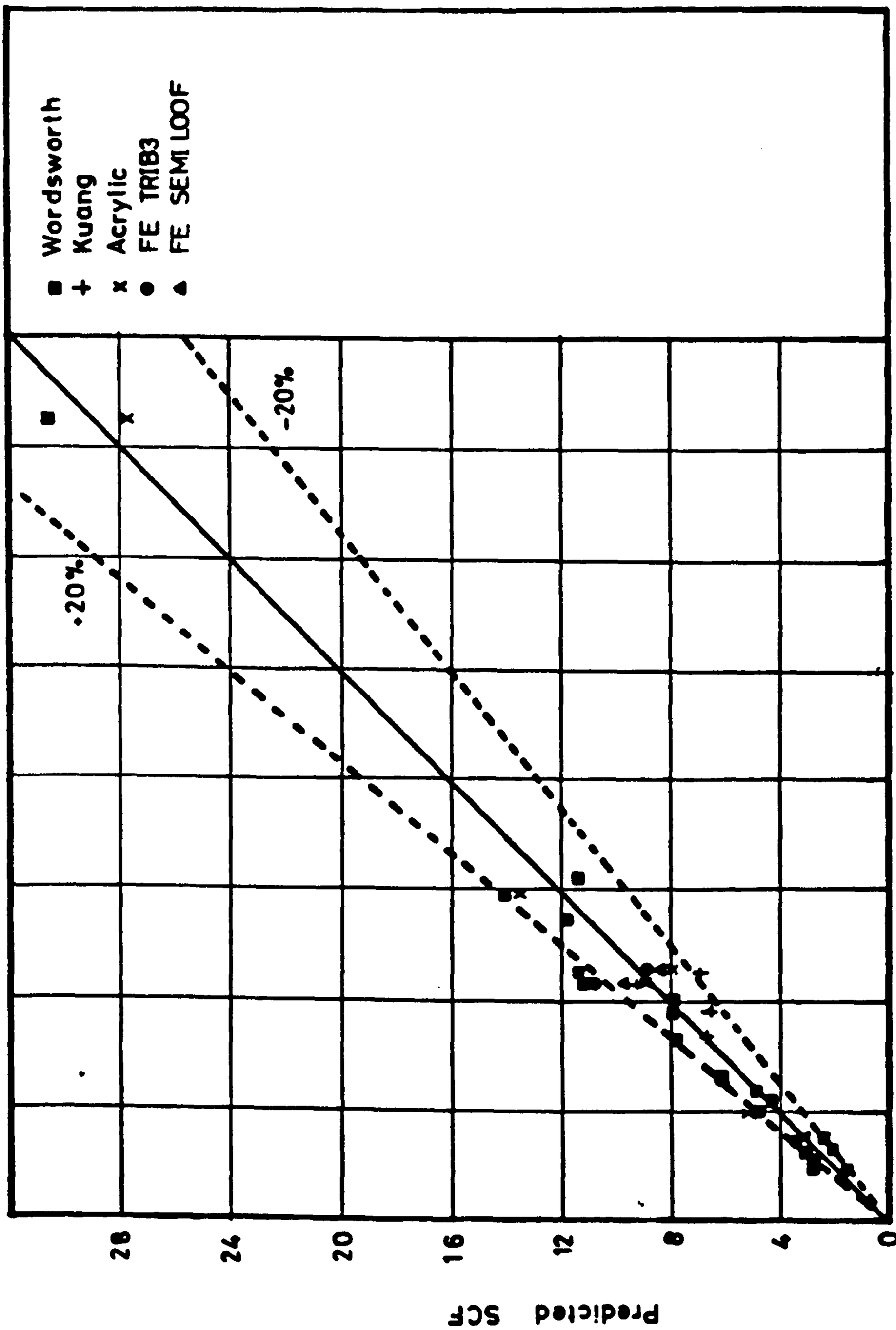

Figure 3.19 Comparison of measured and predicted SCFs for different tubular joints

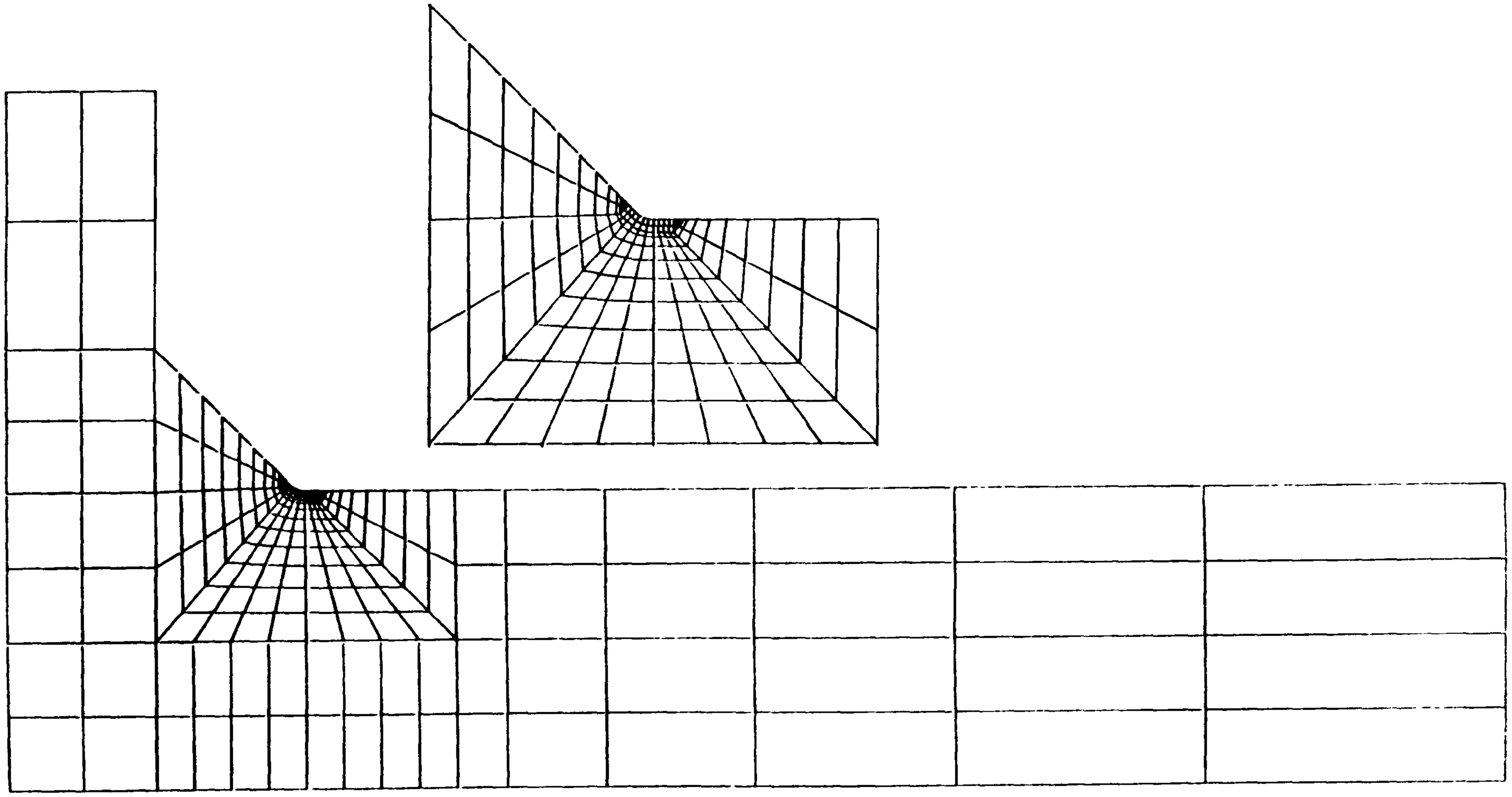

Figure 3.20 FE model used in T-butt joint analysis (ref.3.18)

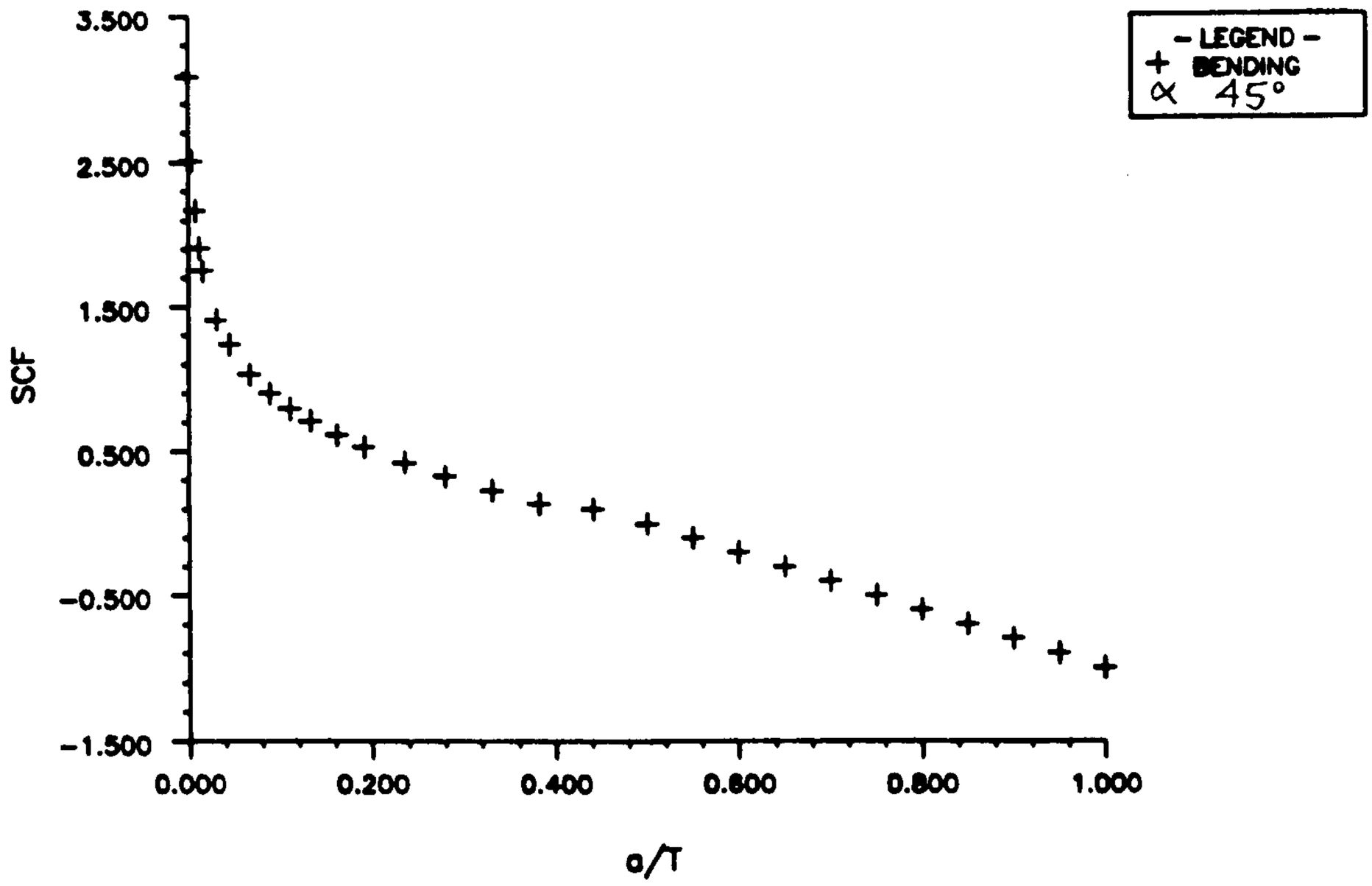

FIGURE 3.21 THROUGH THICKNESS STRESS DISTRIBUTION T–BUTT

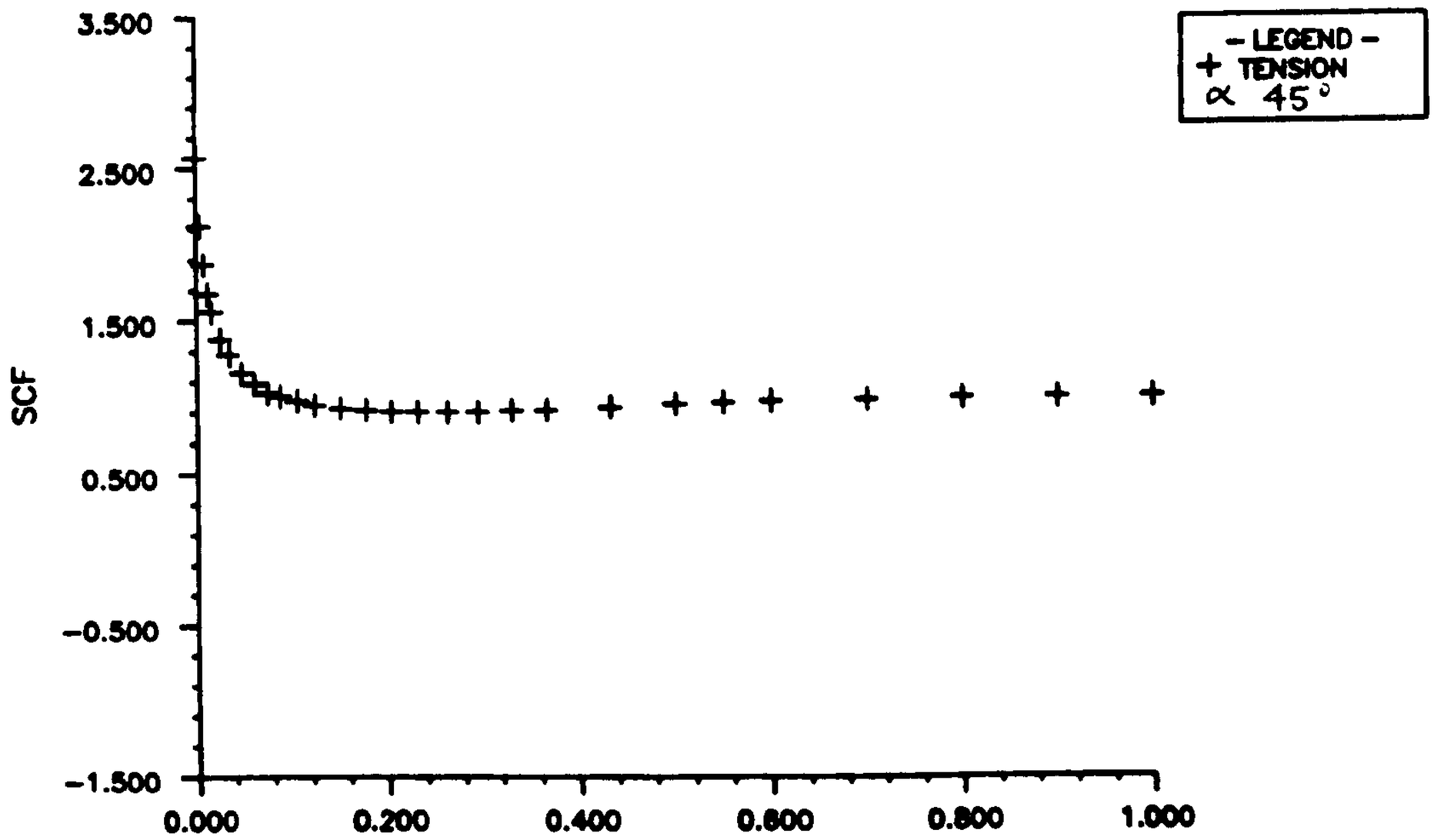

FIGURE 3.22 THROUGH THICKNESS STRESS DISTRIBUTION T–BUTT

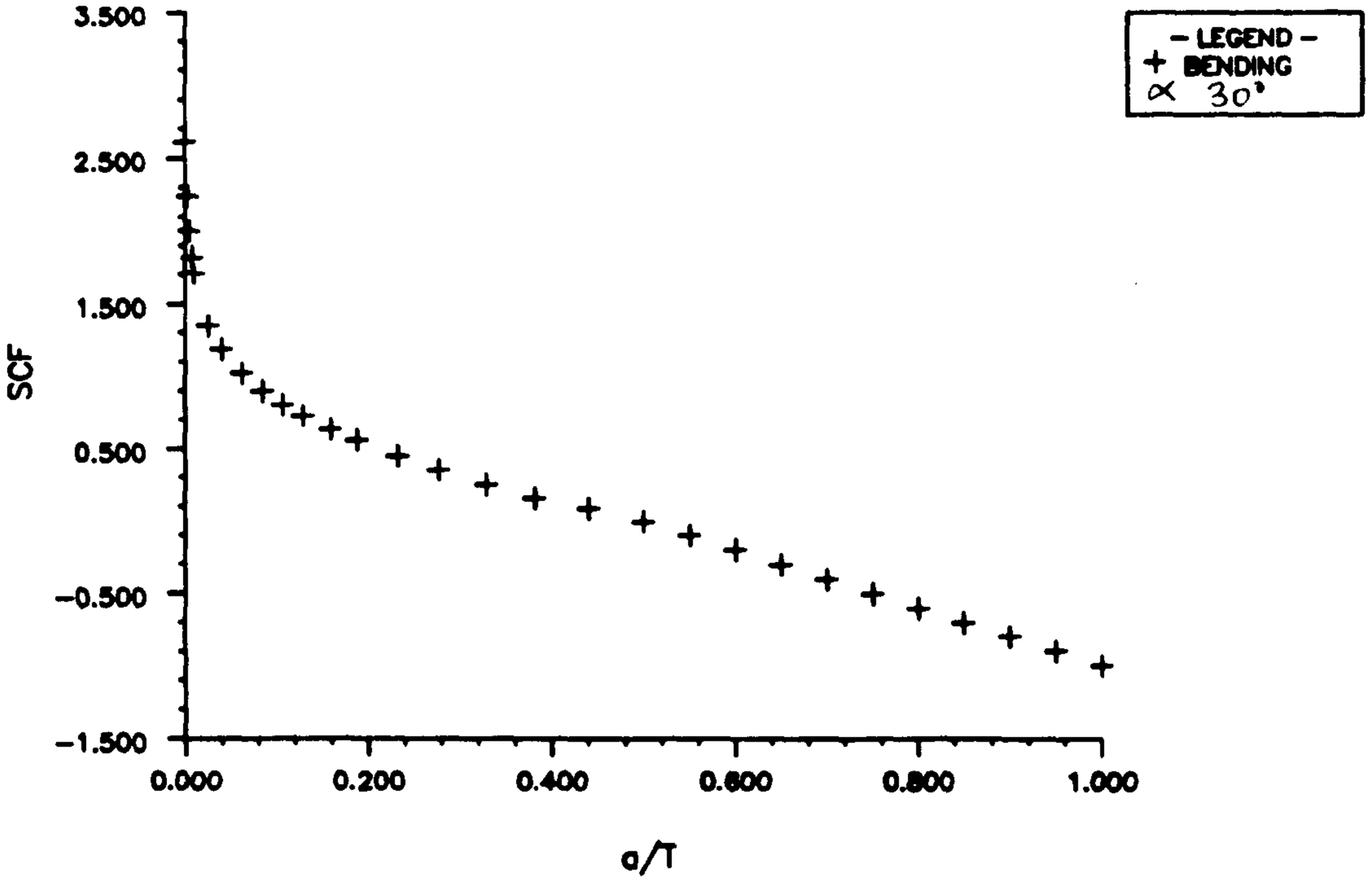

FIGURE 3.23 THROUGH THICKNESS STRESS DISTRIBUTION T–BUTT

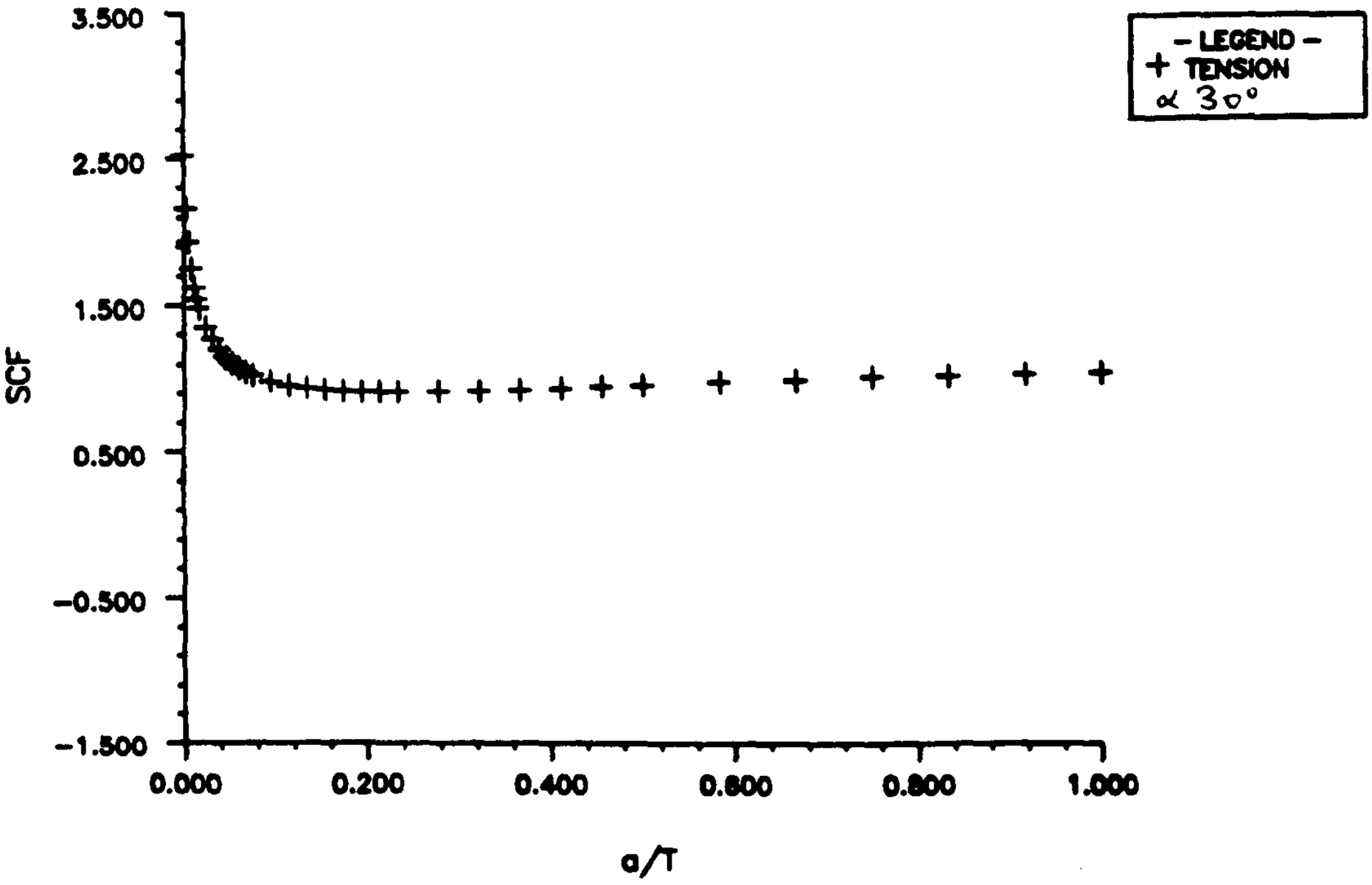

FIGURE 3.24 THROUGH THICKNESS STRESS DISTRIBUTION T–BUTT

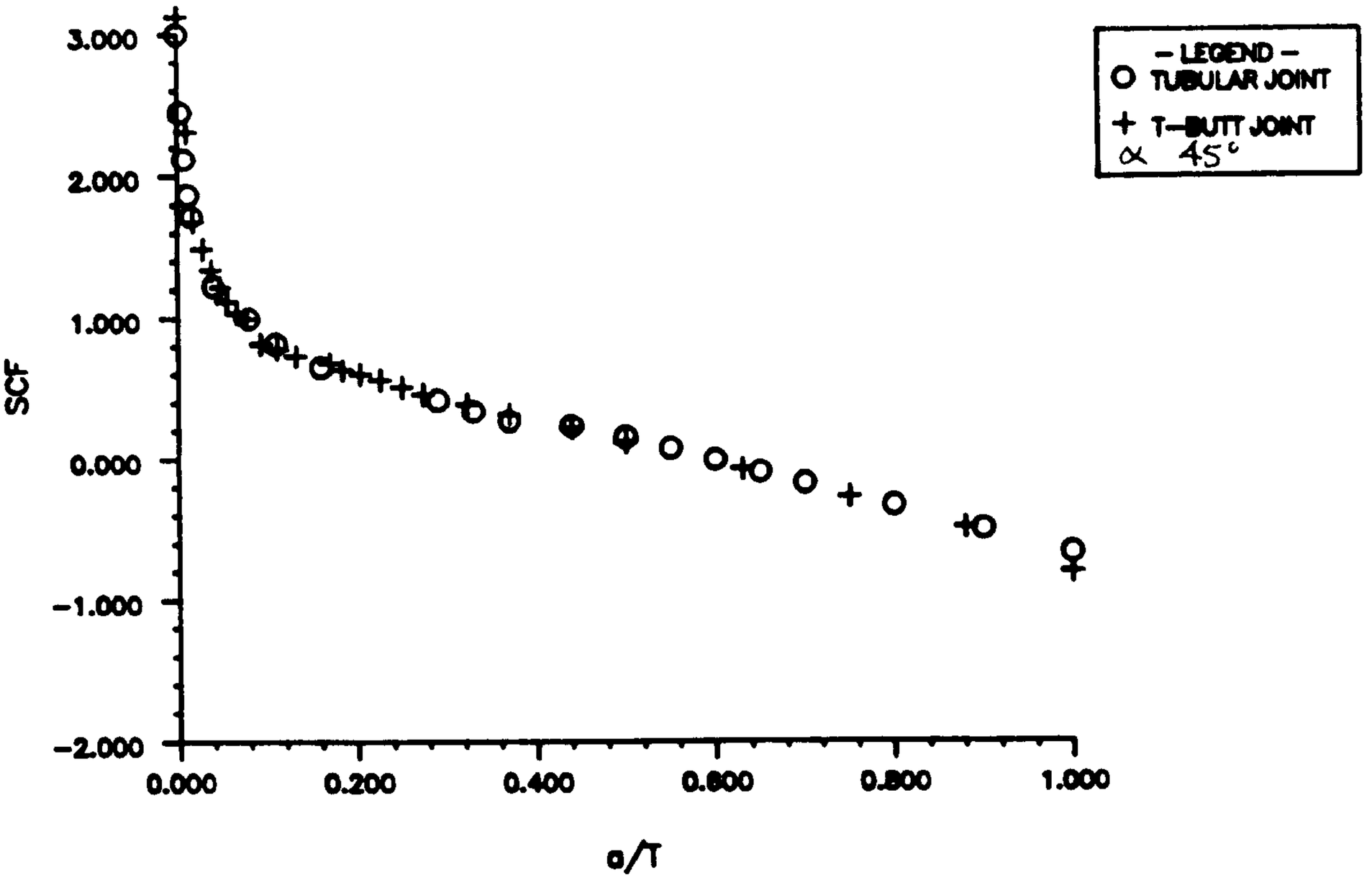

FIGURE 3.25 THROUGH THICKNESS STRESS DISTRIBUTIONS

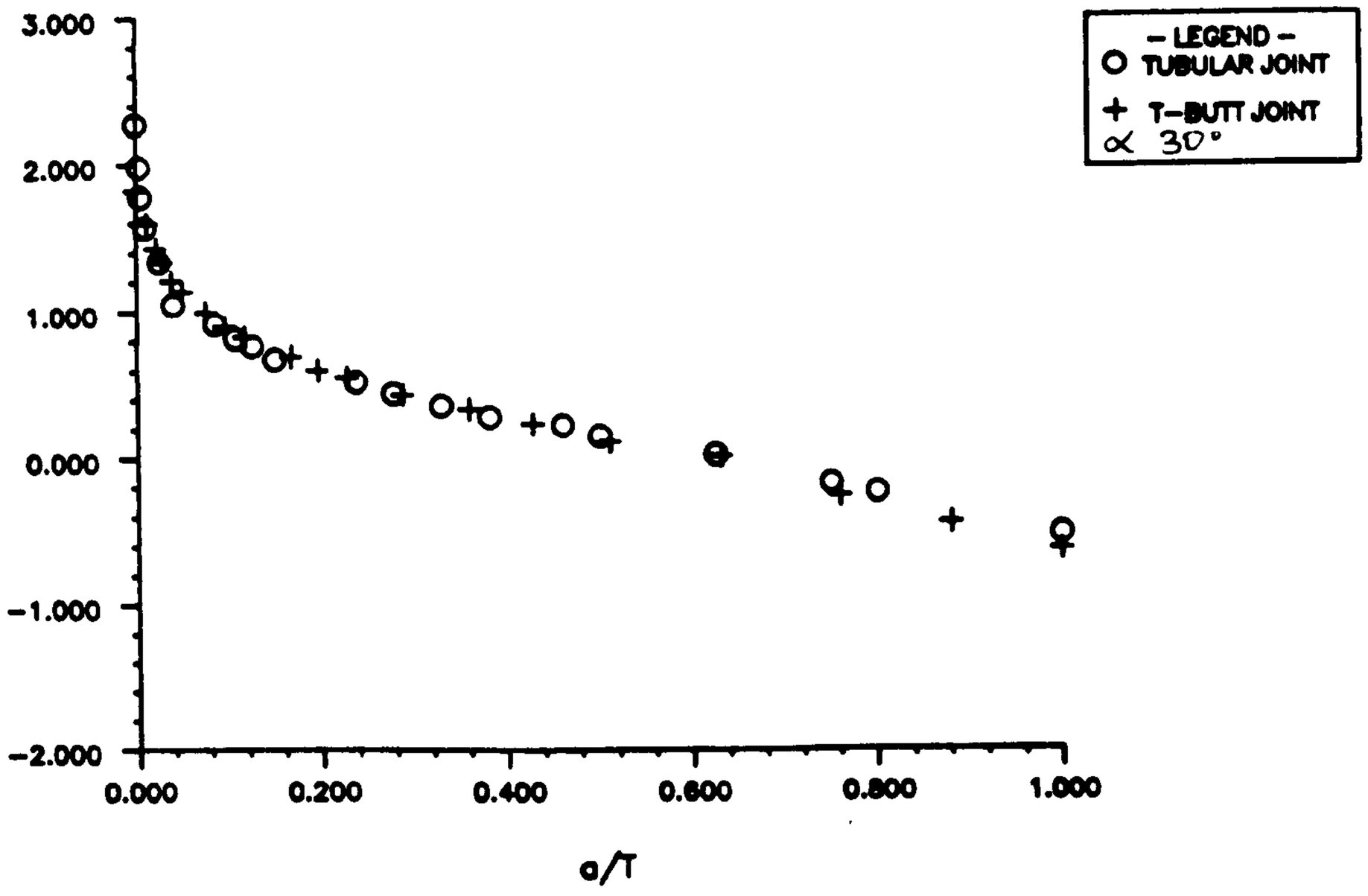

FIGURE 3.26 THROUGH THICKNESS STRESS DISTRIBUTIONS

4 CHAPTER FOUR

FATIGUE TESTING OF STEEL JOINTS

4.1 Scope of chapter

This chapter reports the results of the five fatigue tests conducted on the tubular joints fabricated for this project. These three multiplanar nodes had a variety of weld profiles giving the desired change in the weld angle α and the weld toe radius ρ. The results of the stress analyses studies reported in the previous chapters demonstrated the effects that these changes have produced in reducing the weld toe SCF (K_w) and geometric SCF (K_G). Consequently, the likely changes in total fatigue life resulting from controlling the welding procedure of some braces could be due to the modifications produced in the initiation period as well as subsequent crack growth stage. The established crack growth part of the fatigue life of a structure is governed by the geometric hot spot stress (K_G). But initiation and early crack growth is influenced by the component of stress concentration factor due to the notch at the weld (K_w).

For this reason special care was taken to try and detect the first signs of crack initiation and compare the results for the different profiles studied as well as with the initiation criterion designated by the Department of Energy. A short review of experimental techniques and test instrumentation and automation is presented below.

4.2 Experimental techniques

Many engineering components often fail due to fatigue cracks initiating and growing to catastrophic sizes. The important aspect in assessing the life of a structure depends on the ability to detect these cracks, measure them and characterise them. A number of non-destructive testing techniques (NDT) are available for crack detection. The most widely used method for crack detection in ferromagnetic material, such as BS4360 50D steel, is the Magnetic Particle Inspection method (MPI). It provides location and length of defect and in laboratory conditions it is possible to detect cracks that are smaller than the criterion designated by the Department of Energy Guidance Notes on Offshore Installation [4.1], which considers crack initiation to be a crack of 15mm length with a depth of 1.5mm (N_1). The ability to detect cracks earlier, allows a better assessment of the remaining life of the structure and may also provide

information that will make it possible to produce elasto-plastic fracture mechanics models to study the early crack growth behaviour thus giving rise to more accurate assessment of the total fatigue life.

The early detection of cracks is attempted using the MPI method. This method is used to detect the existence of the cracks and provides the location and length of these defects, it does not measure crack depth. Crack depth is measured using the Alternating Current Field Measurement (ACFM) method. It is possible to use the ACFM technique to detect crack initiation but for very small cracks the MPI method is more efficient. Both techniques are described below.

4.2.1 Magnetic Particle Inspection (MPI)

This method of nondestructive testing is used for locating surface and subsurface discontinuities in ferromagnetic materials. It works on the principle that when the specimen under test is magnetised, discontinuities which lie in a direction transverse to the direction of the magnetic field will cause a leakage field to be formed at and above the surface of the specimen. The presence of this leakage field and therefore the presence of the discontinuity, is detected by the use of finely divided ferromagnetic particles being gathered and held by the leakage field. This magnetically held collection of particles forms an outline of the discontinuity and indicates its location, size, shape and extent.

The specimen to be tested must be magnetised by magnetic fields high enough for leakage field generation. As magnetisation by permanent magnets is in general insufficient, most practical applications use magnetisation generated by electric current flow in an electric circuit. For this project an Ardrox A.C. electromagnetic yoke was used to magnetise the relevant intersection. To check whether a field exists at that particular section under test a Burmah-Castrol strip is used. This strip is made of steel in which there is a fine cut completely encased in a non-ferromagnetic material like brass. When placed in the magnetic field and sprayed with a magnetic ink, the presence of the cut in the steel will be indicated only if the magnetic field exists. A number of these test strips are available with varying degrees of sensitivity.

4.2.1.1 Detecting the distortion in the magnetic field (leakage field)

The effectiveness of the magnetic inspection method is determined by the sensitivity with which the change in magnetic field due to the presence of a defect can be detected. This project utilised the method involving the use of ferromagnetic particles as a suspension in a liquid. While the specimen is being magnetised the liquid suspension is applied to the area under inspection. The particles that come under the influence of the leakage field produced by a discontinuity will be drawn to, and held by this field. These magnetically held particles then provide the visible evidence of the presence of a leakage field, and therefore the presence of some kind of discontinuity.

Leakage field can be produced by conditions other than metallic discontinuities, a magnetic particle pattern does not always mean that a defect is present. Geometric changes in a component such as sharp corners or sharp changes in permeability from any cause will produce such leakage fields.

Strength and concentration of the leakage field is a controlling factor in determining the character and appearance of the indication. It must be strong enough to overcome gravity, surface irregularities and other factors that tend to prevent the gathering and holding of particles to form an indication. The magnetic particles are available in several colours to increase the visibility of the indication under any given condition. Fluorescent magnetic particles which glow in darkness or dim light when exposed to ultra violet radiation (black light) offer the optimum in contrast and visibilty. Flourescent magnetic particles were used once the location of the crack was established.

For this project ultraviolet light was used along with two different types of ferromagnetic particles. Ardrox fluoresecent ferromagnetic ink and Ardrox black ink. Black ink was used during early crack detection of very small cracks (less than 1mm long) where it was applied over a surface coated with white powder thus providing a sharp contrast and improving the technique for detection of very small cracks.

The main advantages of this method are that it is simple and rapid to use and is regarded as a reliable technique for finding surface cracks, especially very fine and shallow ones. It is a very useful method for crack detection for offshore structures as there is no limitation on the size of structure that can be tested. But more important is the fact that no elaborate cleaning is required before conducting an inspection, this makes it very attractive for offshore operators for obvious reasons.

The method does have a number of limitations particularly the fact that it only works on ferromagnetic materials. It does not reliably locate sub-surface cracks, and also demagnetisation following inspection is often necessary. One further disadvantage is that the method is operator dependent.

4.2.2 Alternating Current Field Measurement Technique ACFM

Measureming crack depths of surface flaws is generally a difficult process and it requires a technique that measures some perturbation in an observable property caused by the presence of a crack. This perturbation could be the changes in compliance produced by a growing crack or the changes in the local temperature distribution in the regions near a crack.

One method employed to detect surface flaws in a metal specimen is to pass a high frequency alternating current through the specimen and to probe the plane surface for irregularities in the field produced by the crack. The high frequency a.c. tends to flow in a thin skin along the metal surface. This skin depth δ is dependent on the permeability, and conductivity of the metal and the frequency of the alternating current.

$$\delta = (\mu\mu_0\sigma\pi f)^{\frac{-1}{2}} \qquad 4.1$$

μ_0 is the permeability of free space
μ is the relative permeability of the metal
f is the frequency of the alternating current
σ is the conductivity of the metal

At a chosen operating frequency of 6kHz the skin depth in mild steel given in equation 4.1 is approximately 0.1mm which is small compared to the crack depth of interest.

The use of the ACFM method is illustrated by considering an infinite plate containing an infinitely long surface crack of uniform depth as shown in Figure 4.1. The current is fed in at the sides and the field would be expected to flow as shown. Since constant potential gradient is obtained in the neighbourhood of the crack, then the same potential gradient would exist on the two crack faces. Thus if the voltage is measured in the region near the crack (V_1) and across the crack (V_2) using a probe with a spacing Δ, then the depth can be obtained from the relationship $V_1 \alpha \Delta$ and $V_2 \alpha \Delta + 2a$. The crack depth a is then given by:

$$a = \frac{1}{2}\Delta(V_2/V_1 - 1) \qquad 4.2$$

It can be seen that this approach does not require prior calibration against a test block. Equation 4.2 is known as the one dimensional interpretation of the crack depth and is strictly only valid for the case of an infinitely long crack in an infinite plate, but it can be applied with small error to many types of cracks in finite width plates. For semi-elliptical or circular cracks the above solution does not hold. Dover *et al* [4.2] recognised that the a.c. field measurement technique satisfied Laplace's equation in two dimensions since the depth dependence disappeared due to the skin effect and accordingly further solutions were developed thus enabling accurate measurement of circular and semi-elliptical crack shapes.

4.3 Experimental set up

After the stress analysis all the joints were fatigue tested. Figure 4.2 shows a schematic of the experimental set up used to conduct the fatigue tests. The joint was fixed on the floor using one brace and the load was applied using a second brace at 90° to the fixed brace. The set up allowed for testing to be conducted on two braces simultaneously in the OPB loading mode. For this configuration the highest stresses occur at the saddle positions. Thus each test provided four potential crack growth sites, these are the saddle positions marked A, B, C and D.

The test system is an Instron 250 kN servohydraulic actuator driven by an IBM PC AT interfaced to the mini-controller by the Instron 2490 series intelligent interface. The software used is the commercially available package FLAPS [4.3] which has been developed at UCL to allow automated material testing. Two tests were fully automated and two tests were semi-automated.

For the fully-automated tests probes were fixed to the tubular joint surface after the detection of small cracks was achieved. These probes were connected to a 192 channel switching unit. This switching unit essentially consisted of 192 individual relays mounted on twelve seperate p.c.b. boards (each board consisting of 16 relays). A decoder circuit was used to choose any individual relay and was controlled by a 16 way general purpose interface bus (GPIB) in the IBM PC AT which provided the logic and buffers necessary for parallel transfer of 16 bit data. Therefore to choose a particular site the decoder activates that relay and the output goes to the Microgauge which amplifies the measured voltage. The Crack Microgauge amplifies the small input voltage to a voltage in the range of 0 to 5 volts. This amplified signal goes to a 10 bit analogue to digital converter in the intelligent interface and is then sent to the data base created in the Flaps module in the IBM. Post processing facilities exist in Flaps to present the data in graphics form.

The semi-automated tests were conducted using Flaps to control and drive the test system. Once cracks were detected using the MPI technique the test was then set up to run for a specific number of cycles and then stopped for inspection. This was conducted using the U8 Microgauge and a hand held probe. The brace/chord intersection was probed at 10mm intervals for crack sizing.

4.4 Results of the fatigue tests

All joints were subjected to fully reversed constant amplitude loading. The mode of loading was OPB. Table 4.1 shows the load range and hot spot stress range for each of the individual saddle positions tested.

4.4.1 Tests C1-1-X

For this test a load range of 80.0 kN was applied as shown in Figure 4.2. The different SCF values and differences in nominal stress produced hot spot stress values in the range of 210 - 420 MPa for the four saddle positions A, B, C and D.

Figure 4.3 shows the crack depth as a function of the number of cycles for Positions A, B and D. Figure 4.4 shows curves of crack depth as a function of distance around the brace/chord intersection for Site D. This Figure shows crack shape profile evolution that is typical of these test results. Features that are generally associated with fatigue behaviour of tubular joints are evident, for example cracks initiate after a small portion of the total fatigue life. For Positions A and B cracks

were evident after 1.9 & 0.9 x 10^4 cycles representing 14.6% and 10.6% respectively of the total fatigue life. For Position D initiation was about 33.3% of the total fatigue life.

The number of cycles to crack initiation referred to in this study is not N_1 as defined in the DEn Guidance notes [4.1]. This document designates N_1 as the number of cycles to first discernable crack (defined as a crack of 15 mm length and 1.5 mm depth).

The use of the MPI method allows for the detection of small cracks of approximately 4 mm long with depths of the order of 0.6 mm, (the crack depth is measured using the ACFM method). Thus N_1 is significantly smaller in terms of crack length and depth and therefore initiation is an even smaller part of the total fatigue life of a structure. Table 4.2 shows a comparison of the two values of N_1.

Figure 4.3 shows that the early stages of cracking are a period of slow acceleration. At around the 6 mm crack depth the growth rate becomes constant and independent of depth. These observations are consistent with earlier tubular joint observations reported by Dover *et al* [4.4] and Chaudry [4.5].

These results shown in Figure 4.3 demonstrate the effect of the local and geometric stress distributions on the crack growth rates. Consider the crack growth rates of saddle positions A and D. Site A has the higher weld toe stress concentration factor (K_W), and site D has the higher geometric hot spot stress concentration factor (K_G). Crack initiation occurs after 3.0 x 10^4 cycles at A and 3.8 x 10^4 cycles at D. This is almost 25% longer and would be expected for a difference in their respective K_W values of 7%. Once the cracks begin to grow then the influence of weld toe stresses rapidly decays and the geometric hot spot stress then controls further crack growth. Therefore this should and did result in result crack growth rates at A being less than those at site D, (3.7 x 10^{-7} and 6.3 x 10^{-7} m/cycle respectively).

Saddle position B had a greater weld toe SCF than either A or D and the highest geometric hot spot stress for all four sites. Thus early initiation and rapid growth made this the deepest and longest of all three cracks.

Relatively constant crack growth rates are observed for the latter part of the fatigue life of the three sites. This is attributed to the change in behaviour of the geometric hot spot stress as the crack extends into the chord wall. It is assumed to decay

linearly through the thickness because of the presence of high bending stresses. Such an assumption is supported by the FE results which for these sites predict a comparetively high bending to membrane ratios, (see Table 2.6). For this reason the characteristic exponential increase in crack growth rates, observed in simple specimens such as the compact tension specimen, does not develop.

The curves of the crack depth as a function of the distance around the brace chord intersection show the development of the crack. The early crack shape is long, very shallow and shows an irregular crack profile. Two or in some cases three crack initiation sites were detected. At these locations the cracks grew in depth but quickly coalesced to form one large semi-elliptical crack.

The three crack growth curves shown for this test have different number of cycles for their respective end points. This is due to the fact that the test is conducted at R ratio = -1 which means that when Positions A and B are in tension they should support the same load range as Positions C and D which are then in compression. Testing is conducted without a test frame but instead a brace to brace type of loading is used as shown in Figure 4.2. The four saddle positions experience different hot spot stress ranges, which inevitably leads to cracks initiating at different number of cycles as has been demonstrated. Once one of the braces develops a substantial crack depth at the brace/chord intersection then that particular site can no longer support the same load range as the rest of the positions on the other brace.

In the interest of achieving a more accurate extrapolated N_2 for Position D the test was continued. Consequently any further crack growth at saddle positions A and B was ignored. Thus the different end points for this test. The N_2 values reported are all extrapolated values, no attempt was made to grow any of the cracks to the full duration of N_2. No evidence of crack initiation or growth was detected at saddle position C.

4.4.2 Tests C1-2-X

The test conditions are very similar to those of test C1-1-X and are summerised in Table 4.1. However, the load range is reduced to 55.0 kN thus the geometric hot spot stress range values are 144.9 - 291.0 MPa.

Figures 4.5 shows the crack depth as a function of the number of cycles for Positions A, B and D. Similarly for this test, saddle position C does not show any evidence of crack initiation or growth. Figure 4.6 shows the crack shape profile depth as a function of the distance around the brace chord intersection for Position B. The general features exhibited in C1-1-X are also evident in this test.

Small cracks were detected at all three saddle positions at different stages during the testing. The calculated period of initiation was found to be a small portion of the total life. Table 4.2 shows the N_1 values for all the tests compared with N_1 values calculated according to the Department of Energy definition. Except for saddle position D where initiation accounts for 34%, positions A and B N_1 is less than 15% of the total life of the tubular joint.

The transition between the period of slow acceleration, in crack growth rate, observed in the early stages of the test, and the established growth rates, occurs at the 4-6mm crack depth. Crack depth data acquisition at positions A and B was stopped when it became evident that these positions could no longer support the same load range as positions C and D. This enabled C1-D-2-X to be monitored for a longer number of cycles resulting in the different end conditions for this test.

For this test and particularly for position A initiation occurred at a number of locations around the intersection. This aspect of the fatigue life is governed by the severity of the notch at the intersection, which is a function of the geometry of the last weld bead, and not the geometric hot spot stress. These cracks continued to grow indiviually and exhibited aspect ratios higher than those of test C1-1-X. At around 4mm crack depth, the individual cracks joined to form one long shallow semi-elliptical crack with a slow decreasing aspect ratio. These features are clearly demonstrated in Figure 4.6.

4.4.3 Tests C2-1-Y

The next two tests report on the fatigue behaviour of joint two. For this joint two braces were fabricated with profile A and the other two braces with profile C2. The tests were conducted under fully reversed constant amplitude loading with a load range of 35.0 kN representing stress ranges of 92.2 - 185.3 MPa.

Figure 4.7 shows the crack depth as a function of the number of cycles for Positions A and B. Figure 4.8 shows the crack profile around the brace/chord intersection at different stages of crack growth.

The first occurrance of cracks was detected at saddle position B after 2.5 x 10^5 cycles. Initiation appeared to be at one site only, unlike previous tests where cracks were detected at a number of locations before coalescing into one long semi-elliptical crack. At 6.1 x 10^5 cycles the crack was 2mm in depth, at the deepest point along the crack front. Inspection at sites A and D revealed the first signs of crack initiation for position A, but none at site D.

Both cracks at A and B continued to grow with a slowly increasing crack growth rate up to a depth of approximately 6mm. This appeared to be the stage at which the rate of growth became constant and independent of depth. Again the effect of high bending to membrane stress ratio influences the decay of geometric stress in the through thickness direction (linear decay of stress) thus the constant growth rate is evident.

In view of the fact that the stress range at saddle position B was considerably higher than that measured at site A and also cracking had initiated at B first this led to site B developing the longest and deepest of the two cracks. Testing was stopped at 1.61 x 10^6 cycles and at this point the depth of crack B was 24.4mm and at A 11.5mm. This meant that for Position A the test was not completed but an extrapolation of the curve gives an approximate N_2 value of 2.6 x 10^6, N_2 for B is 1.9 x 10^6.

At Position D crack initiation occured after 1.8x10^6 cycles, this is consistent with the results of C1-1-X and C1-2-X where Position D exhibited the highest number of cycles to initiation compared with the other saddle positions. On completion of the test no significant crack growth was observed at Position D.

Figure 4.8 shows the crack profile developing around the brace/chord intersection as a function of depth in the chord wall. Initial observations suggest that this result is consistent with tubular joint behaviour. However, inspection of the weld profile as well as the chord weld toe revealed that two cracks were present at two sites. One at the weld toe chord side and the other between the 4th and 5th weld bead at what appeared to have been the AWS/CWP profile boundary i.e. where the original weld toe would have been had the joint been manufactured to the standard

AWS weld profile. Both cracks were in the vicinity of the saddle position, the 'hot spot stress site'. The cracks grew in tandem up to 1.02 x 10^6 cycles when the interbead crack stopped growing, at this stage it was 30 mm long and approximately 3.0 mm deep. This depth is approximate because it is experimentally difficult to measure the depth of interbead cracks using the ACFM method due to the nature and profile of each weld bead.

The cracking at the weld toe was one crack that grew around the brace/chord intersection and not a series of small cracks that coalesced into one long semi-elliptical crack.

4.4.4 Tests A-2-Y

The four saddle positions tested here are those located on the two braces of joint two and manufactured to profile A. Testing was conducted under fully reversed constant amplitude loading under a load range of 35.0 kN. The test information is listed in Table 4.2.

Figure 4.9 shows the crack depth as a function of the number of cycles for the three saddle positions A, B, and D. Crack initiation was first detected at position B with an N_1 value representing 13% of the life of the joint. Crack initiation and subsequent growth was established at the other two saddle positions A and D but no evidence of cracking was detected at position C. Testing was stopped when position B measured a crack depth of 24mm.

The cracks at the other two saddle positions A and D were not deep enough to justify extrapolating the values to the full chord wall thickness of 32mm. Consequently, the crack at position B was ground out to its full depth plus the extra region that would have been subjected to fatigue damage. The whole region was inspected using the MPI method to ensure the complete removal of the crack. The section was then welded back to the original profile and the test restarted.

Crack growth was monitored at both saddle positions A and D. Site B was inspected for possible crack reinitiation before the completion of the test. The fatigue life of the repair was unfortunately short and once crack initiation was detected growth was very rapid. It was useful as it provided for further crack growth and thus a more accurate extrapolated N_2 value for A and D. Crack grinding is an approach

frequently exercised by offshore operators, but the maximum reported depth of grinding is 50%. In this case attempts were made to grind a crack of 75% of the chord wall thickness.

Figure 4.10 is a schematic of the crack shape profile around the brace/chord intersection. The crack initiation and growth shown are typical of tubular joint behaviour where the fatigue cracks coalesce and appear to form one long shallow semi-elliptical crack.

Figure 4.11 shows the crack depth as a function of number of cycles for two sets of results A-2-Y and C2-1-Y. In both cases the fully reversed loading was the same; 17.5kN. This is a good example to show the effect of CWP on fatigue endurance i.e. it encapsulates changes in SCF and fatigue crack initiation. This value of load produced a range of hot spot stress values for the eight saddle positions and gives the different fatigue behaviour shown in Figure 4.11. Clearly the use of the CWP approach produces longer initiation periods and for these particular positions a final crack growth rate that is significantly slower than that of the AWS weld profile braces. Crack initiation occurred at position C2-D-1-Y after 1.80×10^6 cycles. A-D-2-Y on the other hand gave initiation at 0.2×10^6 cycles. This is a very good confirmation of the effect of CWP and shows the improvements one gets for the same nominal loading as opposed to the same hot spot stress (i.e. including both improved SCF and fatigue performance). The nett effect as seen in this figure would seem to be at least a four fold increase in fatigue life.

4.4.5 Tests A-1-Z

This test reports on the fatigue behaviour of two braces of joint three. The brace fixed on the floor with the two saddle positions B and D was manufactured to profile A specifications. The second brace through which the load is applied and where positions A and C are located was fabricated to a profile C procedure. Testing was conducted under fully reversed constant amplitude loading with a load range of 27.4 kN.

Figure 4.12 shows the crack depth as a function of the number of cycles for Positions B and D. Figure 4.13 shows the crack profile around the brace/chord intersection at different stages of crack growth. The general features of the fatigue

behaviour of tubular joints are again evident in this test particularly the irregular crack profile which is due to the large number of crack face contacts. These occur due to cracks growing on different planes and then coalescing to form one crack with a series of crack face contacts where overlap occured.

For this test Postion D had the higher geometric SCF and thus a higher hot spot stress. Crack growth initiated after $1.6x10^5$cycles at Position D. For Position B crack initiation occurred after $2.8x10^5$ cycles. Crack growth rate continued to increase for both positions up to a crack depth of about 4-5 mm where the crack growth then continued at a constant rate independent of crack depth. Neither of the chord cracks at B and D were grown to the full chord wall depth of 32mm and therefore N_2 is the extrapolated value from the curves. N_2 for B is $1.16x10^6$ cycles and N_2 for position D is $1.02x10^6$ cycles.

Throughout the fatigue testing of the different braces no crack initiation or growth was detected at any of the sites C due to the low SCF value measured at these sites. However, crack growth did occur at all sites A but in this particular test no crack initiation or growth was observed at site A. This is due to the fact that site A had a CWP and would be expected to have a longer endurance than sites B or D, both of which had considerably higher weld toe SCF and geometric SCF.

4.5 Examination of fracture surfaces

The braces fabricated to the CWP, C1 and C2 exhibited longer time to initiation as well as measurable changes in the crack growth rates for the particular tubular joints. One possible explanation for the longer fatigue life observed for these braces could be due to the possibility that crack initiation for these braces occurs at sites more remote from the intersection giving a crack path that curves underneath the weld toe to the notional point of intersection between brace and chord.

In order to establish the nature of the crack path for these braces saddle position B from joint 2 was cut out and sectioned. Prior to cutting out this section the ACFM technique was used to hand probe the intersection to obtain as accurate a crack depth as possible so that a comparison of this technique with the optical method can be made. This could also be used to gauge the accuracy of the other crack depths as this technique provided data on the crack shape evolution for both types of weld profiles.

Figure 4.14 is a comparison of crack depth measured using the ACFM technique and a hand held probe, and the optical measurement of the crack depth of the same region of the brace/chord intersection. For the deepest section of the crack reasonable agreement is shown between the two methods but in areas on either side of the deepest crack underprediction of results is clearly evident. This is explained by the presence of a number of overlapping crack (cracks growing in different planes) sites. In terms of using the ACFM technique for crack sizing, cracks growing in different planes (overlapping cracks) are considered a worst case situation because if one is using a simple one-dimensional interpretation a serious underprediction will result in the regions close to the crack face contact.

Figure 4.15 shows the brace/chord intersection before it was cut out, the cracks are highlighted using black magnetic ink on white powder, a number of over lapping fatigue cracks are clearly identified. This plate was used by Haq *et al* for a paper published in the Royal Society Journal [4.8].

In terms of investigating the path that a crack grown in a brace fabricated to a controlled weld profile had taken and wether the weld leg length had actually influenced the crack path, it is evident that the crack path does curve underneath the weld toe in the direction of where the original weld toe would have been had the brace been manufactured to the standard AWS profile.

A further interesting aspect of these tests is the frequent occurrance of overlapping crack faces in particular for the tubular joints fabricated to the standard AWS weld profile. The braces containing the CWP did exhibit overlapped crack faces but their occurance was less frequent.

4.6 Fatigue crack shape changes

In the previous sections the measurement of crack growth patterns revealed that initiation occured at multiple sites along the weld toe at the hot spot location where the stress was at a maximum. Also, the use of the ACPD method and the MPI technique enabled the characterisation of these cracks in terms of length and depth or more conveniently by the non-dimensional parameters a/c and a/T where T is the chord wall thickness, a is the crack depth at the deepest point and c is the surface crack half length.

The previous sections have demonstrated that it is reasonable to assume that tubular joint fatigue failures were due to the growth of semi-elliptical surface cracks. In order that fracture mechanics analysis could be used for reliable predictions of tubular joint crack growth rates and fatigue strengths, accurate estimation of stress intensity factors for semi-elliptical surface cracks are thus needed. The differences in crack shape evolution between the two types of weld profile studied is also investigated in terms of their influence on crack growth rates and fatigue lives of the tubular joints studied.

The data for crack aspect ratio changes for the thirteen chord cracks produced for the three tubular joints tested is presented below.

4.6.1 Crack shape evolution

4.6.1.1 Profile A

Figure 4.16 shows the crack aspect ratio changes for the five chord cracks produced for profile A. Early crack growth is characterised by short but comparitively deep cracks hence the high aspect ratio but this only occurs over a small region of the chord wall thickness. The aspect ratio decreases sharply up to 5% of the depth then a gradual increase in the a/c value is observed for all the five cracks. Figure 4.17 shows the early part of crack shape changes. The large scatter shown is due to the fact that the data includes all defects detected thus this represents the evolution of the five major cracks as well as other initiation sites.

4.6.1.2 Profile C1

Figure 4.18 shows the crack aspect ratio changes for profile C1. Six chord cracks are presented in this figure and these were tested at stress ranges of 254-424 MPa. Initial high aspect ratio for early crack growth is not evident in this test as can be seen in Figure 4.19. The number of crack initiation sites is significantly less due to the weld toe being further away from the brace/chord intersection and thus in a lower stress field and also as shown in chapter three the average weld toe radius ρ and the most frequently occuring radius have values greater than those of profile A. This would lead to a reduction in the weld toe notch effect and therefore a reduction in the potential crack initiation sites.

4.6.1.3 Profile C2

Figure 4.20 shows the crack aspect ratio changes for the controlled weld profile C2. The distribution of results is very similar to that exhibited for profile C1 and shows a gradual increase in a/c values as the crack grows through the thickness. Again the weld toe average and most frequent radii values are larger than for profile A and thus show a reduced weld toe notch effect.

The basic differences between the crack shape evolution of the two types of profiles studied in this project appears to be determined by the weld geometric parameters. Controlling the weld profile has been shown to reduce the weld notch effect by altering the initial geometry of the defects i.e. whereas for a standard AWS profile initial defects tend to have a/c values that are similar to a semi-circular shape, defects for profiles C1 and C2 appear to be more semi-elliptical in nature. Also, profile A exhibits higher notch stress value leading to an initial preffered crack growth path through the thickness rather than around the intersection, hence early crack growth is characterised by a decreasing aspect ratio followed by a gradual increase.

4.7 Discussion of fatigue test results

There are two possibilities for comparing the fatigue data to see whether the CWP is effective. Firstly estimates can be made in each case of the life to chord wall penetration; a second possibility is comparison of fatigue crack growth data.

During this period 13 chord cracks were produced and these can be interpreted in terms of fatigue life (S/N) data points (8 CWP, 5 AWS). The data for these 13 tests are given in Table 4.3. and are plotted in Figure 4.22. It should be noted that using the hot spot stress range in all cases means that increased fatigue endurance due to a change in K_G is eliminated. This plot only shows the change in fatigue life for the same hot spot stress range.

Three sets of data are included and these are defined by C1, C2 and A. For C1, there are six data points all at high stresses within the range 253-423 MPa. All are for 32mm chord wall thickness but despite this they show an increased life compared to the 32mm UKOSRP mean S/N line. The predicted lives (using the S/N line) of the test are given in Table 4.3. It would seem that an average improvement of 22% was measurable with individual values of between -4% and + 40%.

For C2 only two data points were produced for the third site D the crack initiated but no significant growth occurred. For these two values an average improvement of 148% can be estimated and individual values of (159% and 138%).

The five results for A were also compared to the predicted life and here the increase was insignificant (average difference +2%). The range of individual values was -3% to +6%.

From these comparisons it would seem that for a given hot spot stress the CWP gives a longer life and it would appear that for the C2 type the improvement is sufficient to restore the fatigue life to the 16mm chord wall thickness curve. It should be noted however that all values used in the comparison are extrapolated from crack sizes ranging from 11-25 mm with an average size of 20 mm which is 63% of the chord wall thickness. In view of the linear type crack growth in the later stages of the fatigue life the accuracy of these extrapolations is probably acceptable.

The biggest improvement measured (C2 compared to A) was about a factor of 2.5 on life as shown in Figure 4.11. If the reduction in the SCF is added to this calculation it is possible to predict for a decrease in SCF of 11% an increase in life of a factor of 1.42. This would give an expected total increase in life of a factor of 3.7. The individual fatigue crack growth curves should show this factor of 3.7 for the same nominal cyclic load. The tests on C2 and A did use the same cyclic load and are given in Figure 4.11. A factor of approximately 4 on life can be seen in Figure 4.11 and confirms the prediction made above. This is larger than any suggested fatigue life penalty for chord wall thickness and indicates that CWP can alleviate the thickness effect. Further tests are needed to confirm this finding in Axial and In-plane bending modes.

A reduction in SCF can easily be interpreted in terms of improved fatigue life. The reason for an improved fatigue life on the basis of identical test values of hot spot stress, however, is less clear. Several features could be the cause of this change. Firstly the measured value of K_w indicated that the CWP welds had lower values than for AWS. This would indicate a longer initiation period for the CWP joints and hence a longer life.

Comparing for example C2-B-1-Y and A-B-1-Z (both tested at about 160 MPa) shows that the total (extrapolated) life differed by a factor of 2.27. The final linear growth rate for C2-B-1-Y was about $2x10^{-8}$ m/cycle that for A-B-1-Z was $4x10^{-8}$ m/cycle. Comparing say C2-B-1-Y and A-D-2-Y (both tested at about 185 MPa) the total life differed by a factor of 2.44. The final linear growth differed by a factor of 2.26. In both cases influence on initiation and early growth was measurable (up to 4mm deep) a factor of about 2.5.

For all four tests crack growth to 4mm occupied 41-48% of total life. Thus the changes in total extrapolated life appear to be equally due to early crack growth and established crack growth. The former can be attributed to possible changes in K_w, the latter could be due to the crack initiation at sites more remote from the intersection. These suggestions cannot be confirmed at present but an effect on both stages of fatigue life is an unexpected benefit from CWP.

4.8 Conclusions

1. The combined effect of lower SCFs, geometric and weld toe gave an improved life by a factor of 4 for the CWP compared to an AWS profile.

2. Fatigue life results showed that an improvement could be obtained with a CWP for tests conducted with the same hot spot stress range. The improvement occured in the early crack growth regime (0-4mm deep) and also during later growth (4-32 mm).

3. It was found to be possible to detect and monitor cracks of a very small size (4mm long by 0.6mm deep).

4. Multiple small crack growth was the most common form of early fatigue damage.These cracks eventually coalesced to form one large semi-elliptical crack. The aspect ratio of these cracks was found to decrease from an initial value of approximately 0.2 to about 0.02 then increase to a final value of 0.18 for profile A whereas profiles C1 and C2 the aspect ratios exhibited a gradual increase to a maximum of 0.2.

5. It was possible to measure early crack growth in several specimens and show that the crack initiation was controlled by the local stress field at the weld toe. Subsequent growth was found to be controlled by the hot spot stress. In both cases the growth rate was influenced by the weld profiles.

6. Inter weld bead cracking was observed in the CWP braces at the boundary of the AWS/CWP. The cracks were small and shallow.

7. The final period of crack growth through the thickness was approximately constant. This is probably due to the pronounced local bending predicted from the FE anaysis. The characteristic increasing crack growth rate observed in standard and other type of specimens does not occur.

4.9 References

4.1 Background to new fatigue design guidance for steel welded joints in offshore structures, Report of the Department of Energy Guidance Notes Revision Drafting Panel, HMSO, London, 1984

4.2 Dover, W.D., Charlesworth, F.D.W., Taylor,K.A., Collins,R., and Michael, D.H. The use of a.c. field measurements to determine the shape and size of a crack in a metal In Eddy Current Characterisation of Materials and Structures. ed. G. Birnbaun and G. Free ASTM 722 pp 401-427, 1982

4.3 FLAPS, Technical Software Consultants 34 Linford Forum Milton Keynes. U.K.

4.4 Dover, W.D., Connolly, M.P.M., Fatigue fracture mechanics assessment of tubular welded Y and K joints. Proc. Int. Conf. on Fatigue and Crack Growth in Offshore Structures. I.Mech.E, London, April 1986

4.5 Chaudry, G.K., Applications of fracture mechanics to random load fatigue of tubular joints (in air and sea water). PhD Thesis, University of London, 1985

4.6 Dover, W.D., et al, Crack growth in tubular joints; out-of-plane bending loading. Offshore Technology Conference Paper OTC 3252 May 1978, Houston Texas

4.7 Dover, W.D., Holdbrook,S.J.,Fatigue crack growth in tubular welded connections. Int. Journal of Fatigue, January 1980

4.8 Haq, R., Michael, D.H., Collins, R., The detection and measurement of overlapping fatigue cracks at welded joints by thin-skin electromagnetic fields. *Proc. Royal Society London* A419, 69-89 1988.

Joint	Mode of Loading	Nominal Load kN	Hot Spot Stress (MPa)	N2 (extrapolated)	R Ratio
T [4.6]	OPB		252.0	$1.6x10^6$	-1
T [4.7]	OPB		246.6	$3.0x10^6$	0.51
T [4.7]	OPB		254.7	$3.7x10^5$	0.51
T [4.7]	OPB		303.8	$2.0x10^6$	0.50
C1-A-1-X	OPB	80	368.7	$1.3x10^5$	-1
C1-B-1-X	OPB	80	420.0	$8.5x10^4$	-1
C1-C-1-X	OPB	80	210.7	No cracks	-1
C1-D-1-X	OPB	80	390.4	$1.02x10^5$	-1
C1-A-2-X	OPB	55	253.5	$2.74x10^5$	-1
C1-B-2-X	OPB	55	291.2	$2.77x10^5$	-1
C1-C-2-X	OPB	55	144.9	No cracks	-1
C1-D-2-X	OPB	55	268.4	$2.64x10^5$	-1
C2-A-1-Y	OPB	35	161.3	$2.64x10^6$	-1
C2-B-1-Y	OPB	35	185.3	$1.90x10^6$	-1
C2-C-1-Y	OPB	35	92.2	No cracks	-1
C2-D-1-Y	OPB	35	170.8	*	-1
A-A-2-Y	OPB	35	181.5	$7.6x10^5$	-1
A-B-2-Y	OPB	35	204.6	$5.50x10^5$	-1
A-C-2-Y	OPB	35	109.5	No cracks	-1
A-D-2-Y	OPB	35	184.9	$7.8x10_5$	-1
A-B-1-Z	OPB	27.4	159.4	$1.16x10^6$	-1
A-D-1-Z	OPB	27.4	166.9	$1.06x10^6$	-1

* Crack initiation occured, no significant crack growth was recorded.

Table 4.1.Table of fatigue data from this project compared with [4.6] & [4.7]

Saddle Postion	N_1	D.En N_1	N_2 (extrapolated)	N_1/N_2	D.En N_1/N_2
C1-A-1-X	$1.9x10^4$	$3.0x10^4$	$1.30x10^5$	0.15	0.23
C1-B-1-X	$9.0x10^3$	$2.0x10^4$	$8.50x10^4$	0.11	0.24
C1-D-1-X	$3.4x10^4$	$3.8x10^4$	$1.02x10^5$	0.33	0.37
C1-A-2-X	$3.5x10^4$	$9.5x10^4$	$2.74x10^5$	0.13	0.35
C1-B-2-X	$3.1x10^4$	$6.5x10^4$	$2.27x10^5$	0.14	0.29
C1-D-2-X	$8.9x10^4$	$1.3x10^5$	$2.64x10^5$	0.34	0.49
C2-A-1-Y	$6.1x10^5$	$1.02x10^6$	$2.64x10^6$	0.23	0.39
C2-B-1-Y	$2.5x10^5$	$5.0x10^5$	$1.90x10^6$	0.13	0.26
A-A-2-Y	$9.0x10^4$	$1.65x10^5$	$7.6x10^6$	0.12	0.22
A-B-2-Y	$6.9x10^4$	$1.1x10^5$	$5.5x10^5$	0.13	0.20
A-D-2-Y	$1.95x10^5$	$2.35x10^5$	$7.8x10^5$	0.25	0.30
A-B-1-Z	$2.8x10^5$	$3.74x10^5$	$1.16x10^6$	0.24	0.32
A-D-1-Z	$1.6x10^5$	$2.76x10^5$	$1.06x10^6$	0.15	0.26
Average				0.19	0.30

Table 4.2.Comparison of actual N_1 values as a fraction of N_2 and N_1 as defined by D.En Guidance Notes as a fraction of N_2.

Joint	Hot Spot Stress (MPa)	N_2 Extrapolated	N_2 Predicted	% Difference
C1-A-1-X	368.7	$1.30x10^5$	$9.31x10^4$	+40
C1-B-1-X	423.6	$8.50x10^4$	$6.14x10^4$	+38
C1-D-1-X	390.4	$1.02x10^5$	$7.84x10^4$	+30
C1-A-2-X	253.5	$2.74x10^5$	$2.86x10^5$	-4
C1-B-2-X	291.2	$2.27x10^5$	$1.89x10^5$	+20
C1-D-2-X	268.4	$2.64x10^5$	$2.41x10^5$	+10
C2-A-1-Y	161.3	$2.64x10^6$	$1.11x10^6$	+138
C2-B-1-Y	185.3	$1.90x10^6$	$7.33x10^5$	+159
A-A-2-Y	181.5	$7.60x10^5$	$7.80x10^5$	-3
A-B-2-Y	204.6	$5.50x10^5$	$5.45x10^5$	0
A-D-2-Y	184.9	$7.80x10^5$	$7.38x10^5$	+6
A-B-1-Z	159.4	$1.16x10^6$	$1.15x10^6$	0
A-D-1-Z	166.9	$1.06x10^6$	$1.00x10^6$	+6

Table 4.3 Comparison of actual N_2 with N_2 obtained from the equation* governing the S/N line [4.1].

* $$\text{Log}(N) = 12.669 - 3 \log(S)$$

$N=N_2$

S=Hot spot stress

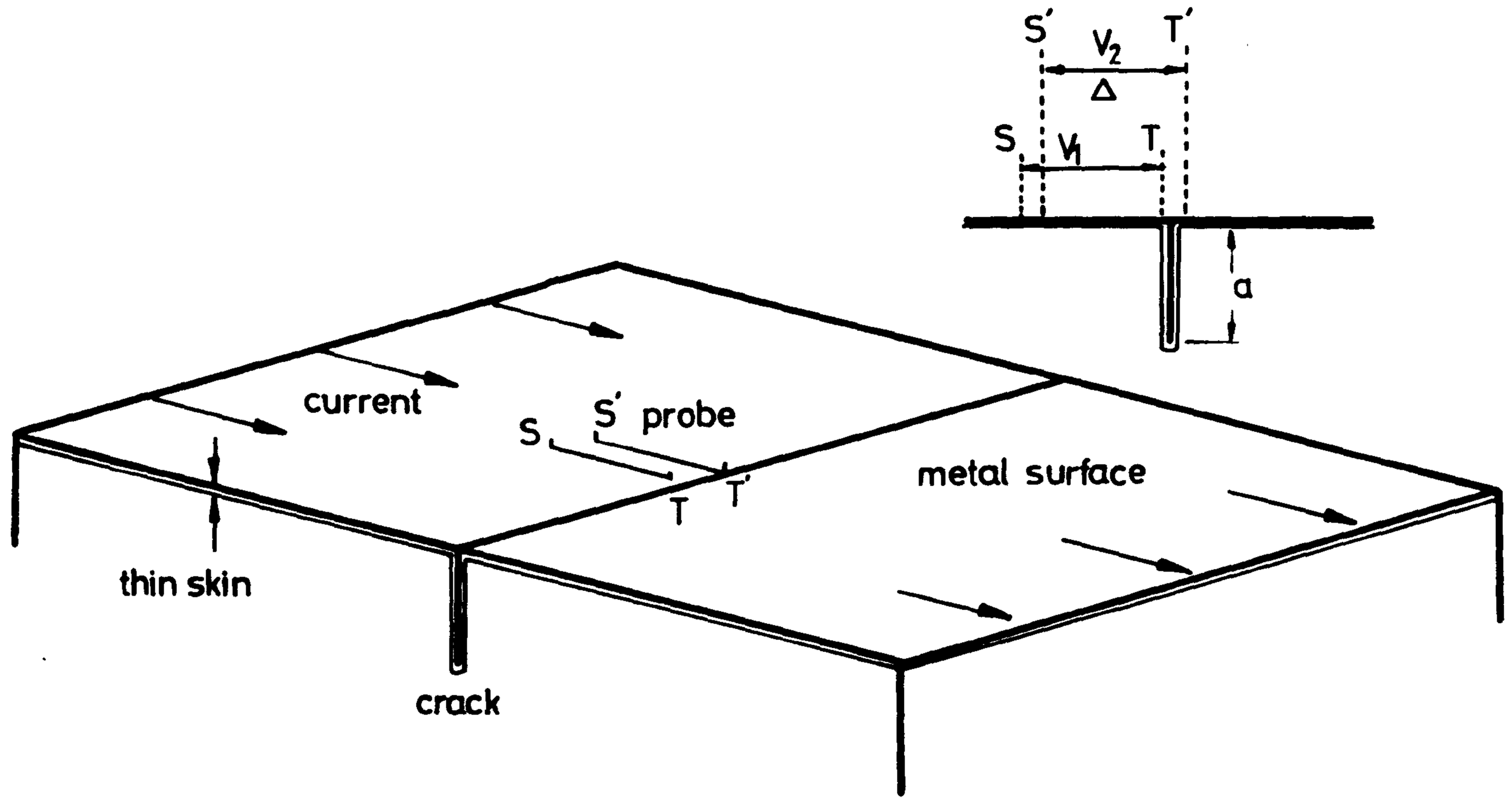

Figure 4.1 The mesurement of crack depth of surface flaws using the a.c. field measurement technique

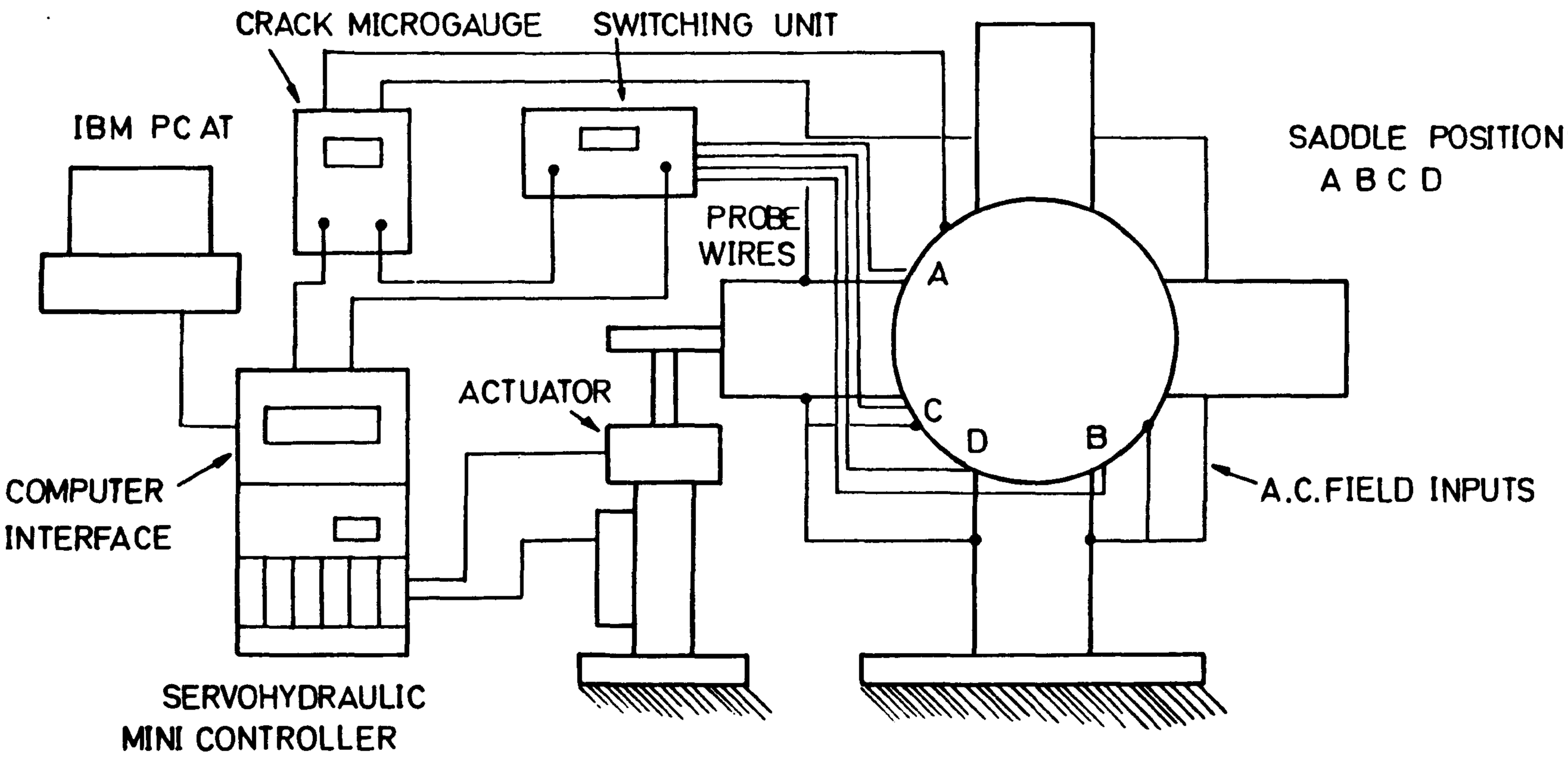

Figure 4.2 Schematic of experimental set up to conduct fatigue testing

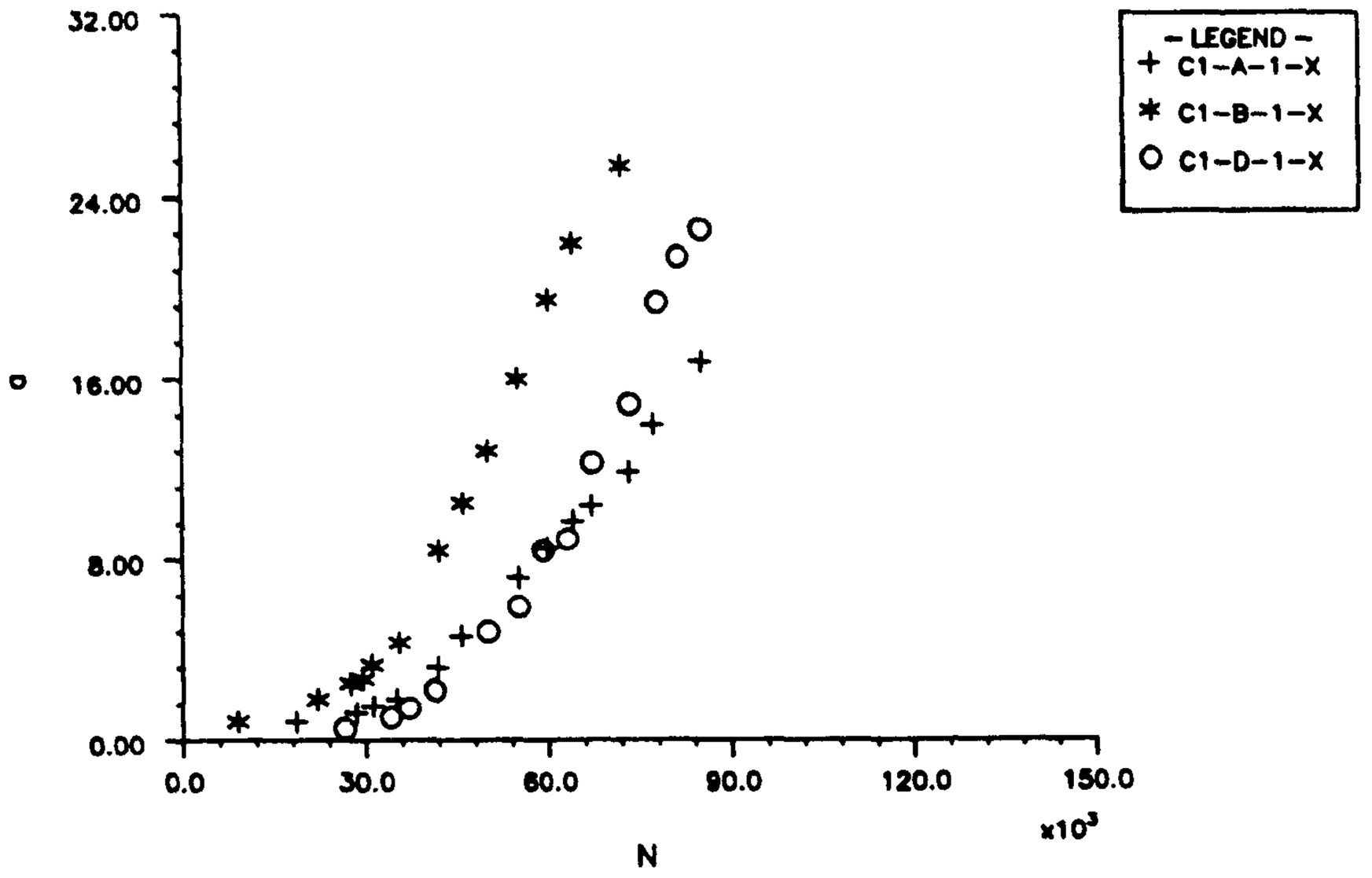

FIGURE 4.3 EXPT. FATIGUE CRACK GROWTH DATA C1–1–X

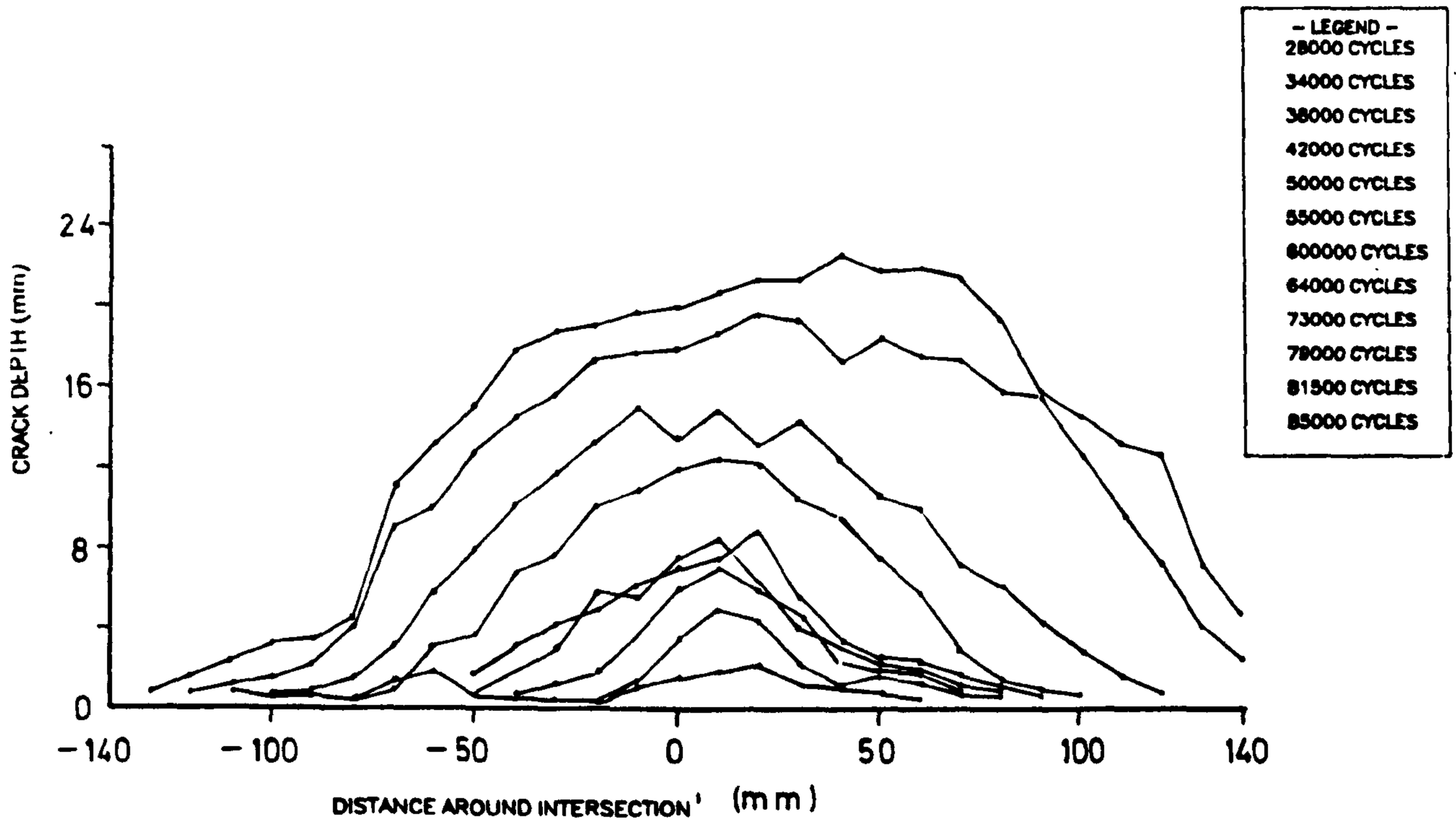

Figure 4.4 Crack shape profile at different number of cycles C1-D-1-X

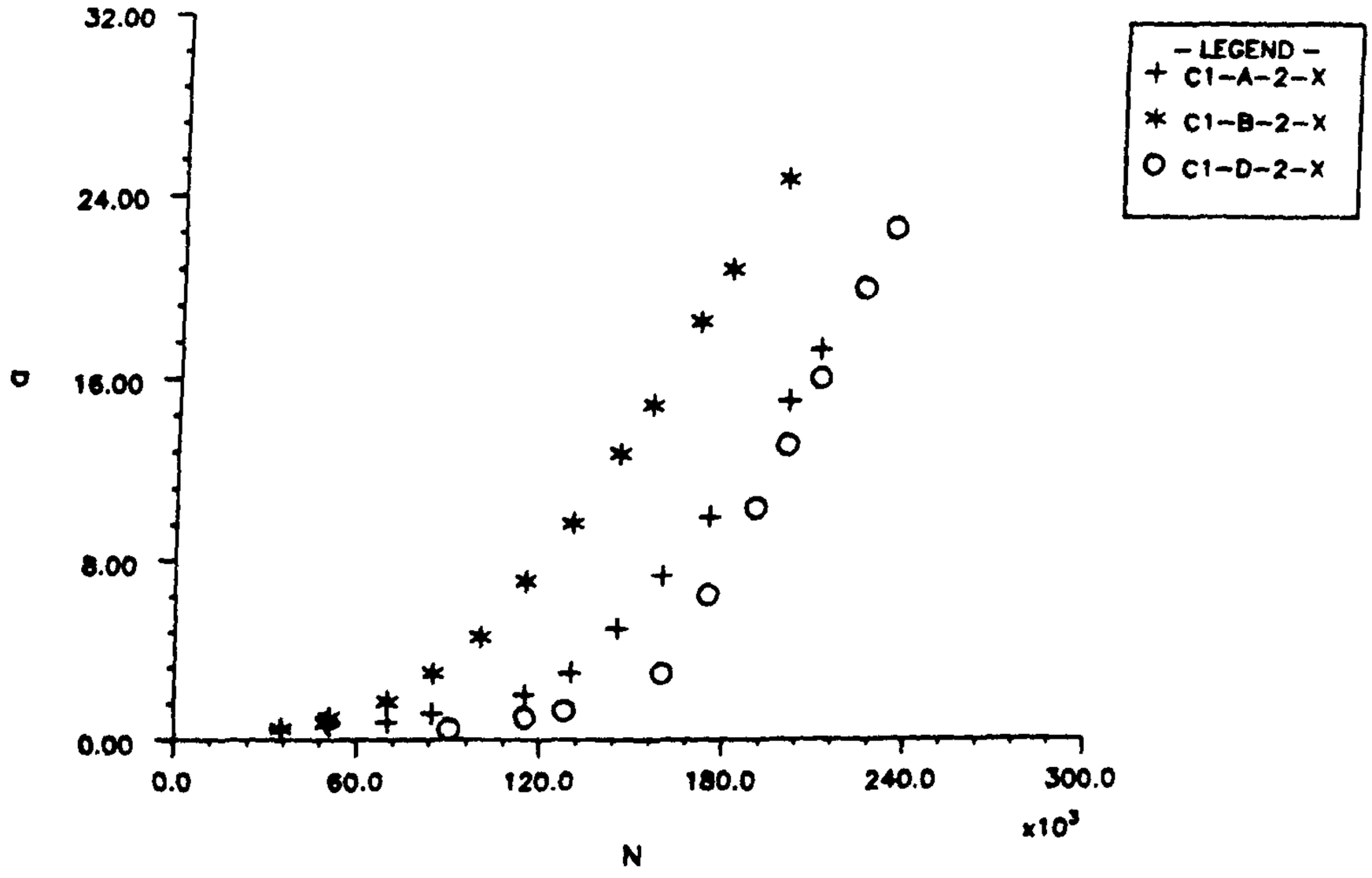

FIGURE 4.5 EXPT. FATIGUE CRACK GROWTH DATA C1–2–X

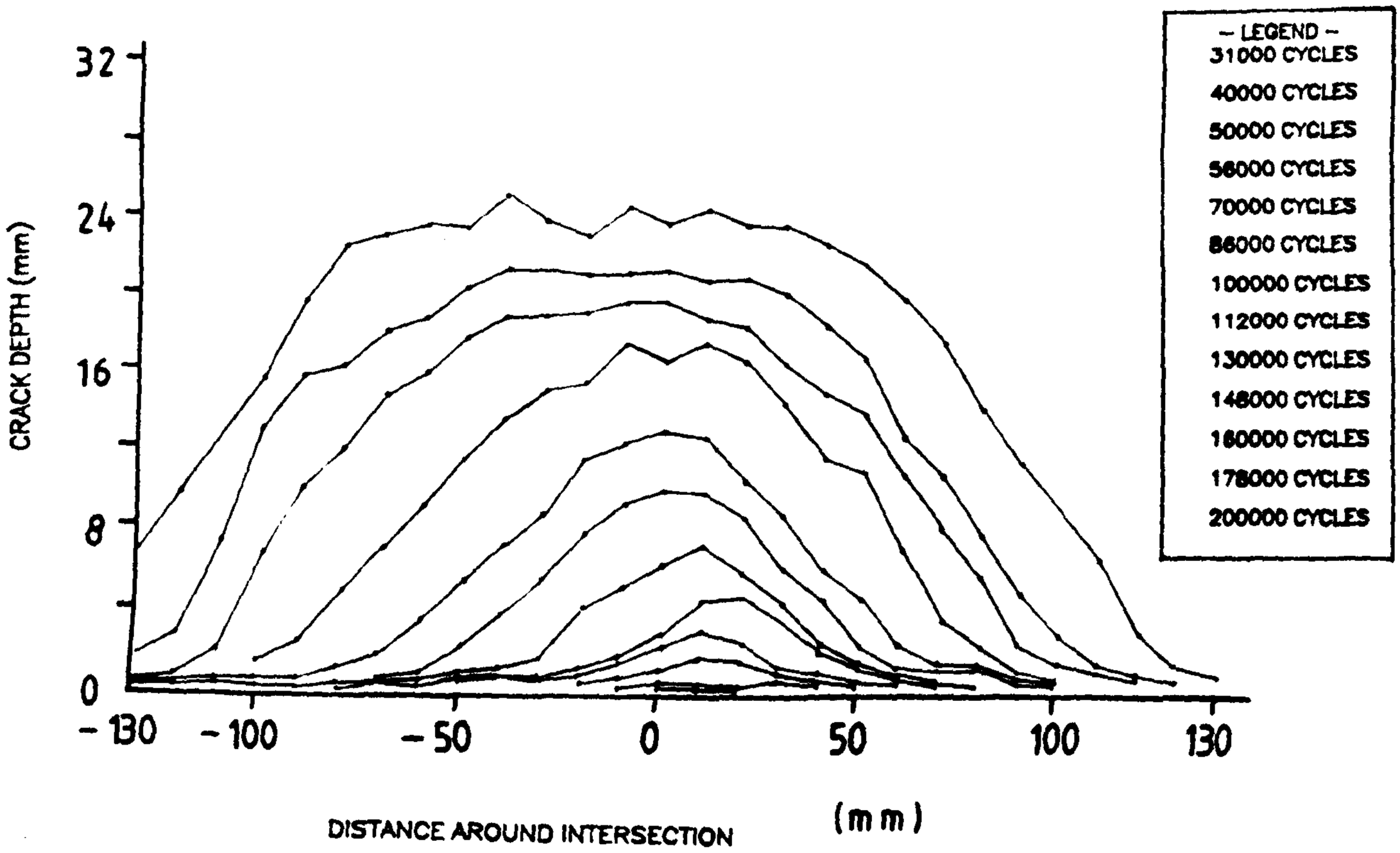

Figure 4.6 Crack shape profile at different number of cycles C1-B-2-X

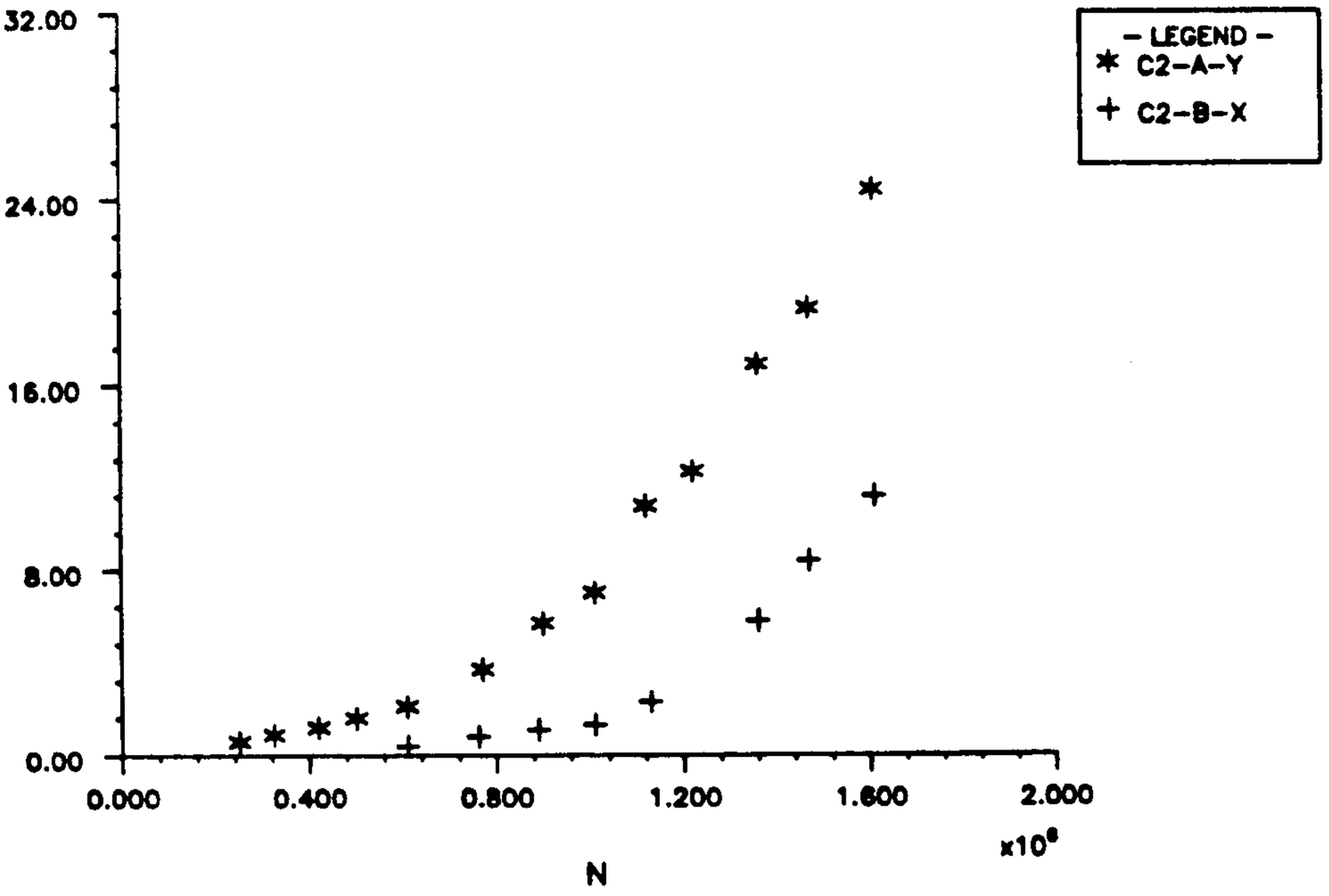

FIGURE 4.7 EXPT. FATIGUE CRACK GROWTH DATA C2–Y

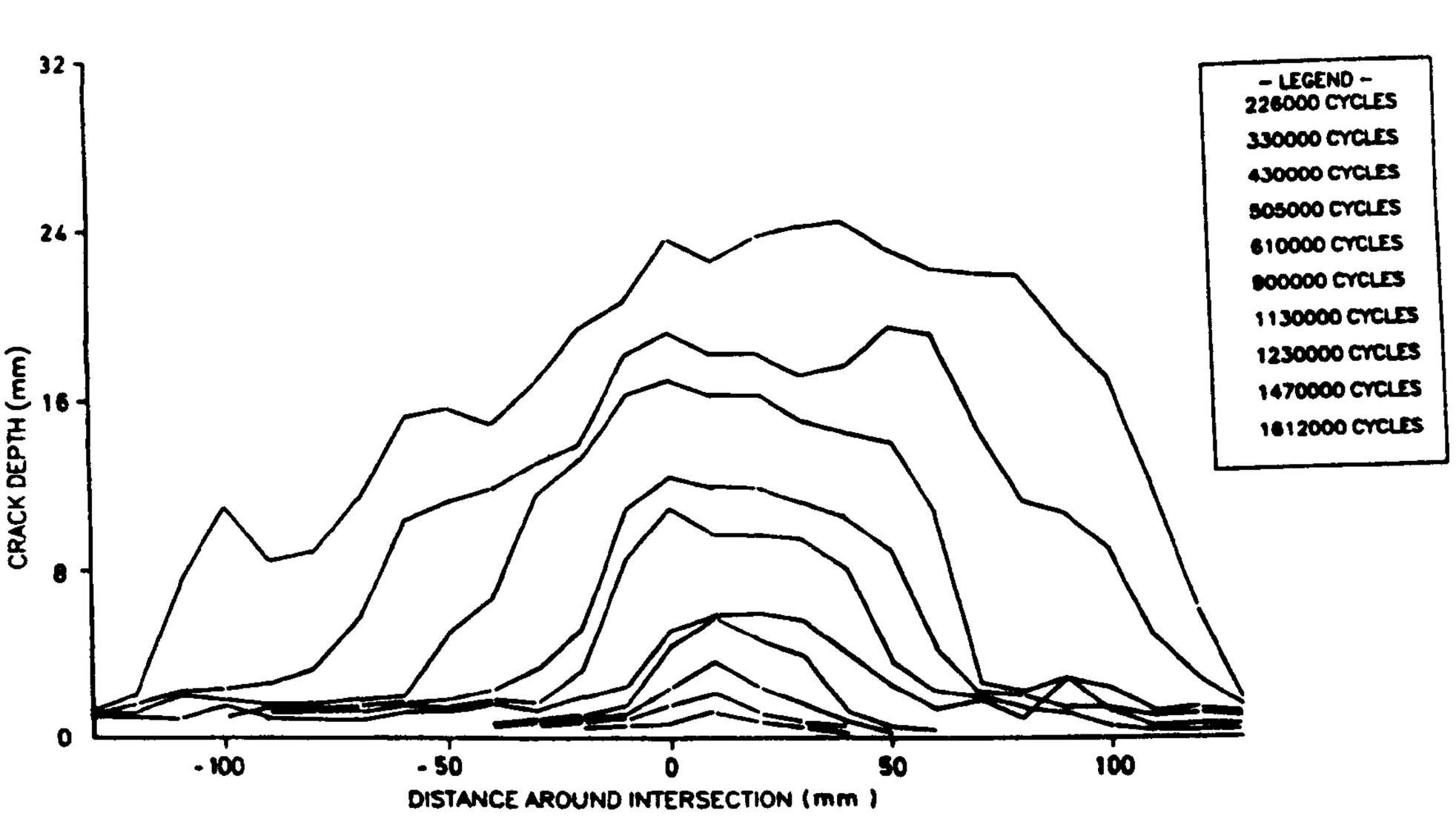

Figure 4.8 Crack shape profile at different number of cycles C2-B-1-Y

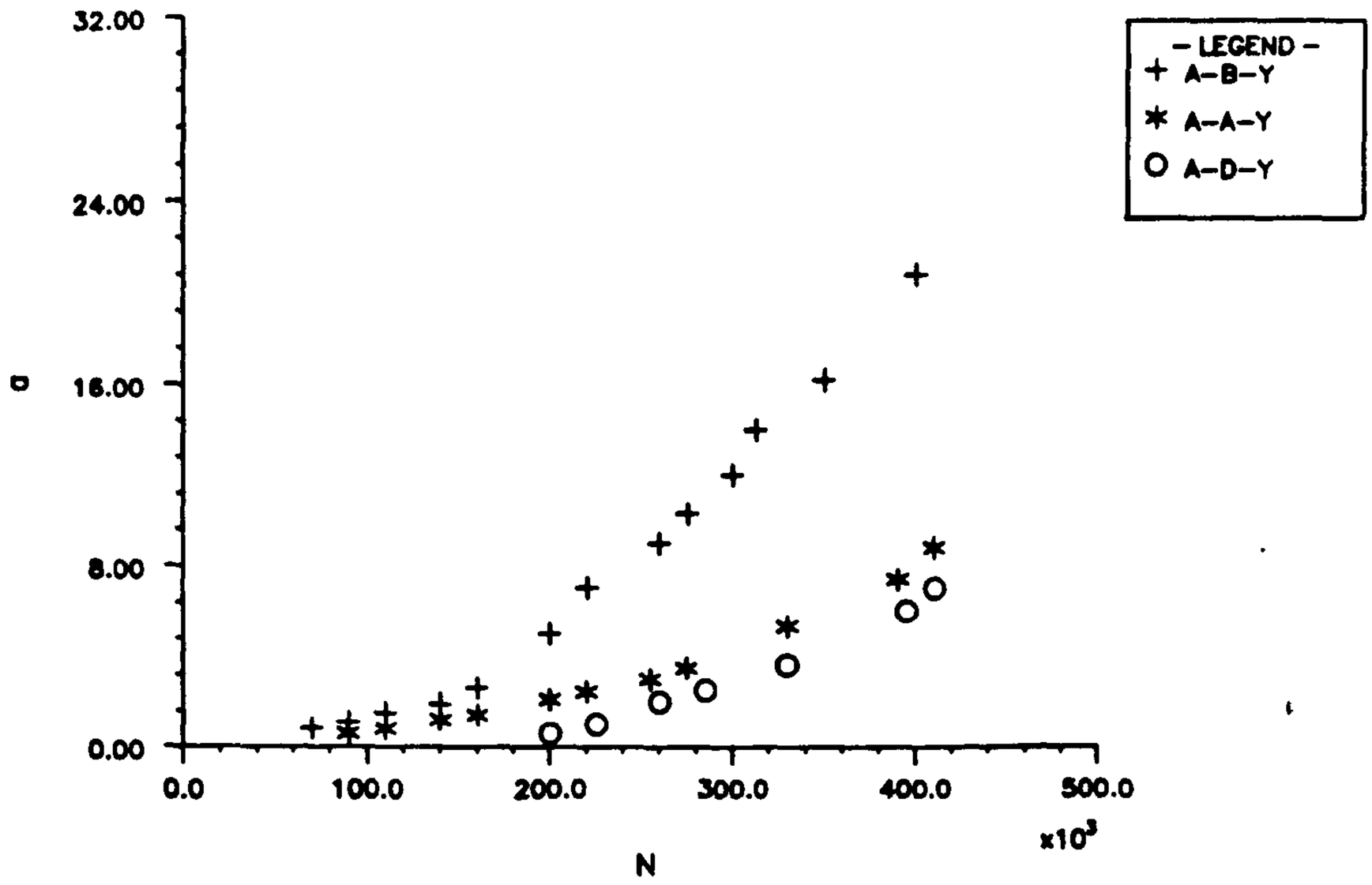

FIGURE 4.9 EXPT. FATIGUE CRACK GROWTH DATA A–2–Y

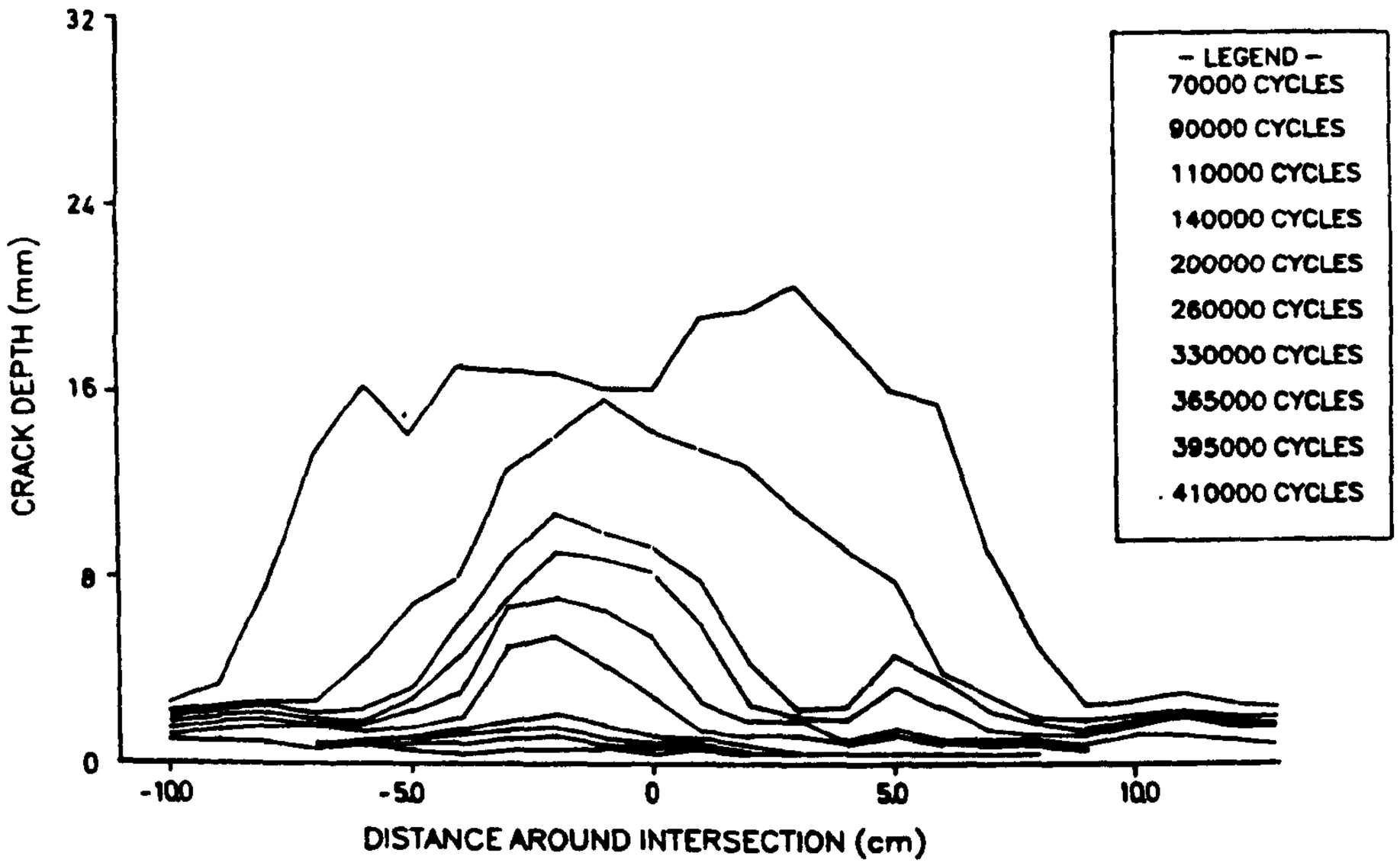

Figure 4.10 Crack shape profile at different number of cycles A-B-2-Y

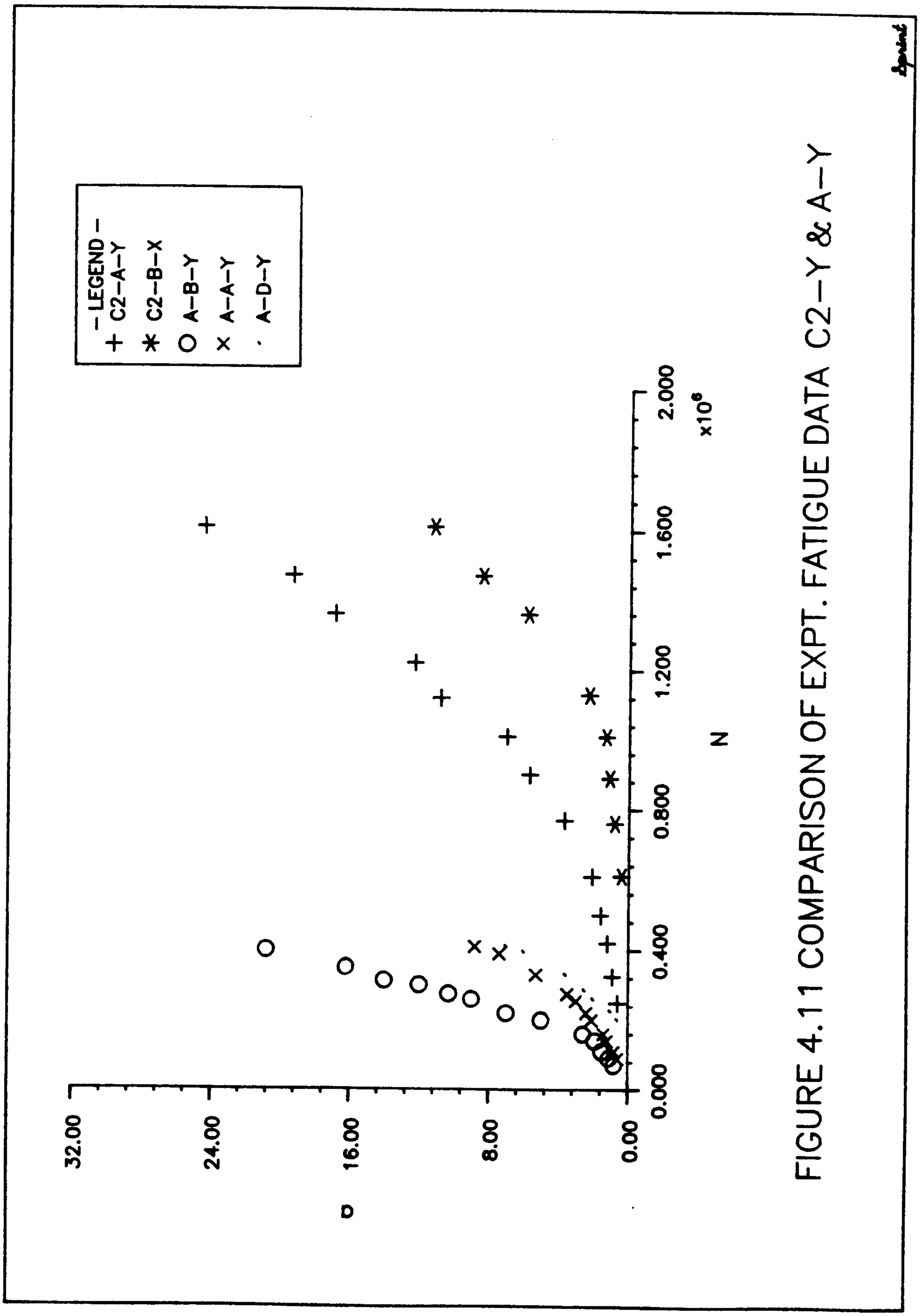
– LEGEND –
+ C2–A–Y
* C2–B–X
O A–B–Y
× A–A–Y
· A–D–Y
32.00
24.00
16.00
8.00
0.00
0.000
0.400
0.800
1.200
1.600
2.000
x10⁶
N
σ
FIGURE 4.11 COMPARISON OF EXPT. FATIGUE DATA C2–Y & A–Y

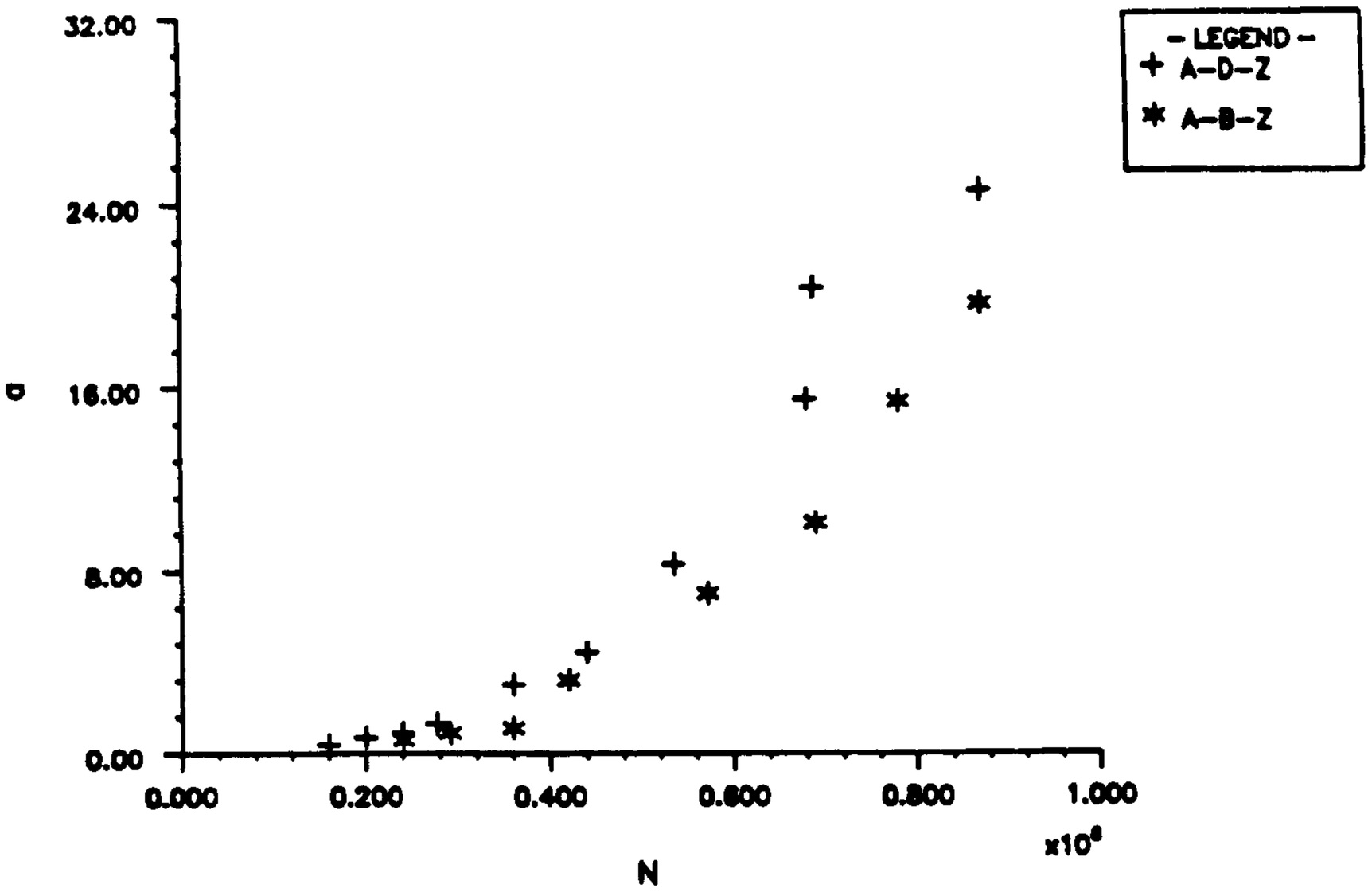

FIGURE 4.12 EXPT.FATIGUE CRACK GROWTH DATA – A– –1–Z

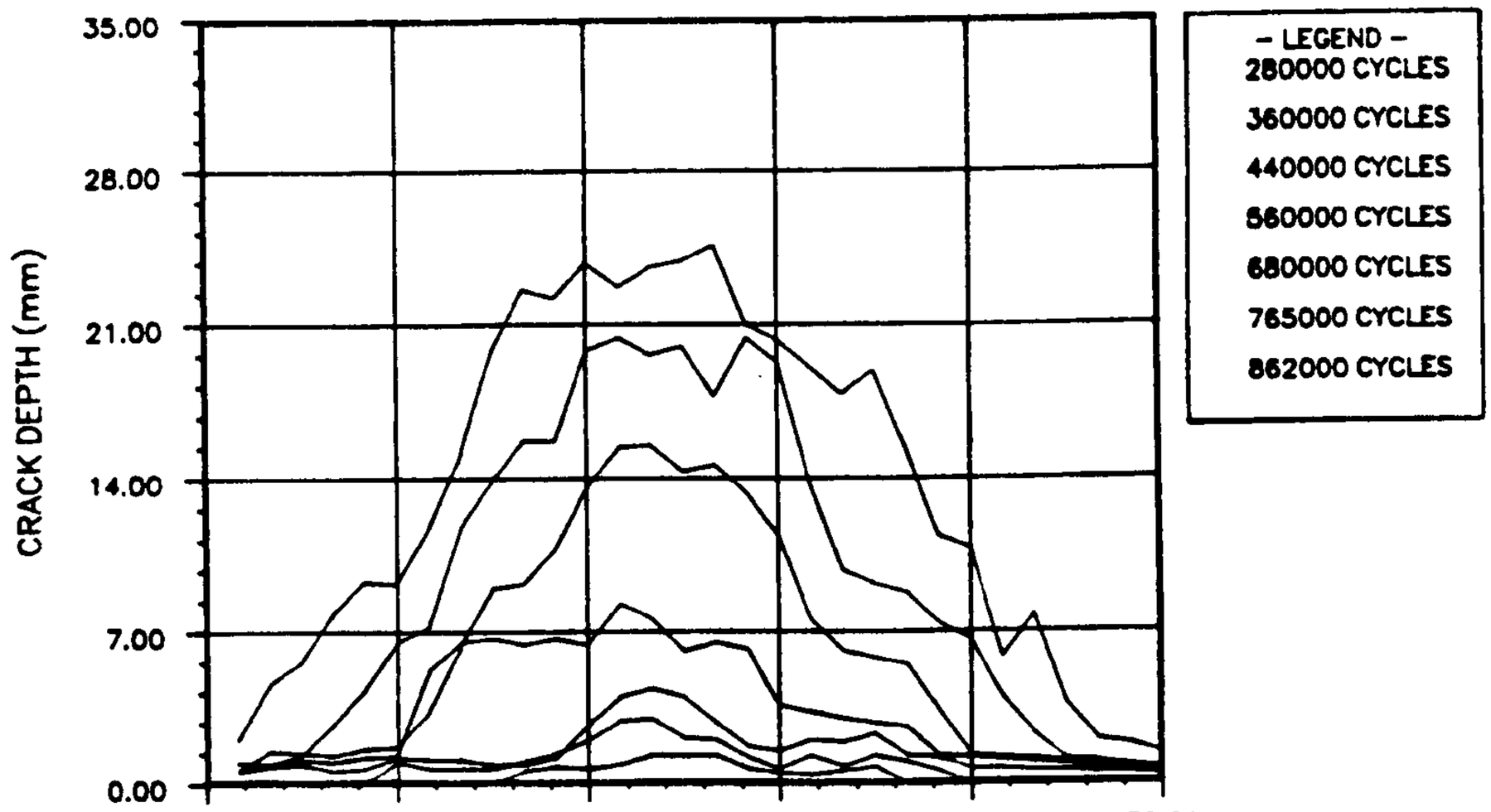

Figure 4.13 Crack shape profile at different number of cycles A-D-1-Z

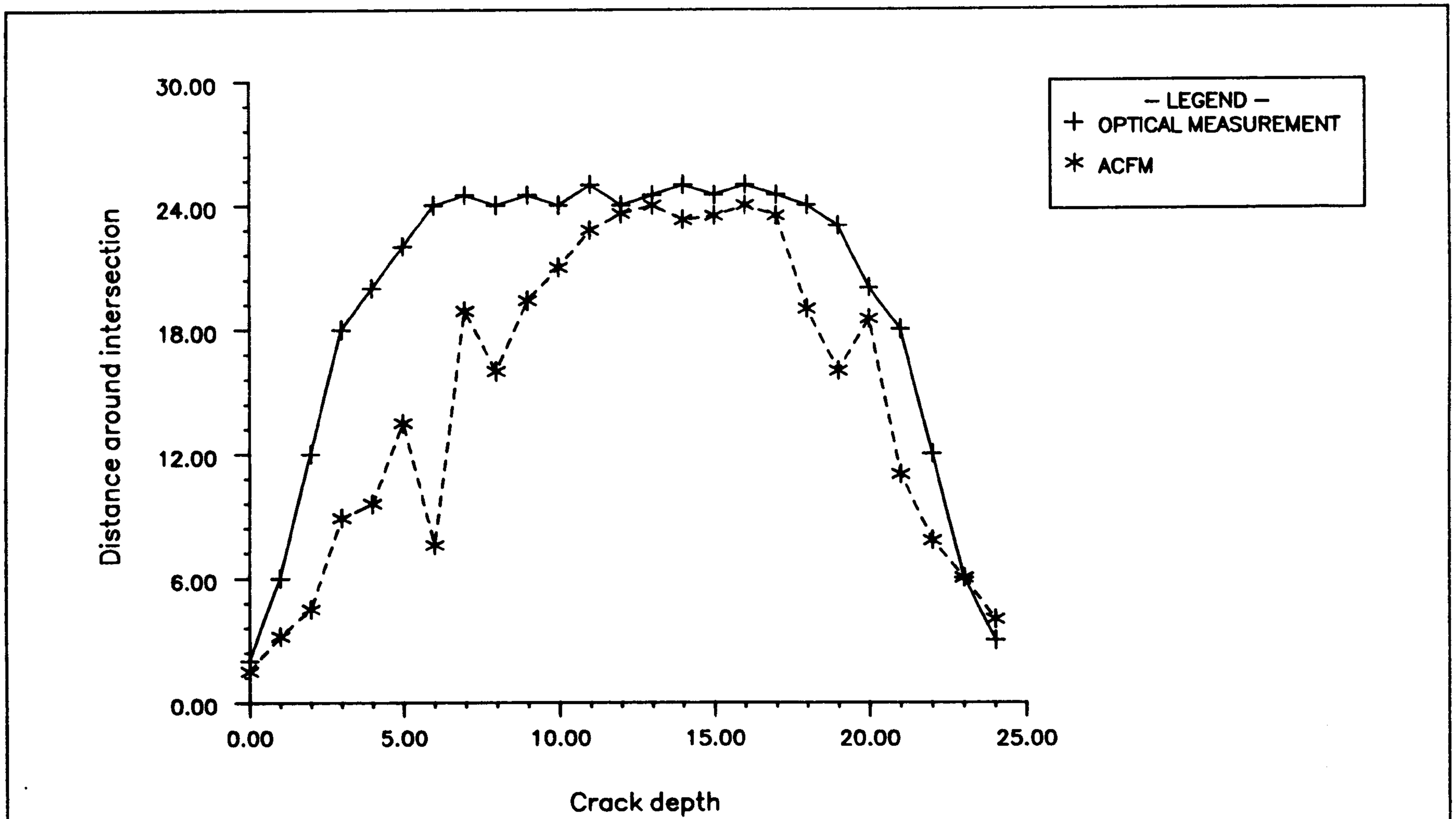

FIGURE 4.14 CRACK DEPTH USING ACFM COMPARED WITH ACTUAL DEPTH

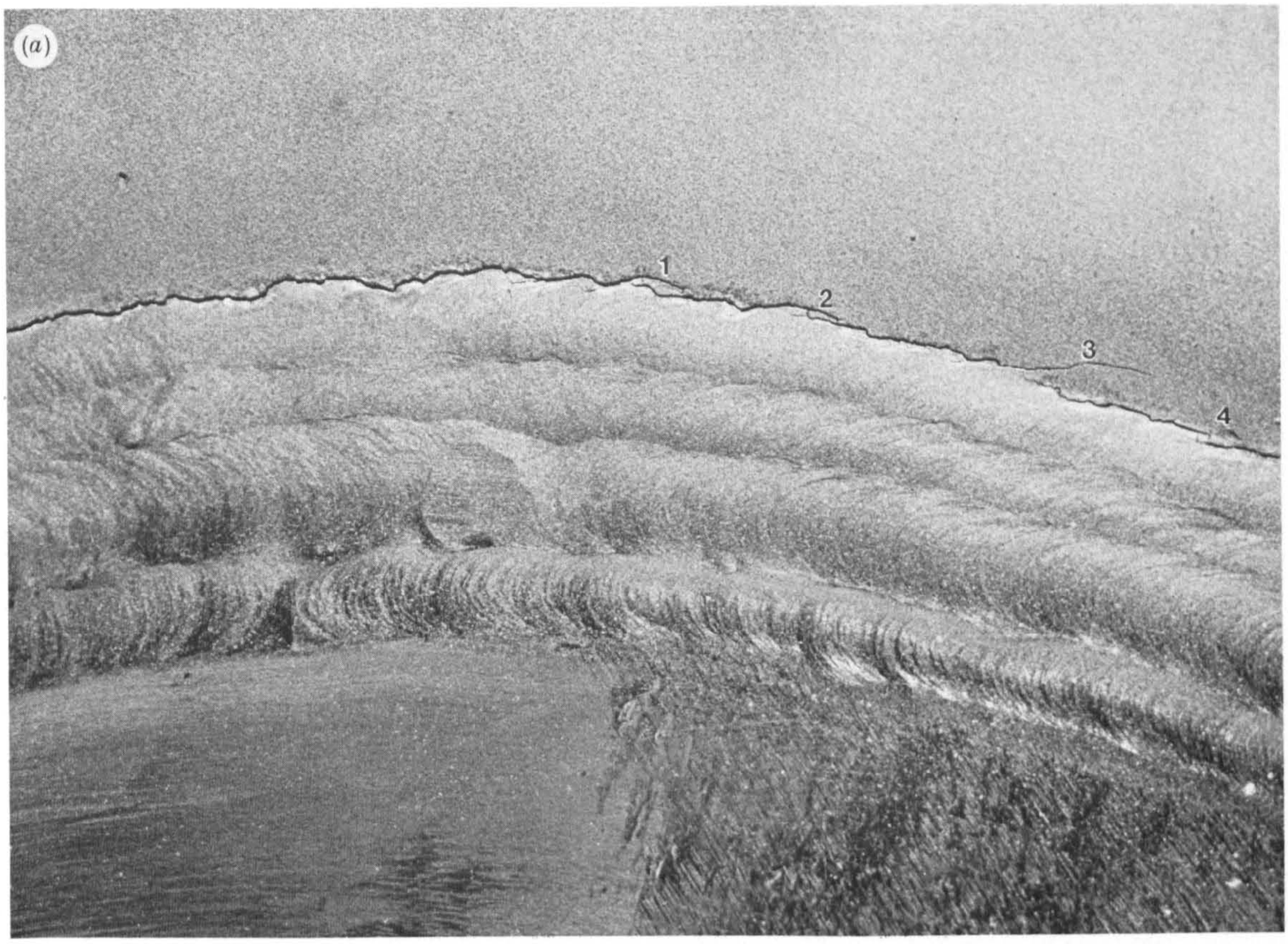

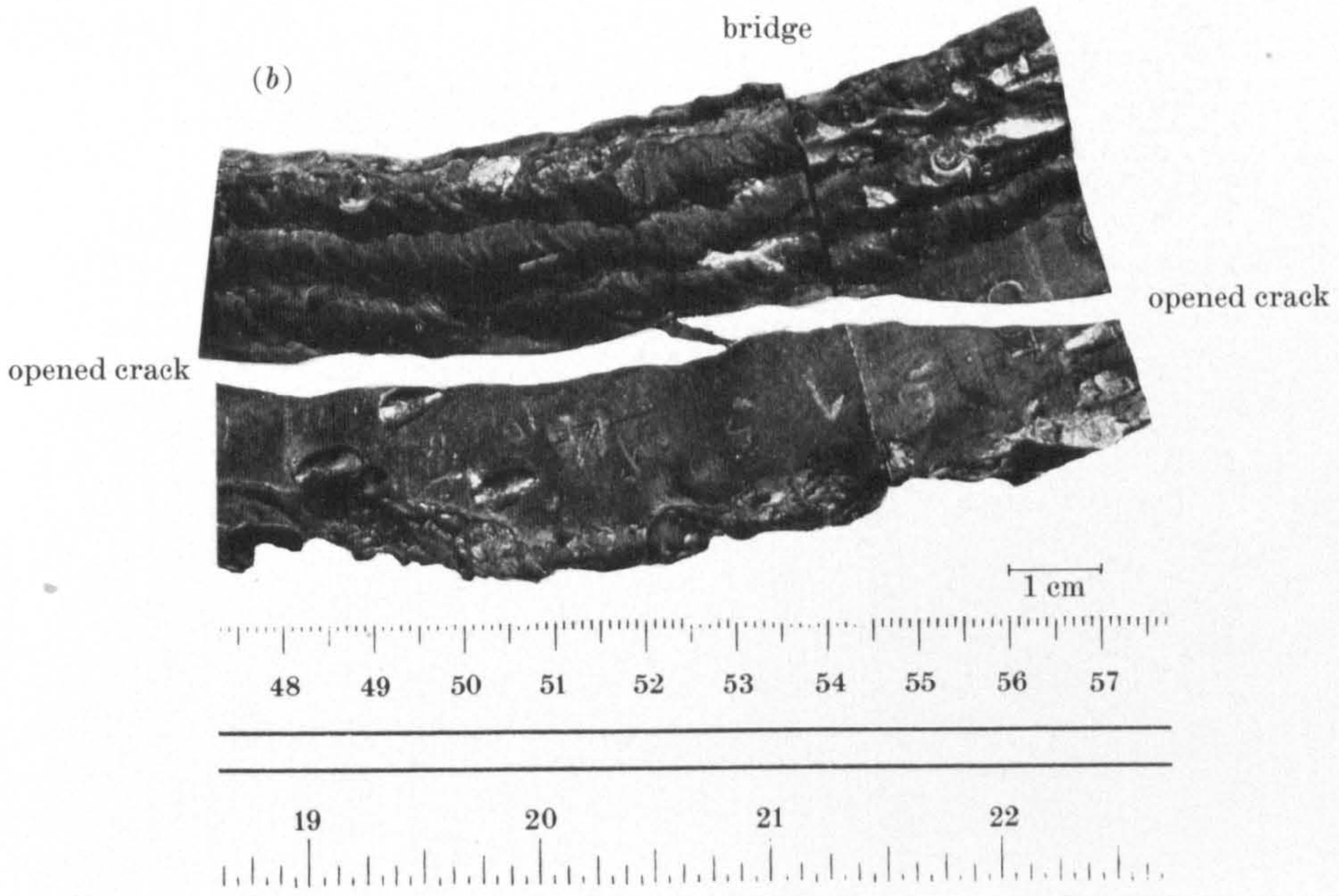

Figure 4.15 (a) Overlapping cracks on a tubular welded joint revealed by magnetic particle inspection; (b) the bridge between the two overlapping cracks reassembled after the cracks have been sectioned and opened

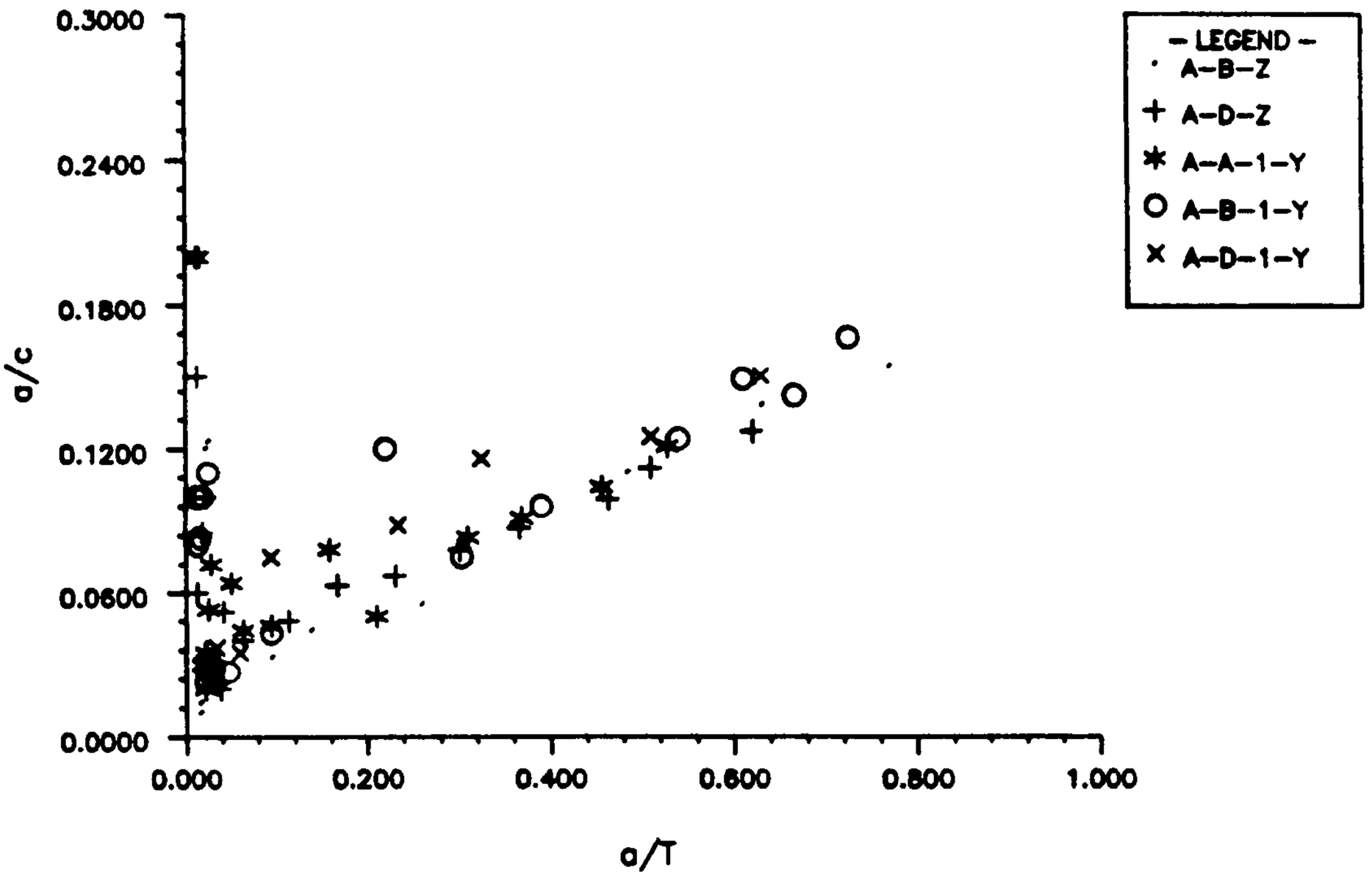

FIGURE 4.16 CRACK ASPECT RATIO CHANGES PROFILE A

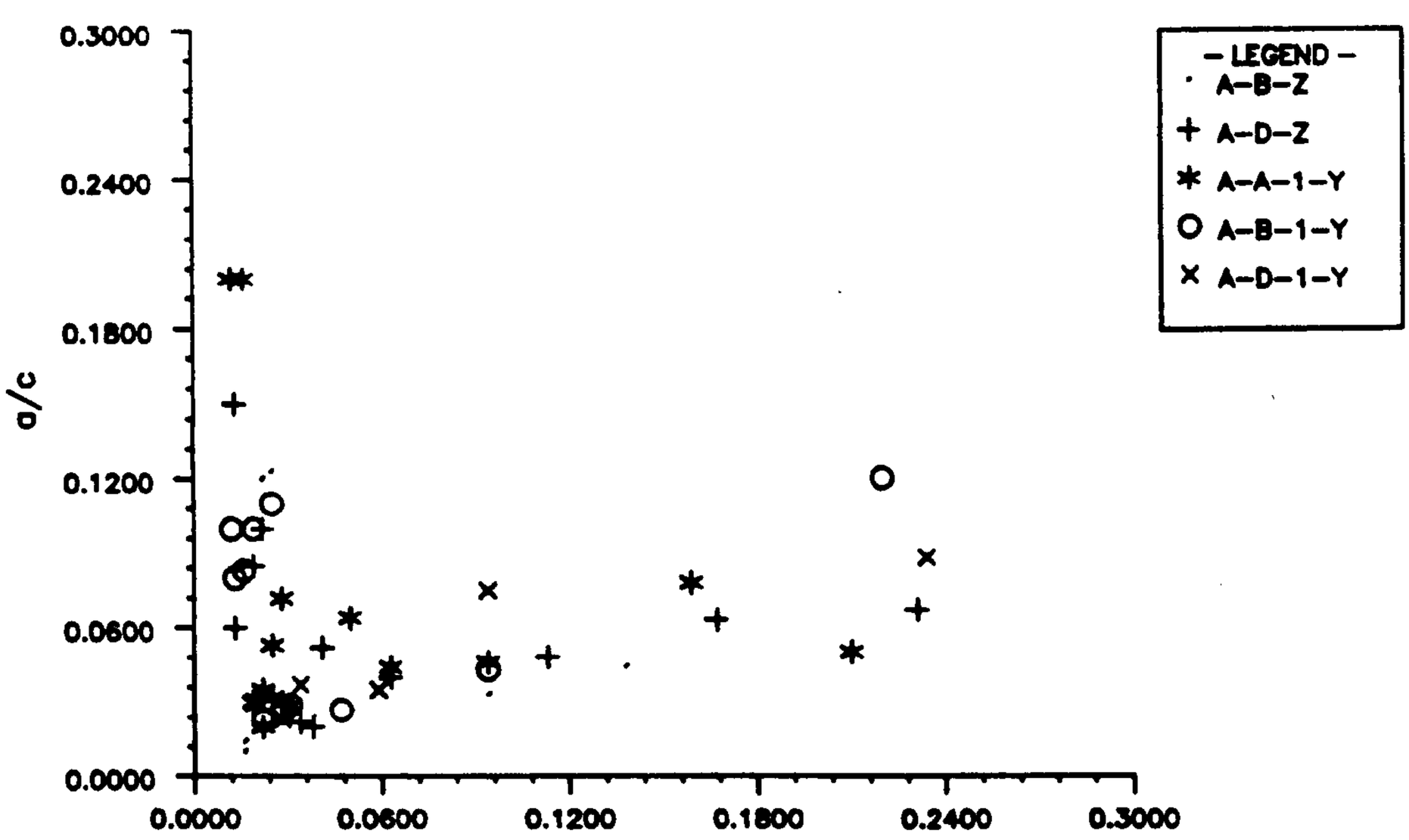

FIGURE 4.17 EARLY CRACK ASPECT RATIO CHANGES PROFILE A

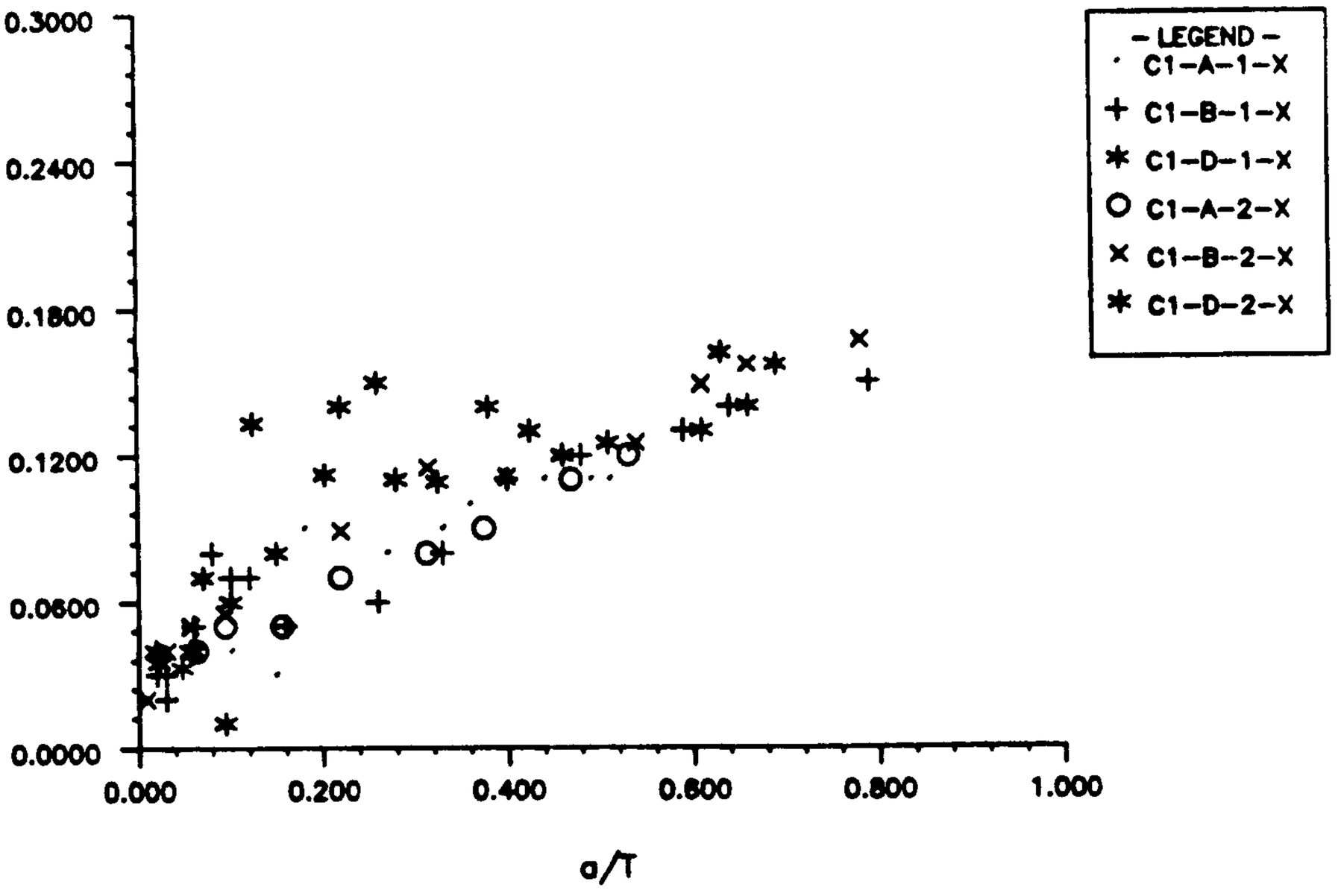

FIGURE 4.18 CRACK ASPECT RATIO CHANGES PROFILE C1

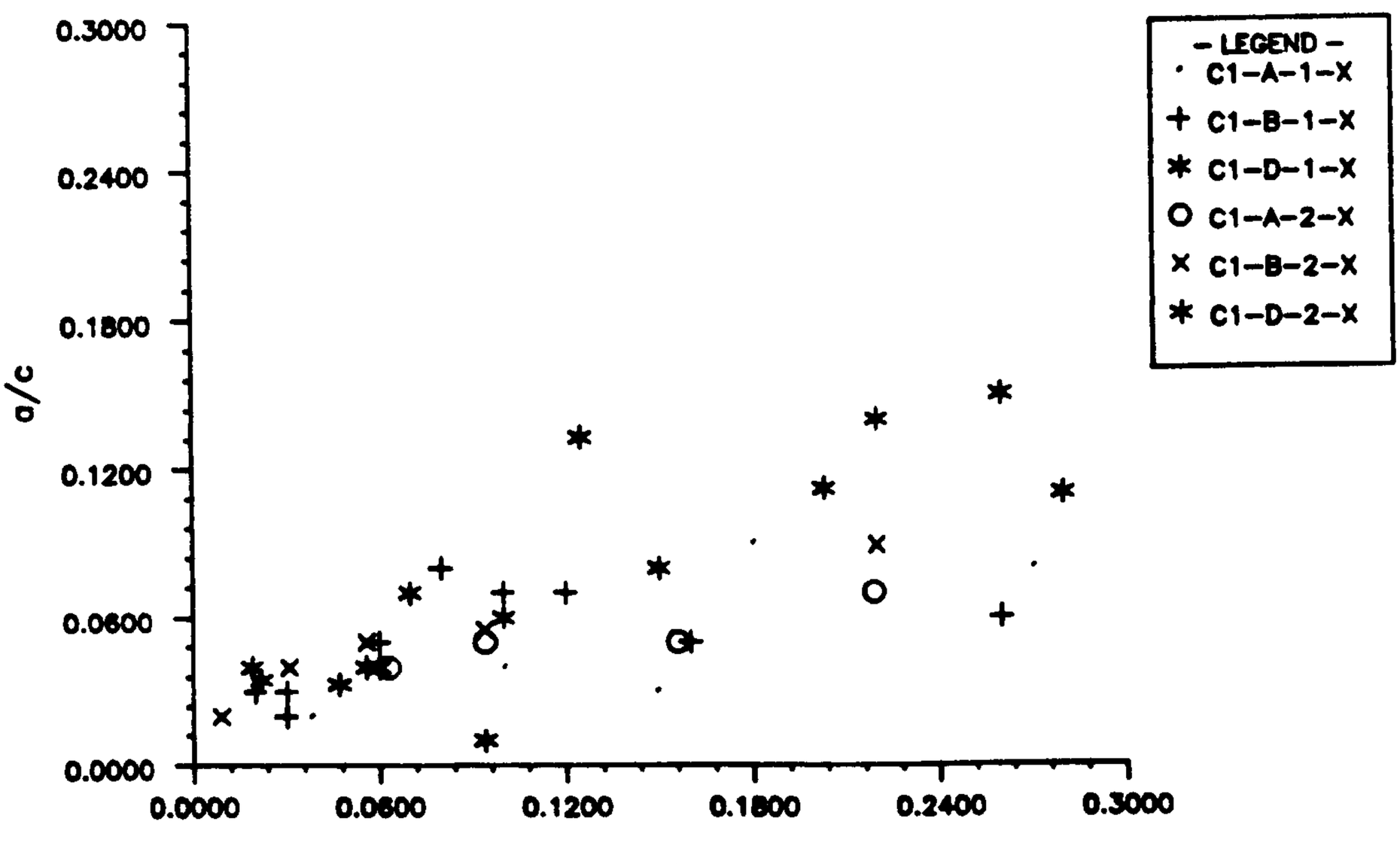

FIGURE 4.19 EARLY CRACK ASPECT RATIO CHANGES PROFILE C1

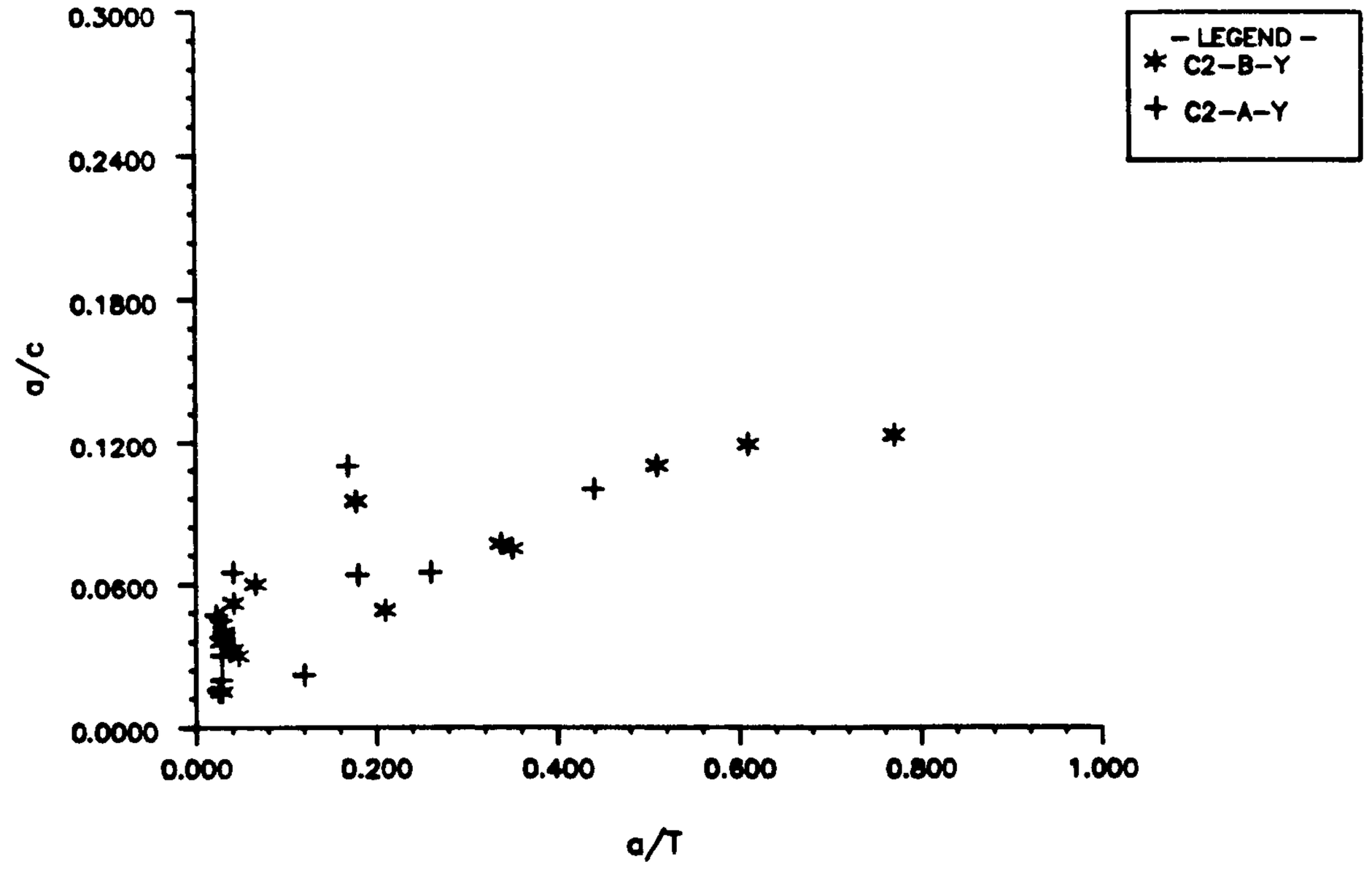

FIGURE 4.20 CRACK ASPECT RATIO CHANGES PROFILE C2

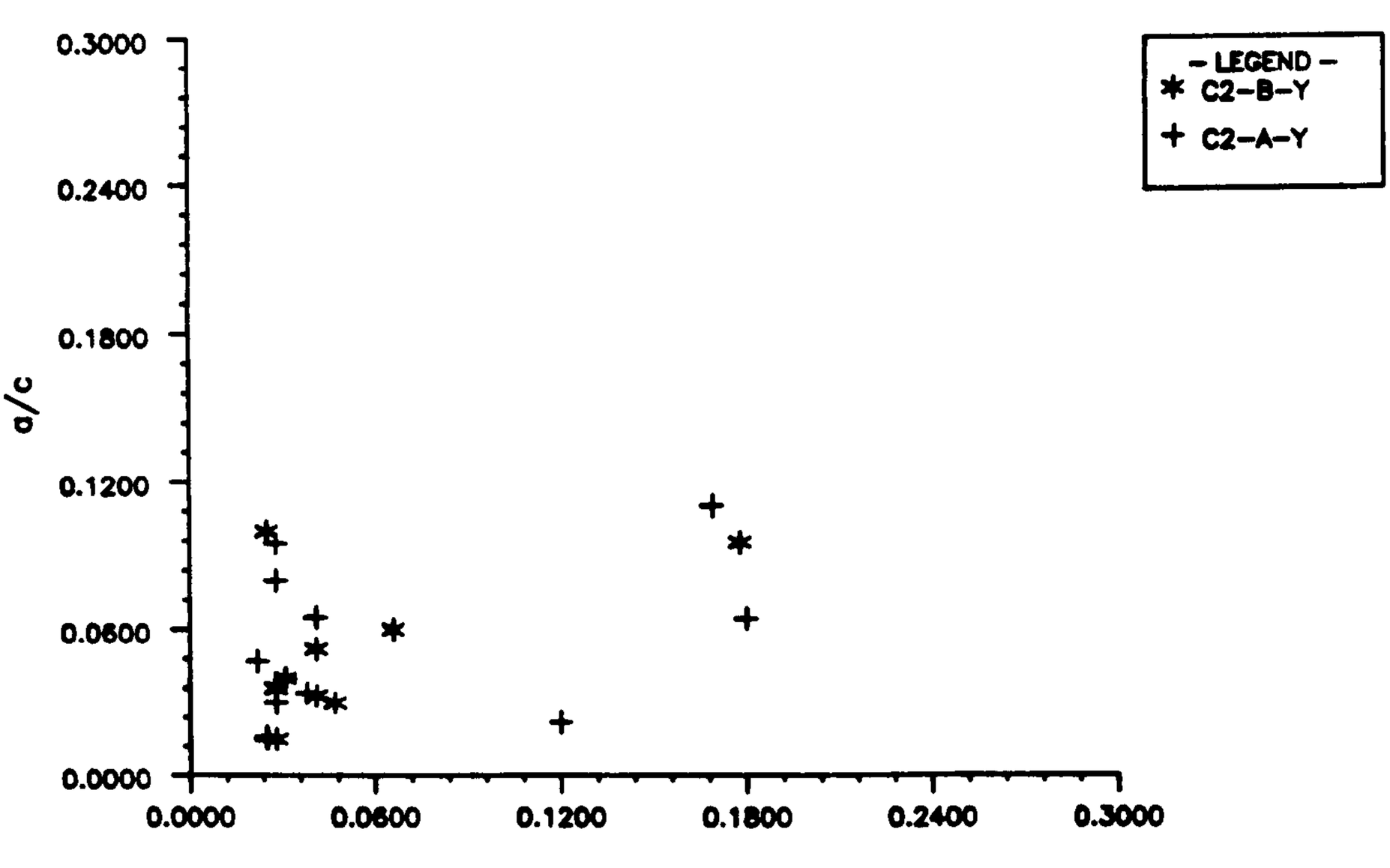

FIGURE 4.21 EARLY CRACK ASPECT RATIO CHANGES PROFILE C2

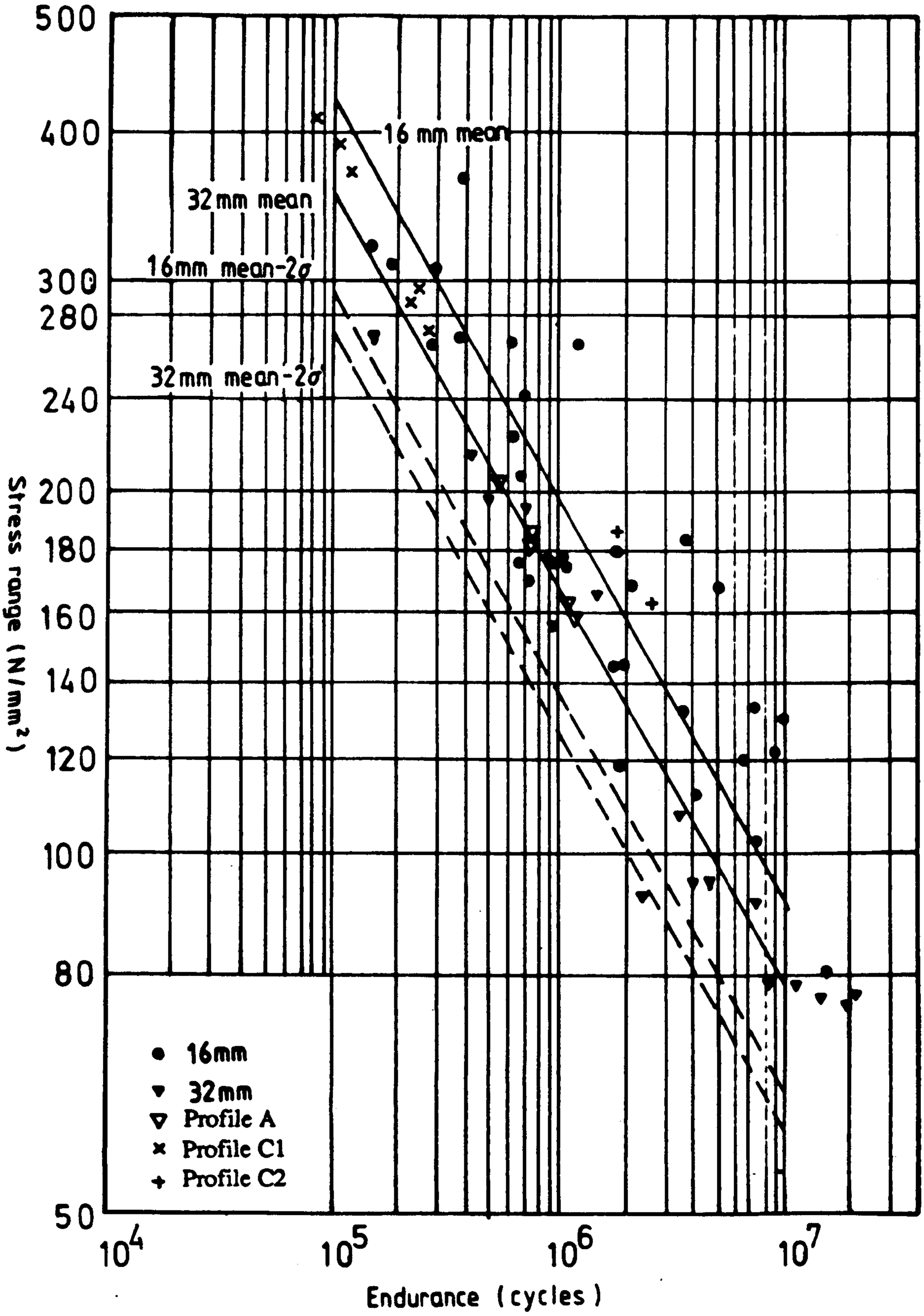

Figure 4.22 Mean and mean -2σ for 16 & 32mm thick joints, (based on experimental hot spot stress and N_2) compared with the 13 data points from this project.

5 CHAPTER FIVE

FRACTURE MECHANICS ANALYSIS OF FATIGUE CRACKS IN TUBULAR JOINTS

5.1 Scope of chapter

This chapter presents a short review of the fracture mechanics approach. It describes briefly some of the stress intensity factor solutions for surface cracks and their applications to tubular joint analysis.

The general weight function method is reviewed with particular reference to the Niu-Glinka weight function for calculating the stress intensity factor for the deepest point of a semi-elliptical surface crack in a welded joint. A comparison of the experimental and analytical values of stress intensity calibration factor Y is conducted.

The effect of moment release on structures such as tubular joints is discussed in terms of incorporating this effect in the calculation of stress intensity calibration factor Y. Two moment release models were developed, a linear model and a quadratic model.

The stress intensity calibration factor Y was calculated using the Niu-Glinka weight function in conjunction with i) the linear moment release model and ii) the quadratic moment release model.

The four sets of values of the geometric stress intensity calibration factor Y are presented and compared in order to determine the best model for estimating the propagation part of the fatigue life of the tubular joints tested.

5.2 Fracture mechanics approach

Fracture mechanics can be used in fatigue analysis to predict the rate of crack growth in a component and consequently the components fatigue crack propagation life. Fracture mechanics relates the local conditions of stress and strain ahead of a crack tip to the global parameters of geometry and applied stress and to the crack depth.

Irwin [5.1] showed that the stresses in the vicinity of a crack tip can be expressed in the form:

$$\sigma_{ij} = \frac{K}{\sqrt{2\pi r}} f_{ij}(\theta) \qquad 5.1$$

The magnitude of the stress field ahead of a crack can, therefore, be described by a single parameter, K, which is known as the stress intensity factor. Once this parameter is known, the complete stress field ahead of a crack is defined. This is the most important parameter used in a fracture mechanics analysis. It can be related to the crack growth rate by the Paris Rule [5.2]:

$$da/dN = C(\Delta K)^m \qquad 5.2$$

a crack size

N number of load cycles

ΔK stress intensity factor range (K_{max} - K_{min})

C & m material constants

By re-arranging and integrating equation 5.2 between limits, the number of cycles taken for a crack to grow from one depth to another can be determined.

$$N = \frac{1}{C} \int_{a_i}^{a_f} \frac{da}{(\Delta K)^m} \qquad 5.3$$

where a_i is the initial crack depth and a_f is the final crack depth. This integration is usually performed by a numerical summation.

The material constants C and m can be determined from fatigue crack growth tests on small standard type specimens, but determining the values of stress intensity factor is often more complex. Consequently, this chapter concentrates on the determination of suitable stress intensity factors for welded tubular joints. Once these can be determined, crack propagation lives can be calculated.

Stress intensity factors can be expressed in the general form:

$$K = Y \sigma \sqrt{\pi a} \qquad 5.4$$

σ representative stress; for tubular joints the 'hot spot' stress

a crack size

Y stress intensity calibration factor. A dimensionless parameter which depends on loading mode, geometry of specimen and crack.

In many simple cases there is a closed form solution for the value of stress intensity factor. For example, in the case of an edge crack subjected to uniform tensile loading:

$$K = 1.12\,\sigma\sqrt{\pi a} \qquad 5.5$$

Stress intensity factors for more complex cases can be obtained by superposing the solutions for simpler cases, if the solutions for the simpler cases are known. Many of these solutions are documented in available handbooks [5.3].

5.2.1 Experimental estimation of Y calibration factors

The development of the a.c. field measurement technique has enabled the characterisation of tubular joint cracks during fatigue tests. This has provided the data about the variation of crack size as a function of the number of cycles and thus the crack growth rate. Using the empirical equation 5.2 proposed by Paris and re-arranged in the form:

$$\Delta K = \frac{1}{C}\frac{da}{dN}^{1/m} \qquad 5.6$$

Dover *et al* [5.4] calculated the crack growth through the wall thickness and obtained the ΔK_{exp} using C and m values obtained from cracked plate specimen tests.

Y_{exp} can be determined by substituting equation 5.4 into equation 5.6 and re-arranging:

$$Y_{exp} = \frac{1}{\Delta\sigma\sqrt{\pi a}}\frac{1}{C}\frac{da}{dN}^{1/m} \qquad 5.7$$

To determine values of the stress intensity calibration factor, Y_{exp}, from equation 5.7, it is necessary to know the crack growth rate, da/dN, at a given crack depth, the stress range, $\Delta\sigma$, and the material constants, C and m. The crack growth rate can be determined from the plots of a versus N given in Chapter 4. The crack growth rate is the gradient of the tangent to the curve at the crack depth being

considered. The term $\Delta\sigma$ is the hot spot stress range at the brace/chord intersection, i.e. at the site of crack initiation. The value of $\Delta\sigma$ was calculated for each of the fatigue tests and shown in Table 4.1.

The values of the material constants C and m are available in the published literature for BS4360 50D steel, the steel from which the test specimens were manufactured. In this study the values for C and m were taken from Ref. [5.5] where $C=2.92 \times 10^{-12}$ and m = 3.0 for ΔK measured in MPa m and da/dN in m/cycle.

5.3 Stress intensity factors for surface cracks

5.3.1 Introduction

Fatigue cracks in welded tubular joints are surface cracks which initiate at the weld toe at a number of sites in the vicinity of the hot spot stress region around the brace/chord intersection. During the early growth period, toe crack depth increases very slowly whereas the crack length on the surface around the intersection increases relatively rapidly to link up forming long shallow semi-elliptical cracks. A large body of literature exists on the stress intensity factor (SIF) solutions for semi-elliptical cracks in finite bodies. For finite thickness plates subjected to uniform tension and bending, solutions in the form of parametric equations based on semi-analytical approaches are available. However,in the cases where a surface crack is located in a more complex body or is subjected to non-uniform loading, other methods e.g. based on numerical techniques are used to calculate the SIFs. Cracks in tubular joints are a case in point.

These cracks are subjected to a stress field in the walls of the tubulars which varies around the intersection. In the through thickness direction the stress field is a combination of tension and bending with a superimposed notch effect in the region of the weld toe. Consequently, attempts have been made to derive semi-analytical models to describe the crack growth behaviour observed in this type of joint.

5.3.2 SIF solutions for cracks in plates subjected to tension or bending

The first solution for calculating the SIF for cracks in three dimensional bodies was derived by Irwin [5.6]. He derived the mode I stress intensity factors, K_I for

the points around an elliptical crack of dimensions 2a and 2c, embedded in an infinite elastic solid subjected to a remote uniform tension, S_t. In this solution which is based on a stress analysis by Green and Sneddon [5.7] the SIFs at the points along the crack front is given by

$$K_I = \frac{S_t\sqrt{\pi a}}{E(k)}\left[\left(\frac{a}{c}\right)^2 \cos^2\phi + \sin^2\phi\right]^{0.25} \qquad 5.8$$

where E(k) is the complete integral of the second kind and is given by:

$$E(k) = \int_0^{\frac{\pi}{2}} (1 - k^2\sin^2\phi)^{0.5} d\phi \qquad 5.9$$

where

$$k^2 = 1 - \left(\frac{a}{c}\right)^2 \qquad 5.10$$

hence

$$E(k) = \int_0^{\frac{\pi}{2}} \left(\frac{a}{c}\cos^2\phi + \sin^2\phi\right)^{0.5} d\phi \qquad 5.11$$

E(k) can be approximated as

$$E(k) = \left[1 + 1.464\left(\frac{a}{c}\right)^{1.65}\right]^{0.5} \qquad 5.12$$

For a semi-elliptical crack in a plate of finite dimensions several differences exist compared to the embedded crack in an infinite body. These are:

i) For a surface crack in a semi-finite body the front surface effects magnifies the SIFs.

ii) For a surface crack in a finite thickness plate, the back surface affects the SIFs.

ii) If a plate is of finite width, this effect magnifies the SIFs.

iv) If the plate is subjected to bending, the stress gradient through the plate thickness also affects the SIFs.

An analytical solution of the problem has proved to be impossible due to the complexity of the geometry involved. Several investigators have attempted to solve this problem by using different techniques. However, one of the approaches considered most accurate particularly for tubular joints is the three dimensional analysis of the joint containing the crack using the finite element method. This method needs a complex mesh generation scheme and is time consuming and expensive. Ritchie *at al* [5.8] used this method to analyse a few cases of tubular joints. They introduced several cracks of varying sizes obtained from fatigue experiments in a finite element model of a T-joint subjected to axial loading. They calculated the SIF for points along the crack front for each crack shape. This required a separate FE analysis of the tubular joint for each of the crack geometries. A simpler approach adopted by a number of investigators was to approximate the cracks in tubular joints by cracks in flat plates subjected to remote tension or bending. Solutions in the form of parametric equations have been proposed by a number of investigators using different methods. The most widely used equations are those of Newman-Raju [5.9], Scott and Thorpe [5.10] and Holdbrook and Dover [5.11].

Newman-Raju [5.9] presented an analysis of surface cracks in plates of finite width using three-dimensional FE with singular crack tip elements to model the rapidly changing stress distribution in the region of the crack tip. They obtained modifications for the embedded flaw results for a range of crack sizes and also included in their results a correction factor to account for the effects of the finite plate width. The SIFs were presented for the case of uinform tension and pure bending as a function around the intersection, the crack depth, surface crack length, plate thickness and plate width.

Holdbrook and Dover [5.11] carried out fatigue tests on specimens of finite dimensions containing a surface crack under tensile loading. Their derived solutions included in their analyses the effect of finite specimen dimensions, the end conditions and induced secondary bending produced by changes in the position of the neutral axis as the crack grows. Using these solutions they obtained good correlation between the through thickness crack and surface crack fatigue data for specimens subjected to tension. Dover and Connolly [5.12] used these solutions to predict changes in the shape of fatigue cracks in specimens subjected to bending and tension. The results showed good agreement with experimental data.

Scott and Thorpe [5.10] reviewed the available SIF solutions and fatigue crack growth data and observed that depending on the type of loading the surface cracks in flat plates try to adopt preffered shapes. They concluded that this change in crack shape is a sensitive test of the accuracy of the SIF solutions. They applied this criterion to examine different available solutions and subsequentky recommended the Newman-Raju solution for pure tension case and Koterazawa and Minamisaka [5.13] for pure bending. In the case of finite width plates the finite dimensions corrections of Holdbrook Dover were recommended.

5.3.3 Discussion

A comparison of results using different models for surface cracks in flat plates were reported by Aaghaakouchak [5.14]. The work involved calculating the stress intensity calibration factor Y for surface cracks with aspect ratio a/c ranging from 0.05 - 1.0. The analyses showed in general that among the available parametric equations those after Newman-Raju, which were based on FE analysis, provide the best SIF results for surface cracks in infinite width plates. The Holdbrook Dover equations which were derived for cracks in plates of finite dimensions, tend to underpredict the SIF for cracks in infinite width plates. For Scott and Thorpe their equations show good agreement with those of Newman-Raju as the earlier work of Raju & Newman provided the basis for the derivation of Scott and Thorpe equations.

However, all the above equations are for surface cracks in flat plates subjected to remote tension or bending. Investigators have simply approximated tubular joint cracks and assumed them to be similar to cracks in flat plates to justify their use of these equations. But plates with surface cracks do not represent the geometry of the surface cracks at the weld toe of a tubular joint. Tubular joints are fundamentally a different geometry, they are more complex and their associated stress fields are complex in nature. In order for a reasonable assessment of the magnitude of the SIF for surface cracks at the weld toe to be undertaken, the weld geometry and it's influence on the stress field at the toe of the weld must be considered. Also the weld is a region where stress concentrations occur, these were shown to introduce changes in the through thickness stress field for a/t values of up to 0.2.

Therefore, for welded tubular joints an appropriate method of calculating the stress intensity factors would be one which incorporated the effects of the weld geometry, changes in the through thickness stress field and changes in the crack aspect ratio as the crack initiates and starts to grow. The weight function method would appear to account for these effects.

The recently derived Niu-Glinka [5.15] weight function for calculating the stress intensity factors for the deepest point of a surface crack emanating at the toe of a T-butt welded joint will be used for this study. Stress analyses studies were conducted with different weld toe angle α and different weld toe radius ρ. The effects of such variables on the through thickness stress field were reported in chapter 3. Niu conducted a similar analysis and concluded that both weld toe angle α and weld toe radius ρ affect the through thickness stress distributions.

The calculated SIF values using the weight function method for a T-butt joint having a surface crack subjected to pure tension or bending showed that the SIFs were affected over much larger distances compared with the effect on the stress distribution. The weld toe radius ρ had negligible effect on the SIFs for $a/t > 0.05$. For weld toe angle α the effect was negligible for $a/t > 0.35$ and not very significant for $a/t > 0.15$, but for $a/t < 0.35$ measurable differences were reported. This indicates that the effects of joint geometry on the fatigue strength cannot be estimated on the basis of stress distributions, thus the argument that the stress distribution incorporates the geometry effect is not totally accurate for SIF considerations.

The major disadvantage in using the Niu-Glinka weight function is that the SIF values are calculated for the deepest point of the crack and not for all points along the crack front.

In view of the fact that this study places considerable emphasis on the early crack growth period with particular reference to the differences between the two weld profiles studied, it would appear that the Niu-Glinka weight function is the most appropriate method. Crack aspect ratio changes reported in chapter 4 showed significant differences between the two different weld profiles studied as demonstrated in plots of crack aspect ratio as a function of the non-dimensional crack

depth a/t shown in Figures 4.16-4.21. These differences can be incorporated in this weight function and their impact assessed in terms of the propoagation part of life.

A review of the general weight function technique is therefore presented and the Niu-Glinka method and it's application is also presented.

5.4 Weight function method

The weight function method is a technique used to calculate the stress intensity factor for a crack subjected to a non-uniform stress field. Bueckner [5.16] and Rice [5.17] have demonstrated that for a crack in a given geometry, there exists a particular function, known as the weight function, which is the property of the cracked body. The general expression for such a function can be obtained based on the principle of the strain energy release rate. For plane problems it can be given by the relation:

$$m(x,a) = \frac{H}{K_r}\frac{\partial u_r}{\partial a} \qquad 5.13$$

where K_r is the reference stress intensity factor, and $m\ (x,a)$ is the reference crack opening displacement at x for a crack of length a.

Rice showed that the weight function is unique to the given cracked geometry and independent of the loading from which it was derived. Consequently, the stress intensity factor can be calculated by integrating the product of weight function $m(x,a)$ and stress distribution $\sigma(x)$ in the potential crack plane:

$$K = \int_o^a \sigma\,(x)\, m\,(x,a)dx \qquad 5.14$$

where $\sigma(x)$ is determined for the uncracked body.

The application of the weight function method to a practical problem where a crack exists is usually associated with the use of the superposition technique. This technique allows one to resolve complex loading geometry configuration into a number of separate simpler configurations which have simpler boundary conditions and thus known stress intensity factors.

The methodology of the weight function consists of the following steps:

1) Determine the stress distribution of the uncracked body along the potential crack site.

2) Obtain an appropriate weight function for the cracked geometry under consideration.

3) Perform an integration according to equation 5.14 using numerical or analytical methods depending on the form of the weight function and the stress acting on the surfaces.

The major advantage of the weight function method is that the amount of stress analysis is markedly reduced. Once the stress distribution has been determined for a given geometry, the stress intensity factor can be calculated for any crack size and shape. This is done by an integration and the need to include the crack explicitly in the stress analysis for each crack size is not required.

5.4.1 Niu-Glinka weight function

Niu [5.18] derived a number of weight functions for both edge and semi-elliptical surface cracks in flat plates and plates with angular corners. The procedure used was based on the theory of weight functions developed by Bueckner and Rice [5.16 & 5.17] in conjunction with the Petroski-Achenbach [5.19] method.

In order to derive the weight function (equation 5.13), a reference stress intensity factor K_r for a given geometry under any stress system S_r needs to be known Figure 5.1 together with the corresponding crack opening displacement field $u_r(x,a)$. An appropriate reference stress intensity factor K_r can often be found in the literature, but the corresponding crack opening displacements $u_r(x,a)$ are difficult to find because these data are seldom accompanied by the stress intensity factor solutions. To overcome this difficulty, Petroski and Achenbach [5.19] proposed an approximate crack opening displacement function $u_r(x,a)$ for plane problems:

$$u_r(x,a) = \frac{\sigma_0}{H\sqrt{2}}\left[4F\sqrt{a(a-x)} + \frac{G(a-x)^{3/2}}{\sqrt{a}}\right] \qquad 5.15$$

where

$$F = K_r / \sigma_0\sqrt{\pi a} \qquad 5.16$$

For equation 5.15 the only unknown is the parameter G (parameter of the crack opening displacement function). Petroski Achenbach derived a solution for G; details are in Reference [5.19]. Once this was resolved it was then possible to derive a general form of a weight function which was analagous to that derived by Bueckner [5.16] for an edge crack;

$$m(x,a)=\frac{2}{\sqrt{2\pi(a-x)}}\left[1+M_1\left(\frac{a-x}{a}\right)+M_2\left(\frac{a-x}{a}\right)^2\right] \qquad 5.17$$

where

$$M_1=\frac{8F'a+4F+3G}{4F} \qquad 5.18$$

$$M_2=\frac{2G'a-G}{4F} \qquad 5.19$$

$$F'=\frac{\partial F}{\partial a};\ ]G'=\frac{\partial G}{\partial a}$$

Therefore the derivation of a weight function for any particular geometry can be reduced to the determination of parameters M_1 and M_2 only.

Full details of the derivations and listing of the different weight functions by Niu *et al* are presented in Reference [5.18].

The particular weight function of interest in this work is that derived for a semi-elliptical surface crack in a finite thickness plate with an angular corner α. It was assumed that the relative effect of corner angle α was the same for edge and semi-elliptical cracks. Consequently Niu argued that the ratio of the stress intensity factor for an edge crack in a flat plate to that of an edge crack emanating from a corner is equal to the analogous ratio for semi-elliptical cracks (Figures 5.2 & 5.3) of the same depth and under the same stress system $\sigma(x)$:

$$K_s^{\alpha}=\frac{K_e^{\alpha}}{K_e^{P}}K_s^{P} \qquad 5.20$$

K_s^{α} stress intensity factor for a semi-elliptical surface crack emenating from an angular corner α in a finite thickness plate with a step.

K_e^{α} stress intensity factor for an edge crack emenating from an angular corner α in a finite thickness plate with a step.

K_s^P stress intensity factor for a semi-elliptical surface crack in a finite thickness flat plate.

K_e^P stress intensity factor for an edge crack in a finite thickness flat plate.

Thus using the weight functions already derived Niu proposed the following expression for the refence stress intensity factor required by equation 5.16.

$$K_r = \sigma_o \frac{\int_o^a m_e^{\alpha}(x,a,a/t,\alpha)dx}{\int_o^a m_e^{P}(x,a,a/t)dx} \int_o^a m_s^{P}(x,a,a/t,a/c,c/w)dx \qquad 5.21$$

where

$$K_r = F_r \sigma_o \sqrt{\pi a} \qquad 5.22$$

$$F_r = \frac{2\sqrt{2}}{15\pi} \cdot \frac{F^{\alpha}}{F^{90}} \cdot \frac{15 + 5M_{e1}^{90} + 3M_{e2}^{90}}{15 + 5M_{e1}^{P} + 3M_{e2}^{P}} \cdot (15 + 5M_{s1}^{P} + 3M_{s2}^{P}) \qquad 5.23$$

Therefore the desired weight function can be expressed as shown in equation 5.24.

$$m_s^{\alpha}(x,a/t,a/c,c/w,\alpha) = \frac{2}{\sqrt{2\pi(a-x)}}\left[1 + M_{s1}^{\alpha}\left(\frac{a-x}{a}\right) + M_{s2}^{\alpha}\left(\frac{a-x}{a}\right)^2\right] \qquad 5.24$$

where

$$M_{s1}^{\alpha} = A_s^{\alpha} + 3B_s^{\alpha} - 4$$

$$M_{s2}^{\alpha} = 5\left[\frac{\sqrt{2}\pi}{4}F_r - \frac{A_s^{\alpha} - 1}{3} - B_s^{\alpha}\right]$$

$$A_s^{\alpha} = \frac{2F'_r a}{F_r}$$

$$B_s^{\alpha} = \frac{5\sqrt{2}\pi \int_o^a F_r^2 a\,da}{8a^2 F_r}$$

5.4.1.1 Application of Niu-Glinka weight function to tubular joints

Niu [5.20] wrote a Fortran 77 program which uses the Niu-Glinka weight function to calculate the stress intensity factor for the deepest point of a semi-elliptical surface crack in a welded joint. The main routine of this program is module CRK3D. This routine receives input data on crack geometry and stress distributions. These are the crack aspect ratio a/c and the dimensionless crack depth a/t where a is the crack depth at the deepest point and c is half the crack length and t is the plate thickness. The stress distribution is supplied as the stress normalised by the nominal stress. As the weight function accounts for the effects of the weld toe angle α and plate width, on the stress intensity factor, these variables are also supplied.

The module CRK3D calculates the coefficients of the weight function and evaluates the stress intensity factors by calling on subroutines which integrate the weight function with the specified stress distribution. All necessary integrations and differentiations were conducted using numerical procedures. This weight function has recently been developed by Niu to calculate stress intensity factors for the full plate thickness. This is the first opportunity available where analytical Y values can be calculated for $a/t > 0.5$ for either T-butt welded joints or tubular joints. This is an important development particularly for tubular joints since the remaining fatigue life beyound 0.5T is still significant.

5.4.2 Comparison of analytical and experimental stress intensity calibration factor Y

Stress intensity calibration factors were calculated for the thirteen chord cracks produced in this work. The test details and fatigue data are presented in chapter 4. Procedures for the calculation of experimental values of stress intensity calibration factor Y are described in section 5.2.1.

The Niu-Glinka weight function was used to calculate the calibration factor Y at a number of crack depths. The crack depths chosen were those measured by the a.c. field measurement technique during testing in order that the experimentally obtained aspect ratios could be used in the calculation. The weld toe angle values for the two different weld profiles reported in chapter 3 were also incorporated in

the analysis. The function c/w was assumed to be zero as the deepest point of the crack occurred at the saddle position i.e. the mid point of the 2000mm long chord wall.

The theoretically calculated values of the calibration factor Y using the weight function method are compared with the experimental Y values. The comparison is expressed in the form of Y as a function of the non-dimensional parameter a/t. Figures 5.4-5. 6 show the results for the two different weld profiles studied. For small crack depths a/T < 0.15 the Y values decrease sharply. This decay is associated with the sharp decrease in stresses away from the weld toe region in which the effect of the weld toe notch causes high stress concentrations to occur. A comparison of these results with other experimental Y values is not possible due to the paucity of data on early crack growth. This is mainly due to:

i) Experimental difficulties associated with measuring small cracks.

ii) Small cracks at the weld toe are significantly affected by the weld geometry. This was clearly demonstrated in the crack aspect ratio changes for the two weld profiles reported in this study. The differences are highlighted in Figures 4.16-4.20. Consequently stress intensity factors will also be significantly affected by weld geometry. Since no reliable data about the geometry of the weld is reported with the available fatigue data a comparison is therefore not possible.

Above a certain crack size a/t > 0.15 both experimental and analytical Y values exhibit very slight decay, almost constant Y values independent of crack depth. The stress intensity factor and crack growth rates begin to increase. This increase in SIF is due to the crack growing through the thickness. The general trend and features observed in these curves is consistent with other Y calibration values reported in References [5.12, 5.14 & 5.21] for Y, K and T steel tubular joints.

In comparing the experimental and calculated vales of Y significant disagreement is observed. This is due to the fact that experimental Y calibration factors are calculated from fatigue test data which encompasses all the parameters affecting the behaviour of the tubular joint and in particular the crack growth characteristics. In the case of the calculated Y calibration values, these are obtained from information regarding the uncracked section i.e. distribution of stress conducted on the uncracked tubular joint. Obviously crack aspect ratio changes are considered in

the weight function method but possible load redistribution once the crack initiates and starts to grow are not included. It is this significant observation reported by Dover *et al* [5.22] and Aaghaakouchak *et al* [5.23] which could possibly explain such obvious differences between the experimental Y calibration factor values and calculated Y values for the same tubular joint.

Aaghaakouchak [5.14] conducted FE analysis on 2-D plates and rings with edge cracks in an effort to establish a relation that can describe the mechanism of the moment release model. The FE analyses were conducted under different boundary conditions. He reports that for the 2-D plates or rings studied the behaviour of the cracked section approached that of a hinge.

In the presence of some degree of redundancy this change of behaviour caused a load redistribution in the body and in effect released the loads transmitted across the cracked section. Aaghaakouchak established a trend for the moment release in the section as a function of the crack size. The rate of increase in SIF in the statically indeterminate structure was significantly lower than that of the statically determinate structure.

5.4.3 Effect of moment release on tubular joints

In the case of tubular joints it was proposed that these can be regarded as redundant structures because tubular joints can maintain equilibrium even if the cracked section is replaced by a hinge. Under such a condition there would be no moment in the cracked section, only a membrane and shear force would exist. The membrane force in the chord wall of a tubular joint is due primarily to the transfer of applied loads from the brace to the chord. The bending moment is a secondary load resulting from the rigidity of the brace/chord intersection. Therefore, in order to compare the calculated and experimental stress intensity calibration factors Y, the load shedding effect would have to be assessed and incorporated in the analysis.

The load shedding model assumes that the membrane force at the section containing the surface crack remains constant, but the bending moment releases as the crack grows. This assumption is based on the simple analysis of 2-D plates and rings containing an edge crack. The tubular joint however, is a more complex structure and significantly more difficult to analyse.

There is no therotical basis for the load shedding model, the concept was introduced on the basis of the results of FE analyses conducted on 2-D plates and rings under different boundary conditions. Use of this model appears to account for the differences between the experimental calibration value Y and the calculated Y value for the tubular joints. To date no numerical analyses have been conducted on tubular joints to obtain confirmation for this hypothesis or to attempt to validate the moment release models proposed by Aaghaakouchak *et al* . The models they proposed are linear and parabolic. These are presented graphically in ref 5.23 where M is the the bending moment at the cracked section and M_0 is the bending moment at the uncracked section. The calculated Y calibration factors are simply multiplied by this ratio of M/M_0 shown in ref.5.23

Aaghaakouchak concludes that the parabolic model produced a totally wrong result and this was subsequently discarded. The linear model was of the following form

$$S_b = S_{bo}\left(1 - \frac{a}{t}\right) \qquad 5.28$$

S_b bending stress

S_{bo} bending stress in uncracked body

a & t crack depth and tubular wall thickness respectively.

The equation produced results which showed good agreement with the Y_{exp} values calculated from the fatigue data base available at UCL [5.24]. The above equation obtained from ref.[5.23] does not specify the method used to decompose the hot spot stress into bending and tension components in order that the load shedding model could be used. Consequently, in this work a development of this technique is undertaken and two models are presented where the elements of each are explicitly defined.

Therefore, the rate of release of the bending moment as the fatigue crack grows through the thickness of the chord wall is modelled as a linear decaying function. The second model is based on a quadratic function. The introduction of the quadratic model has no theoretical basis and is purely an attempt to find the best model that can describe the load shedding concept.

The two moment release models can therefore be incorporated in the equation for calculating the stress intensity factor, thus equation 5.14 is modified accordingly

$$K(a) = \int_0^a m(x,a)\,\sigma(x,a)dx \qquad 5.29$$

It should be noted that stress σ in equation 5.29 is not only a function of x but also a function of a, the crack depth. The function $m(x,a)$ is unaffected.

The basic assumptions of the moment release models is that the tension component remains constant whereas the bending moment is released. Therefore the hot spot stress must be decomposed into the tension and bending in order to allow the analysis to be conducted. The stress analyses reported in chapter 3 have already established that T-butt through thickness stress distributions for bending and tension could be combined using the relation 3.10 in chapter 3, (where the R ratio is the bending to tension ratio of the tubular joint), to produce the equivalent stress distribution for a tubular joint.

Figures 3.25 & 3.26 of chapter 3 show excellent agreement between the combined bending and tension T-butt joint results and the tubular joint results. Therefore for the moment release models the T-butt results for tension and pure bending for the 30° and 45° weld toe angles representing the controlled weld profile and the AWS weld profile respectively will be used to assess the effect of load shedding on the calculated Y values.

Therefore, $\sigma(x,a)$ in equation 5.29 where σ is the non-dimensional stress value can then be expressed as

$$\sigma(x,a) = \left(\frac{R}{1+R}\right)\sigma_B(x) + \left(\frac{1}{1+R}\right)\sigma_T(x) \qquad 5.30$$

σ_B component of stress in bending

σ_T component of stress in tension

R ratio of bending to tension stress

However, in order to realise the load shedding effect a function needs to be introduced in equation 5.30 to modify the bending component. Thus equation 5.29 should be expressed as

$$\sigma(x,a) = \left(\frac{R}{1+R}\right)\sigma_B(x)\,f(a) + \left(\frac{1}{1+R}\right)\sigma_T(x) \qquad 5.31$$

where f(a) = 1 - a/t for the linear moment release model

and f(a) for the quadratic moment release model is presented in Appendix II.

5.4.4 Comparison of analytical and experimental stress intensity calibration factor Y including moment release models

The Niu-Glinka weight function used in conjunction with the moment release models was used to calculate the stress intensity calibration factors for the thirteen chord cracks produced in this work. These sets of results were incorporated with the data shown in section 1.4.2 and presented in Figures 5.17-5.29. The results for each type of profile are compared below.

5.4.4.1 Profile C1

Figures 5.17-5.12 show the four sets of Y calibartion factor distributions. The general trend associated with Y factors for tubular joints tested under bending moment loading is apparent. The early crack growth period a/T < 0.1 Y factors calculated in conjunction with moment release models exhibit substantially higher values than the Y_{exp} or analytica! Y values. In some cases the over-prediction can be up to 25% as shown for tests C1-A-1-X and C1-B-1-X. Both Y values calculated using linear and quadratic models exhibit sharp decay for very small values of a/t, this is the region where high concentration of stress occurs due to the weld notch effect. The sharp decay is consistent with the behaviour of the stress distribution and reflects the effect that the stress distribution has on the calculation of Y values.

For a/t > 0.1 both models begin to demonstrate a reduction in Y as compared with Niu-Glinka results and for a/T > 0.2 the Y values are very close to Y_{exp} results. The distribution of Y for the linear model is consistently higher than that shown for the quadratic model results.

5.4.4.2 Profile C2

Figure 5.23 & 5.24 represent the data for profile C2. The figures clearly show that for early crack growth all three values i.e. analytical, linear load shedding

and quadratic load shedding models significantly overpredict the Y factor values for a/t < 0.25. For a/t > 0.25 the correction due to the use of the load shedding models improves but does not correspond to the same value as the $Y_{exp.}$ Clearly the lower notch stresses associated with this weld profile give rise to a much lower Y_{exp} values for initial and early crack growth. Also as reported in chapter 2 the hot spot stress concentration factor is lower than either profile A or C1. Thus for the same nominal stress values lower hot spot stress is measured thus leading to a reduced crack growth rate.

It would therefore appear that the two load shedding models do not provide the necessary correction and this could lead to the predicted propagation part of life to be much reduced. It must be noted that the theoretical model uses stress distribution for T-butt joints calculated on the basis of a smaller weld toe radius as compared with that observed for profile C2. This would therefore contribute to possible overestimation in the calculated Y factors.

5.4.4.3 Profile A

Figures 5.15-5.19 show the four values of stress intensity calibration factors Y for the different methods used. Firstly, a larger number of data points are available for early crack growth period for the AWS weld profile. This is due to the fact that the most frequent weld toe radii measured were significantly smaller than for either C1 or C2 profiles. This leads to bigger region at the brace/chord intersection where the notch stresses are high. Consequently, the probability that a larger number of initiation sites could exist is higher.

Again a sharp decay in the Y values occurs for small values of a/t. This is a reflection of the effect of stress distribution on Y values. For the stress distributions associated with a weld angle of 45° the notch effect close to the weld toe the influence is clearly visible and results in higher values in Y distributions compared with profiles C1 and C2.

In considering the whole distribution of Y factors the quadratic load shedding model produces lower values than the linear model and both approaches do not fully correct for the overprediction until the crack has reached approximately 35-40% of the wall thickness.

5.4.5 Discussion

In order to calculate the fatigue life of a structure it is important to determine the stress intensity factors for the defects in the particular structure. For simple components a number of solutions exist but for complex bodies such as tubular joints the task is extremely difficult because of the geometry and the influence of the changing weld profile on the local stress fields.

Therefore, in the case of tubular joints there are no solutions available to accurately calculate the SIF values. However, the recently developed Niu-Glinka weight function derived in closed form was used in this study. This weight function is capable of dealing with non-linear through thickness stress distributions and can incorporate effects due to different weld angle α and weld toe radius ρ. In view of the advantages of this approach the results produced are not sufficiently accurate to predict the correct crack propagation part of the fatigue life of the tubular joints. In this case, the Niu-Glinka weight function significantly overpredicted the SIFs. These features are demonstrated in Figures 5.4-5.16. It must be noted that the general trend for Y values was accurately predicted by this weight function.

The stress distribution used in calculating the Y values is that of the uncracked body but for tubular joints it is felt that the presence of a crack causes changes in the local bending stress. It is thought that the reduction in local bending moment and associated increase in local flexibilty can be modelled by systematic moment release. The mechanism for tubular joints is not fully understood yet, but the linear and quadratic models have been tried. These attempts shown in Figures 5.17-5.29 show the linear moment release model slightly overpredicts the overall distribution of Y factors whereas the quadratic model provides good agreement between the experimental and predicted values.

In using the stress distributions derived for the T-butt welded joints, small errors were introduced in the values of Y for very early crack growth in the case of the controlled weld profiles C1 and C2. This is due to the weld toe radius modelled being smaller than that measured for either of the two profiles. This did not occur for profile A and consequently the benifit of using the moment release models is realised for the whole distribution of Y values.

The ability of the linear model to reduce the value of Y calibration factor in particular for crack depth up to 25% of the chord wall was not sufficient. Consequently the quadratic model approach was introduced in an attempt to model a more significant drop in Y values for a/T < 0.25. Both models were specifically derived on a simple approach, the linear model on a straight line and the quadratic model is based on part of a circle. However, the actual problem associated with predicting the behaviour of the structural response and possible load redistribution in a tubular joint in the presence of a crack is probably much more complicated. The moment release concept appears to be the right approach but its implementation in this context may be too simplistic.

It would seem that the moment release models linked with the Niu-Glinka weight function could provide a fast procedure for the calculation of stress intensity factors for tubular joints. The evidence so far suggest that their application to fatigue life assessment may provide improvement in the predictions of the number of cycles in the crack propagation part of life. These models will be further applied in the life calculation of the tubular joints used in this study and their possible validation discussed in the next cahpter.

5.5 conclusions

1) Stress intensity calibration factors Y were produced for the deepest point of the crack from experimental data. These values decreased rapidly during early crack growth. The general trend of the distribution of Y values associated with tubular joint behaviour was observed.

2) The Niu-Glinka weight function capable of incorporating the effects of weld angle and weld toe radius was successfully used to predict the general trend of values of Y for for the deepest point of the crack for this study. However, the values for the whole distribution were over conservative.

3) The moment release concept applied to tubular joint SIF calculation was successfully incorporated with the Niu-Glinka weight function.

4) Two moment release models were developed namely, linear and quadratic models. The results produced using the Niu-Glinka weight function in conjunction with these models showed significant improvements in the predicted Y values compared with Y values calculated from experimental data.

5.6 References

5.1 Irwin, G.R., Analysis of stress and strain near the end of a crack traversing a plate, *J. of Applied Mechanics, ASME*, No. 3, 1957.

5.2 Paris, P., Erdogan, F., A critical analysis of crack propagation laws, *J. of Basic Eng., Trans. ASME*, Vol. 85, 1963, pp 528-534.

5.3 Rooke, D.P., Cartwright, D.J., Compendium of stress intensity factors. HMSO, London, 1976

5.4 Dover, W.D., Dharmavasan, S., Fatigue analysis of tubular joints using fracture mechanics, *Offshore China conference* 1983.

5.5 Johnson, R., Bretherton I., Fatigue data from constant amplitude tests on BS 4360 50D steel in air and seawater. UKOSRP Interim report 3/40, February 1979.

5.6 Irwin, G.R., Crack extension force for a part-through crack in a plate . *Journal of applied mechanics, ASME*, Vol.29, N0.4, 1962.

5.7 Green, A.E., Sneddon, I.N., The distribution of stress in the neighbourhood of a flat elliptical crack in an elastic solid. Proceedings , *Cambridge philosophical society*, Vol. 46, 1950.

5.8 Ritchie, D., Voermans, C.W.M. Stress intensity factors in an offshore tubular joint test specimens, Private communication 1986.

5.9 Newman, J.C., Raju, I.S., An Empirical Stress Intensity Factor Equation for the Surface Crack, *Engineering Fracture Mechanics*, Vol. 15, No. 1, 1981, pp 185-192.

5.10 Scott, P.M., Thorpe,T.W., A critical review of crack tip stress intensity factors for semi-elliptical cracks. *Fatigue of engineering materials and structures*, Vol 4, No. 4, 1981.

5.11 Holdbrook, S.J., Dover, W.D., The stress intensity factors for a deep surface crack in a finite plate. *Engineering fracture mechanics*, Vol. 12, 1979.

5.12 Dover, W.D., Connolly, M.P., Fatigue fracture mechanics analysis of tubular welded Y and K joints. *Int'l Conf. on Fatigue and Crack Growth in Offshore Structures*. IMech E London 1986.

5.13 Koterazawa, R., Minamisaka, S., Stress intensity factors of semi-elliptical surface cracks in bending. *J. Soc. Material Science,* Japan, Vol. 26, 1977.

5.14 Aaghaakouchak, A.A., Fatigue fracture mechanics analysis of ring-stiffened and simple tubular joints for offshore structures. PhD. Thesis Unversity of London 1989.

5.15 Niu, X., Glinka, G., Stress intensity factors for semi-elliptical surface cracks in welded joints. *Int'l J. of Fracture*, 1989 (To be published).

5.16 Bueckner, H.F., A Novel Principle for the Computation of Stress Intensity Factors, *Zeitschrift fur Angewandte Mathematik und Mechanik,* 50, 1970, pp 529-546.

5.17 Rice, J.R., Some remarks on elastic crack tip stress fields. *Int'l J. of solid structures,* Vol. 8, 1972.

5.18 Niu, X., Glinka, G., Weight functions for edge and surface semi-elliptical cracks in flat plates and plates with corners. *Engineering Fracture Mechanics*. 1989 (To be published).

5.19 Petroski, H.J, Achenbach, J.D., Computation of the weight function from a stress intensity factor. *Engineering Fracture Mechanics,* Vol. 10, N0. 2, 1978, pp. 257-266.

5.20 Niu, X., User manuel, Module NGWFUNC, version 1.0 UCL NDE Centre, 1989.

5.21 Dharmavasan, S., Fatigue fracture mechanics analysis of tubular Y-joints. PhD. Thesis, University of London, 1983.

5.22 Dover, W.D., Niu, X., Aaghaakouchak, A.A., Kare, R.F., Topp, D.A., Fatigue crack growthin X joints and multi-brace nodes. *Fatigue of Offshore Structures. Int'l Conf. Engineering Integrity Society*. London 1988.

5.23 Aaghaakouchak, A.A., Glinka, G., Dharmavasan, S., A load shedding model foe fracture mechanics analysis of fatigue cracks in tubular joints. *OMAE 89 Conference*, The Hague, Netherlands. 1989.

5.24 Fatigue data base. University College London. Mech. Eng. Dept. Torrington Place London WC1 E 7JE.

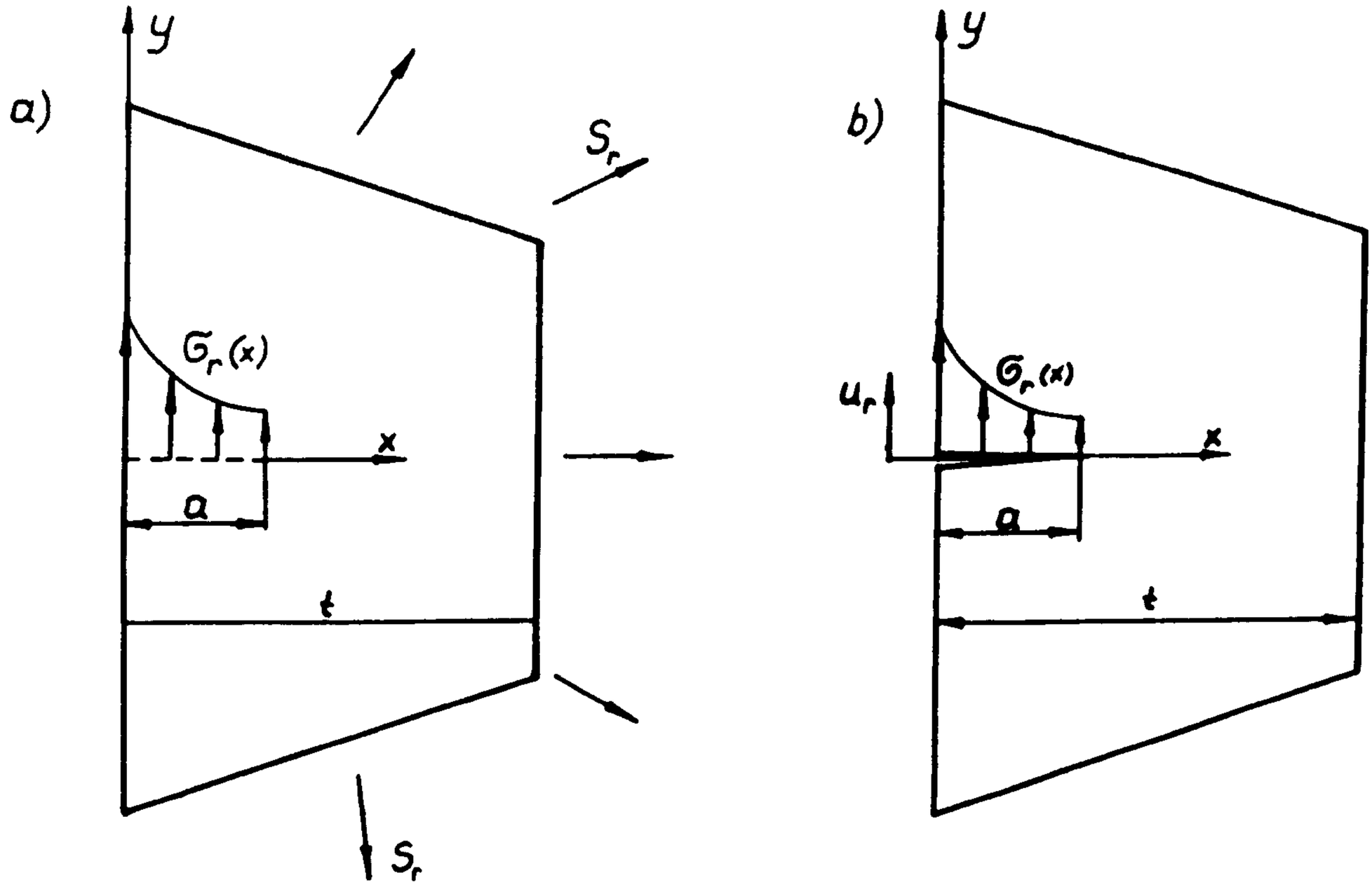

Figure 5.1 Stress system $S_r \sigma_r(x)$ and displacement U_r necessary for the derivation of the weight function $m(x,a)$

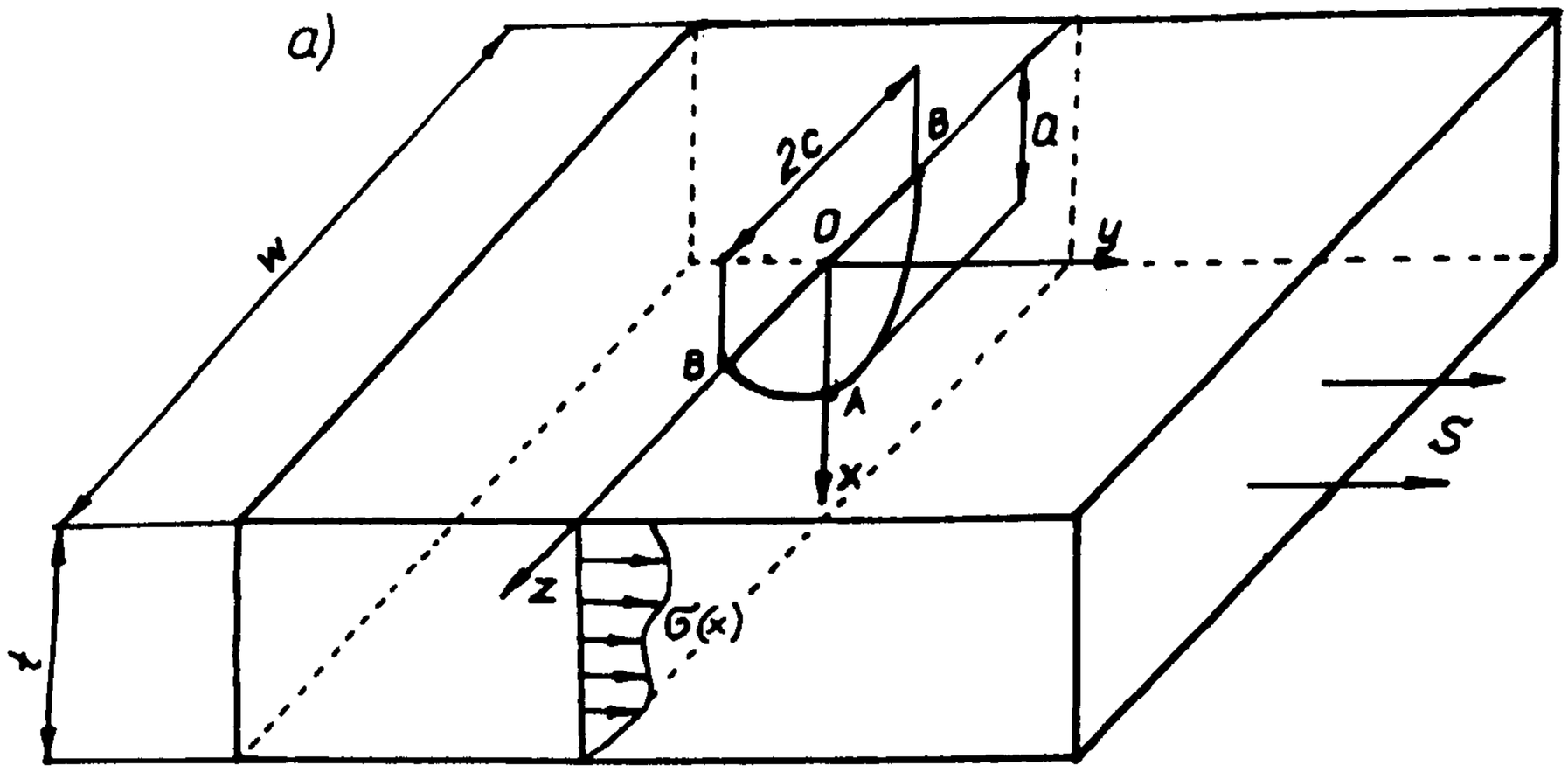

Figure 5.2 Surface semi-elliptical crack in a finite thickness flat plate.

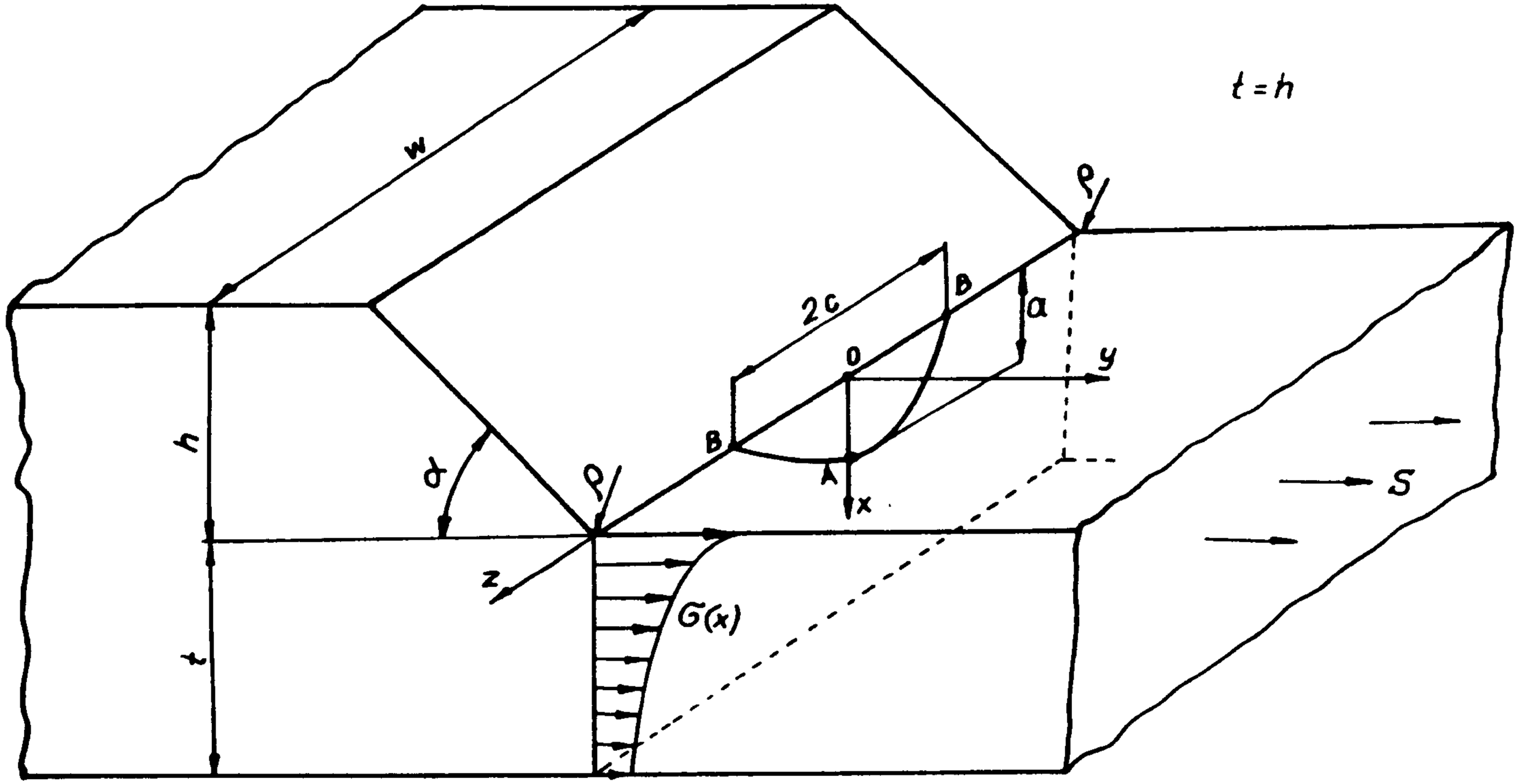

Figure 5.3 Crack emenating from a corner in a finite thickness plate

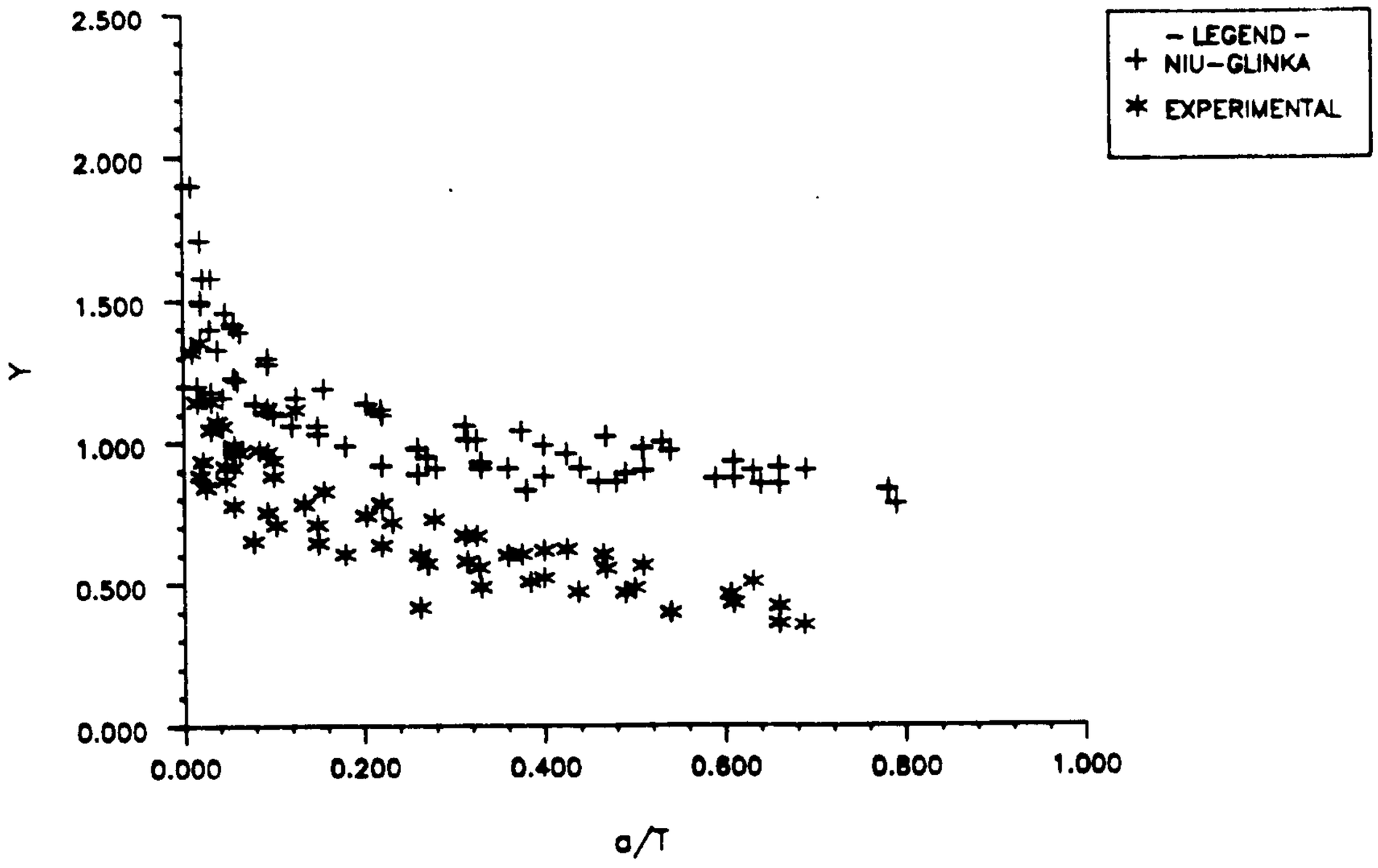

FIGURE 5.4 Y – CALIBRATION FACTORS. PROFILE C1

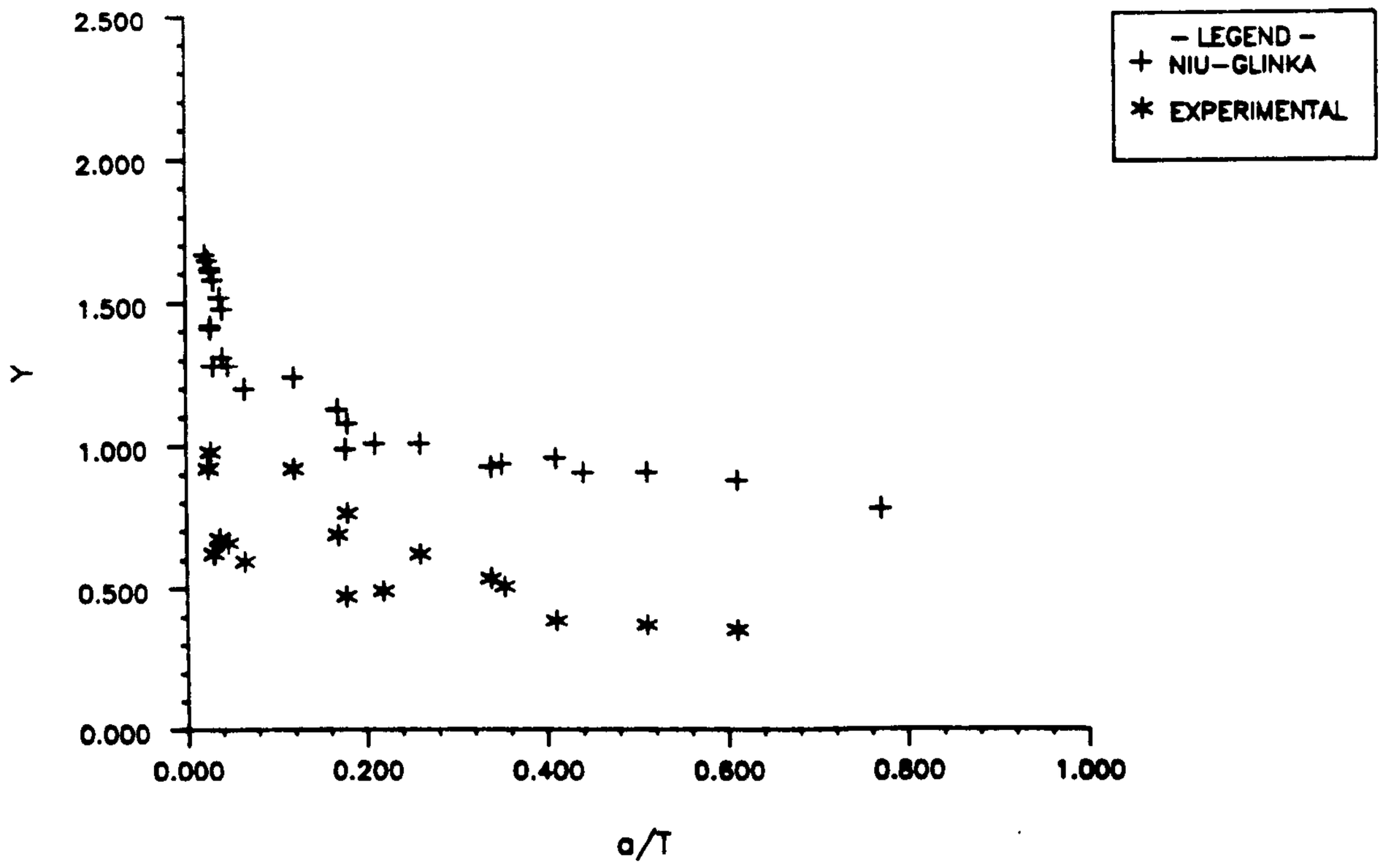

FIGURE 5.5 Y – CALIBRATION FACTORS. PROFILE C2

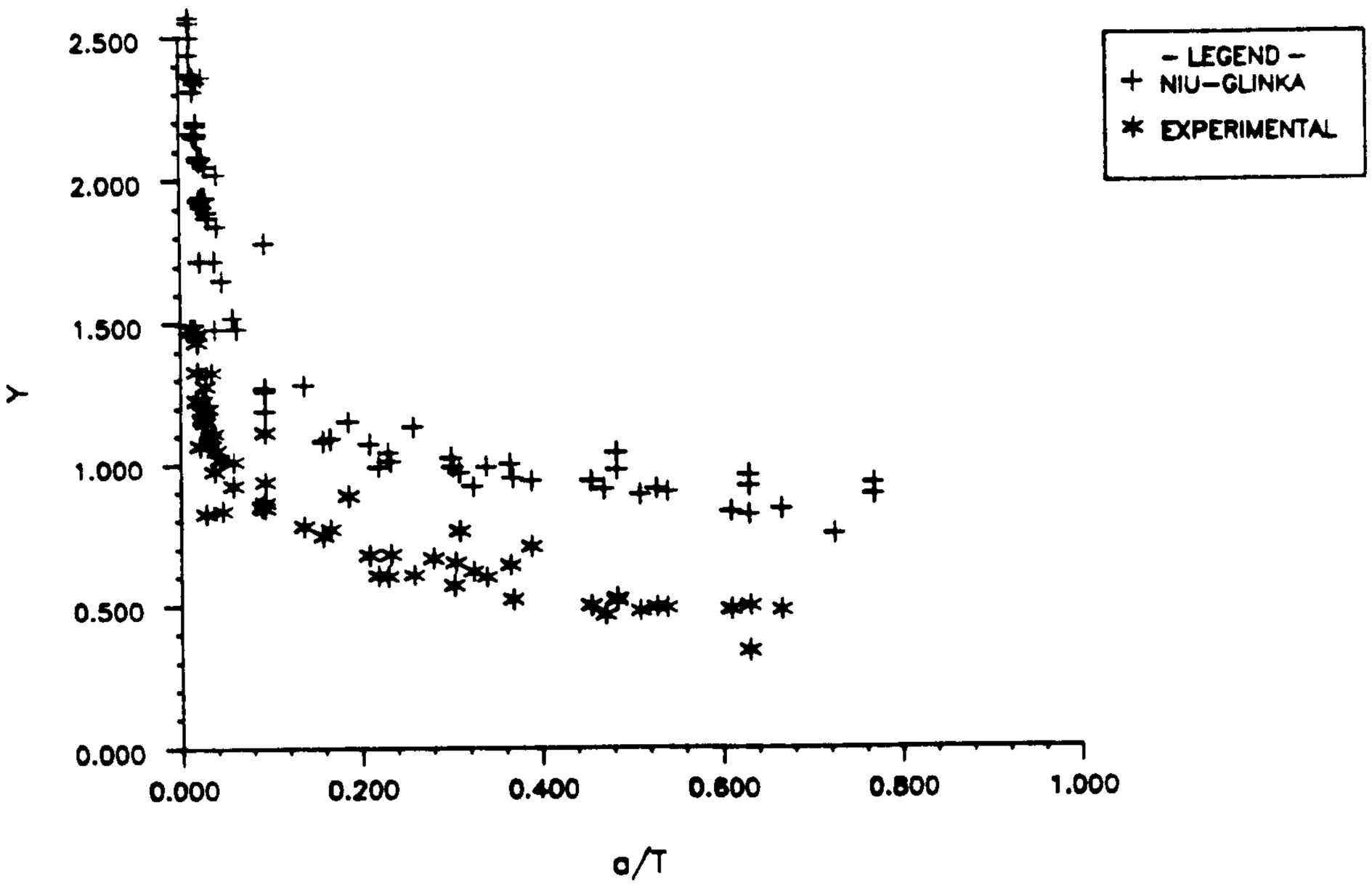

FIGURE 5.6 Y – CALIBRATION FACTORS. PROFILE A

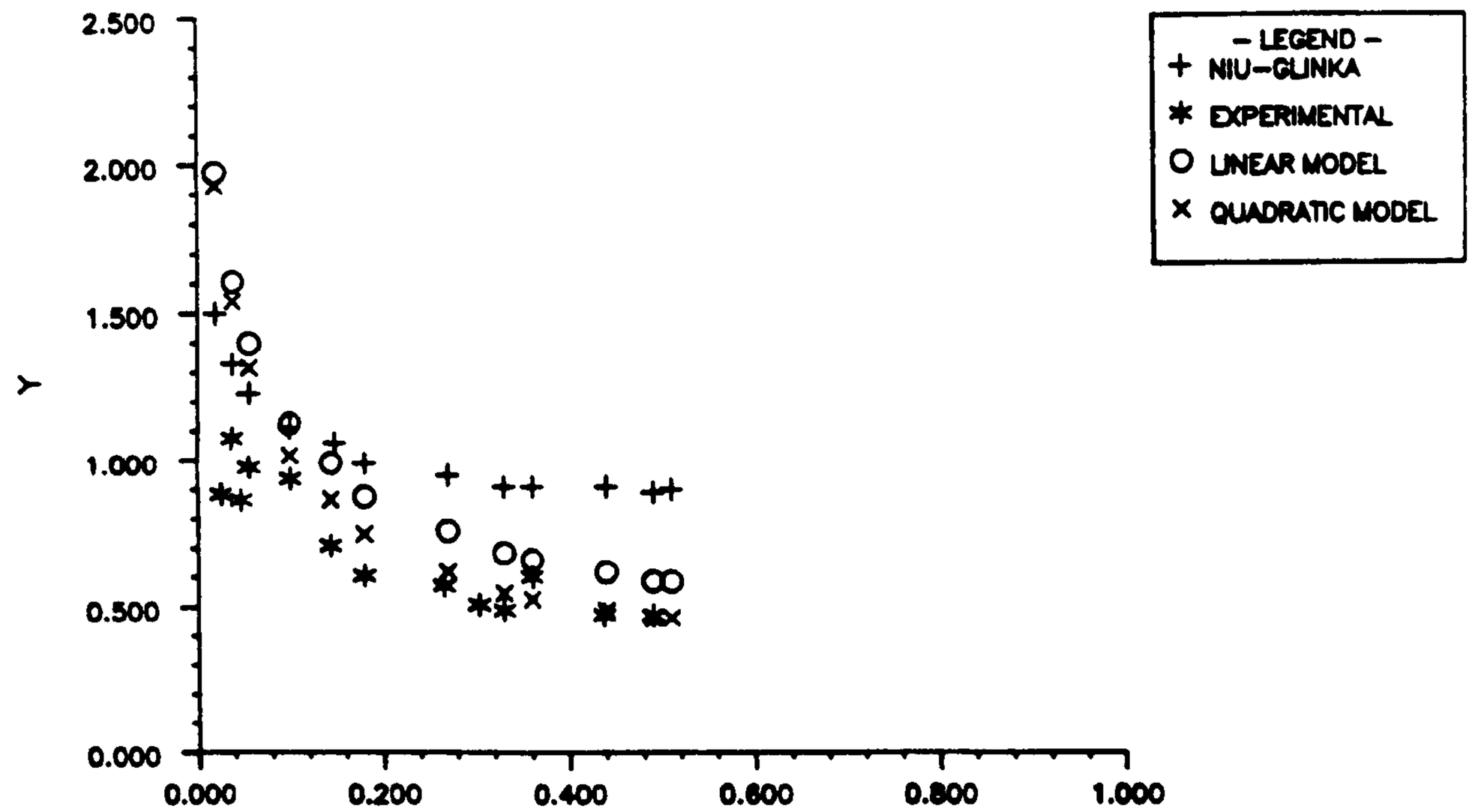

FIGURE 5.7 Y – CALIBRATION FACTORS. C1–A–1–X

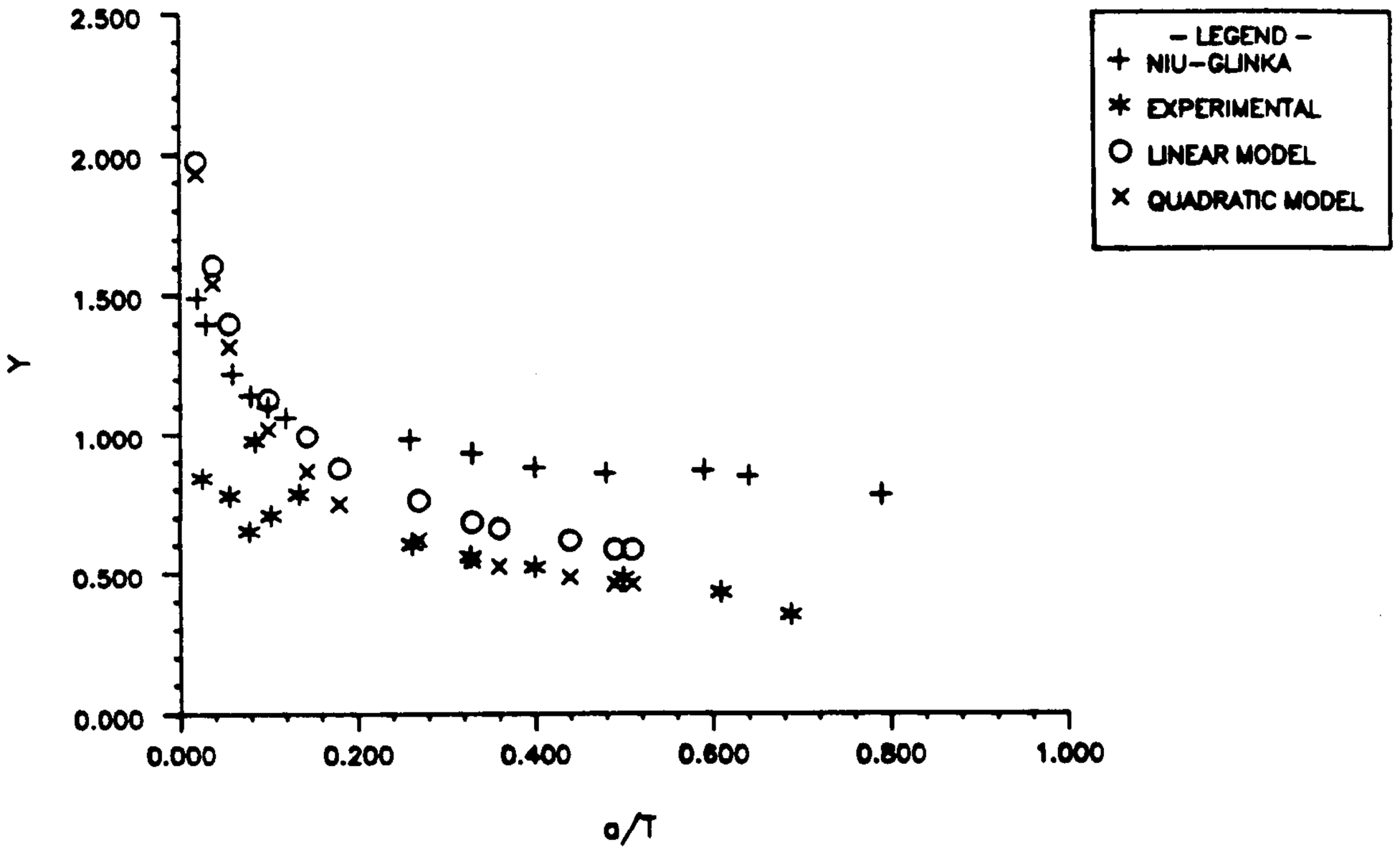

FIGURE 5.8 Y – CALIBRATION FACTORS. C1–B–1–X

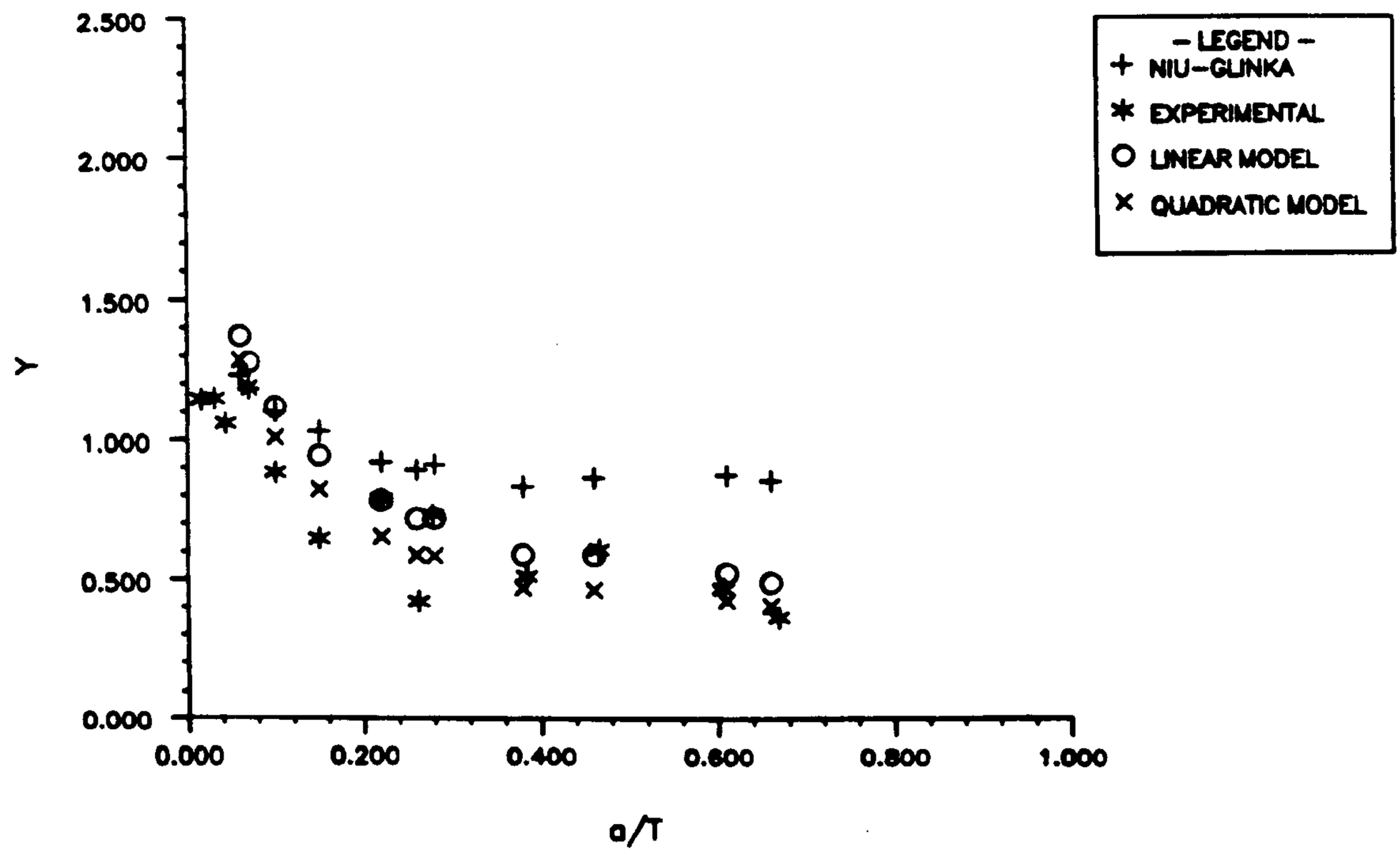

FIGURE 5.9 Y – CALIBRATION FACTORS. C1–D–1–X

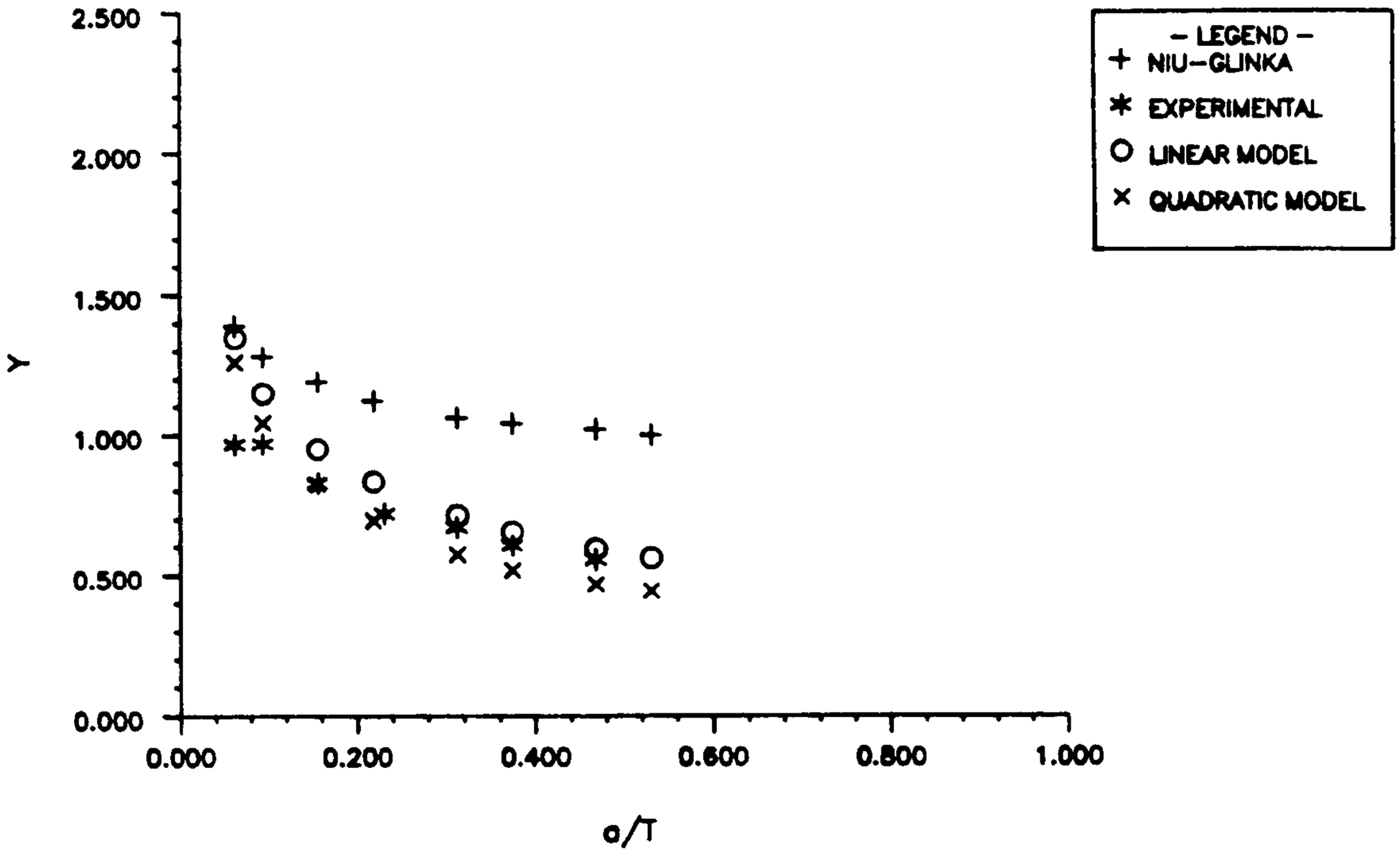

FIGURE 5.10 Y – CALIBRATION FACTORS. C1–A–2–X

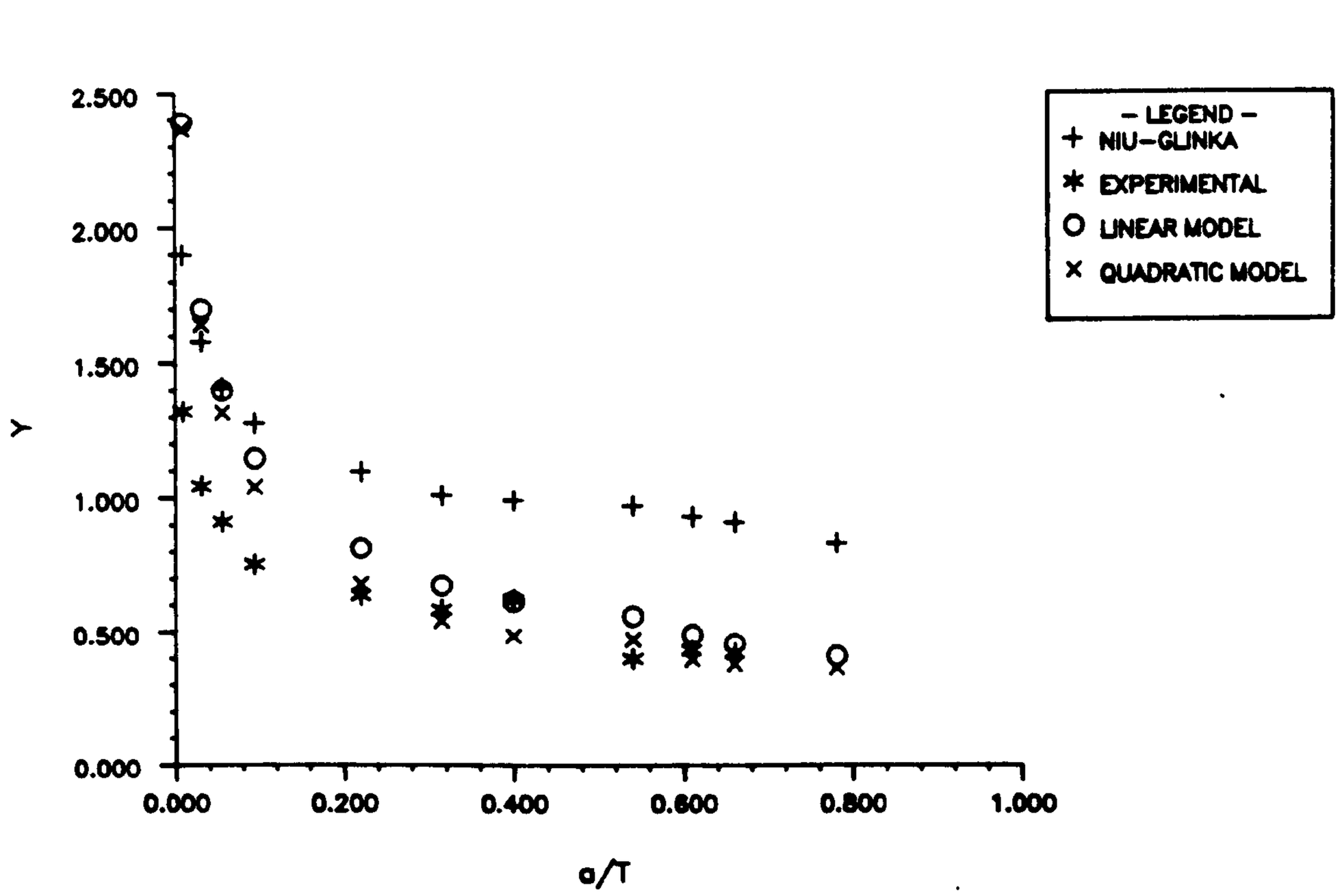

FIGURE 5.11 Y – CALIBRATION FACTORS. C1–B–2–X

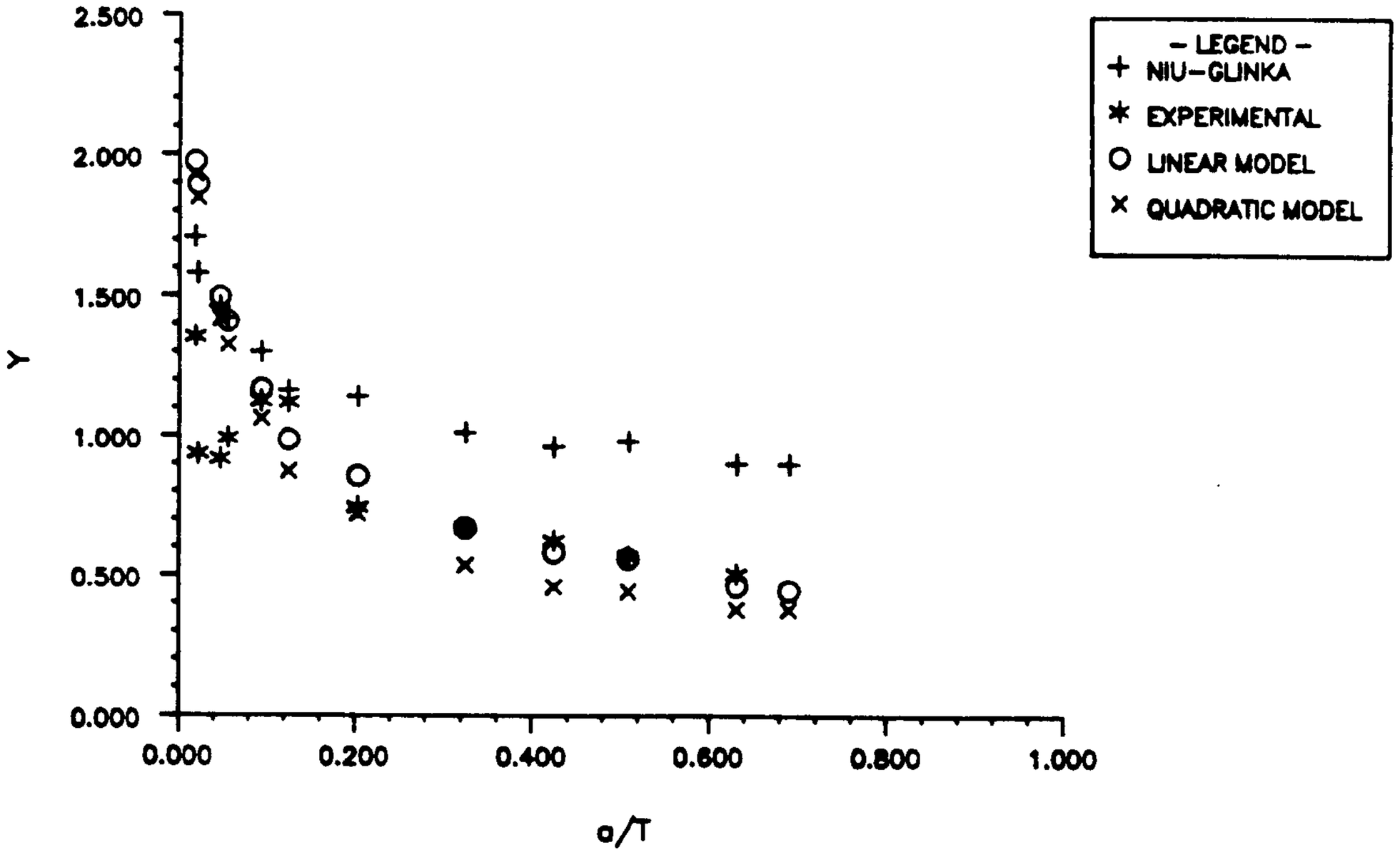

FIGURE 5.12 Y – CALIBRATION FACTORS. C1–D–2–X

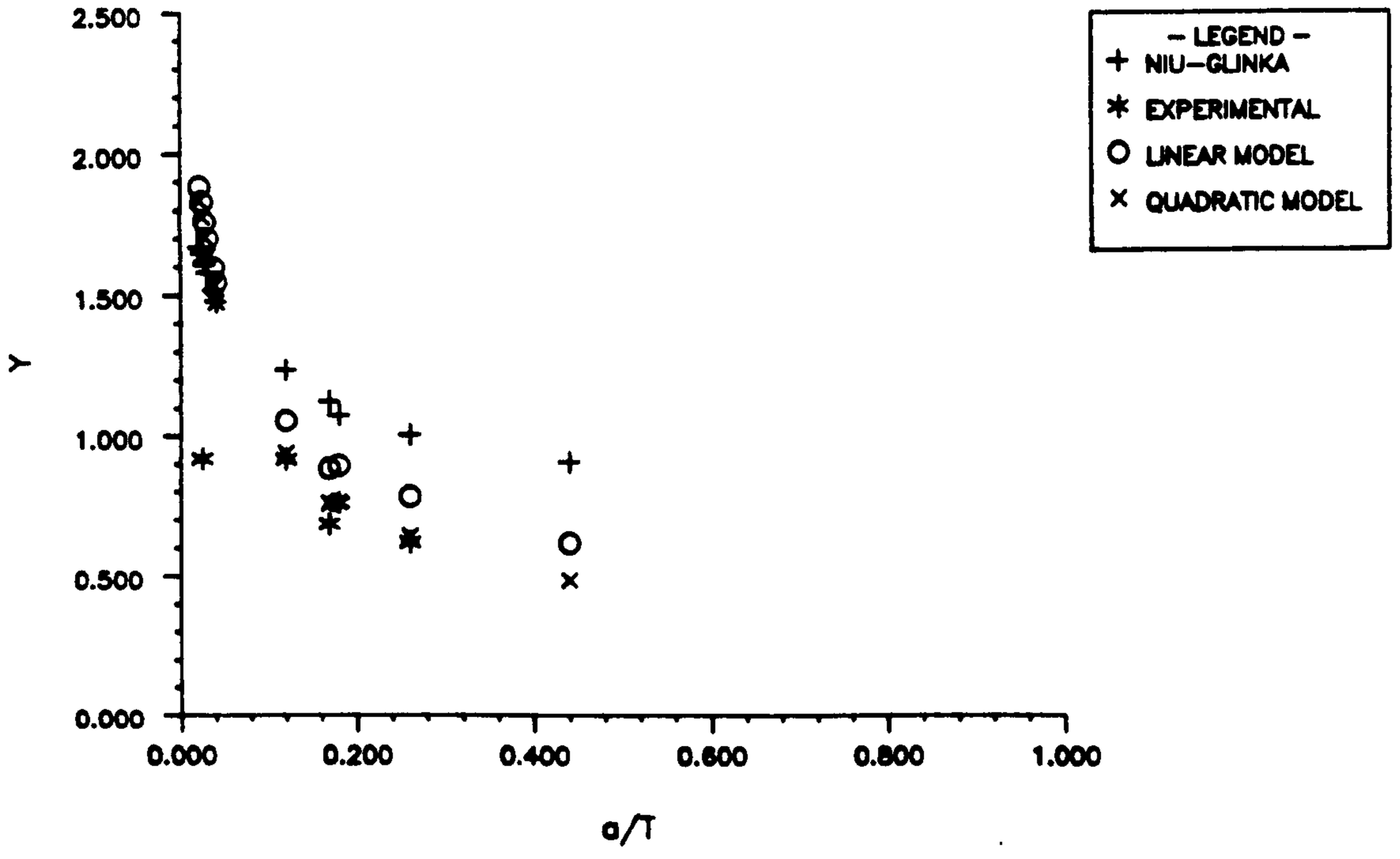

FIGURE 5.13 Y – CALIBRATION FACTORS. C2–A–Y

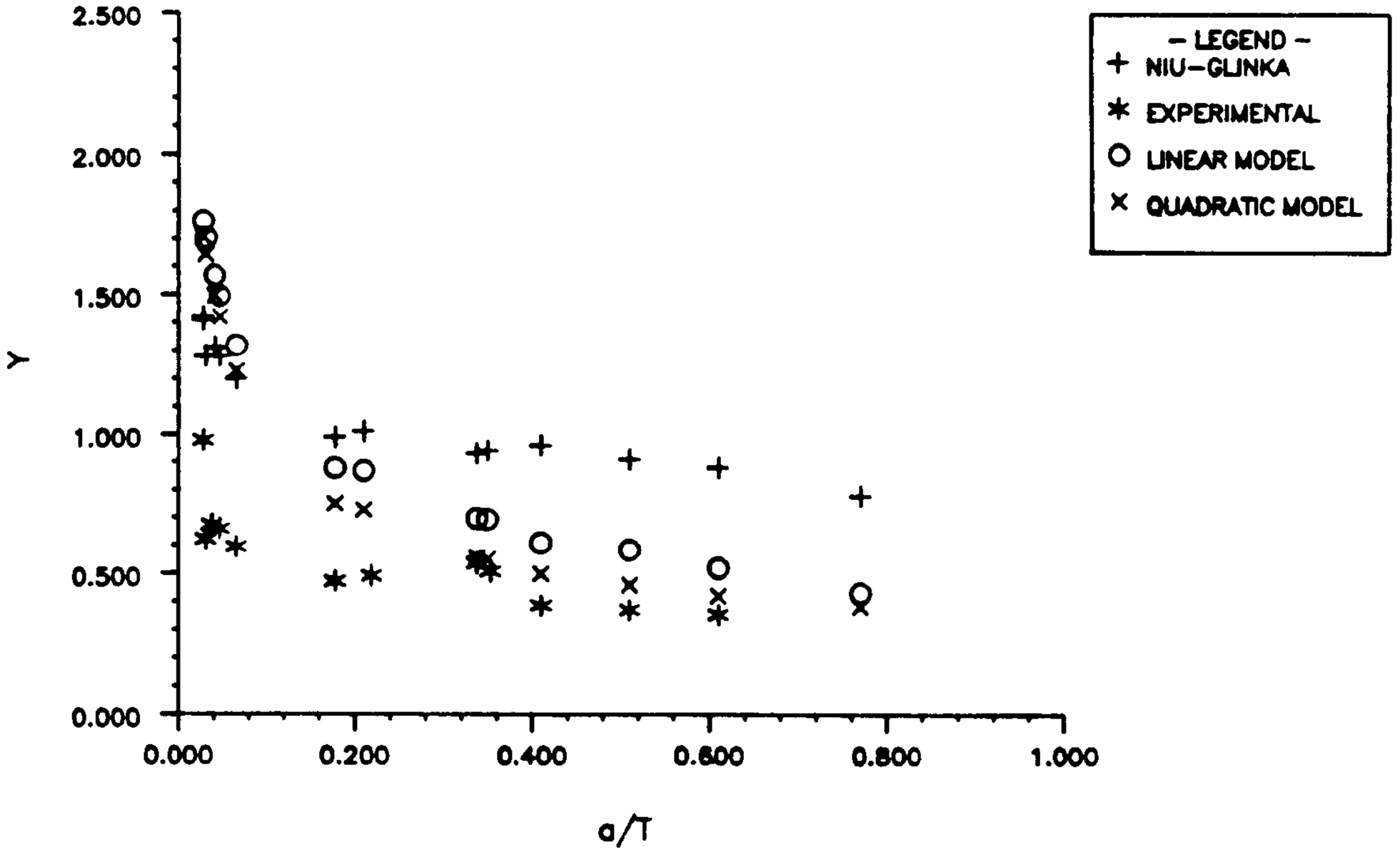

FIGURE 5.14 Y – CALIBRATION FACTORS. C2–B–Y

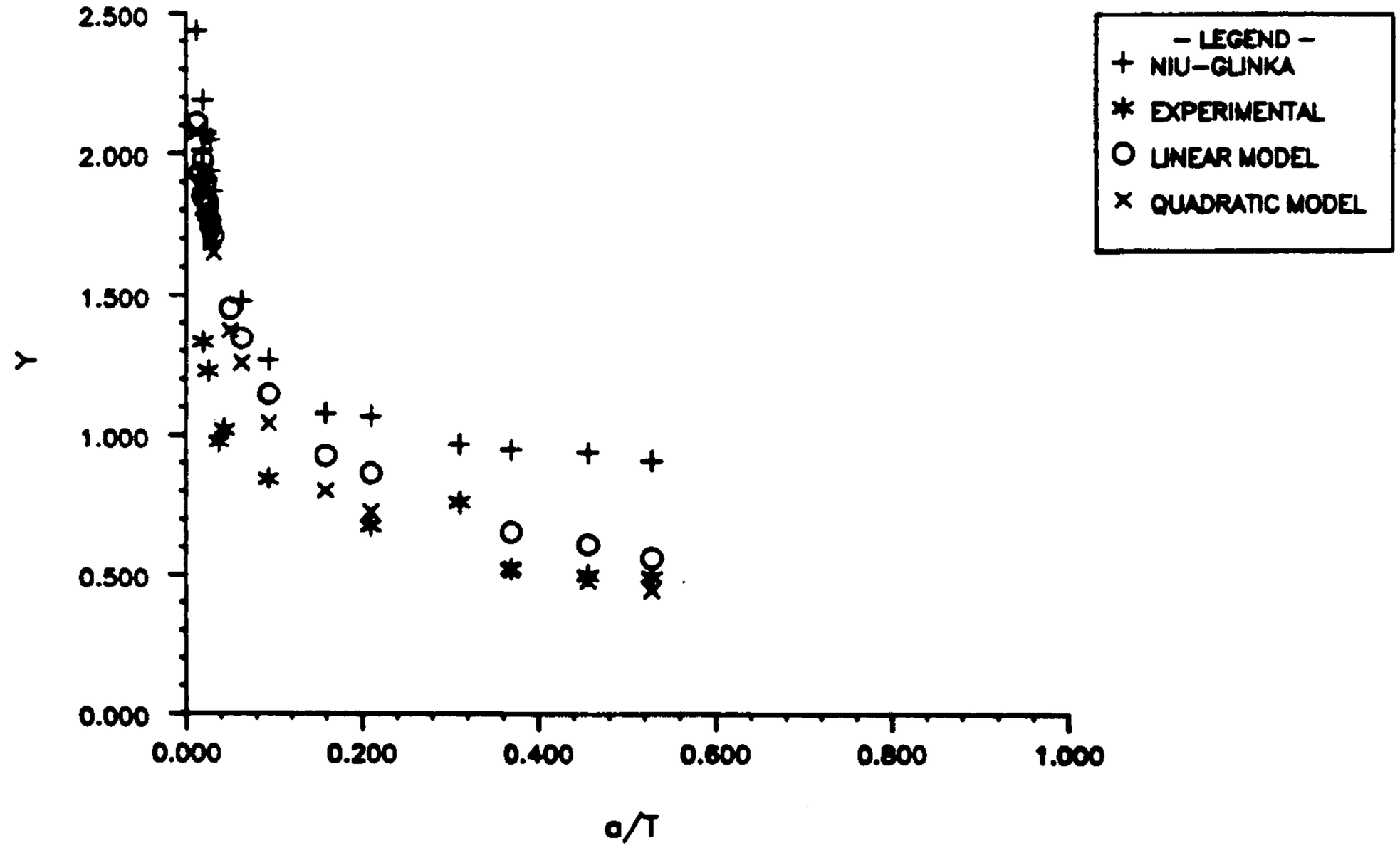

FIGURE 5.15 Y – CALIBRATION FACTORS. A–A–Y

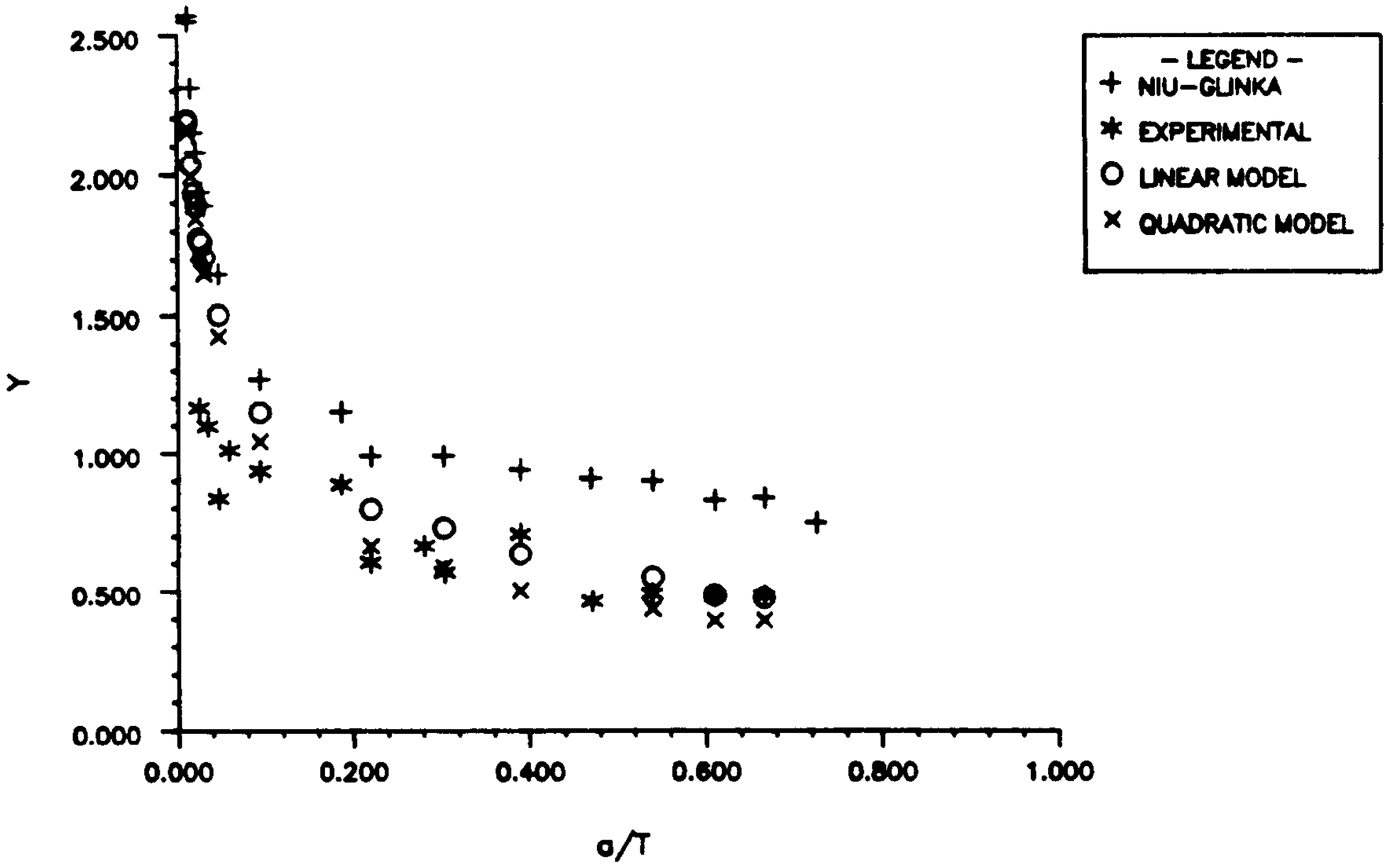

FIGURE 5.16 Y – CALIBRATION FACTORS. A–B–Y

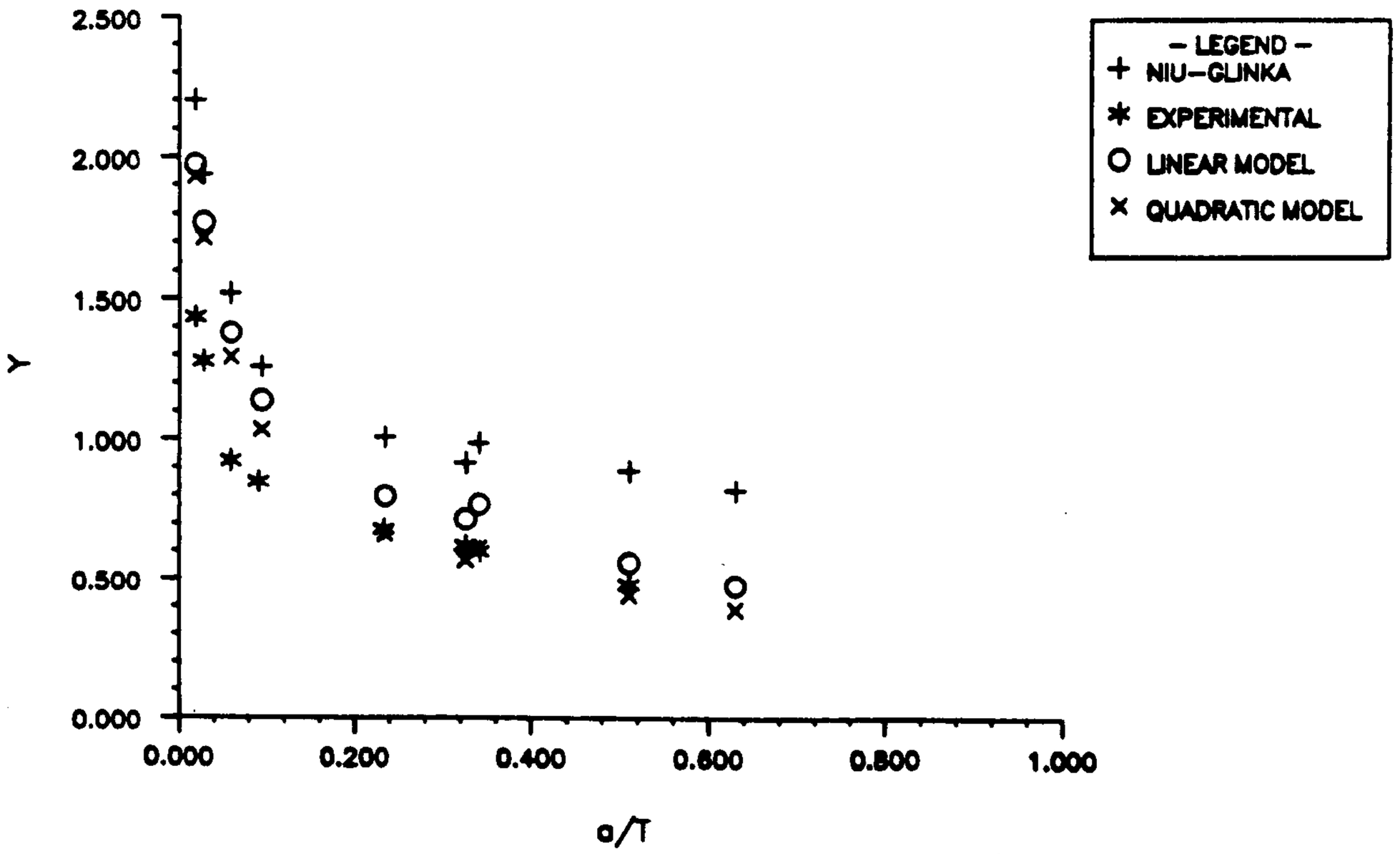

FIGURE 5.17 Y – CALIBRATION FACTORS. A–D–Y

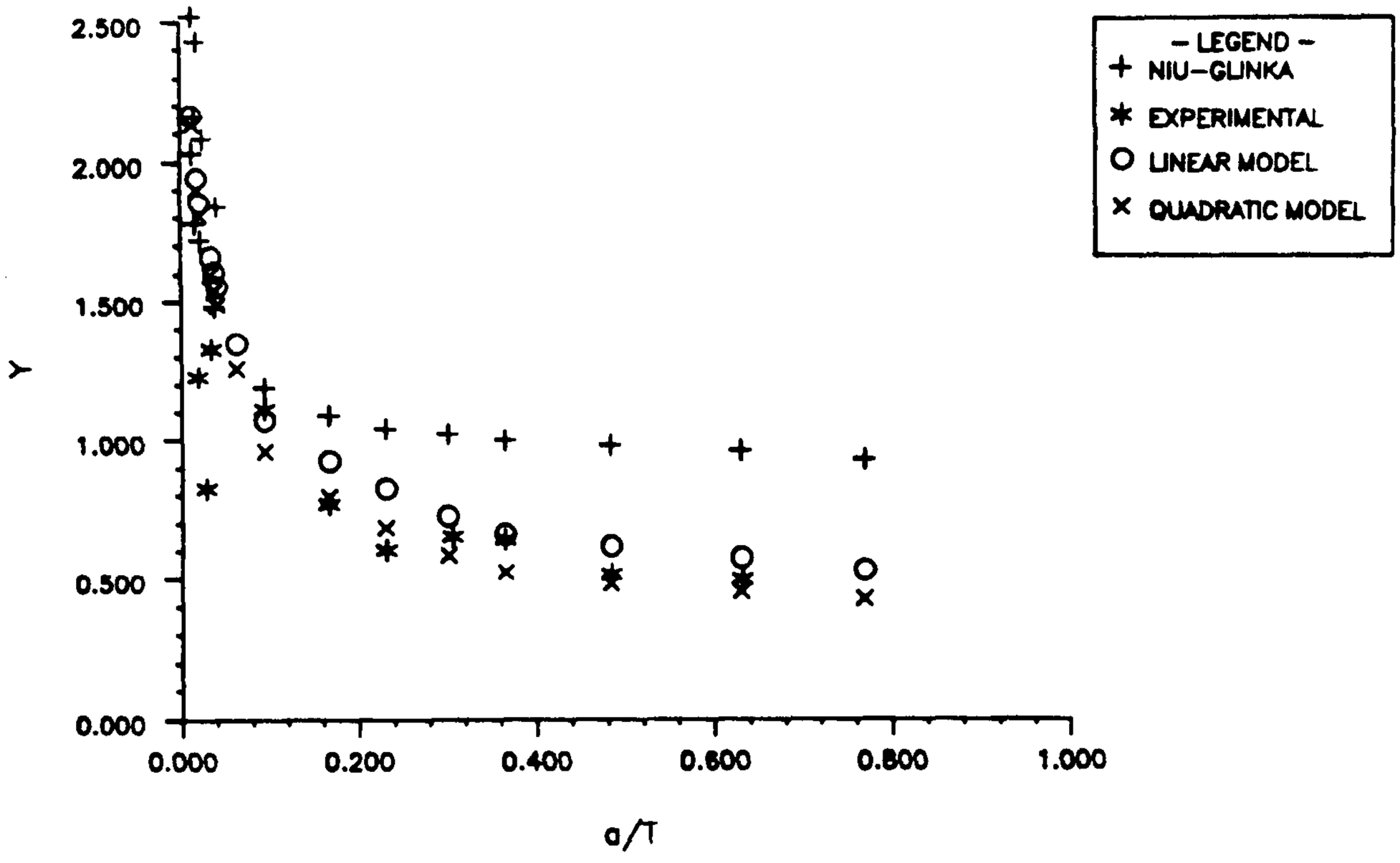

FIGURE 5.18 Y – CALIBRATION FACTORS. A–B–Z

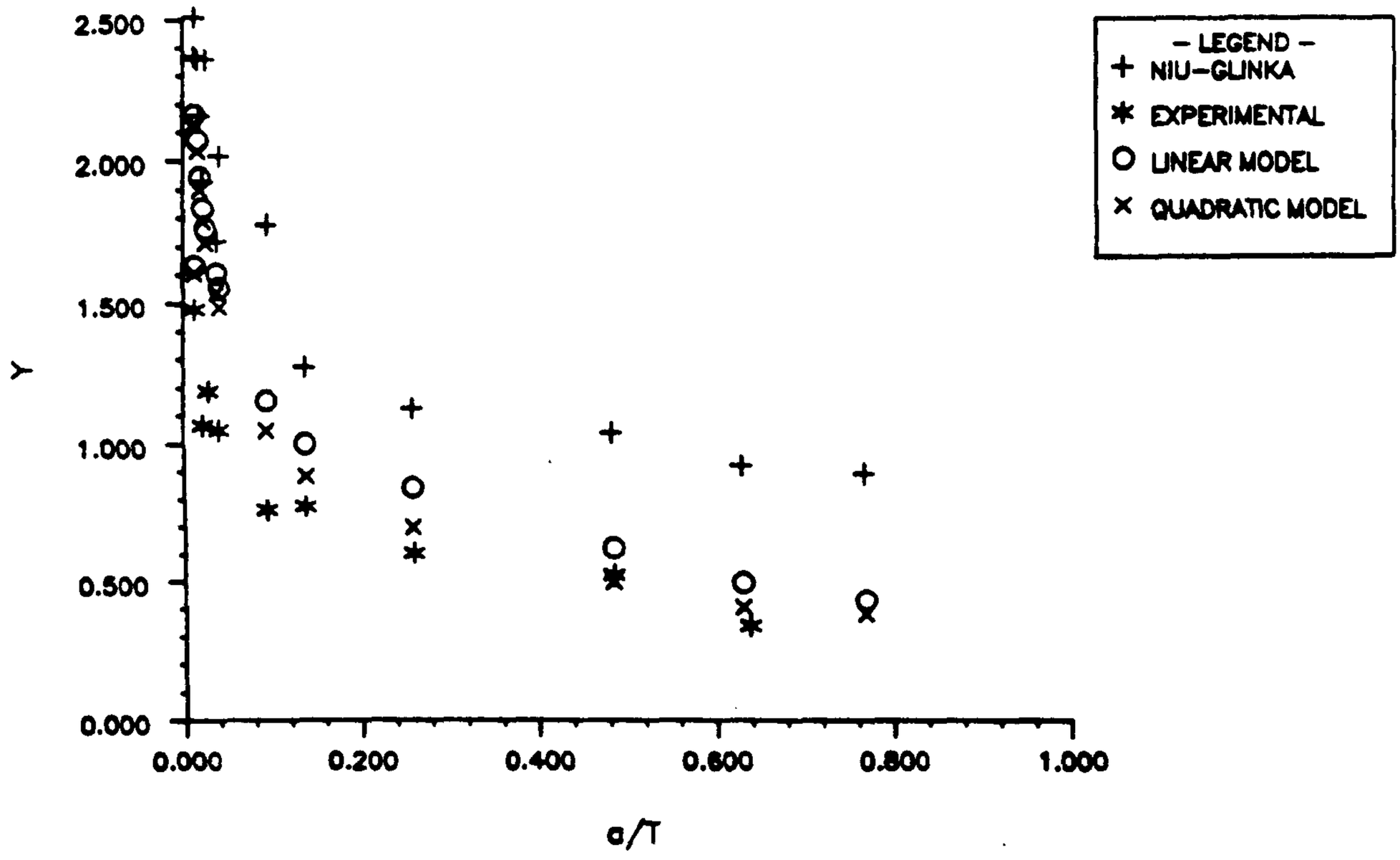

FIGURE 5.19 Y – CALIBRATION FACTORS. A–D–Z

6 CHAPTER SIX

FATIGUE LIFE PREDICTION OF TUBULAR JOINTS

6.1 Scope of chapter

To calculate the predicted total fatigue life of the tubular joints and compare the results with the experimental data obtained for the thirteen chord cracks. This will involve calculating the number of cycles to crack initiation and the number of cycles for the crack to propagate through the chord wall thickness. The two techniques used were:

i) The local strain approach to predict the number of cycles to initiation.

ii) Linear elastic fracture mechanics to calculate the crack propagation part of life.

6.2 The local strain approach

The aim of the local strain approach is to predict the number of loading cycles necessary to initiate a crack in a component. Unfortunately at present there is no clear definition of initiation i.e. a specific crack size which determines that initiation has occurred. Consequently the fraction of life taken up by initiation depends on the criterion used.

If a component does not contain an initial crack or sharp crack-like defect at the beginning of its life, the most likely place for it to start is in the most highly stressed notch root. In steel welded tubular structures the weld toe notch area is the site of potential crack initiation. The basis of the predictive technique is the postulation that the fatigue behaviour of a notch can be approximated by a small plain specimen subjected to the same stress-strain history as the notch-tip. Specifically, the number of loading cycles to crack initiation in the notch-tip is expected to be equal to that in the plain specimen if crack initiation is defined in both as a common small crack size and both experience the same stress strain history.

Components are generally designed so that when subjected to cyclic loading, general yielding does not occur. The deflections of the component are therefore related to the applied load in a linear elastic manner. However, because of the stress raising

effect of any notch in the component, localised plastic straining may occur at these sites. This results in the local strains in the notch-tip not being linearly related to the applied load.

The local strain approach to fatigue life prediction consists of three principal stages. Firstly, the local notch stress and strain histories must be determined for given load or nominal stress histories. Secondly, a cycle counting procedure has to be employed, and thirdly, fatigue damage must be calculated. The elements of the local strain approach were briefly presented in chapter one, further discussion on the subject can be obtained in references [6.1 & 6.2].

The initiation criterion used for this study is based on crack depth i.e. initiation is said to have occured when a crack of 0.5mm depth has been detected.

6.2.1 Fatigue initiation life calculations

The input data required for the complete initiation life calculation are as follows:

i) material cyclic stress-strain curve σ - ε

ii) material fatigue characteristics given by the Manson-Coffin strain-life curve [6.3].

iii) nominal stress history - S

iv) stress concentration factor - K_t

Table 6.1 shows a list of the fatigue data used for calculating initiation life for BS4360 50D steel, the material used for fabrication of the tubular joints. Using this data it is possible to determine the local notch-tip strain-stress history due to a given nominal load or stress variation.

The main steps of the fatigue initiation life calculation procedure are listed below:

a) determine loading/nominal stress history P or S

b) determine notch-tip elastic stress based on the elastic stress concentration factor

$$\sigma = S_t K_t$$

c) determine the corresponding notch-tip elastic-plastic stress-strain histories using:

- material cyclic properties
- material memory model
- Neuber's rule or equivalent strain energy density concept

d) identify closed stress-strain loops and calculate strain range $\Delta\varepsilon$ and mean stress σ_m for each loop

e) calculate fatigue damage associated with each stress-strain loop - D_i

f) calculate total fatigue damage caused by given load/nominal stress history $D = \Sigma D_i$

g) calculate fatigue life - $N_f = 1/D$

The procedure described above has been incorporated into a Fortran IV computer program known as TLIFE which is written to run on a DEC PDP/11 computer. Both constant amplitude and random loading can be input as nominal stress or load histories. The solution of Neuber's rule and the energy density method is based on an approximation of the material cyclic stress-strain curve to a series of straight lines [6.4].

Newport [6.5] demonstrated that the equivalent strain energy density concept gave more accurate notch-tip stress-strain predictions than Neuber's rule [6.6] and thus the energy density concept will be used for this work. Also in considering the fact that multi-axial stress field exists at the notch-tip the analysis was therefore conducted under plane strain conditions. In the case of the stress concentration factors the calculations were not based on the therotical stress concentration factors at the notch-tip but instead on values of strain measured at the weld toe using the small single element gauges, gauge length 0.3mm, described and reported in chapter 3.

The values calculated using TLIFE program will be compared with the number of cycles to initiate a crack of 0.5mm deep in the chord wall of the tubular joints in the following section.

6.2.2 Comparison of predicted and calculated number of cycles to crack initiation

Predictions of fatigue crack initiation lives were made using the local strain approach for the tubular joints tested in this study. The hot spot stress ranges to which the tubular joints were subjected are listed in Table 4.3. Cyclic and fatigue properties of BS 4360 50D steel are listed in Table 6.1.

Experimental values of crack initiation for the thirteen chord cracks were obtained either directly from experimental fatigue data or by extrapolating the curve of crack depth versus number of cycles (Figures 4.3, 4.5, 4.7 & 4.9) back to 0.5mm crack depth as this is the criterion used to define the onset of crack initiation for this study.

6.2.2.1 Profile C1

The four braces manufactured to profile C1 produced six fatigue cracks at the weld toe chordside of the tubular joint. Test one i.e. all C1-1-X saddle positions were tested at relatively high values of hot spot stress range (368.7-423.6 MPa) and would therefore be expected to show the lowest number of cycles to initiation. A comparison of the theoretical and experimental values of N_1 shown in Figure 6.1 show good agreement for saddle position A but a conservative estimate, by a factor of 2 and 6, for positions B and D respectively.

Test two C1-2-X also shown in Figure 6.1 exhibits a larger amount of scatter between the two sets of values. The local strain approach predicts a higher number of cycles for sadddle positions A and B by a factor of 3.5 and 1.8 respectively whereas position D an underestimate of N_1 value by a factor of 4.4 is evident.

6.2.2.2 Profile C2

Two fatigue chord cracks are reported for profile C2. The hot spot stress range for these two cracks were 161.3 and 185.3 MPa. Figure 6.2 shows the two sets of data of N_1 values. The theoretical method produced a small underprediction in number of cycles to initiation for saddle position B and an equally small

overprediction for position A. An average of the two sets of values produces remarkable agreement between the local strain method and experimental results.

6.2.2.3 Profile A

Five chord cracks were produced from the braces fabricated using profile A welding procedure. The hot spot stress ranges used were 159.4-204.6 MPa. For two of the five cracks, shown in Figure 6.3, the theoretical method produced good agreement between the two N_1 values i.e. for positions A-B-Y and A-D-Z. However, the other three cracks sgnificant differences are apparent. The local strain approach underpredicts the number of cycles to initiation by a factor ranging from 4.8 times to 14.4 times of the actual experimental values.

6.2.2.4 Discussion

In attempting to validate the local strain approach using the available experimental data the thirteen chord cracks shown in Figure 6.4, appear to have produced conflicting signals as to the reasons behind the differences in predicted and experimental N_1 values. The large degree of underprediction shown for some cracks of profile A cannot be attributed to the method of measuring the stress concentration at the weld toe. The technique used was the same for all cracks. It would appear from the results that the degree of agreement was dependent on the type of weld profile investigated.

Consider the two controlled weld profiles C1 and C2. Profile C2 produced the best agreement between experimental and theoretical values. C1 on the whole could be considered to have produced reasonable comparison of results and accurately predicted the measured trend in crack initiation life. The major discrepencies however, appear when comparing the results of profile A with the theoretically predicted N_1 values.

The differences in results can probably be attributed to the different geometric parameters of the two weld profiles. It was shown in chapter 3 that for profile A the most frequent weld toe radius value was significantly smaller than the equivalent radius value for either C1 or C2. This would lead to profile A having a potentially larger number of crack initiation sites. These observations were

subsequently confirmed in chapter 4. Therefore, the existence of a number of crack initiation sites could have led to possible crack interaction and thus resulted in higher N_1 values.

A further factor regarding possible inaccuracies is that the experimental value of stress concentration used in the therotical calculation may not be the actual value of SCF that corresponds to the site of where initiation occurrs. This could have occured because the brace/chord intersection was not fully strain gauged.

It is arguable whether such a predictive technique which relies on fatigue data obtained from testing smooth specimens can be justifiably applied to tubular joints which are of complex geometry and the potential crack initiation site occurs in regions of complex stress fields. In order to use the local strain approach the relation between the stress-strain range has to be accurately established. The energy density equation or Neuber's rule are usually used. However, it should be noted that this relation between stress-strain range has only been validated and applied for a limited number of cases e.g. smooth specimens. In the case of tubular joints these are complex structures and the stress-strain range can be affected by a number of different factors. It is possible that this approach may not be capable of accounting for such complex geometries such as tubular joints and therefore would not provide an accurate relation for the stress-strain range.

It is also felt that a more accurate relation for the material properties could be developed specifically for tubular joints. Finally a more comprehensive validation process would be required before this technique could be reasonably applied to tubular joint fatigue life assessment.

6.3 Fracture mechanics model to predict fatigue crack propagation for tubular joints

In this section the second part of the process to calculate the total fatigue life of the tubular joints studied is presented. This is the technique based on fracture mechanics analysis. It attempts to predict the number of cycles required to grow a crack from an initial depth of $a_i = 0.5$mm to a final depth $a_f = 32.0$mm. These values are then compared with the fatigue data reported in chapter 4.

The methodology of the fracture mechanics model used in this thesis is based on the Paris equation [5.2] in conjunction with the stress intensity factor range calculated using the Niu-Glinka weight function. The following are required for the proposed model.

1) Derive an equation that describes the changes in crack aspect ratio as a function of the non-dimensional crack depth for each of the three weld profiles investigated based on the experimental fatigue data.

2) Calculate the stress intensity factor in conjuction with the linear and quadratic moment release models.

3) Integrate the Paris equation,equation 6.1 shown below,between limits. The number of cycles taken for the crack to grow from an initial depth of 0.5mm to a final depth of 32.0mm can be determined.

$$N = \frac{1}{C} \int_{a_i}^{a_f} \frac{da}{(\Delta K)^m} \qquad 6.1$$

6.3.1 Curve fitting for a/c versus a/T

The Niu-Glinka weight function was derived for a semi-elliptical surface crack in a finite thickness plate with an angular corner α. It only calculates the stress intensity factor for the deepest point of the crack when the crack geometry is known. However, the stress intensity factor is influenced by the crack geometry. Therefore changes in crack shape need to be described in order to continue to calculte the stress intensity factor for increasing crack depth. Consequently the crack aspect ratio changes as a function of crack depth are required as input data in order to use the Niu-Glinka weight function. This can be achieved by establishing the required relation based on available experimental data.

The experimental data points for crack aspect ratio changes as a function of crack depth for each of the three weld profiles studied were used along with an existing Fortran program available on the micro VAX II and linked to the NAG library to achieve the best fitting curve through the data points. The NAG routine is a curve fitting program which provides the best fitting curve using the Chebyshev approximation [6.7]. The coefficients of the polynomials are derived using the least squares method. The process was based on trial and error and required

engineering judgement to choose the curve that describes the changes in a/c versus a/T most accurately. The general form of the Chebyshev polynomial is given below:

$$f(x) = \sum_{k=1}^{N} C_k T_{k-1}(x) - \frac{1}{2} c_1 \qquad 6.2$$

The expressions for T_k are given as follows:

$$T_0(x) = 1$$

$$T_1(x) = x$$

$$T_2(x) = 2x^2 - 1$$

$$T_3(x) = 4x^3 - 3x$$

$$T_4(x) = 8x^4 - 8x^2 + 1$$

$$T_{n+1}(x) = 2xT_n(x) - T_{n-1}(x) n >= 1$$

The above equations and expressions were used for both profiles C1 and C2. However, for profile A the differences in crack aspect ratio changes in the early part of the crack growth meant that a modified version of the above was used i.e. the variable x in the expressions for T_k were replaced by $(x)^{0.5}$. This modification was required in order to be able to accurately fit the sharp decay in a/c exhibited in the early part of crack growth. For established crack growth the expressions were the same as those for profiles C1 and C2. The coefficients for T_k are given in Table 6.2.

Figure 6.5 is the fatigue data for a/c versus a/T for the six chord cracks produced for the braces fabricated with profile C1.

Figure 6.6 shows the fatigue data for profile C2 and the best fit curve for the crack aspect ratio changes as a function of crack depth. This curve and that shown in Figure 6.6 for profile C1 are similar in shape in particular for a/T > 0.4. The geometric parameters of the weld profiles are essentially the same and it would be expected that the behaviour exhibited in these two Figures to be very similar.

Figure 6.7 shows the changes in fatigue crack behaviour in terms of a/c and a/T for profile A. The early part of crack growth is characterised by higher aspect ratios than for either profile C1 or C2. This initially high value of a/c decreases sharply for small inceases in a/T. The initial drop in a/c is followed by a gradual increase as the crack grows deeper through the chord wall. This part of the curve is of similar trend to that observed for the two controlled weld profiles C1 and C2. In order to achieve this shape curve the analyses was split in two parts as described above.

6.3.2 Calculation of SIF incorporating the moment release models

The fracture mechanics model proposed here calculates one set of disribution of geometric stress intensity calibration factor Y for each of the three weld profiles C1, C2 and A. The calculation of these analtyical Y values is conducted using the Niu-Glinka weight function which requires as input data the following:

i) Stress distributions for T-butt welded joints for tension and pure bending calculated for 30° and 45° weld angles. These distributions should be normalised with the hot spot stress value.

ii) Initial value of bending to tension ratio.

iii) Details of weld geometry.

iv) Details of the linear and quadratic moment release models.

The distribution of geometric stress intensity calibration factor Y as a function of the non-dimensional crack depth a/T was calculated analytically for each of the three weld profiles studied. Figures 6.8-6.10 show the distributions for the three weld profiles. Each figure shows the Y values calculated from the fatigue data with two curves superimposed on top of the experimental data. These curves represent the analytical Y values which include the moment release models. The linear load shedding model appears to constantly predict higher values for all three profiles as compared to the quadratic load shedding model. Both sets of the analytically predicted Y values are used to calculate the SIFs for each test conducted. The results of the two models are then compared with the experimental results.

6.3.3 Calculation of crack propagation

The propagation part of the fatigue life of the tubular joints is calculated by integrating the Paris equation. Numerical routines available from the NAG library are used to perform the integration.

6.3.4 Comparison of experimental N cycles with the fracture mechanics model results

The elements of the fracture mechanics model discussed above were incorporated in a Fortran 77 program module LIFE written on a micro VAX II computer. Two versions of the program are available; one for calculating the fatigue propagation life using the linear moment release model and the other is for the propagation life using the quadratic moment release model. The number of cycles for crack propagation were calculated for the thirteen chord cracks. The results are discussed in terms of the weld profile.

6.3.4.1 Profile C1

Figures 6.11-6.16 show the plots of crack depth a, versus number of cycles, N produced using the fracture mechanics model proposed for this thesis. The experimental a versus N values are also presented in an attempt to validate the proposed techniques for estimating the propagation part of the fatigue life.

Test C1-1-X the three chord cracks at saddle positions A,B and D all show similar results i.e. the fracture mechanics model for linear and quadratic moment release predict higher initial crack growth rates as compared with the experimental results. For crack depth a > 0.15T the differences between the two models begin to emerge with the linear model clearly underpredicting the number of cycles for through thickness crack growth. However, closer agreement is evident between the experimental and quadratic model.

Test C1-2-X the three sets of results show the same trend as that reported for C1-1-X, the only difference being that the results from the two models fall either side of the experimental data. The linear model results are conservative and the quadratic results are non-conservative.

6.3.4.2 Profile C2

Two chord cracks are reported for this profile and these are shown in Figures 6.17 & 6.18. The fracture mechanics model for linear moment release and quadratic moment release show significant underprediction in the number of cycles for through thickness crack growth. This is not unexpected given that the predicted distribution of geomtric stress intensity calibration factor Y for this profile is much higher than the experimental values for almost the whole range of a/T values. These differences could be attributed to lower weld toe notch stresses and lower hot spot stress values for a given nominal stress.

6.3.4.3 Profile A

The five chord cracks reported here and presented in Figures 6.19-6.23 show the same trend as those of the controlled weld profile results C1. the linear moment release model again underpredicts the number of cycles to through thickness crack growth and closer agreement is shown for the quadratic model. The linear model predicts constant crack growth rate, the quadratic model however, exhibits an initial constant crack growth rate but a change in gradient occurs at 0.25T. This feature appears to be a characteristic of the model and occurs in the prediction of all types of weld profiles investigated.

6.3.4.4 Discussion

In this section the aim is to formulate a mathematical model to predict fatigue crack propagation in welded tubular joints that produced reasonable agreement with the experimental data available for the thirteen chord cracks. The results from this model are presented in Figures 6.11-6.23. It is apparent that in the case of linear moment release a conservative estimate of the number of cycles to through thickness crack propagation was predicted. The quadratic model however, was non-conservative and in some cases the results agreed well with experimental data. However, neither model produced accurate results.

The inaccuracies in the results can be attributed to a number of assumptions made when formulating the fracture mechanics model. These assumptions are:

i) The fracture mechanics model was based on an ideal semi-elliptical crack profile.

ii) Only one crack was assumed to initiate and grow through the thickness.

iii) For each type of weld profile only one curve was derived to describe the relation between crack aspect ratio changes as a function of crack depth. This disregards complicated weld geometry and hot spot stress range.

iv) The load shedding model is itself an assumption without numerical or experimental validation.

Consider the curve fitting that is required. This is basically an averaging process which produces one curve for each type of weld profile. This curve is based on experimental data and must therefore be subject to experimental error. Also fatigue crack initiation and the number of initiation sites can be considered a random process and therefore subject to errors.

The use of curve fitting techniques in conjunction with load shedding models to calculate Y factors can produce either an overestimation or an underestimation and this is reflected in the fatigue life predictions. Also the early part of crack growth which involves multiple crack initiation sites and therefore possible crack interaction could introduce inaccuracies.

Therefore the discrepencies shown in the results cannot be exclusively attributed to the load shedding models. Furthermore, if one of the load shedding models produced good agreement with the experimental data it should not be considered as necessarily validating that particular model. But it could suggest that the set of assumptions used for the fracture mechanics model is more applicable to the results obtained.

In view of the fact that the calculations are based on a range of assumptions the results produced provided fairly good agreement with experimental data and could prove to be a useful tool for the design engineer. One observation on the difference between the two load shedding models is that the linear model accurately predicted the shape of the crack growth curve, a versus N, for all thirteen cracks. This is an important feature of the model because, if the extent to which the model is conservative can be quantified then given that the shape of the curve is accurately modelled a correction factor could be calculated to

produce closer agreement with the experimental results. This could then provide the design engineer with a more realistic approach to estimating crack propagation part of life.

This however does not suggest that the linear model is more accurate but does imply that a combination of the assumptions in conjunction with this model produce a set of useful results. It is felt that from the results of the two load shedding models presented either model could be used for predicting crack propagation life of a tubular joint. These could be used in conjunction with average values of N_1 for crack initiation calculated from experimental results to predict the total fatigue life of a tubular joint. It is felt that the inaccuracies associated with the application of the local strain approach to tubular joint analysis must disqualify this technique in this context.

Therefore a totally predictive approach to total fatigue life calculation is presently not possible. Further analysis and experimental validation of the local strain approach would be required before it could be successfully applied to tubular joint analysis.

6.4 Conclusions

1) The local strain approach was used to predict N_1 values for the 13 chord cracks. Various degrees of accuracy was obtained for the different cracks. It was concluded that the method requires further development for tubular joint application.

2) A set of equations was derived based on fatigue experimental data to describe the crack aspect ratio changes as a function of crack depth.

3) A fracture mechanics model to predict the propagation part of life of a tubular joint was developed in conjunction with the Niu-Glinka weight function and the moment release models. The Paris equation was used to predict N_2.

4) The linear moment release model produced conservative estimates of the propagation part of the fatigue life. However, the quadratic model was not conservative, it tended to overpredict N_2 values.

5) The linear model accurately predicted the shape of the fatigue life curve, a versus N.

6) A predictive approach to total fatigue life of tubular joints was not possible due to inaccuracies in the local strain approach. In order to calculate total number of cycles of the fatigue life of a structure, an average experimental N_1 value would have to be used.

6.5 references

6.1 Glinka, G., Fatigue life prediction of thraded connection-Reprt. UCL Mech. Eng. Dept. Torrington Place London WC1E 7JE.

6.2 Dowling, N.E., Fatigue failure prediction for complicated stress-strain histories. *Journal of Materials, MJLSA,* Vol.7 No. 1.

6.3 Wetzel, R.M., (ed), Fatigue Under Complex Loading: Analyses and Experiments. Advances in Engineering, Vol. 6, *Society of Automative Engineering,* Warrendate, Pa.1979.

6.4 Neuber, H., Theory of stress concentrations for shear strained prismatical bodies with arbitary non-linear stress-strain law. *Transactions ASME Journal of Applied Mechanics. Vol. 8 1961.*

6.5 Newport, A., Stress and fatigue analysis of threaded tether connections. PhD Thesis. University of London, 1989.

6.6 Neuber, H., Theory of stress concentrations for shear-strained prismatical bodies with arbitrary non-linear stress-strain law. *Transactions ASME Journal of Applied Mechanics*. Vol. 8, Dec., 1961.

6.7 Press. W.H., Flannely, B.P., Peukolsky, S.A., Vetterling, W.T., Numerical Recipies, The Art of Scientific Computing. Cambridge University Press, 1987.

yield stress σ_y	386 MPa
ultimate tensile stress σ_{UTS}	560 MPa
Modulus of elasticity E	210,000 MPa
cyclic yield strength σ'_y	312 MPa
cyclic strength coefficient K′	1063
strain hardening exponent n′	0.177
fatigue strength coefficient σ'_f	982 MPa
fatigue ductility coefficient ε'_f	0.72
fatigue strength exponent b	-0.102
fatigue ductility exponent c	-0.604

Table 6.1 Mechanical properties of BS 4360 50D steel

Index	Coefficient			
	Profile A (I)	Profile A(II)	Profile C1	Profile C2
0	0.1574	0.2000	0.2132	0.1634
1	-0.0495	0.0461	0.0586	0.0524
2	0.0440	-0.0081	-0.0206	-0.0132
3	-0.0278	-0.0024	0.0059	0.0021
4		-0.0022	-0.0010	
5		0.0000	0.0005	

Table 6.2 List of the coefficients of the polynomials for the curve fitting. Profile A(I) and Profile A(II) refer to the two parts of the curve for profile A.

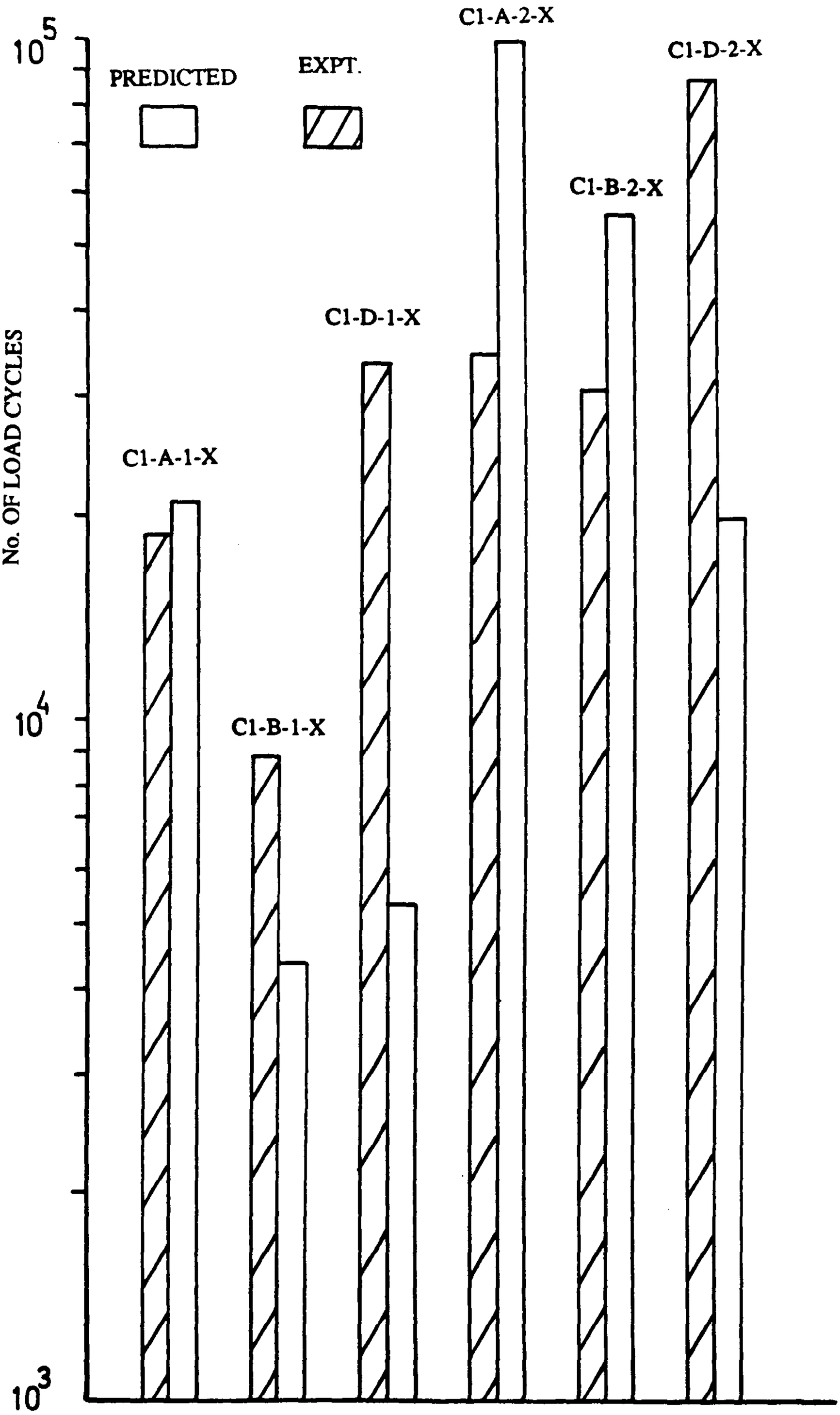

Figure 6.1 Comparison of initiation life experimental and predicted. C1-X

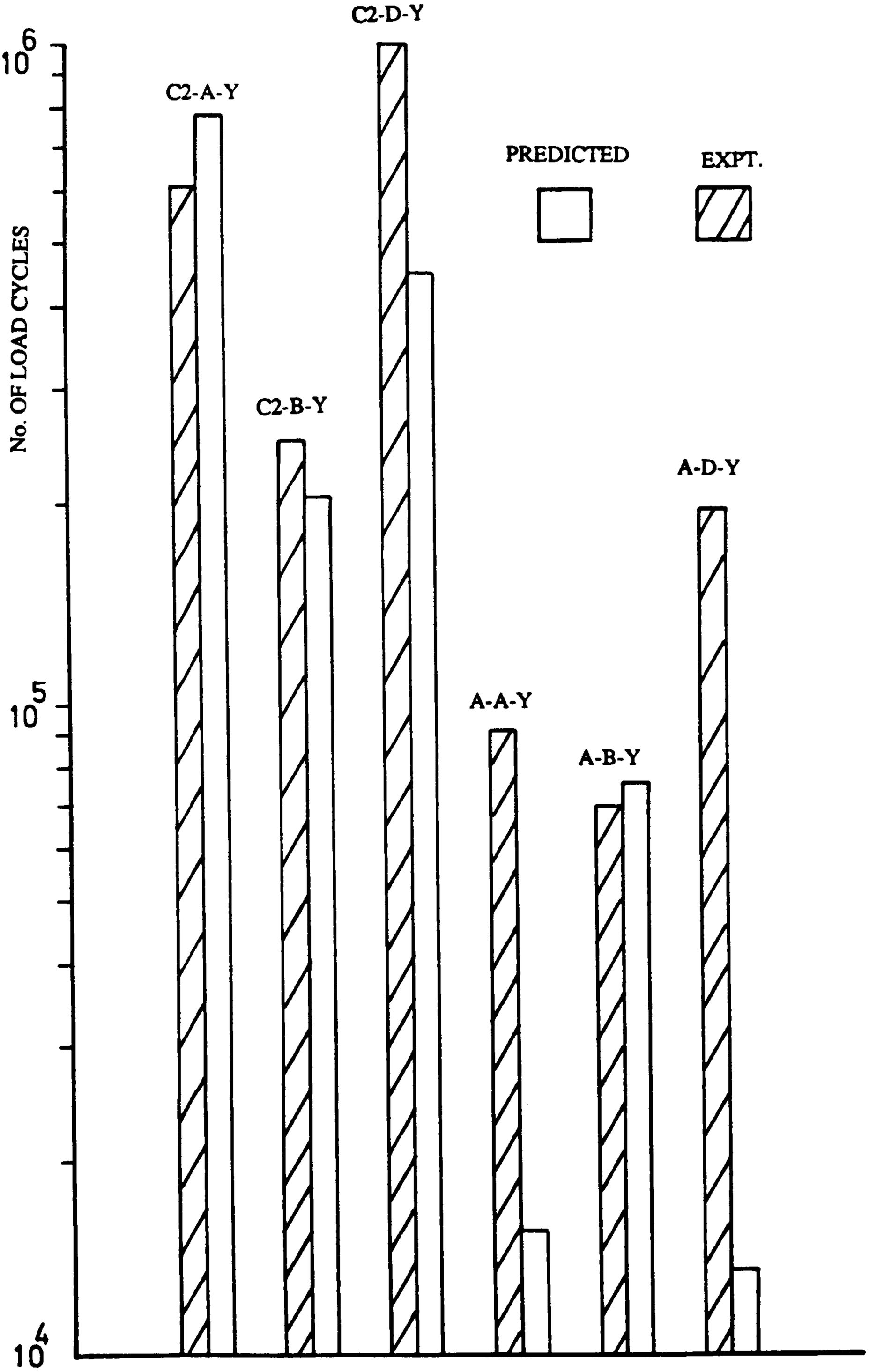

Figure 6.2 Comparison of initiation life experimental and predicted. C2-Y and A-Y

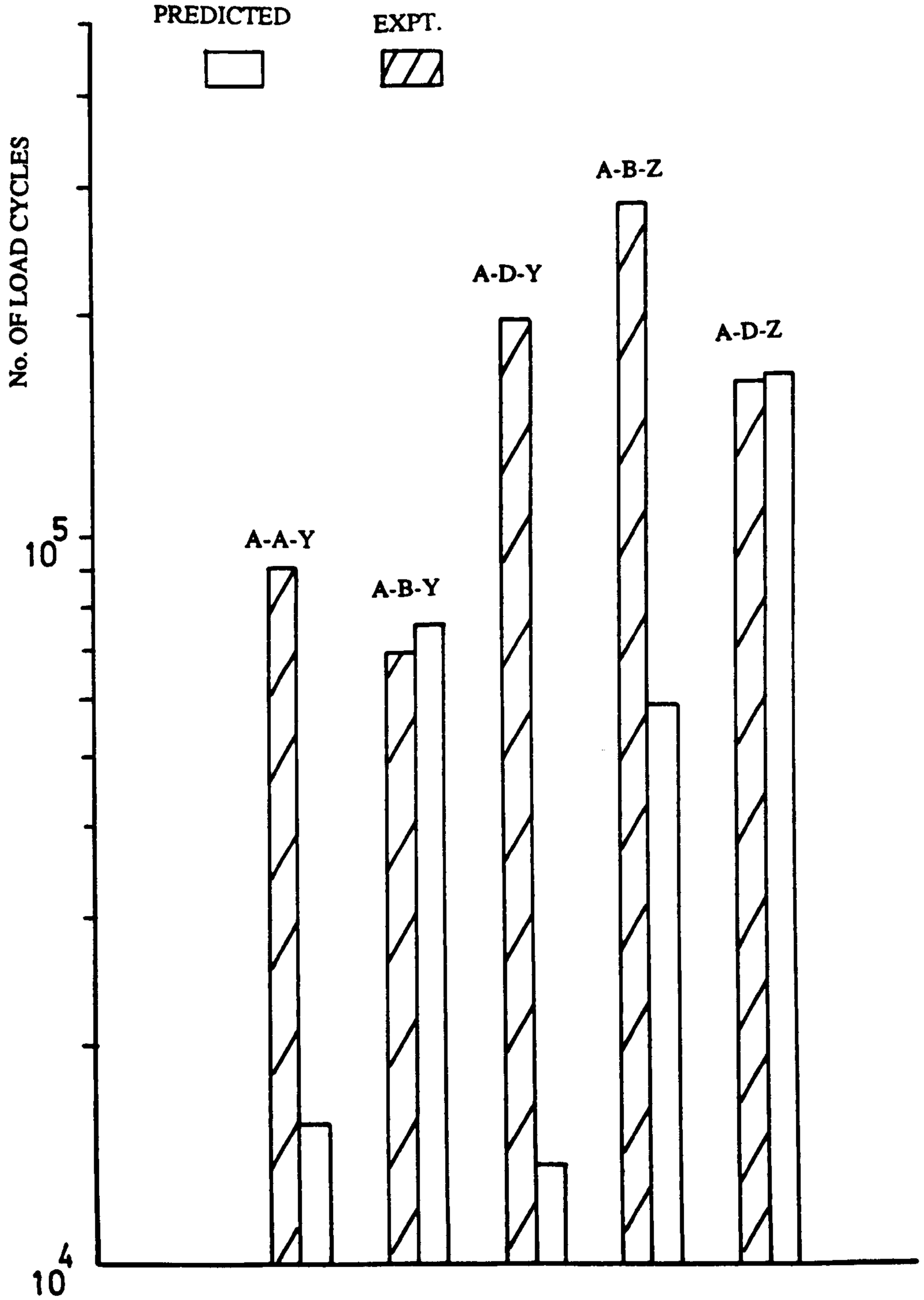

Figure 6.3 Comparison of initiation life experimental and predicted. A-Y and A-Z

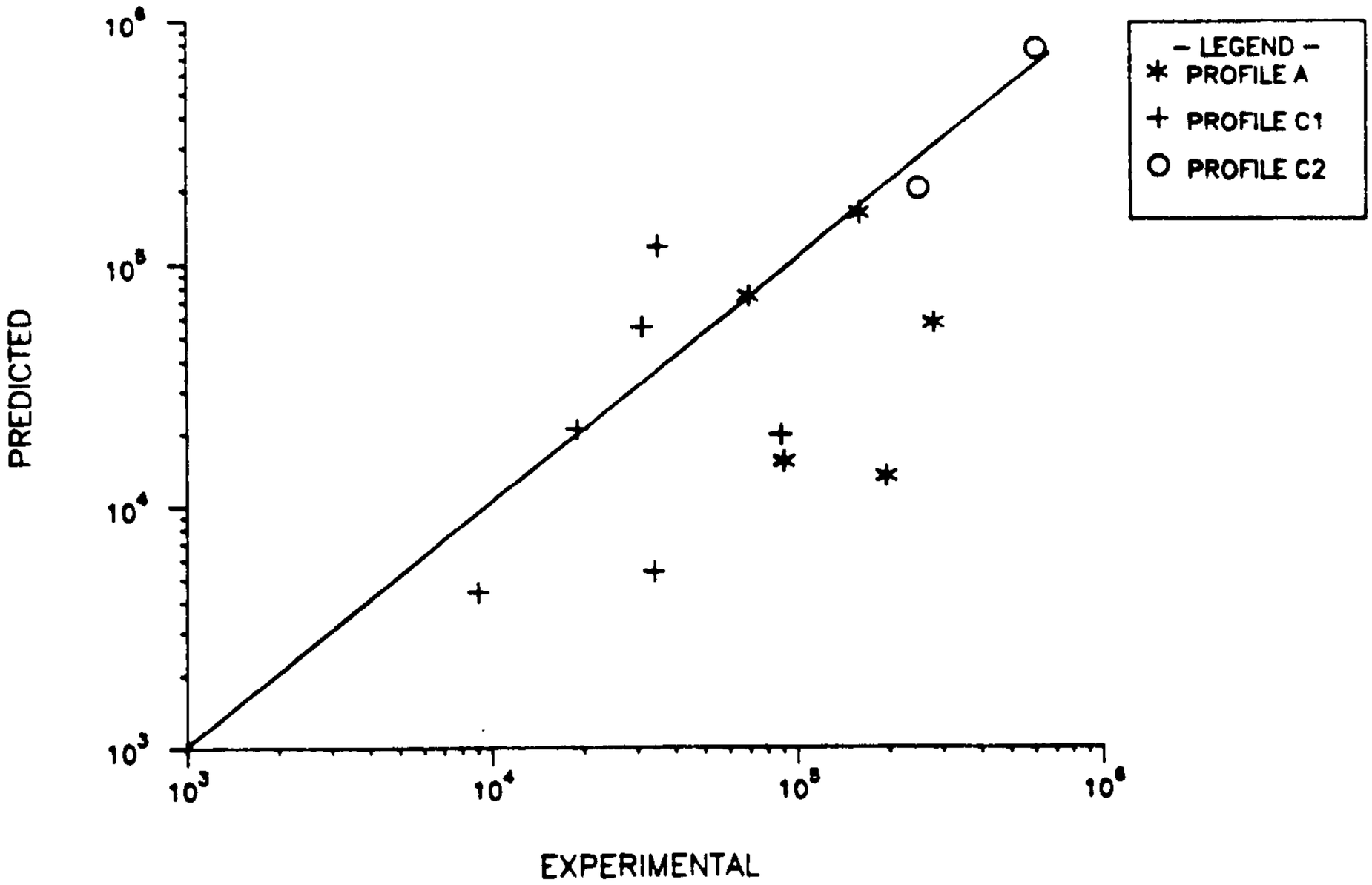

FIGURE 6.4 COMPARISON OF INITIATION LIFE EXPT. & PREDICTED

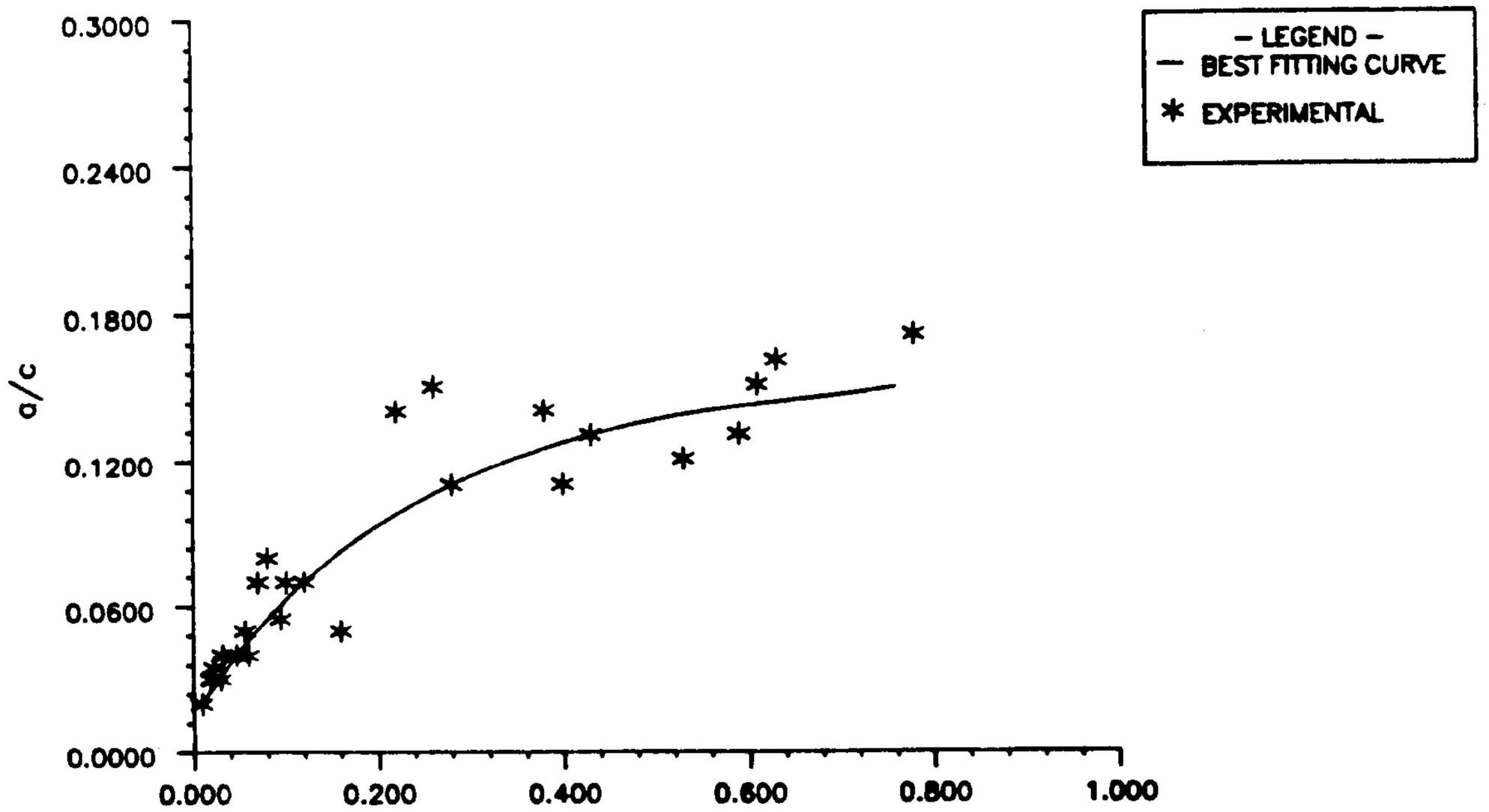

FIGURE 6.5 CRACK ASPECT RATIO CHANGES PROFILE C1

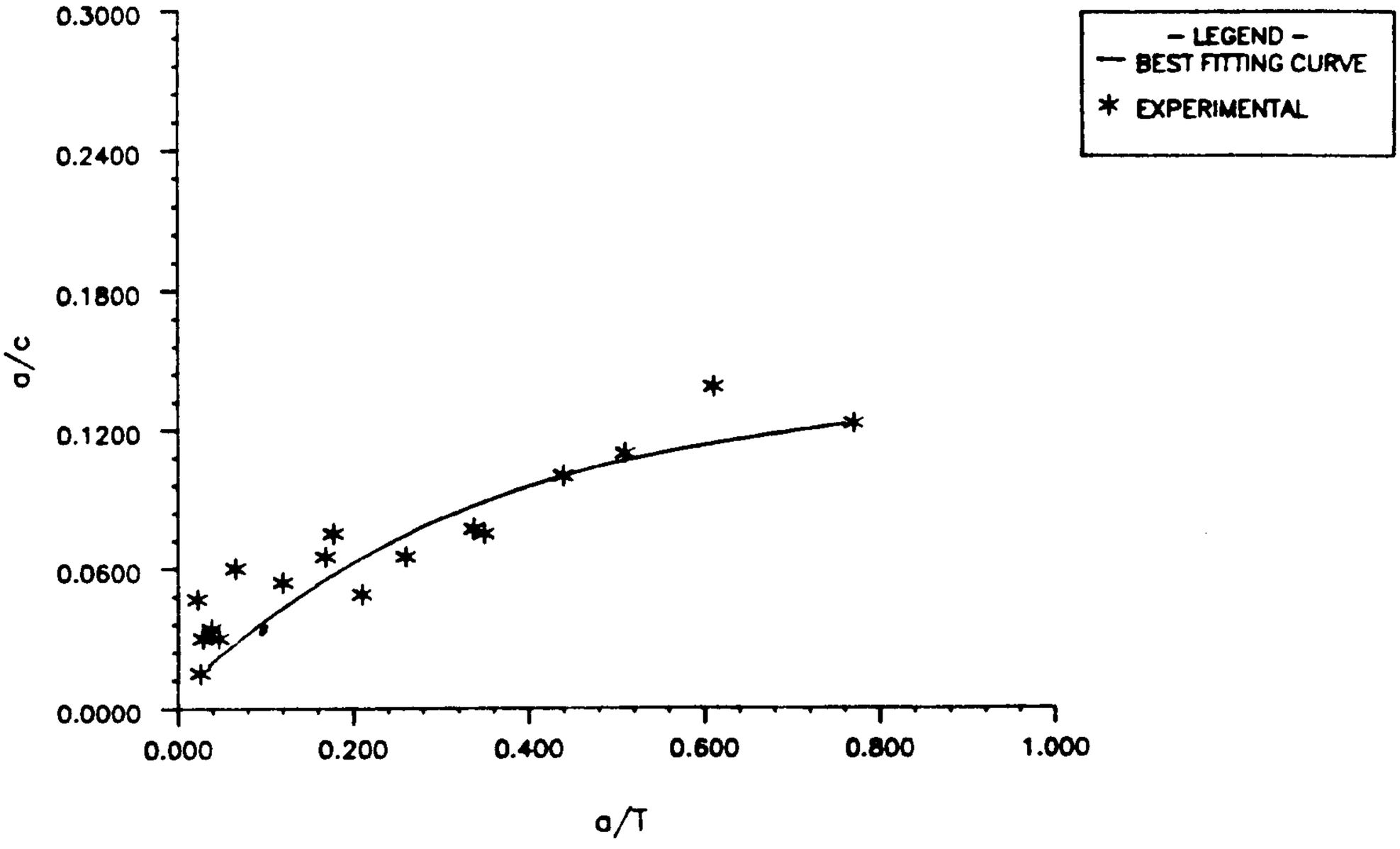

FIGURE 6.6 CRACK ASPECT RATIO CHANGES PROFILE C2

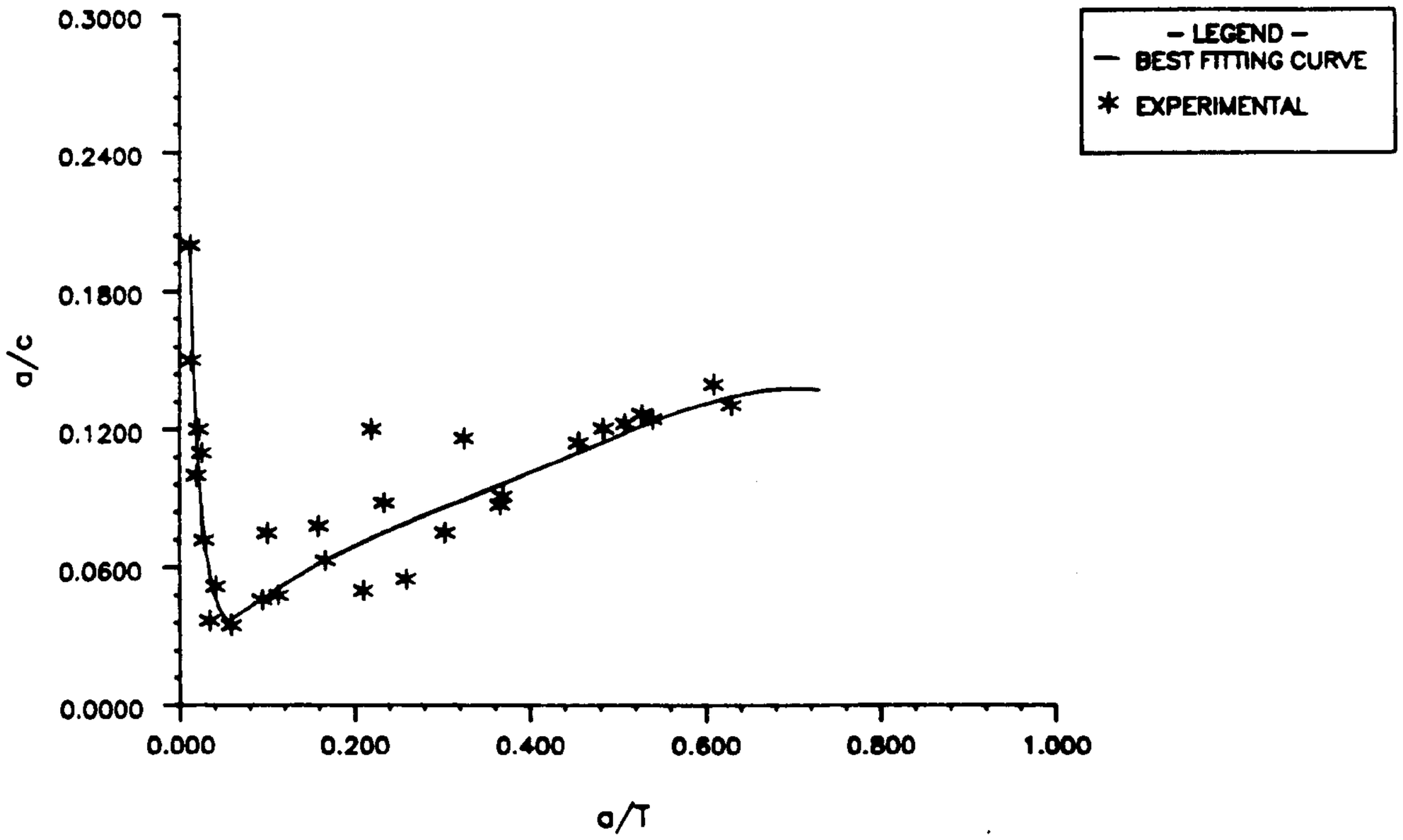

FIGURE 6.7 CRACK ASPECT RATIO CHANGES PROFILE A

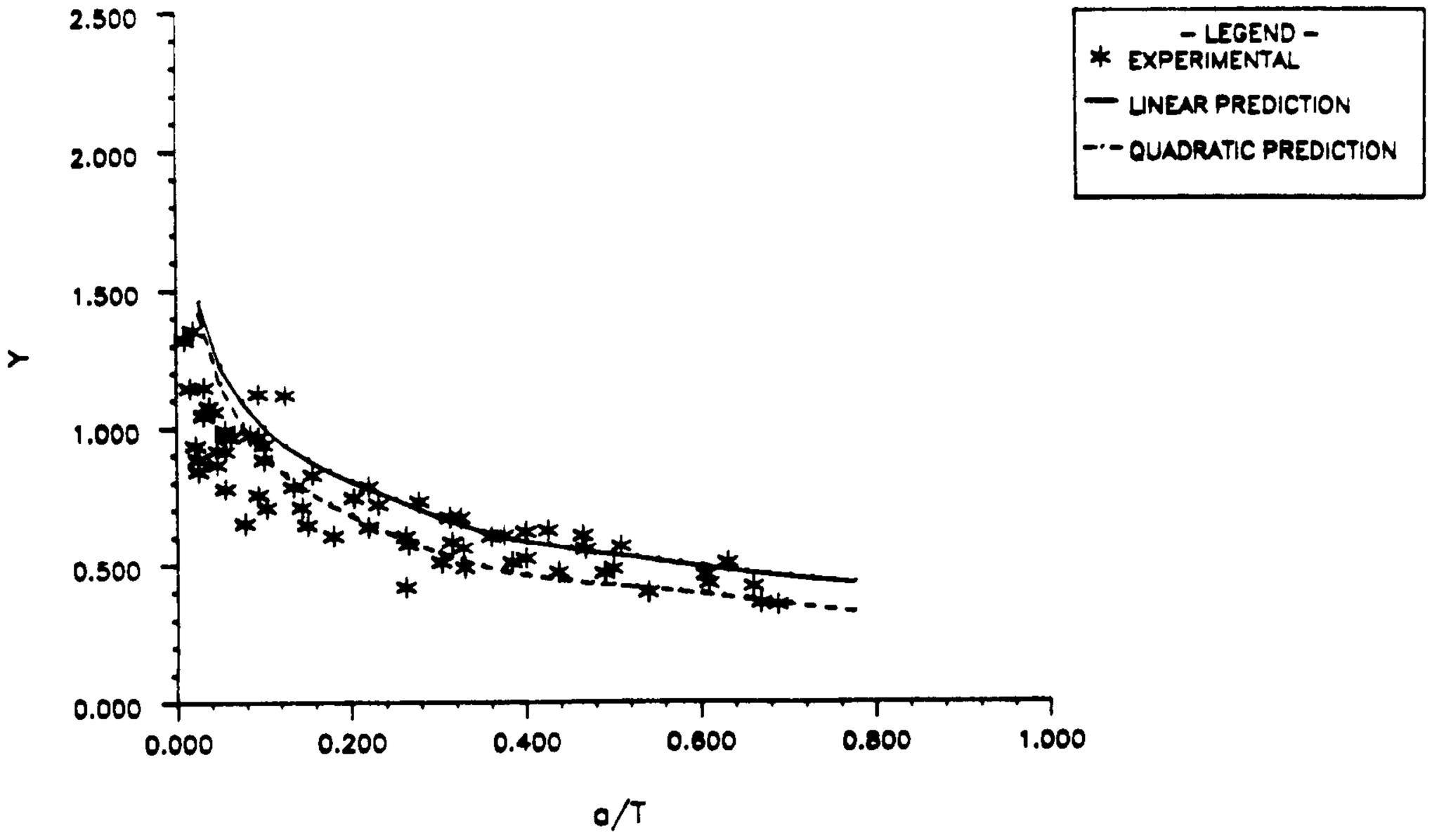

FIGURE 6.8 PREDICTED DISTRIBUTIONS OF Y C1–X

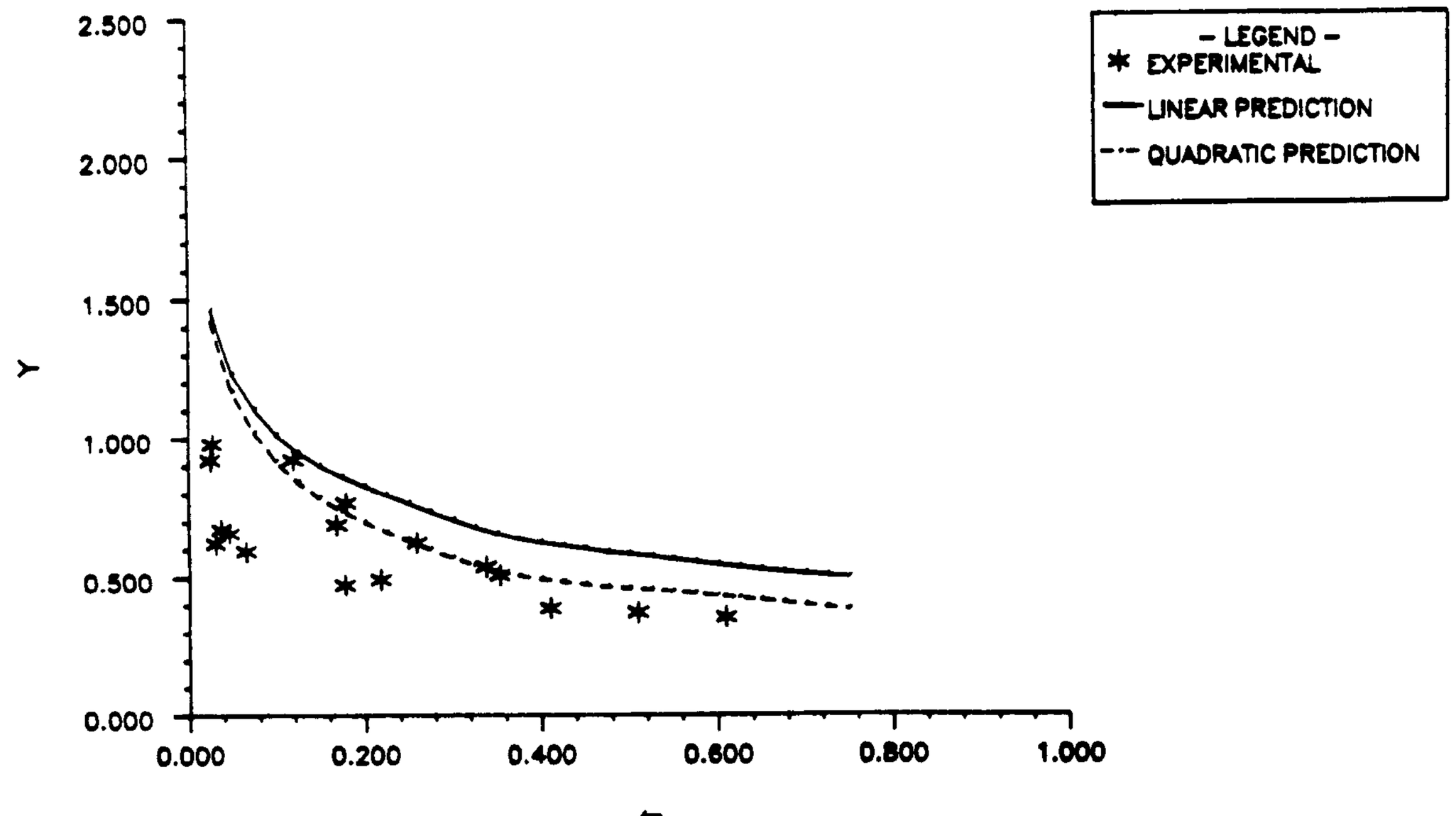

FIGURE 6.9 PREDICTED DISTRIBUTIONS OF Y C2–Y

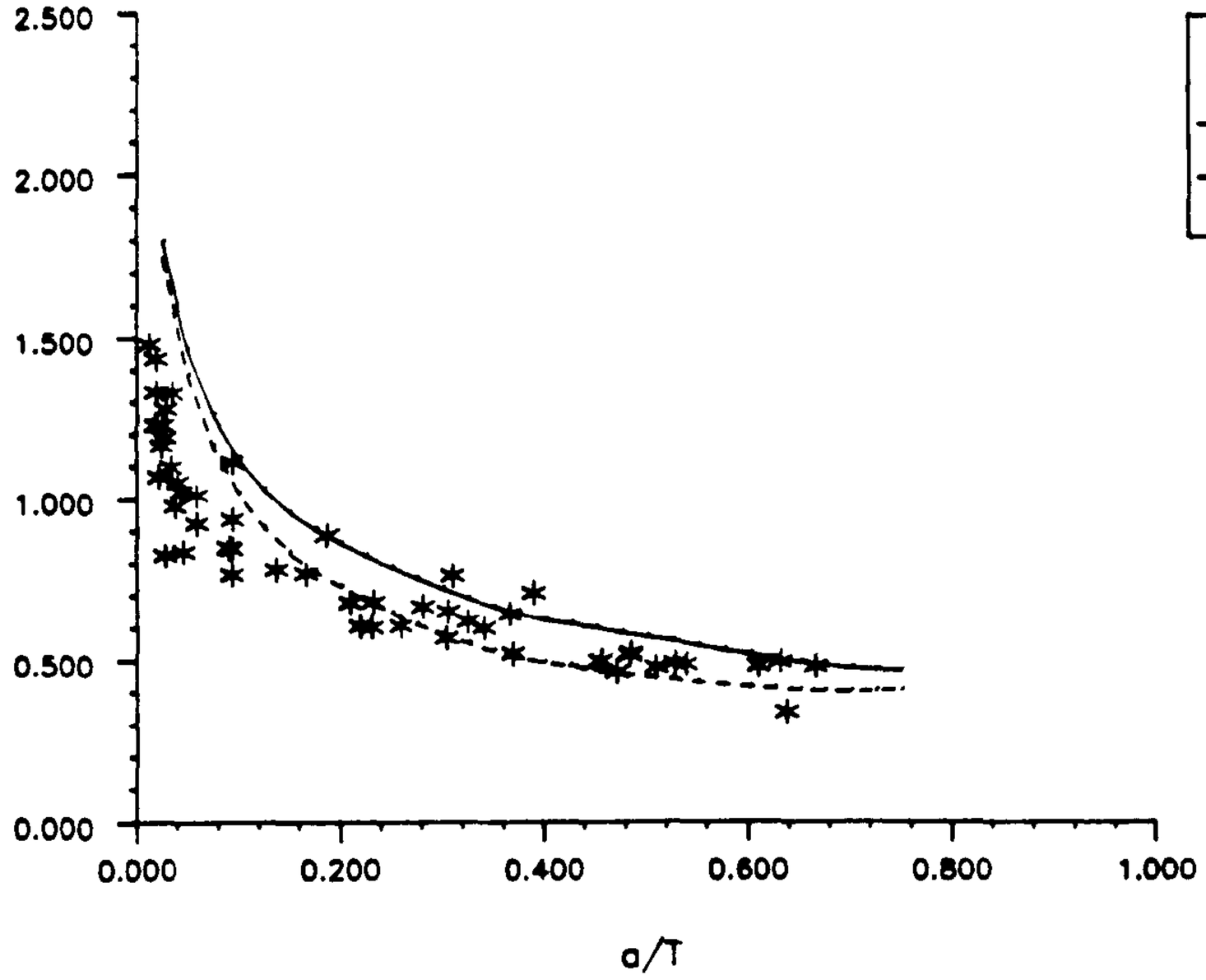

FIGURE 6.10 PREDICTED DISTRIBUTIONS OF Y PROFILE A

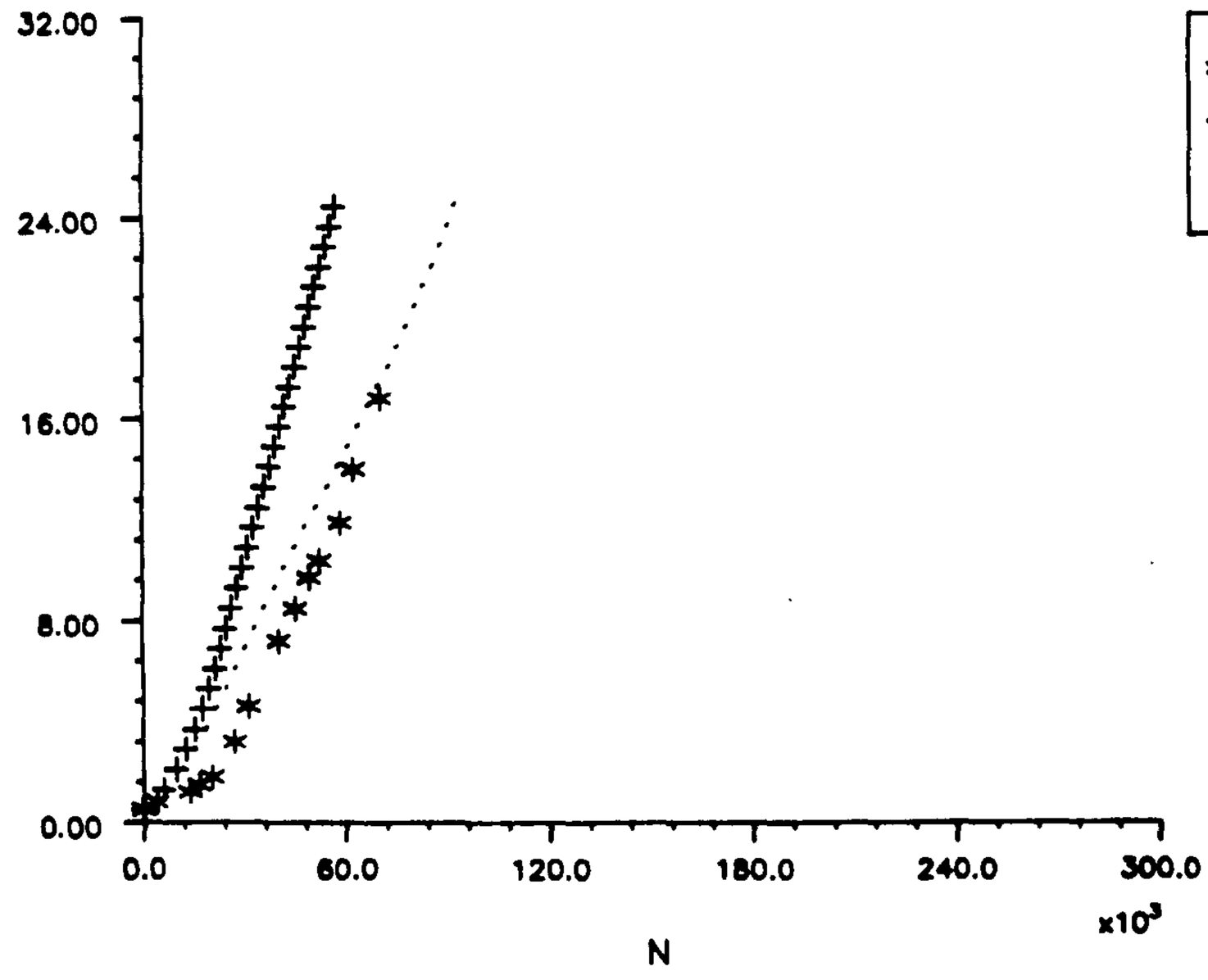

FIGURE 6.11 COMPARISON OF FATIGUE LIFE DATA C1–A–1–X

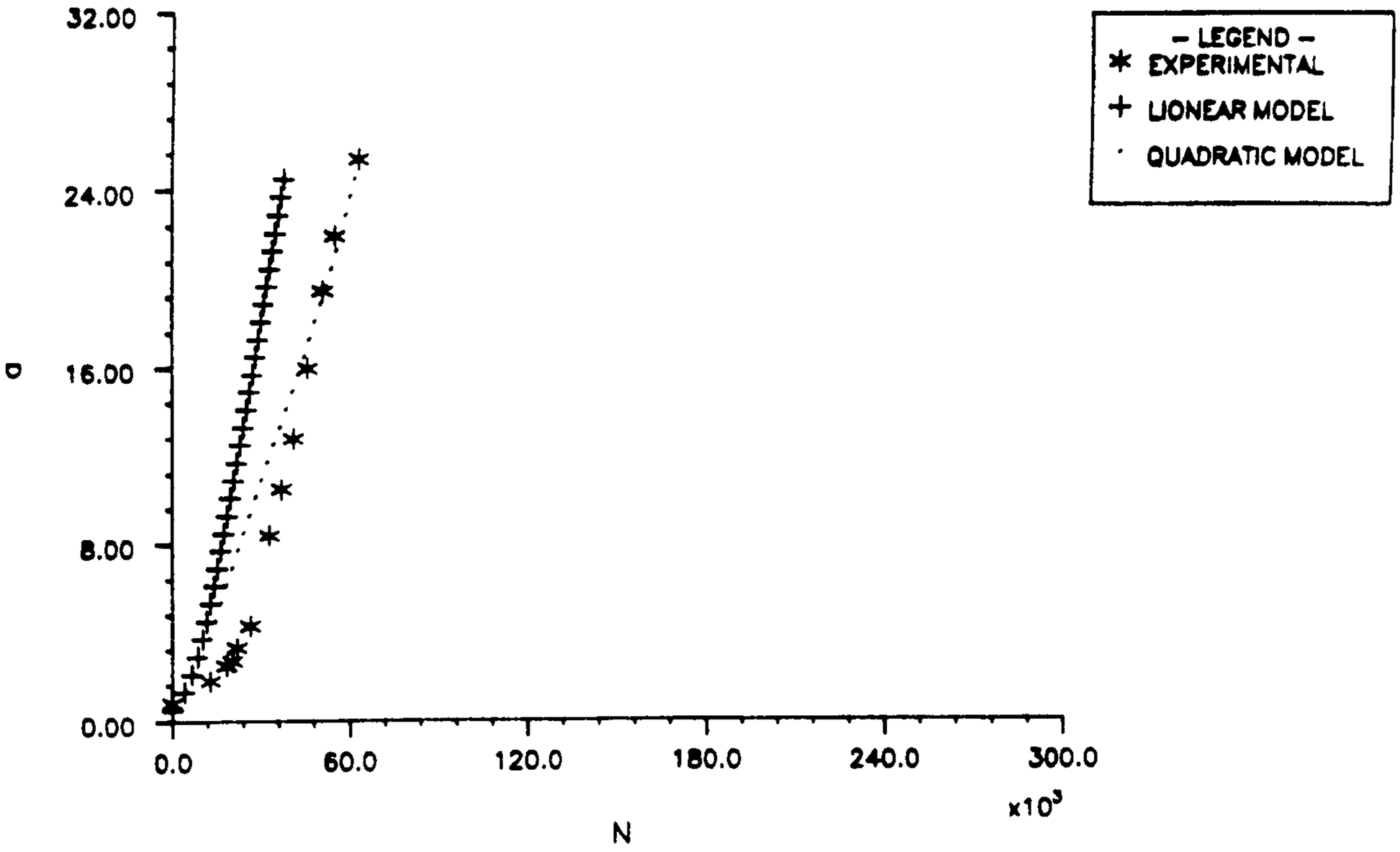

FIGURE 6.12 COMPARISON OF FATIGUE LIFE DATA C1–B–1–X

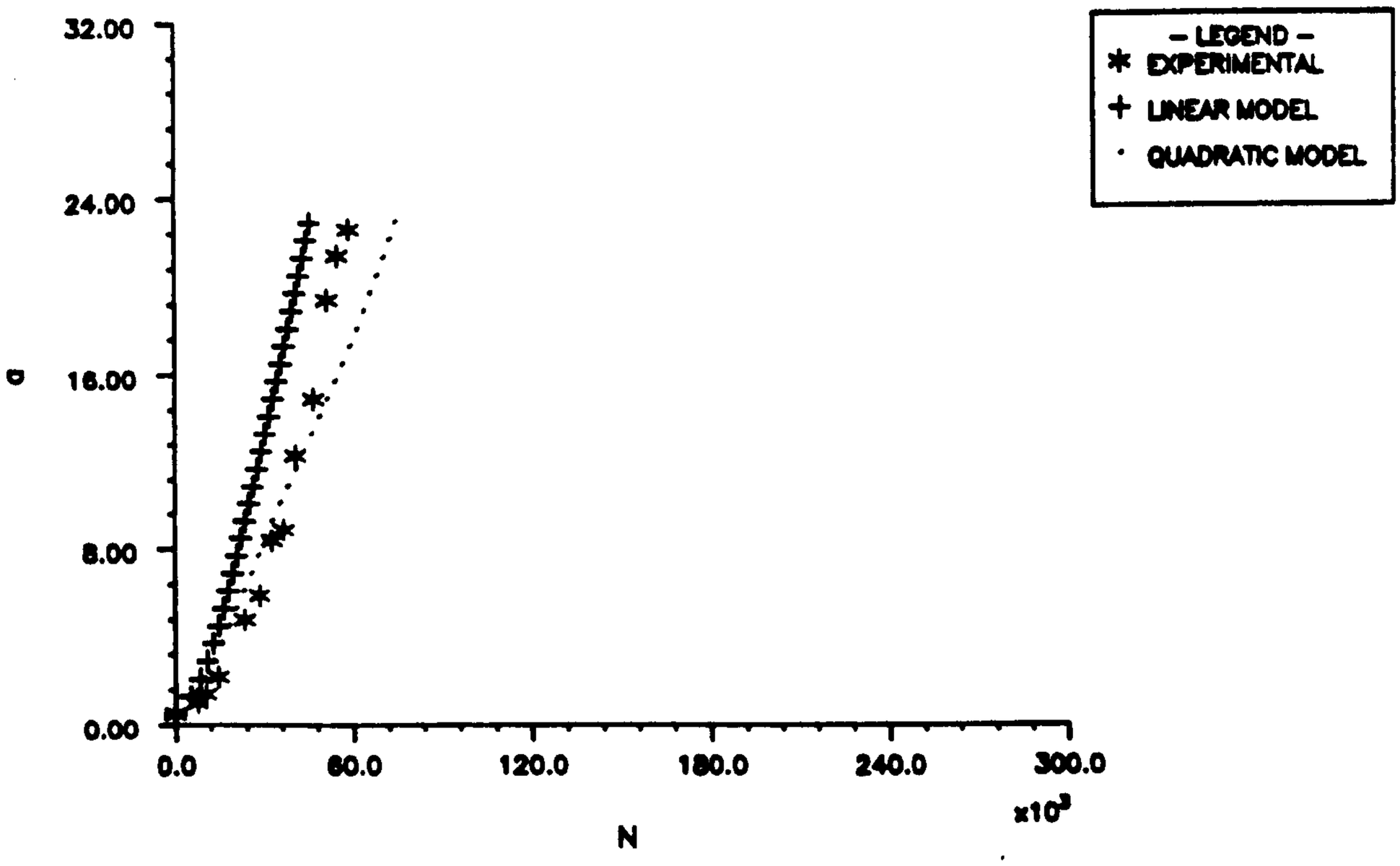

FIGURE 6.13 COMPARISON OF FATIGUE LIFE DATA C1–D–1–X

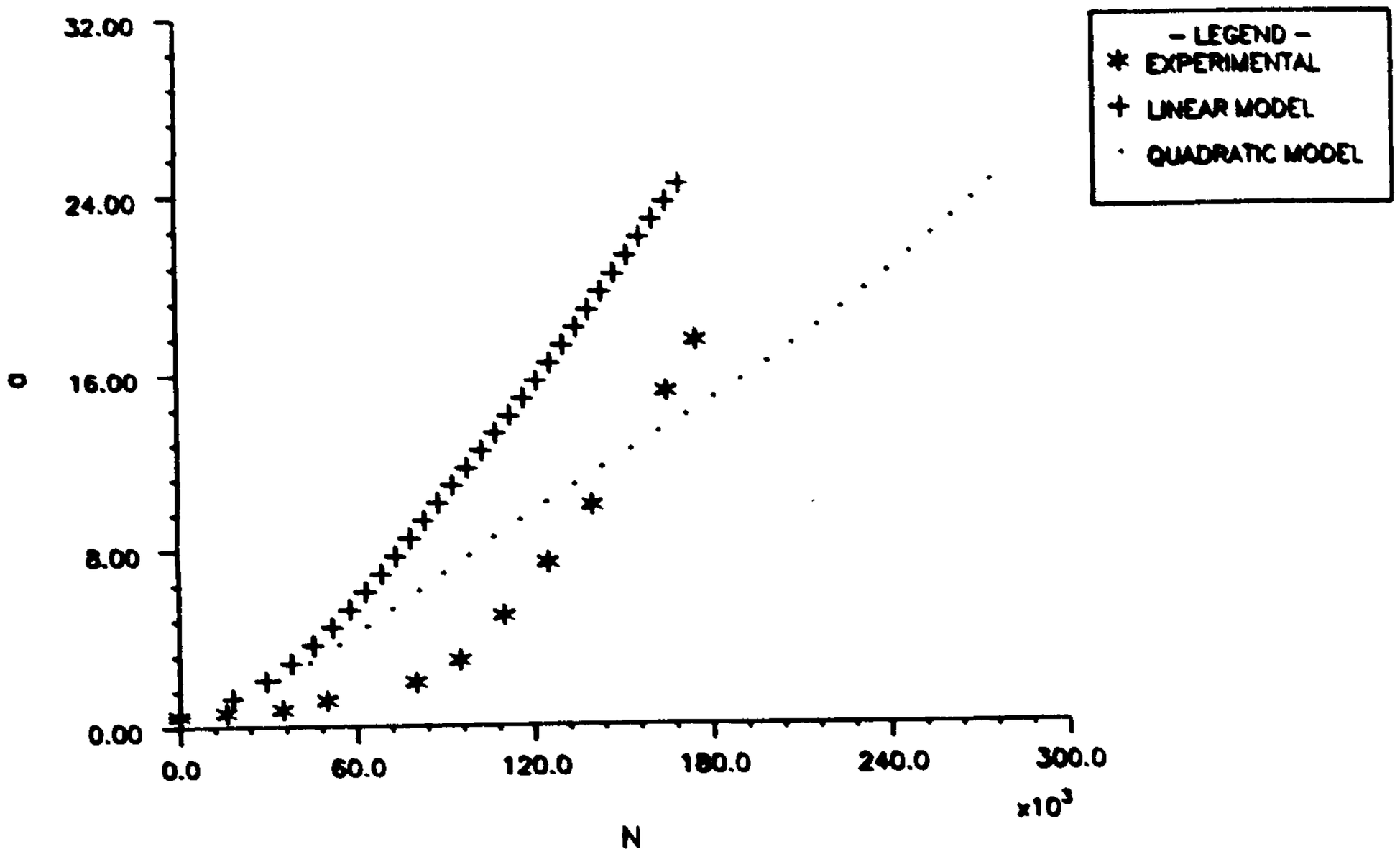

FIGURE 6.14 COMPARISON OF FATIGUE LIFE DATA C1–A–2–X

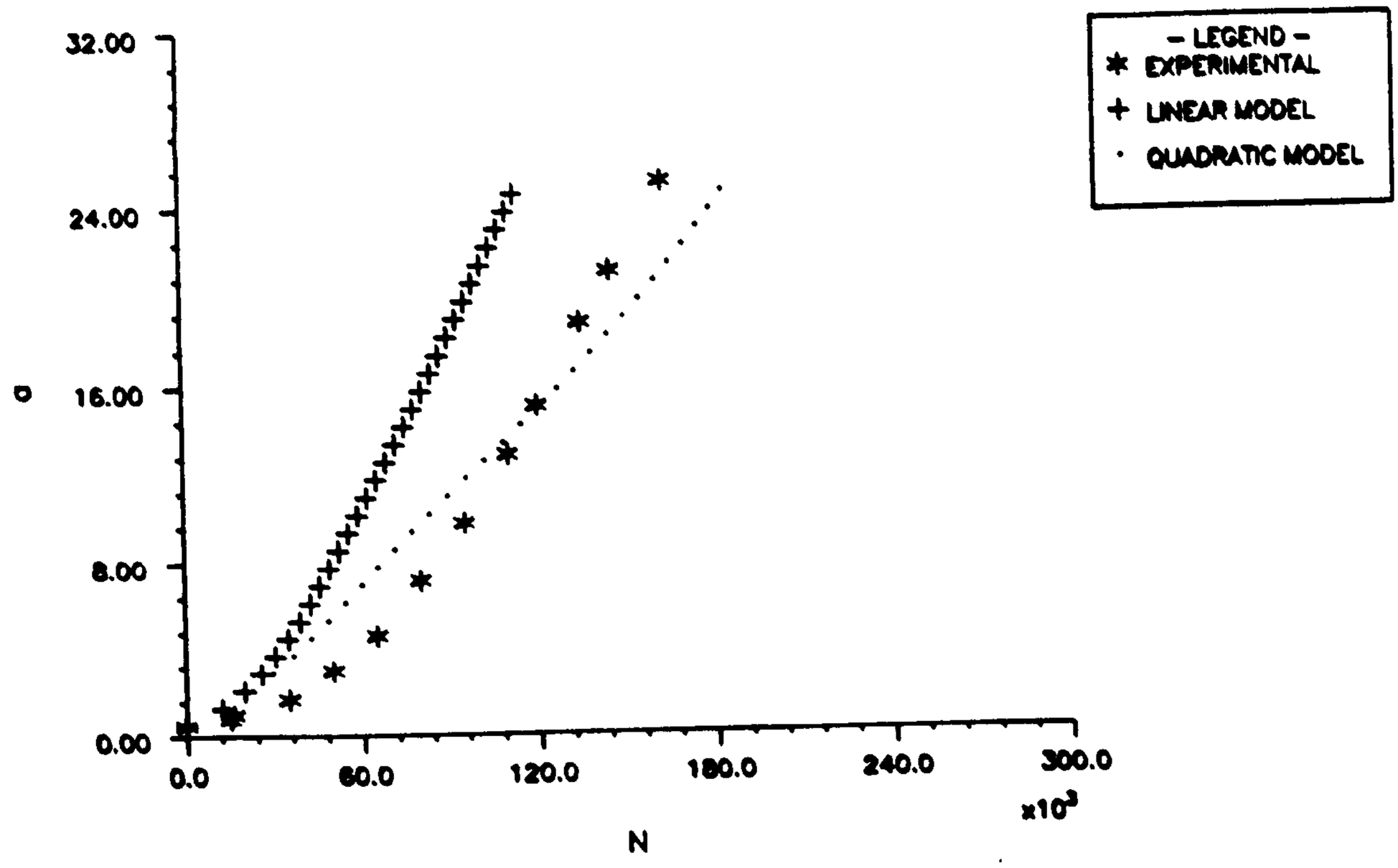

FIGURE 6.15 COMPARISON OF FATIGUE LIFE DATA C1–B–2–X

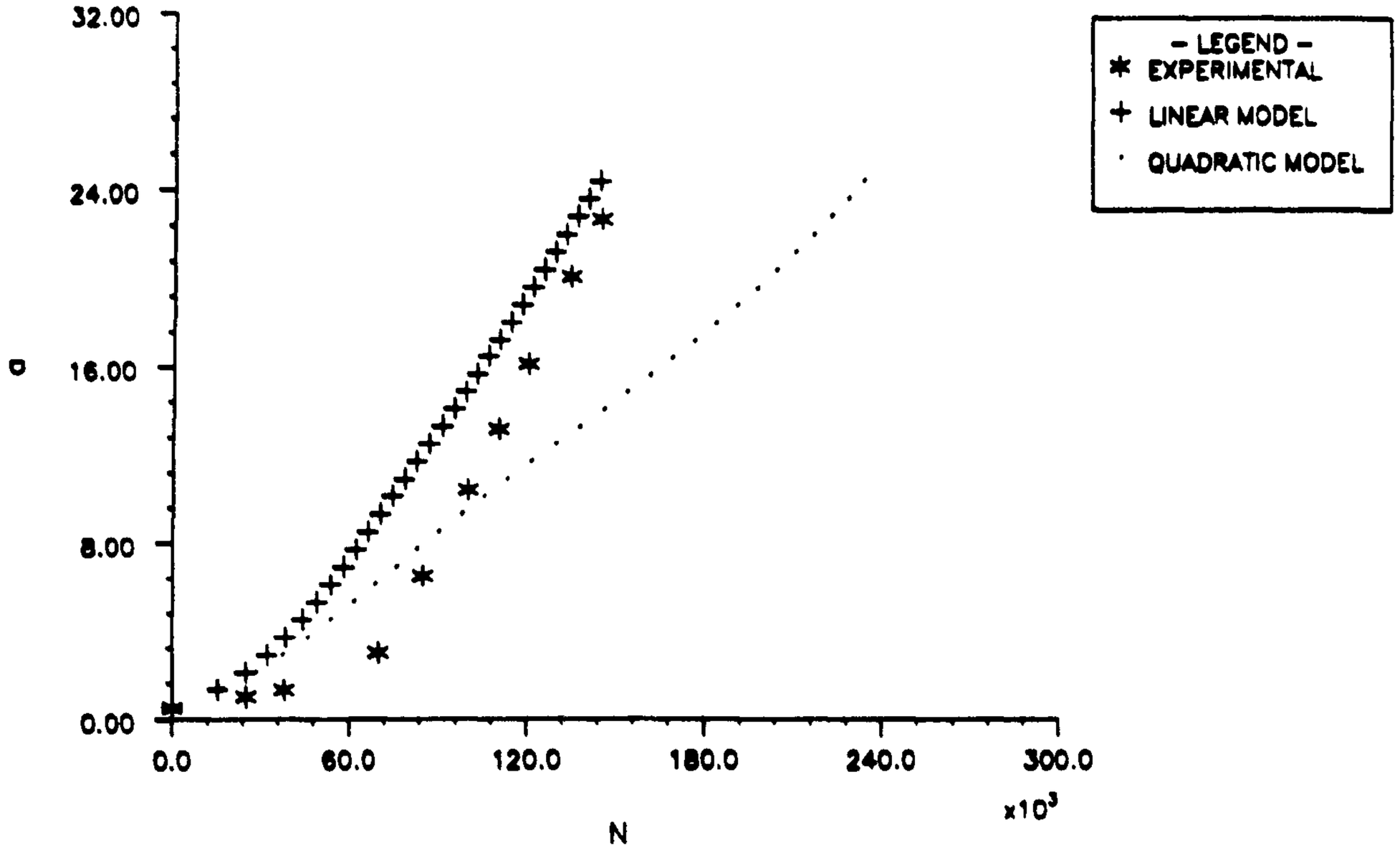

FIGURE 6.16 COMPARISON OF FATIGUE LIFE DATA C1–D–2–X

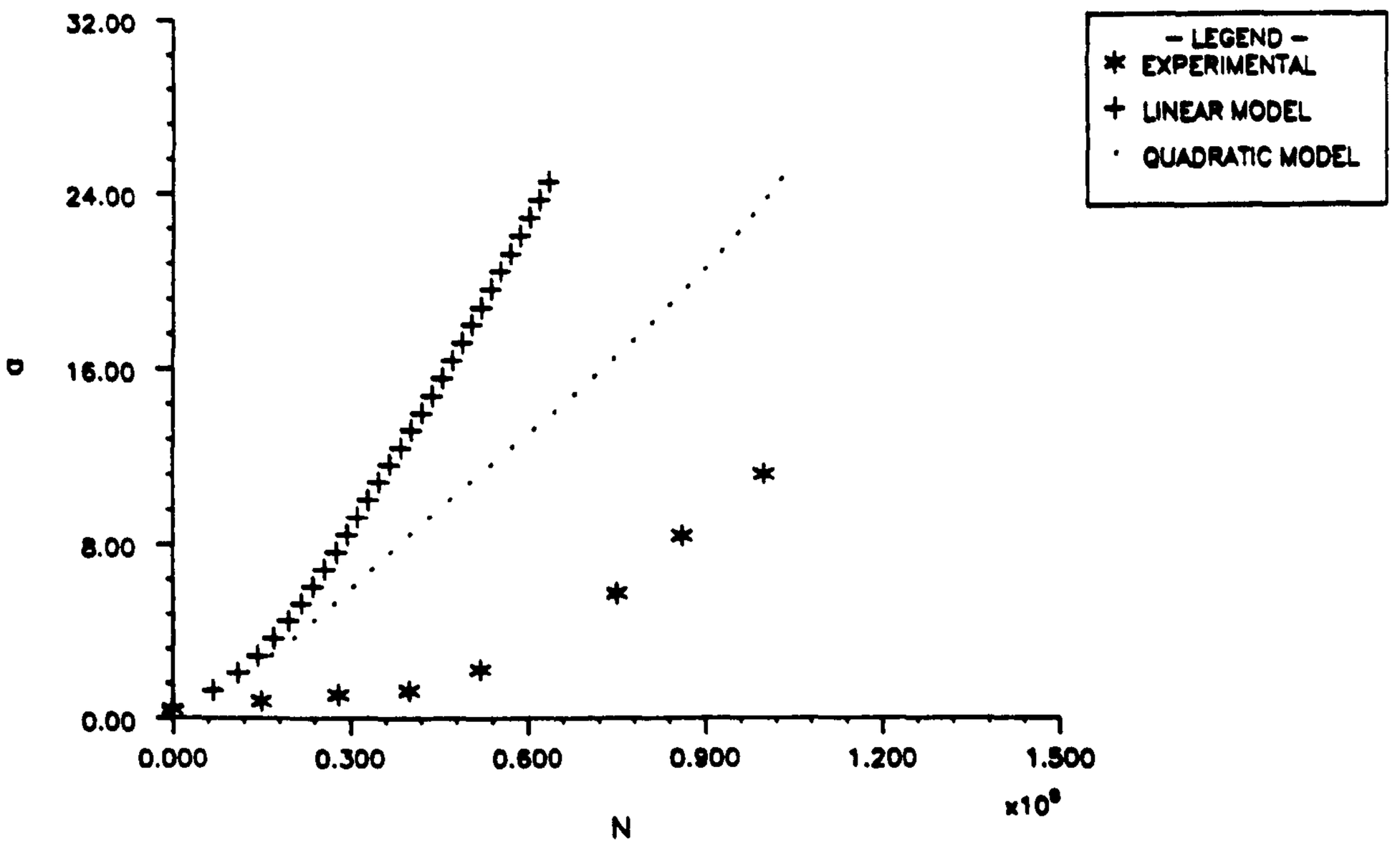

FIGURE 6.17 COMPARISON OF FATIGUE LIFE DATA C2–A–Y

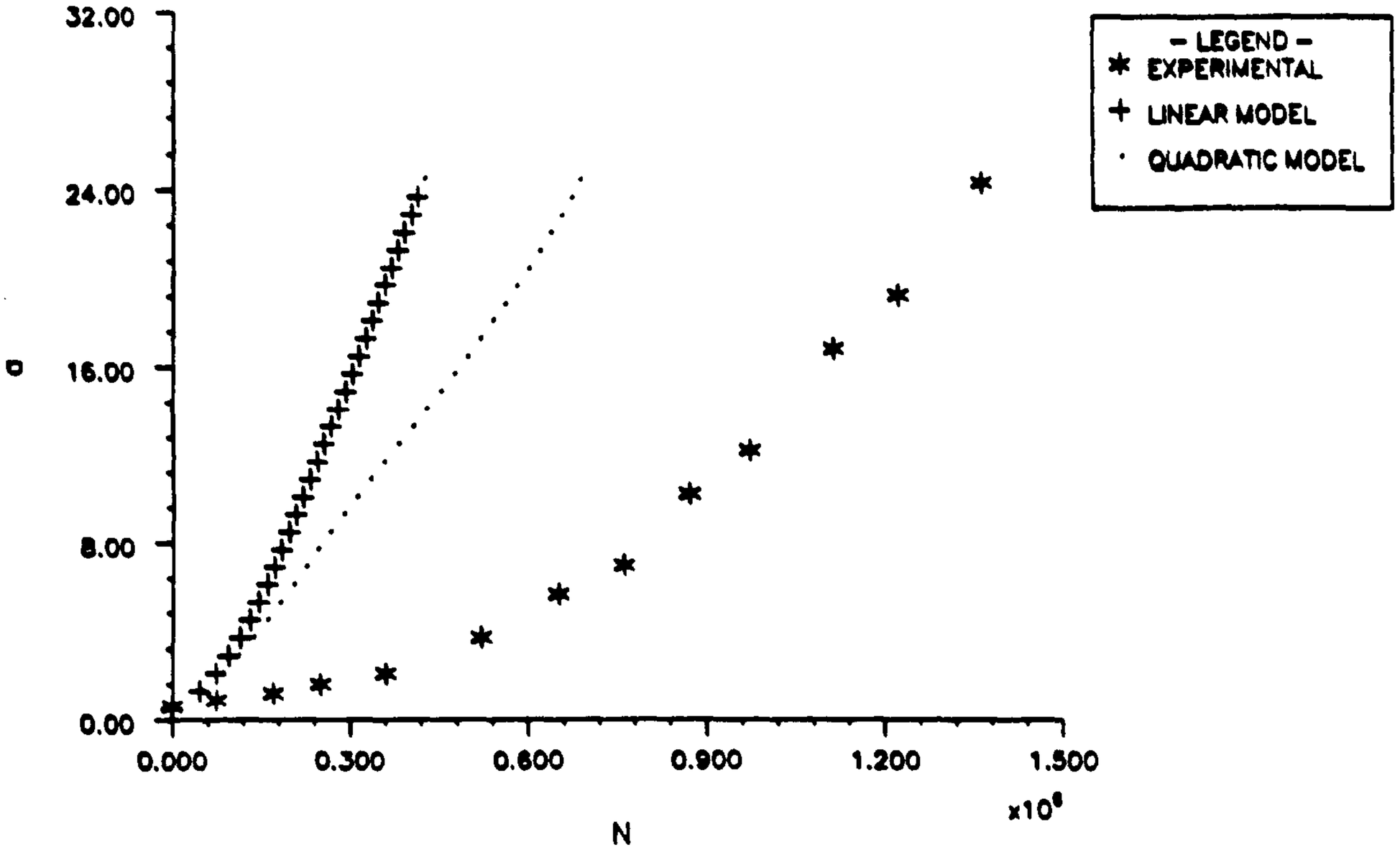

FIGURE 6.18 COMPARISON OF FATIGUE LIFE DATA C2–B–Y

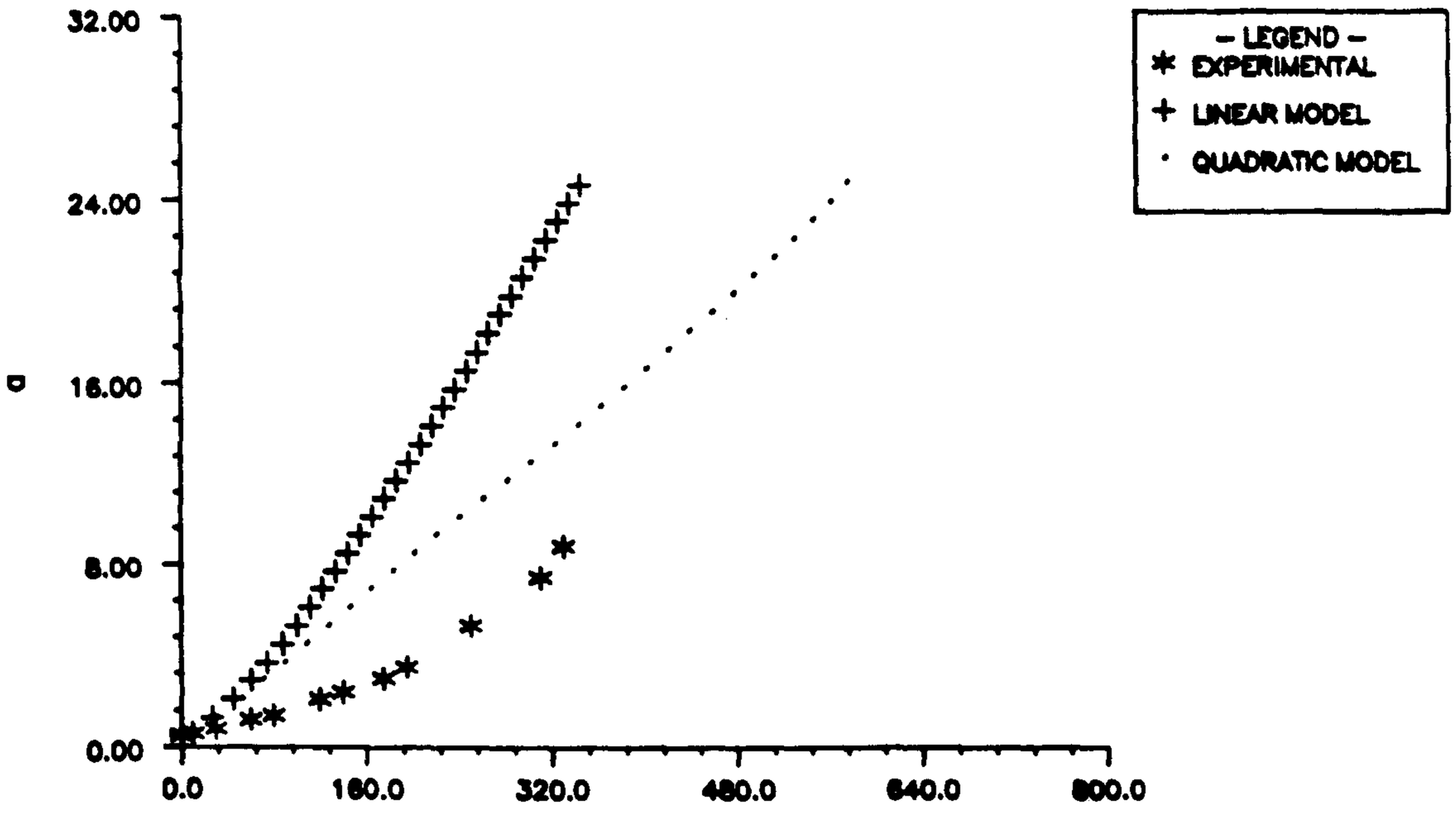

FIGURE 6.19 COMPARISON OF FATIGUE LIFE DATA A–A–Y

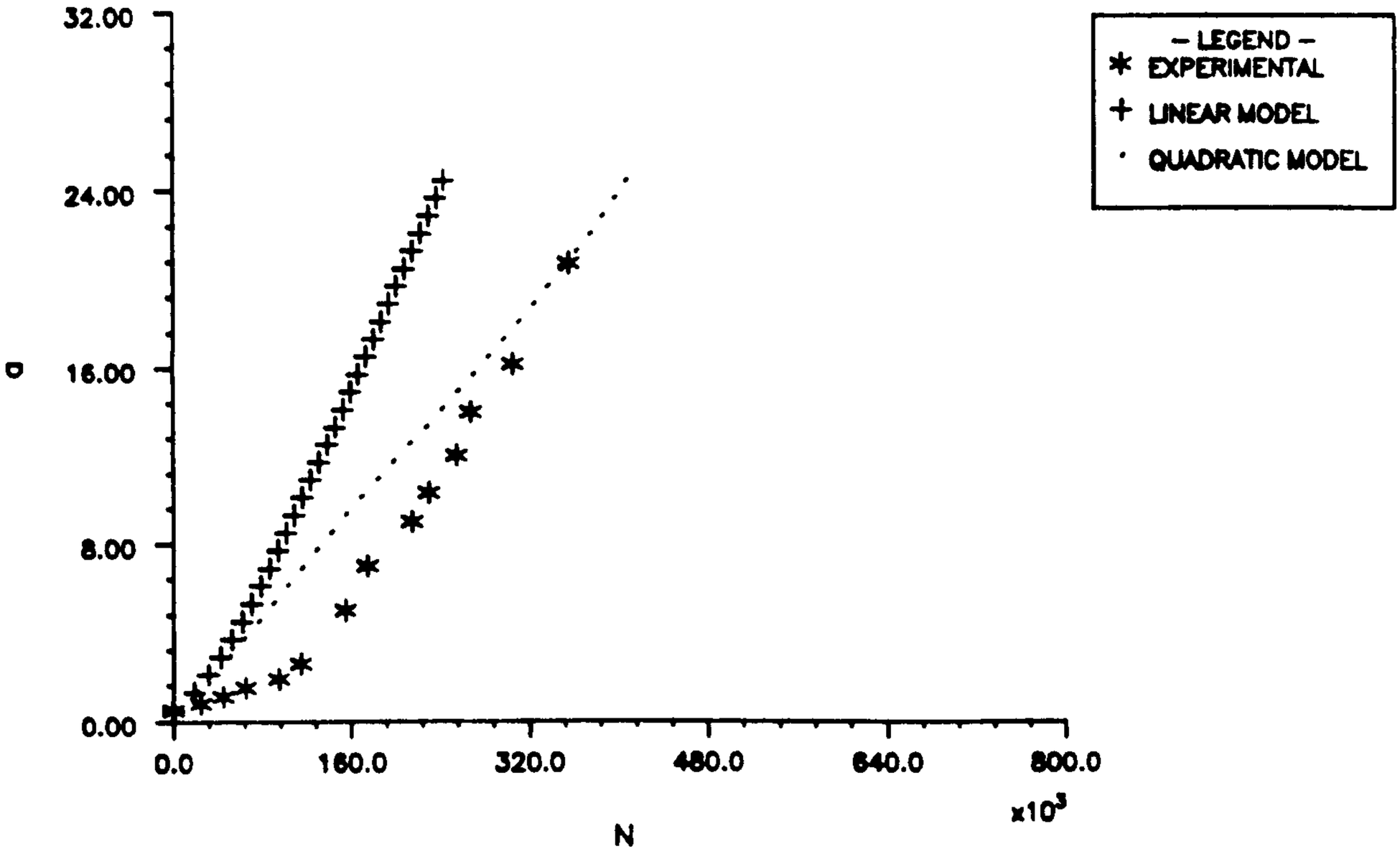

FAIGURE 6.20 COMPARISON OF FATIGUE LIFE DATA A–B–Y

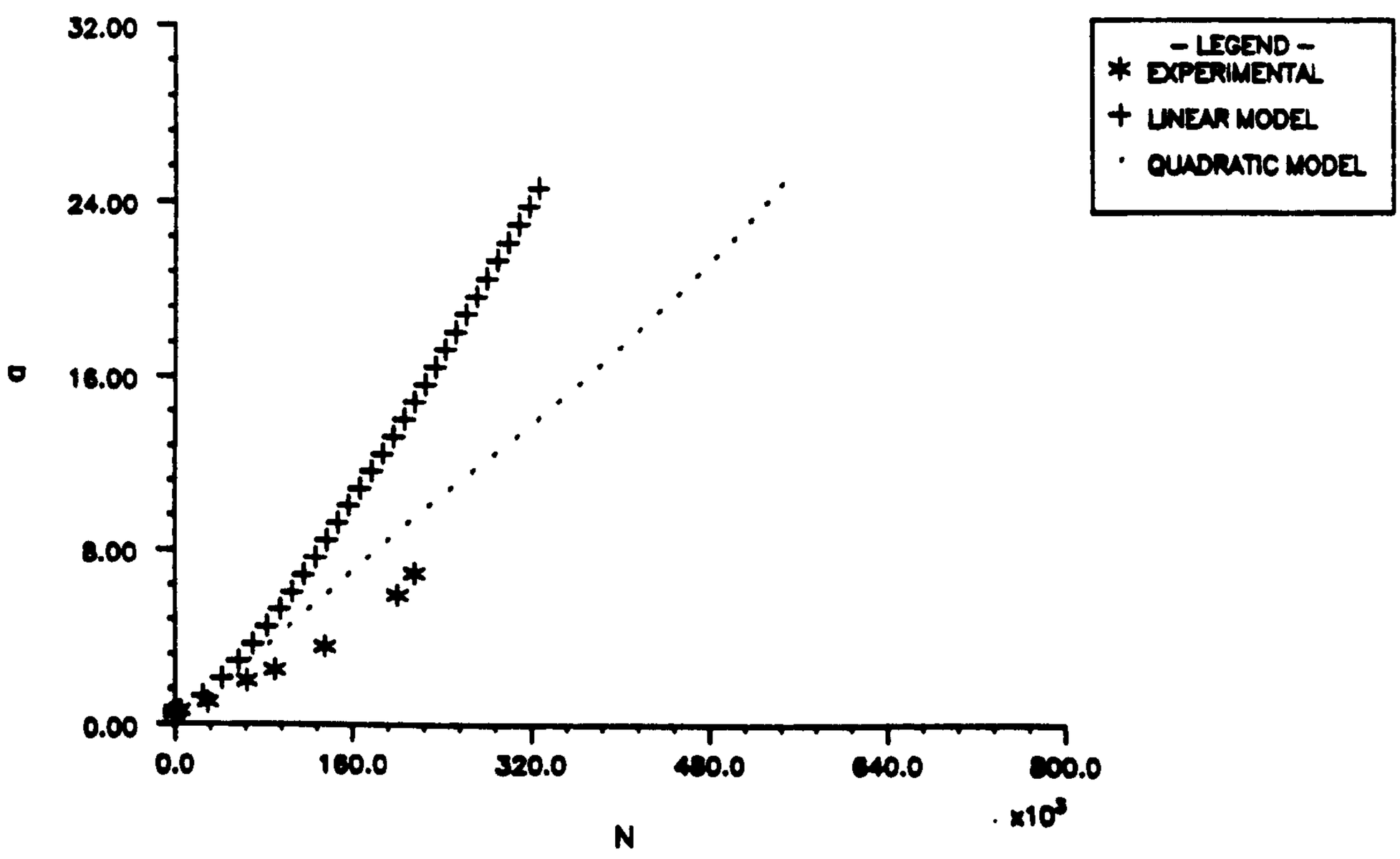

FIGURE 6.21 COMPARISON OF FATIGUE LIFE DATA A–D–Y

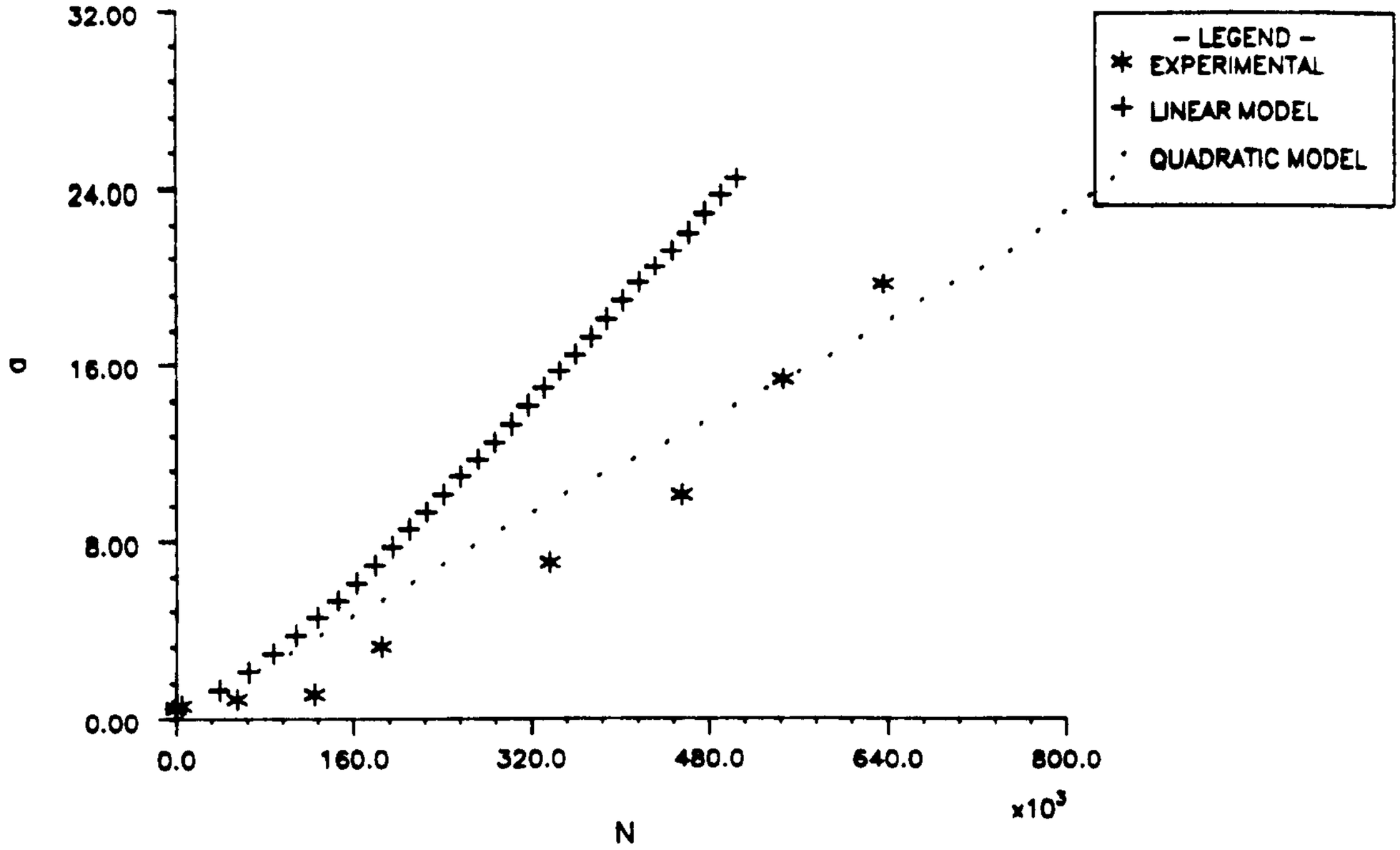

FIGURE 6.22 COMPARISON OF FATIGUE LIFE DATA A–B–Z

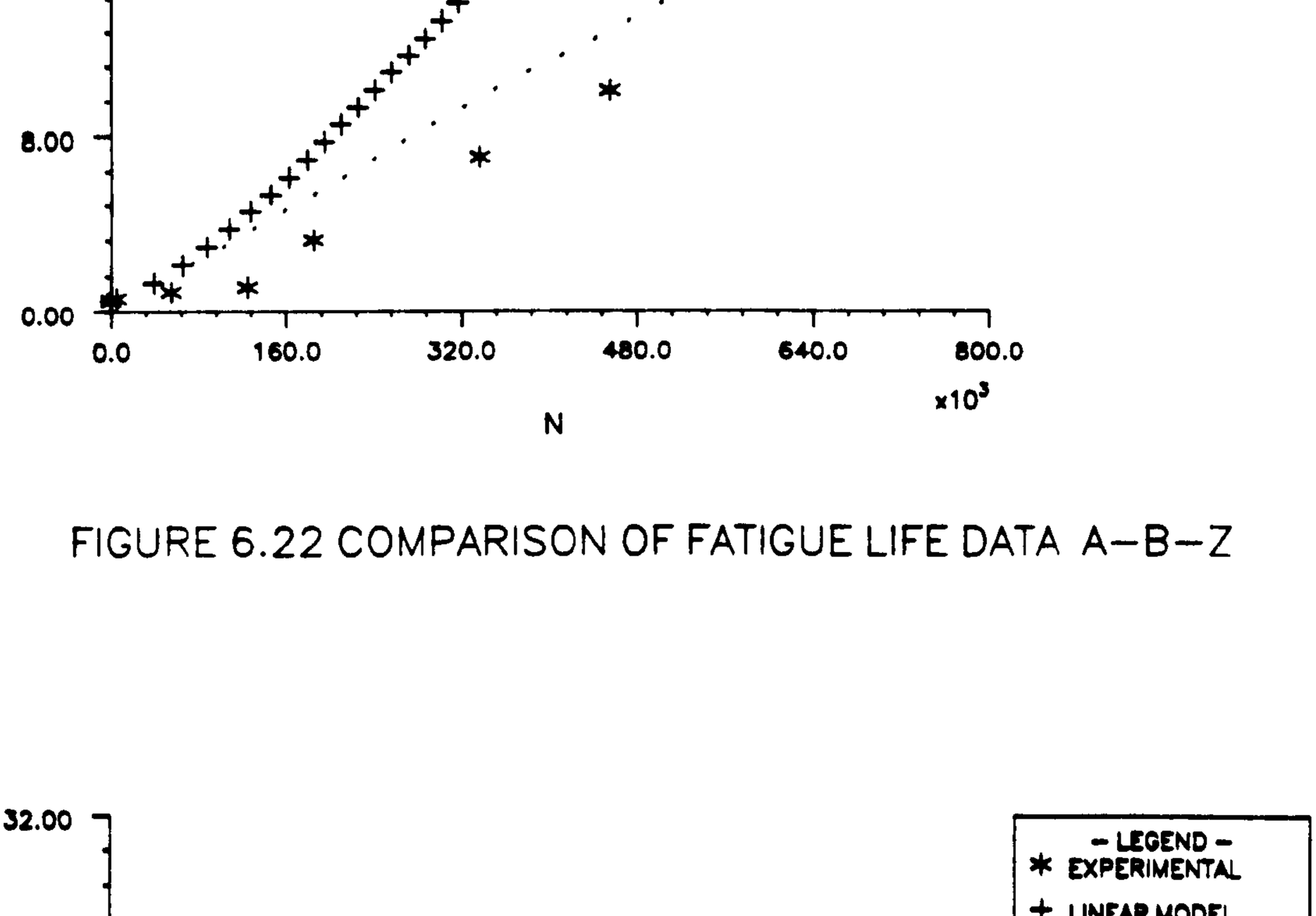

FIGURE 6.23 COMPARISON OF FATIGUE LIFE DATA A–D–Z

7 CHAPTER SEVEN

SUMMARY CONCLUSIONS AND FUTURE WORK

7.1 Scope of chapter

This chapter presents a summary of the main findings of this thesis. Recommendations are made for future work that could be undertaken to possibly enhance and extend the findings presented here.

7.2 Summary of Thesis

The aim of this Thesis has been to investigate the extent to which controlling the weld profile could affect the fatigue crack growth in welded steel tubular joints. A new welding procedure was developed based on the use of extra weld beads to cause a change in the geometric parameters of the weld profile. It was considered that this change could lead to modifications in the stress fields at the brace/chord intersection along the outer surface of the tubular joints and in the through thickness direction resulting in longer initiation time and possibly slower crack growth rates. To assess this possibilty three multiplanar nodes were fabricated with a variety of weld profiles giving the desired change in the geometry of the weld profile.

Large scale automated fatigue tests were conducted using out-of-plane bending loading. Prior to fatigue testing a comprehensive stress analysis study was conducted using the experimental strain gauged method, the finite element method and parametric equations.

Chapters two and three report on the main findings of the stress analysis study. The hot spot stress along the brace/chord intersection of the tubular joint was evaluated using strain gauged steel models and the FE method. The steel model results provided a comparative study of the global stress distributions for the different weld profiles. The results showed that using a different welding procedure, where the geometry of the weld profile could be controlled, produced a measured reduction in the average value of the hot spot stress of 11%. Both types of weld profile produced a range of SCF values for the four saddle positions. This variation in values was reflected in the

FE results and is probably due to the different boundary conditions applied during the testing i.e. brace to brace loading. However, the FE results predicted lower SCF values than the steel results. The underprediction was about 40%.

The conclusions from the FE analyses of the axial and in-plane-bending loading suggest that brace to-brace-loading for tubular joint analyses produces significant differences in the predicted SCF values at the position of the hot spot stress. These conditions considered in terms of local restraint suggest that where a repair has been conducted and the local restraint altered, then important differences in the distributions of stress around the brace/chord intersection could occur. This situation could be important in multimode multinodal studies.

In chapter three the stress analysis study was extended to investigate the local stress fields in the vicinity of the weld toe. The through thickness stress distributions were also investigated. The study attempted to quantify the differences in the stress fields due to the changes in weld geometric parameters. The results from the small single element gauges reported an average reduction in the weld notch effect by 15% for the controlled weld profile. This observation combined with the reduction in hot spot SCF values could lead to a twofold benefit in terms of longer time to initiation and a slower crack growth rate.

The values of the geometric parameters namely, weld toe radius ρ, weld angle α and weld leg length L taken from steel model measurements were used to construct 2-D models of a saddle position. Using the substructuring technique a number of FE analyses were conducted. The results provided specific information on the through thickness stress distribution. The changes in weld toe radius ρ, weld angle α and weld leg length L have been shown to significantly influence the through thickness stress distribution. It is predicted that such changes will ultimately affect the fatigue life of a structure through their influence on the behaviour of the stress intensity factor.

The comparison of through thickness stress distributions between tubular joint results and the combined tension and bending results of T-butt joints (based on equation 3.10) showed excellent agreement. This indicates that it is no longer necessary to conduct tubular joint analyses under complex boundary conditions to calculate through thickness stress distributions.

The reduction in stress values reported in chapters two and three were reflected in the fatigue crack initiation and growth observed in chapter four. The combined effect of lower SCFs, geometric and weld toe, gave an improved life by a factor of 4 for the controlled weld profile compared to an AWS profile. The improvement occurred in the early growth regime. Multiple small crack growth was the most common form of early fatigue damage. These cracks eventually coalesced to form one long semi-elliptical crack. It was possible to measure early crack growth and show that initiation was controlled by the local stress field.

The fatigue data presented in chapter four and the stress distributions reported in chapter three were used in fracture mechanics models. The geometric stress intensity calibration factor Y was calculated from the experimental fatigue data and analytically using the Niu-Glinka weight function method. The Niu-Glinka weight function was based on measured values of weld angle α and weld toe radius ρ taken from chapter three. The analytical results were over conservative. This is probably due to changes in local bending stress that occur as a consequence of the presence of a crack. It was considered that the reduction in local bending moment due to cracking and allied increase in local flexibilty could be modelled by systematic moment release. The mechanism for tubular joints is not fully understood but models using either linear or quadratic moment release produced significant improvements in the analytically calculated Y factors.

These were incorporated in a fracture mechanics model which was used to predict the propagation part of the fatigue life of a structure. The initiation part was predicted using the local strain appraoch. This predictive technique produced anomolies which could not be explained on the basis of the available fatigue data but tended to indicate that the technique was not fully developed to deal with complex structures such as tubular joints.

7.3 Summary of conclusions

1) The combined effect of lower SCFs, geometric 11% lower, weld toe 15% lower, produced an improvement in life by a factor of 4 for the controlled weld profile. This is sufficient to offset any penalty due to chord wall thickness.

2) Reacting brace loads through another brace at 90°, rather than by torsion at the chord ends would seem to give different values of SCF when compared to simple T-joints. This could indicate that the parametric equations should be reassessed in terms of the boundary conditions and could have important implications for multimode multinode situations.

3) The geometric parameters of the weld profile α, ρ and L were shown to significantly influence the through thickness stress distributions.

4) Equation 3.10 was successfully applied using through thickness stress distributions obtained from T-butt joint analysis to demonstrate that T-butt joint results could be used instead of complex tubular joint analysis.

5) The Niu-Glinka weight function used in conjunction with linear and quadratic moment release models formed the basis of the fracture mechanics model. This provided reasonable agreement with experimental fatigue data on the propagation part of life. The linear model was conservative but it accurately predicted the shape of the life curve. The quadratic model was non-conservative and did not predict the shape of the curve accurately.

6) The degree of accuracy provided by the local strain approach in assessing initiation life was not sufficient. This approach requires further development for use in tubular joint analysis.

7.4 Future work

Recommendation for future work that would contribute to a better understanding of the fatigue properties of tubular joints based on the findings of this thesis are listed below.

1) To conduct a comparative stress analysis study on steel joints with different weld profiles under axial and in-plane-bending loading to complement the findings of chapters two and three.

2) Further tests are needed under axial and IPB loading to confirm the findings that the CWP produced significant improvement on life. This is important as it could offset any penalty due to chord wall thickness.

3) Accurate material properties need to be developed for tubular joints to use in the local strain approach.

4) The stress-strain range relation based on Neuber's rule or the energy density method has not been validated for tubular joints, this could explain the inaccuracies in the initiation predictions using the local strain approach. Further development in terms of tubular joint application is required.

5) The use of the Niu-Glinka weight function in conjunction with the two moment release models produced improvements in modelling the fatigue crack propagation part of life. The concept of load shedding is not fully understood and further research could lead to improvements in the models proposed. A numerical and or an experimental analysis would be required to validate this approach.

APPENDIX I

Nominal stress calculations for the four saddle positions A,B,C, and D for the OPB loading mode.

Using the beam theory:

$$\frac{M}{I} = \frac{\sigma}{Y}$$

M bending moment

I second moment of area

σ bending stress

Y distance from neutral axis to the point under consideration

$$I = \left(\frac{\pi}{64}\right)(d_2^4 - d_1^4)$$

t 16.7mm

d_1 inner diameter of brace. 290.6mm

d_2 outer diameter of brace. 324.0mm

I $1.91 \times 10^8 mm^4$

Y 162.0mm

1 kN force produces a nominal stress at A and C

$$Bending\,\sigma = \frac{(1000\,x\,970x\,162)}{(1.91x10^8)}$$

Hence

$$\sigma = 0.823$$

For positions B and D

$$Bending\,\sigma = \frac{(1000\,x\,1370x\,162)}{(1.91x10^8)}$$

$$\sigma = 1.162$$

$$Tension\,\sigma = \frac{1000}{\pi x 324 x 16.7}$$

$$\sigma = 0.059$$

Consider case one for positions A and B in tension thus C and D are in compression i.e

At postion D (-1.162-0.059) = - 1.22 MPa

At position B (+1.162-0.059) = 1.103 MPa

Consider case two for positions A and B in compression C and D in tension

At postion D (1.162+0.059) = 1.22 MPa

At position B (-1.162+0.059) = -1.103 MPa

Therefore the nominal stress for the saddle positions A B C and D is as follows:

σ_n A 0.823 MPa

σ_n B 1.103 MPa

σ_n C 0.823 MPa

σ_n D 1.220 MPa

APPENDIX II
QUADRATIC MOMENT RELEASE MODEL

The rate of moment release is described using the general equation of a circle Consider a circle with centre (a,b) in a coordinate system X and Y where the axes are tangents to the circle at coordinates (0,1), and (1,0). The centre of the circle lies on a 45° line passing through the origin. Thus (a=b). A further point with coordinates (0,d) and (d,0) is considered.

$$r^2 = (x-a)^2 + (y-b)^2$$

$$r^2 = a^2 + (1-b)^2$$

$$r^2 = b^2 + (1-a)^2$$

$$r^2 = (d-a)^2 + (d-b)^2$$

$$r^2 = (1-a)^2 + a^2$$

$$r^2 = 2(d-a)^2$$

$$r = \pm\sqrt{2}\,(d-a)$$

$$0 = (1-a)^2 + a^2 - 2(d-a)^2$$

$$1 - 2d^2 = (2-4d)a$$

$$a = \frac{(2d^2-1)}{(4d-2)}$$

The parameter d is input during the calculation. It governs the position of the centre of the circle and thus alters the curvature giving different degrees of load shedding.

For the present work a number of values of d were used. The final results are presented for d=0.45.